Title

Pavement Recycling: Shrinkage Crack Mitigation in Cement-Treated Pavement Layers—Phase 2b Laboratory Testing and Performance Modeling

Authors

Louw, Stephanus
Jones, David D.
Hammack, Joseph
et al.

Publication Date

2023

DOI

10.7922/G24Q7SBF

January 2023
Research Report: UCPRC-RR-2020-04

Pavement Recycling: Shrinkage Crack Mitigation in Cement-Treated Pavement Layers—Phase 2b Laboratory Testing and Performance Modeling

Authors:
Stephanus Louw, David Jones, Joseph Hammack, and John Harvey

Partnered Pavement Research Center (PPRC) Project Number 4.52b and 4.65 (DRISI Tasks 2709 and 3194):
Microcracking of Cement-Treated Pavement Layers

PREPARED FOR:

California Department of Transportation
Division of Research, Innovation and System Information
Office of Materials and Infrastructure Roadway Research

PREPARED BY:

University of California
Pavement Research Center
UC Davis and UC Berkeley

TECHNICAL REPORT DOCUMENTATION PAGE

1. REPORT NUMBER UCPRC-RR-2020-04	2. GOVERNMENT ASSOCIATION NUMBER	3. RECIPIENT'S CATALOG NUMBER
4. TITLE AND SUBTITLE Pavement Recycling: Shrinkage Crack Mitigation in Cement-Treated Pavement Layers—Phase 2b Laboratory Testing and Performance Modeling		5. REPORT PUBLICATION DATE January 2023 6. PERFORMING ORGANIZATION CODE
7. AUTHOR(S) Stephanus Louw (ORCID 0000-0002-1021-7110) David Jones (ORCID 0000-0002-2938-076X) Joseph Hammack (ORCID: 0000-0002-2410-0896) John Harvey (ORCID: 0000-0002-8924-6212)		8. PERFORMING ORGANIZATION REPORT NO. UCPRC-RR-2020-04 UCD-ITS-RR-20-108
9. PERFORMING ORGANIZATION NAME AND ADDRESS University of California Pavement Research Center Department of Civil and Environmental Engineering, UC Davis 1 Shields Avenue Davis, CA 95616		10. WORK UNIT NUMBER 11. CONTRACT OR GRANT NUMBER 65A0628
12. SPONSORING AGENCY AND ADDRESS California Department of Transportation Division of Research, Innovation, and System Information P.O. Box 942873 Sacramento, CA 94273-0001		13. TYPE OF REPORT AND PERIOD COVERED Research Report June 2019 to June 2022 14. SPONSORING AGENCY CODE

15. SUPPLEMENTAL NOTES
doi:10.7922/G24Q7SBF

16. ABSTRACT

The California Department of Transportation (Caltrans) has been using full-depth recycling (FDR) as a pavement rehabilitation strategy since 2001. Early projects were recycled with foamed asphalt and cement. Cement-only treatments were permitted from 2015 to improve the properties of more marginal materials. However, shrinkage cracking associated with the hydration and curing of the cement-treated layers remains a concern, especially with regard to crack reflection through asphalt concrete surfacings and the related problems caused by water ingress.

Crack mitigation has been studied for decades, and a range of measures related to improved mix designs and construction practices have been implemented by road agencies. One of the most promising measures, used in conjunction with appropriate mix designs, is that of microcracking the cement-treated layer between 48 and 72 hours after construction. In theory, this action creates a fine network of cracks in the layer that limit or prevent the wider and more severe block cracks typical of cement-treated layers. Limited research to assess microcracking as a crack mitigation measure has been completed on a number of projects in Texas, Utah, and New Hampshire. Recommendations from these studies were first implemented by the Texas Department of Transportation and then later by other state departments of transportation. However, longer-term monitoring on a range of projects in Texas, California, and other states had revealed that microcracking has not always been successful in preventing cracking. Some projects showed reflected transverse and block cracks in a relatively short time period, attributable to a number of factors including but not limited to cement content, cement spreading, the method of curing, and the interval between base construction and placement of surfacing.

Discussions with researchers in Texas indicated that additional research was necessary to better understand the microcracking mechanism, and to identify the key factors influencing performance, including but not limited to aggregate properties, cement content, the time period before microcracking starts, layer moisture contents, roller weights and vibration settings, the number of roller passes, the field test methods and criteria used to assess the degree of microcracking, and the effects of early opening to traffic. A multiphase project was therefore initiated at the University of California Pavement Research Center (UCPRC) to investigate these outstanding issues. The second phase of this study is discussed in this report. This phase covered the design, construction, monitoring, and associated laboratory testing of a 37-cell test road to evaluate shrinkage crack mitigation procedures. The study found that microcracking is an effective mitigation measure, provided that design strengths do not exceed 600 psi (4.1 MPa) and that microcracking is done between 48 and 56 hours after compacting the layer.

17. KEY WORDS full-depth recycling with cement, FDR-C, cement treatment, cement stabilization, shrinkage cracking, crack mitigation, microcracking	18. DISTRIBUTION STATEMENT No restrictions. This document is available to the public through the National Technical Information Service, Springfield, VA 22161	
19. SECURITY CLASSIFICATION (of this report) Unclassified	20. NUMBER OF PAGES 200	21. PRICE None

UCPRC ADDITIONAL INFORMATION

1. DRAFT STAGE Final	2. VERSION NUMBER 1
3. PARTNERED PAVEMENT RESEARCH CENTER STRATEGIC PLAN ELEMENT NUMBER 4.65	4. DRISI TASK NUMBER 3194
5. CALTRANS TECHNICAL LEAD AND REVIEWER(S) Allen King and Deepak Maskey	6. FHWA NUMBER CA223194B

7. PROPOSALS FOR IMPLEMENTATION
   (1) Base decision on which full-depth recycling strategy to use on field investigation findings.
   (2) Follow the mix design procedure recommendations in the In-Place Recycling Guide, which includes doing an initial consumption of stabilizer test.
   (3) Consider reducing the target allowable strength for FDR-C mix design strengths to 250 to 450 psi (≈1.7 MPa to 3.1 MPa), with a maximum of 600 psi (4.1 MPa).
   (4) Revise nSSP/Section 30 specification language for microcracking as follows:
   (5) "During the period from 48 to 56 hours after compaction, microcrack the surface by applying 2 to 3 single passes, equivalent to 2.8 to 4.3 kN/cm2 (4,060 to 6,235 psi) of energy, using a 12-ton vibratory steel drum roller at maximum vibration amplitude (centrifugal force of 200 to 300 kN [≈45,000 to 67,500 lb.]) traveling from 2 to 3 mph."
   (6) If a performance-based specification is preferred over a method specification, a 40% stiffness reduction after microcracking, measured with a soil stiffness gauge, should be considered.

8. RELATED DOCUMENTS
   UCPRC-TM-2015-02; UCPRC-RR-2015-02; UCPRC-RR-2016-07; UCPRC-GL-2020-01; UCPRC-RR-2019-05

9. VERSION UPDATES
   None

10. LABORATORY ACCREDITATION
    The UCPRC laboratory is accredited by AASHTO re:source for the tests listed in this report

11. SIGNATURES

S. Louw **FIRST AUTHOR**	J.T. Harvey **TECHNICAL REVIEW**	C. Fink **EDITOR**	J.T. Harvey **PRINCIPAL INVESTIGATOR**	A. King and D. Maskey **CALTRANS TECH. LEADS**	T.J. Holland **CALTRANS CONTRACT MANAGER**

DISCLAIMER STATEMENT

This document is disseminated in the interest of information exchange. The contents of this report reflect the views of the authors who are responsible for the facts and accuracy of the data presented herein. The contents do not necessarily reflect the official views or policies of the State of California or the Federal Highway Administration. This publication does not constitute a standard, specification or regulation. This report does not constitute an endorsement by the Department of any product described herein.

For individuals with sensory disabilities, this document is available in alternate formats. For information, call (916) 654-8899, TTY 711, or write to California Department of Transportation, Division of Research, Innovation and System Information, MS-83, P.O. Box 942873, Sacramento, CA 94273-0001.

ACKNOWLEDGEMENTS

The University of California Pavement Research Center acknowledges the following individuals and organizations who contributed to the project:

- The California Department of Transportation
- University of California, Davis Transportation and Parking Services
- Tom Scullion and Stephen Sebesta, Texas Transportation Institute, Texas A&M University
- Marco Estrada, and the recycling team from Pavement Recycling Systems
- Jeff Wykoff, California Nevada Cement Association
- CalPortland, Cemex, Lehigh Cement Company, and Nevada Cement Company
- Alegre Trucking and Conti Trucking
- Ed Hall, Humboldt Manufacturing
- Gary Aiken, Kessler Engineering

PROJECT OBJECTIVES

This study is a continuation of PPRC Project 4.52b addressing the project titled "Microcracking of Cement-Treated Layers." The objective of this project is to develop guidelines for mitigation measures to limit/prevent shrinkage cracking in cement-treated layers. This will be achieved in two phases through the following tasks (revised after completion of Phase 1):

- Phase 1: Literature review, preliminary laboratory testing, field testing, and modeling (completed)
  - Task 1: Conduct a literature review on research related to crack mitigation in cement-treated pavement layers.
  - Task 2: Conduct preliminary laboratory testing to understand crack mitigation mechanisms and identify criteria for modeling the effects of crack mitigation on long-term pavement performance.
  - Task 3: Monitor the construction and early performance of FDR-C projects where crack mitigation measures have been used.
  - Task 3: Model the effects of crack mitigation on long-term pavement performance.
  - Task 4: Prepare a summary report with recommendations for Phase 2 testing, if appropriate.

- Phase 2: FDR-C Test Road and pilot study construction and monitoring, and laboratory testing
  - Task 1: Update the literature review.
  - Task 2: Continue monitoring the construction and performance of FDR-C field projects where crack mitigation measures have been used.
  - Task 3: Design, construct, and monitor a test road to better understand the effects of different crack mitigation strategies without the influence of traffic.
  - Task 4: Conduct laboratory testing of specimens sampled from the test road and other field projects to compare laboratory test results with measurements on constructed roads and to identify suitable criteria for refining mechanistic-empirical design procedures and performance models for pavements with cement-treated layers.
  - Task 5: Prepare research reports and guidelines for crack mitigation in FDR-C layers.

This report covers Phase 2b (Tasks 4 and 5) and should be read in conjunction with the report prepared for Phase 2a (Tasks 1, 2, 3, and 5; Research Report UCPRC-RR-2019-05).

EXECUTIVE SUMMARY

Introduction

Cement-treated layers, including full-depth recycled layers using cement as a stabilizer (FDR-C), are prone to cracking. This is, and has been, a concern for using cement to improve the strength and stiffness properties of recycled materials that have limited amounts of fine materials and/or plasticity. The research discussed in this and a companion report, which focused on identifying and understanding appropriate shrinkage crack mitigation procedures for recycled pavement layers treated with cement, builds on previous work by the Texas Transportation Institute and others on microcracking as a shrinkage crack mitigation measure. The process involves a combination of optimum curing times before microcracking and number of roller passes (or stiffness reduction) to minimize drying shrinkage crack width, which will maximize long-term stiffness and fatigue life.

Studies by the Texas Transportation Institute and other organizations agreed that microcracking is a potentially effective shrinkage crack mitigation study. However, gaps in the knowledge were identified, specifically a full understanding of microcracking mechanisms, influence of cement content/design strength, optimal timing of microcracking, and roller type. This study addressed these gaps primarily through continued long-term monitoring of pilot studies, the construction and monitoring of a 37-cell FDR-C Test Road (Phase 2a), and a comprehensive laboratory testing study, followed by development of an understanding of the processes and layer behavior through modeling and simulation (Phase 2b).

Summary of Phase 2b Research

Refinement of the Resilient Modulus Test for Treated Materials

The AASHTO T 307 method for testing resilient modulus was originally developed for unbound materials and has been found to significantly underestimate the stiffness of treated materials. Research was conducted to assess four alternative linear variable differential transformer (LVDT) placements to determine whether more realistic stiffness values could be collected. Based on the results, the method was modified to collect on-specimen measurements using three equally spaced LVDTs, instead of the single externally mounted LVDT used in the standard method.

Laboratory results using the new setup corresponded to backcalculated falling weight deflectometer (FWD) results collected on roads with FDR layers.

Development of a Laboratory Microcracking Procedure

A laboratory procedure for inducing microcracking in cement-treated specimens, based on the refinements to the resilient modulus test, was developed to provide a controlled method for reducing the stiffness of compacted specimens that would simulate the results from the FDR-C Test Road.

Laboratory Testing

Laboratory testing on specimens produced with material sampled during construction of the FDR-C Test Road included stiffness testing with microcracking, long-term indirect tensile strength (ITS) tests, short-term ITS tests, short-term unconfined compressive strength (UCS) tests, and drying shrinkage tests. The laboratory microcracking test results were consistent with the backcalculated stiffness results from the FDR-C Test Road in terms of the range of stiffnesses measured and the trends among the different applied energies. The main findings from this part of the study include the following:

- Stiffness Change
  - The laboratory microcracking procedure effectively simulated microcracking in the field, with results showing similar trends between laboratory- and field-measured stiffnesses.
  - The stiffness of the 2.5% cement-content specimens after microcracking recovered through autogenous healing to equal or exceed the stiffness of the control specimens at the same age.
  - The 4% cement-content specimens after microcracking had a significant long-term reduction in stiffness with microcracking effort and curing time before microcracking.
  - Microcracking resulted in damage to the specimens in the form of internal cracks that led to stiffness reduction.
  - The critical factor affecting differences in stiffness behavior was the difference in water-to-cement-for-cementation ratio (w/c_c) for the two cement contents, with the 2.5% cement-content material having a w/c_c of 9.8 and the 4% cement-content material having a w/c_c of just 2.5. As a result, the 2.5% cement-content specimens had significantly more free water available for rehydration of cement after microcracking.
  - The long-term effect of microcracking on stiffness was also dependent on the w/c_c ratio, with microcracked material with higher w/c_c ratios recovering stiffness more effectively than material with a lower w/c_c. Materials with higher w/c_c ratios also achieved stiffness

levels similar to or greater than specimens/pavement layers that were not microcracked, depending on energy input. Microcracked material with lower w/c_c ratios had levels of recovery that were dependent on curing time after compaction and energy input from the roller. Longer curing times and increased energy input reduced the level of stiffness recovery.

  - Microcracking facilitated the movement of moisture through the induced microcracks due to increased permeability, allowing access to any unhydrated cement. The higher cement-content specimens did not have the same free water available for this later hydration, which in turn limited stiffness recovery after microcracking. Compaction of FDR-C layers in the field is typically performed at or close to the optimum moisture content (OMC) of the material. In order to benefit from the ability of the material to gain stiffness after microcracking, the w/c_c should be optimized. However, increasing the moisture content above the OMC to increase the w/c_c can result in a mix that will have a lower density, reduced strength and stiffness, and increased shrinkage cracking. This supports selection of cement contents for FDR-C layers that meet the minimum recommended target strength requirements (i.e., 300 to 450 psi [≈2.1 to 3.1 MPa]) while still meeting the initial consumption of stabilizer (ICS) plus 1% cement durability requirement.
  - Stiffness reduction was log-linearly correlated with energy input, and independent of the number of cycles or the order of stress sequences.
  - The rate of stiffness reduction with energy input was similar for the different cement contents and microcracking times, except for the 4% cement-content specimens microcracked at 72 hours, which had the lowest rate of stiffness reduction due to the increased strength of the material.

- Indirect Tensile Strength and Stiffness
  - The ITS of the specimens was shown to be linearly correlated with stiffness. It is thus expected that reducing the ITS by microcracking will result in shorter crack spacings, while lowering the stiffness will reduce crack widths. This was, however, not observed in the first four months of FDR-C Test Road crack monitoring. It is hypothesized that the cracks existed, but due to their frequency, they were not visible or had not reflected through the microsurfacing four months after construction.
- Unconfined Compressive Strength with Different Microcracking Efforts
  - UCS was not significantly affected by the reduction in stiffness due to microcracking. This is likely due to the mechanics of the test method, which applies an axial load on the specimen and compresses the cracks to their original state before the specimen fails in shear. The UCS was also poorly correlated with the stiffness after different microcracking efforts.

- Effect of Microcracking on Strength (UCS and ITS)
  - Microcracking at 72 hours, and at 48 hours and again at 72 hours (i.e., two microcracking actions), effectively reduced the ITS in both the short-term (i.e., after microcracking) and longer-term (i.e., after 56 days). The UCS, tested two days after microcracking, was not significantly affected by microcracking.
  - The stiffness of both the 2.5% and 4% cement-content specimens were linearly correlated with the ITS.

Development of Behavior Models from Laboratory Test Results

A series of models using data from the FDR-C Test Road and laboratory testing was developed for predicting the effects of microcracking on stiffness. Key factors influencing model prediction trends were cement-content and the water-to-cement-for-cementation ratio.

Simulating Microcracking on the FDR-C Test Road

Microcracking simulations using the laboratory-determined material models, field observations, and published crack width and crack spacing models provided information to further describe the development of shrinkage cracks in FDR-C layers for different microcracking efforts. The results showed the importance of distributing the shrinkage strain over several cracks to minimize crack widths in order to mitigate reflective drying shrinkage cracking. Important findings from this part of the study include the following:

- Microcracking Time and Effort
  - Microcracking is a drying shrinkage crack-control method that reduces strength and effective layer thickness to promote additional shrinkage crack development.
  - Microcracking induces high compressive stresses under the roller drum and high tensile stresses at the bottom of an FDR-C layer. This can lead to crushing on carbonated layers and/or bottom-up cracking from bending failure, which could lead to an effective layer-thickness reduction in terms of stiffness/traffic carrying capacity.
  - The timing of microcracking can affect the crack width based on the remaining shrinkage potential after microcracking. Early microcracking can minimize the difference in crack widths among the different cracks, but it could result in increased reflective cracking in some cases.
- Shrinkage Crack Development
  - Increasing the number of drying shrinkage cracks in an FDR-C layer to reduce slab lengths between the cracks minimizes the accumulation of shrinkage strain over individual cracks and increases the number of cracks over which the shrinkage strain can be distributed.

    - Reducing the widths of drying shrinkage cracks in an FDR-C layer can reduce the number of reflected cracks in the asphalt concrete surface layer. Not all drying shrinkage cracks in an FDR-C layer will reflect through the asphalt concrete layer.
- Design Strength
    - Increasing the cement content to increase the strength and stiffness in anticipation of better fatigue performance of the "intact layer" can adversely affect shrinkage crack widths because the resistance to shrinkage cracking increases. A minimum acceptable design strength should be considered for the mix design of FDR-C layers that satisfies both the durability requirement (UCS at ICS-determined cement content plus 1% cement), as well as the minimum design strength required by the transportation agency.
- Fatigue Life
    - Microcracking can increase the effective fatigue life in pavements with FDR-C layers, since the location that controls fatigue life is the area in the vicinity of wide, reflected shrinkage cracks.

Conclusions

The conclusions drawn after completion of the Phase 2a research were further supported by the results from the work completed in this phase of the study. Revised conclusions based on the research conducted in both Phase 2a and Phase 2b (this report) include the following:

- Microcracking of FDR-C layers does not prevent shrinkage cracking, but it is an effective shrinkage crack mitigation procedure. Microcracking induces a network of fine cracks, which generally do not reflect through asphalt concrete surfacings as wide shrinkage cracks tend to do.
- Microcracking has limitations and will not mitigate all shrinkage cracks on all FDR-C projects. Design strength, construction procedures, curing time before microcracking, number of microcracking passes, and stiffness reduction achieved during microcracking will all influence the level of mitigation achieved.
- The original stiffness prior to microcracking is mostly recovered, and often exceeded, after microcracking on FDR-C layers with strengths at the lower end of the specified target range (i.e., 300 psi [≈2.1 MPa]). Stiffness is significantly reduced on higher-strength layers (i.e., >600 psi [≈4.1 MPa]) after microcracking, and it may not recover to the same stiffness measured before microcracking.
- Microcracking will be most effective if the seven-day UCS of the treated material falls in the range of 250 to 450 psi (1.7 to 3.1 MPa) and preferably no higher than 600 psi (4.1 MPa). Layers with design strengths greater than 600 psi will likely have shrinkage cracks forming before the road can be microcracked.

- Higher-strength FDR-C layers are more sensitive to the timing of microcracking. The greatest reduction in the long-term stiffness is associated with microcracking at 72 hours, with significantly lower stiffnesses measured than those measured when the layer is microcracked between 48 and 56 hours of curing. Statistical modeling on a small data set indicated that microcracking as soon as 24 hours after final compaction may be beneficial on higher-strength layers.
- Microcracking can increase the fatigue life of FDR-C layers by reducing crack widths. Given that failure in pavements with cement-treated layers initiates in the vicinity of reflected wide shrinkage cracks, reducing crack widths by forcing the development of additional cracks in the FDR-C layer will reduce the likelihood of early failures around the cracks and therefore increase fatigue life through improved load transfer efficiency and aggregate interlock. This in turn reduces stresses and strains adjacent to the cracks at the bottom of the layer. The hypothesis proposed early in the study that microcracking would increase the fatigue life of pavements with cement-treated layers was therefore confirmed.
- Microcracking can increase the long-term stiffness of FDR-C layers, which in turn also increases the effective fatigue life of the pavement for comparable conditions. Adjusting mix designs to maximize the water-to-cement-for-cementation ratio, together with applying the appropriate energy input during microcracking, will maximize stiffness in the post-cracked phase in the form of secondary cementation and hydration of unhydrated cement through the mobilization of free water through induced microcracks.
- The current Caltrans method specification for microcracking of FDR-C layers, as it is currently phrased, could lead to significantly different stiffness reduction results given that 12-ton rollers from different manufacturers apply different levels of energy.

Recommendations

The recommendations made after completion of the Phase 2a research were further supported by the results from the work completed in this phase of the study. Revised recommendations based on the research conducted in both Phase 2a and Phase 2b (this report) include the following:

- The mix design procedure for FDR-C layers should include an initial consumption of stabilizer (ICS) test to ensure an optimum cement content that will result in a durable layer is selected. The starting cement content in mix design tests should be the ICS plus 1%. If this results in a seven-day UCS higher than 450 psi (3.1 MPa), the pavement design and or choice of stabilizer/recycling agent should be reviewed.
- Microcracking of FDR-C layers will be most effective if the seven-day UCS falls in the range of 250 to 450 psi (1.7 to 3.1 MPa) and preferably no higher than 600 psi (4.1 MPa).

- Microcracking of FDR-C layers should be done as close as possible to 48 hours after final compaction, especially if design strengths exceed 450 psi (3.1 MPa). Further investigation into microcracking higher-strength FDR-C layers after 24 hours is warranted.
- The Caltrans method specification language for microcracking should be changed to the following (the energy requirement will encourage contractors to check the ratings of their rollers):
  - During the period from 48 to 56 hours after compaction, microcrack the surface by applying 2 to 3 single passes, equivalent to 2.8 to 4.3 kN/cm^2 (4,060 to 6,235 psi) of energy, using a 12-ton vibratory steel drum roller at maximum vibration amplitude (centrifugal force of 200 to 300 kN [≈45,000 to 67,500 lb.]) traveling from 2 to 3 mph.
- If a performance specification is considered, then a maximum stiffness reduction of 40%, measured with a soil stiffness gauge is recommended (i.e., initial measurement before the first roller pass and then measurements after each roller pass until a 40% reduction in stiffness is achieved).
- The research cited in the literature review and testing in this study assessed microcracking on cement-treated layers between 10 and 12 in. (250 and 300 mm) thick. Research on layers thinner than 10 in. should continue to determine if microcracking effort needs to be reduced on thinner layers to prevent permanent damage (i.e., loss of stiffness) to the layer. Research on layers thicker than 12 in. should also continue to assess whether uniform compaction and effective microcracking can be achieved over the full depth of the layer, especially on weak subgrades, and the implications on shrinkage and fatigue cracking if it cannot.
- Although the soil stiffness gauge is considered an appropriate instrument for measuring stiffness reduction during microcracking, testing procedures will need to be refined and precision and bias statements prepared to ensure that reasonable quality control and quality assurance procedures are followed.
- Based on the research findings to date, further research on the following topics, in addition to those noted above, is warranted:
  - Interaction between the water-to-cement-for-cementation ratio and energy input to determine if these can be optimized to maximize stiffness recovery after microcracking, while still ensuring durability of the mix.
  - Quantification of the relationship between crack width, load transfer efficiency, and stress and strain at the bottom of the FDR-C layer adjacent to drying shrinkage cracks, to develop appropriate factors to increase the tensile stress and strain as determined from layer elastic theory for pavement design.

TABLE OF CONTENTS

LIST OF TABLES

LIST OF FIGURES

LIST OF ABBREVIATIONS

AASHTO	American Association of State Highway and Transportation Officials
AMPT	Asphalt mix performance tester
ASTM	American Society for Testing and Materials
Caltrans	California Department of Transportation
CSH	Calcium silicate hydrate
ESAL	Equivalent single axle load
FDR	Full-depth recycling
FDR-EA	Full-depth recycling with emulsified asphalt emulsion
FDR-FA	Full-depth recycling with foamed asphalt
FDR-N	Full-depth recycling with no stabilizer
FDR-C	Full-depth recycling with portland cement
FEM	Finite element method
FWD	Falling weight deflectometer
HVS	Heavy Vehicle Simulator
ICS	Initial consumption of stabilizer
IDT	Indirect tensile
ITS	Indirect tensile strength
LTE	Load transfer efficiency
LVDT	Linear variable differential transformer
LWD	Light weight deflectometer
MC	Microcracking
OMC	Optimum moisture content
RAP	Reclaimed asphalt pavement
RVE	Representative volume element
SEM	Scanning electron microscopy
SNR	Signal-to-noise ratio
SSE	Sum of the square of the error
SSG	Soil stiffness gauge
TS	Test setup
UCPRC	University of California Pavement Research Center
UCS	Unconfined compressive strength
UTM	Universal testing machine
w/c_c	Water-to-cement-for-cementation ratio

TEST METHODS CITED IN THE TEXT

AASHTO

T 180 Standard Method of Test for Moisture-Density Relations of Soils Using a 4.54-kg (10-lb) Rammer and a 457-mm (18-in.) Drop

T 307 Standard Method of Test for Determining the Resilient Modulus of Soils and Aggregate Materials

ASTM

D1557 Standard Test Methods for Laboratory Compaction Characteristics of Soil Using Modified Effort (56,000 ft-lbf/ft^3 [2,700 kN-m/m^3])

D1633 Standard Test Methods for Compressive Strength of Molded Soil-Cement Cylinders

D2487 Standard Practice for Classification of Soils for Engineering Purposes (Unified Soil Classification System)

D6931 Standard Test Method for Indirect Tensile (IDT) Strength of Asphalt Mixtures

CONVERSION FACTORS

SI* (MODERN METRIC) CONVERSION FACTORS				
APPROXIMATE CONVERSIONS TO SI UNITS				
Symbol	**When You Know**	**Multiply By**	**To Find**	**Symbol**
		LENGTH		
in.	inches	25.40	millimeters	mm
ft.	feet	0.3048	meters	m
yd.	yards	0.9144	meters	m
mi.	miles	1.609	kilometers	km
		AREA		
in^2	square inches	645.2	square millimeters	mm^2
ft^2	square feet	0.09290	square meters	m^2
yd^2	square yards	0.8361	square meters	m^2
ac.	acres	0.4047	hectares	ha
mi^2	square miles	2.590	square kilometers	km^2
		VOLUME		
fl. oz.	fluid ounces	29.57	milliliters	mL
gal.	gallons	3.785	liters	L
ft^3	cubic feet	0.02832	cubic meters	m^3
yd^3	cubic yards	0.7646	cubic meters	m^3
		MASS		
oz.	ounces	28.35	grams	g
lb.	pounds	0.4536	kilograms	kg
T	short tons (2000 pounds)	0.9072	metric tons	t
		TEMPERATURE (exact degrees)		
°F	Fahrenheit	(F-32)/1.8	Celsius	°C
		FORCE and PRESSURE or STRESS		
lbf	pound-force	4.448	newtons	N
lbf/in^2	pound-force per square inch	6.895	kilopascals	kPa
APPROXIMATE CONVERSIONS FROM SI UNITS				
Symbol	**When You Know**	**Multiply By**	**To Find**	**Symbol**
		LENGTH		
mm	millimeters	0.03937	inches	in.
m	meters	3.281	feet	ft.
m	meters	1.094	yards	yd.
km	kilometers	0.6214	miles	mi.
		AREA		
mm^2	square millimeters	0.001550	square inches	in^2
m^2	square meters	10.76	square feet	ft^2
m^2	square meters	1.196	square yards	yd^2
ha	hectares	2.471	acres	ac.
km^2	square kilometers	0.3861	square miles	mi^2
		VOLUME		
mL	milliliters	0.03381	fluid ounces	fl. oz.
L	liters	0.2642	gallons	gal.
m^3	cubic meters	35.31	cubic feet	ft^3
m^3	cubic meters	1.308	cubic yards	yd^3
		MASS		
g	grams	0.03527	ounces	oz.
kg	kilograms	2.205	pounds	lb.
t	metric tons	1.102	short tons (2000 pounds)	T
		TEMPERATURE (exact degrees)		
°C	Celsius	1.8C + 32	Fahrenheit	°F
		FORCE and PRESSURE or STRESS		
N	newtons	0.2248	pound-force	lbf
kPa	kilopascals	0.1450	pound-force per square inch	lbf/in^2

*SI is the abbreviation for the International System of Units. Appropriate rounding should be made to comply with Section 4 of ASTM E380. (Revised March 2021)

Blank page

1 INTRODUCTION

1.1 Background

The California Department of Transportation (Caltrans) has been using full-depth recycling (FDR) as a rehabilitation strategy since 2001. Most projects to date have used a combination of foamed asphalt (FDR-FA) and portland cement as the recycling agent. However, emulsified or foamed asphalt are not always appropriate recycling strategies for all projects, and therefore alternative FDR strategies need to be considered. This study investigates the use of portland cement alone (FDR-C) as a stabilizer, specifically for projects where more marginal materials are present in the recycled layer.

Cement-treated (or stabilized) materials in FDR projects are mixtures of recycled asphalt pavement (RAP), aggregate base/subbase, and/or soil together with measured amounts of portland cement and water, which are shaped and compacted to form new subbase or base layers in pavement structures. Subgrade soils can also be treated in place to improve the properties of the pavement foundation. Cement-treated layers have been widely used as pavement bases for highways, roads, streets, parking areas, airports, and materials-handling and storage areas. Because they typically have better bearing capacity and durability than bases constructed with untreated materials, they allow for thinner and often more cost-effective pavement structures. They have been widely used in the past in California, nationally, and internationally, and considerable published research by numerous organizations has been undertaken and experience gained on their design, construction, and long-term performance *(1)*. This report does not document this past research on cement-treated layers.

A well-documented concern about cement-treated layers, and therefore FDR-C layers, is the potential for shrinkage cracking associated with the hydration and curing of the treated layers. Observations of this cracking date back to ancient Roman times, when horsehair was added to concrete roadways and the structural members in buildings in an attempt to reduce the risk of cracking while the concrete set *(2)*. As hydration and curing progress, the drying shrinkage of cement-treated materials is known to contribute the most to shrinkage cracking *(3-5)*. In semi-rigid pavements, shrinkage cracks from the underlying cement-treated layers, including FDR-C layers, can reflect through the asphalt concrete surfacing, allowing water to infiltrate into the

treated layer. Frequent cracks coupled with water infiltration leads to a loss in stiffness in the treated layer, resulting in a faster rate of overall deterioration compared to pavements that are not cracked.

Although no costs for shrinkage crack repair are readily available for California highways, the Texas Department of Transportation estimated savings of between $3.3 million and $8.6 million in annual net present value maintenance costs if shrinkage cracking could be prevented on projects where cement-treated layers are placed *(6)*.

A variety of crack mitigation approaches have been investigated in recent years, including but not necessarily limited to the following:

- Optimizing pavement designs with a specific focus on cement content and design strengths.
  - The Caltrans non-standard special provision for FDR-C current at the time this research was undertaken specified a design strength range of 300 to 600 psi (≈2.0 to 4.1 MPa), considerably lower than the standard specification design-strength envelope for Class A cement-treated base layers (minimum unconfined compressive strength [UCS] of 750 psi [≈ >5.1 MPa] after a seven-day cure).
  - The Portland Cement Association recommends an FDR-C mix design strength range of 250 to 400 psi (≈1.7 to 2.8 MPa) to limit shrinkage cracking *(7)*.
- Improved construction procedures with a specific focus on curing and on microcracking of the treated layers with a vibrating steel drum roller to alter shrinkage crack development patterns.
- Microcracking (sometimes termed precracking) of the treated layer. The process entails driving a vibrating steel drum roller over the layer between 48 and 72 hours after its construction. In theory, this action creates a fine network of cracks in the layer that limits or prevents the wider and more severe block cracks typical of cement-treated layers.
- Limited documented *(8)*, but unpublished research to assess the influence of using small quantities of emulsified or foamed asphastelt in combination with the cement to alter the hydration process and potential shrinkage.

Microcracking is currently the most commonly used shrinkage crack mitigation approach because of its relative simplicity, low cost, and measurable effect. The technique was originally developed in Austria to limit the amount of shrinkage cracking in cement-treated layers. At the time of starting this study, limited testing had been completed on a number of projects in Texas, Utah, and New Hampshire. Recommendations from these studies have been implemented by Caltrans and other state departments of transportation. However, longer-term monitoring on a range of

projects in California, Texas, and other states revealed that microcracking has not always been successful in preventing cracking, with some projects showing reflected transverse and block cracks in a relatively short time period (Figure 1.1). Discussions with the Texas researchers indicated that additional research was necessary to better understand the microcracking mechanism and to identify the key factors that influence performance. These include, but are not limited to, aggregate properties, cement content and design strength, the time period before microcracking is initiated, layer moisture contents, curing procedures, roller weights and vibration settings, the number of roller passes applied, the time period before placing the surfacing, the time period before opening the road to traffic, and the field test methods and criteria used to assess the degree of microcracking achieved.

Figure 1.1: Reflected shrinkage cracks on an FDR-C pavement seven years after construction.

1.2 Related Studies

During the period covered by the 2011–2014 Caltrans-UCPRC Partnered Pavement Research Contract, a test track was constructed to assess four different FDR strategies (with no stabilization [FDR-N], using foamed asphalt with portland cement [FDR-FA], using emulsified asphalt [FDR-EA], and using only portland cement [FDR-C]) *(9)*. An additional microcracking experiment was included in the FDR Test Track design, but problems with the control of the cement application by the contractor on the day of construction prevented any testing on this lane and limited any further research on microcracking at the time. A 0.2 ft. (60 mm) asphalt concrete surfacing was placed on all the recycled layers. Accelerated wheel-loading tests with a Heavy Vehicle Simulator (HVS) were carried out on sections on the four lanes under dry and then wet conditions. Limited laboratory testing on cores sampled from the FDR Test Track was also undertaken. The FDR-C

sections designated for HVS testing were not microcracked and some shrinkage cracking was observed on the tested base approximately 15 days after construction and through the asphalt concrete surfacing approximately six months after construction:

- On the dry test, no cracking was observed in the asphalt concrete on the test section after more than one million wheel-load repetitions (≈43.3 million equivalent single axle loads [ESALs]) under dry conditions. However, deflection tests indicated considerable loss of stiffness in the structure during the testing period (i.e., from ±2,900 ksi [20 GPa] to ±1,885 ksi [13 GPa]), which was attributed in part to shrinkage, potential fatigue cracking in the FDR-C layer, and breakdown of the cemented bonds during trafficking. Continued HVS testing on this section may therefore have led to the cracks reflecting through the asphalt concrete surface. The average surface rut depth after testing was 1 mm.
- The wet test, started approximately 12 months after the end of the dry test, was conducted on an untrafficked section that included an original reflected shrinkage crack. New reflected shrinkage cracks were observed after approximately 100,000 load repetitions (100,000 ESALs). These eventually developed into fatigue cracks covering most of the section during the remainder of HVS testing. Terminal cracking (0.75 ft./ft^2 [2.5 m/m^2]) was reached after 530,000 load repetitions (≈1.69 million ESALs). Localized loss of stiffness was observed in the vicinity of the reflected shrinkage cracks. The average surface rut depth after testing was 3.2 mm.

1.3 Problem Statement

Microcracking is a promising technique for limiting or preventing shrinkage cracking in FDR-C and other cement-treated layers that could reflect through asphalt concrete and other types of asphalt surfacings. However, insufficient research has been conducted to fully understand its mechanism, to develop procedures for microcracking (i.e., time interval between final compaction and microcracking, vibration settings, the number of microcracking cycles, etc.), and to identify suitable criteria for mechanistic-empirical design procedures and performance models of pavement structures that incorporate a microcracked FDR-C or cement-treated layer (which could theoretically have a different mechanistic behavioral life cycle than structures with FDR-C or cement-treated layers that have not been microcracked). The Caltrans Standard Specifications at the time of starting this research required microcracking only on FDR-C layers, with instructions stating only that:

> During the period from 48 to 72 hours after compaction, microcrack the surface by applying 3 passes of the vibratory steel drum rollers used during final compaction at high amplitude, regardless of whether asphaltic emulsion has been applied.

One pass is considered to be the roller movement in one direction only (i.e., three passes would be 1) start to end, 2) end to start, and 3) start to end.

No additional information was provided, and no tests were required by the specification to determine whether microcracking was effective in reducing initial stiffness. The results of using this method specification had not been evaluated in California prior to the start of this UCPRC study.

At the start of this study, the following problem statements requiring additional research or refinement/calibration of existing information for California conditions were identified:

- No comprehensive guidelines exist to guide design engineers, contractors, and project specification writers on how to decide on the optimal microcracking procedure for a specific layer design and how to determine whether the desired result has been achieved.
- The research completed in Texas was limited to a small number of projects with a limited range of materials and cement contents. Subsequent observations have found that cement content, curing, and layer durability can have a significant influence on the effectiveness of microcracking. Additional research is required to determine the key factors that influence the effectiveness of microcracking. These may include, but are not limited to, the following:
  - Adjusting the time interval between the completion of construction and the start of microcracking (i.e., curing time)
  - Selecting a specific weight of roller
  - Selecting specific vibration settings
  - Selecting one or multiple microcracking actions
  - Setting required specific changes in measured stiffness after microcracking
- There is no established procedure for accurately measuring the effectiveness of microcracking actions. Currently, a percentage change in stiffness measured with a falling weight deflectometer (FWD), light weight deflectometer (LWD), or soil stiffness gauge (SSG) is recommended. Implementable guidelines based on actual field performance need to be prepared for this activity. Consideration needs to be given to whether the load applied during FWD testing causes additional microcracking in the drop zone, thereby influencing conclusions regarding the level of stiffness change that was achieved by the roller.
- There is no procedure for simulating microcracking in the laboratory as part of a mix design/ pavement design process. Such a procedure needs to be developed.
- There is no documented research linking microcracking with layer curing, opening to traffic, and the period between constructing the treated layer and placing the asphalt concrete surfacing.

- There is no documented research investigating the use of alternative strategies to microcracking to reduce shrinkage cracking, such as adding fibers, adding small quantities of emulsified or foamed asphalt, or synthetic polymer emulsion, to enhance crack mitigation when using microcracking, or using retarders to slow the rate of hydration.
- There is limited research quantifying the benefits of microcracking in terms of extended pavement life.

1.4 Project Objective/Goal

This study is a continuation of PPRC Project 4.36 ("Guidelines for Full-Depth Reclamation of Pavements") and addresses the project titled "Microcracking of Cement-Treated Layers." The objective of this project was to develop guidelines for mitigation measures to limit/prevent shrinkage cracking in cement-treated layers. It was planned that this would be achieved in two phases through the following tasks (revised workplan after completion of Phase 1 *[10]*). Accelerated wheel-load testing was originally included in the workplan as a potential third phase but was removed with the agreement of Caltrans based on findings from the early phases of the FDR research study *(9)* and from Phase 1 of the FDR-C crack mitigation research (completed in 2016 *[3,11]*):

- Phase 1: Literature Review, Preliminary Laboratory Testing, Field Testing, and Modeling
  - Task 1: Conduct a literature review on research related to crack mitigation in cement-treated pavement layers.
  - Task 2: Conduct preliminary laboratory testing to understand crack mitigation mechanisms and identify criteria for modeling the effects of crack mitigation on long-term pavement performance.
  - Task 3: Monitor the construction and early performance of FDR-C projects where crack mitigation measures have been used.
  - Task 4: Prepare a summary report with recommendations for Phase 2 testing if appropriate.
- Phase 2: Test Road and Pilot Study Construction and Monitoring
  - Task 1: Update the literature review.
  - Task 2: Continue monitoring the construction and performance of FDR-C field projects where crack mitigation measures have been used.
  - Task 3: Design, construct, and monitor an experimental FDR-C Test Road to better understand the effects of different crack mitigation strategies without the influence of heavy traffic.

Task 4: Conduct laboratory testing of specimens sampled from the FDR-C Test Road and other field projects to compare laboratory test results with measurements on constructed roads and to identify suitable criteria for refining mechanistic-empirical design procedures and performance models for pavements with FDR-C layers.

Task 5: Prepare research reports and guidelines for crack mitigation in FDR-C layers.

This report covers Phase 2b (Tasks 4 and 5) and should be read in conjunction with the report prepared for Phase 2a (Tasks 1, 2, 3, and 5, report number UCPRC-RR-2019-05 *[12]*) and guidelines for partial- and full-depth recycling in California *(13)*.

1.5 Study Hypotheses

The hypotheses for this research are:

- Microcracking can mitigate the effects of drying shrinkage cracking by inducing a network of hairline cracks to relieve the restraint stress and minimize drying shrinkage crack widths.
- Improved mix design and laboratory characterization methods can increase the effective fatigue life of an FDR-C layer by accepting the presence of drying shrinkage cracks in the layer and focusing the mix design to minimize the effects of these cracks.

These hypotheses are based on the current understanding of the theoretical fatigue mechanism of cement-treated layers under traffic originally proposed by De Beer and illustrated in Figure 1.2 *(14)*. Cement-treated layers develop drying shrinkage cracks due to the restraint stresses that develop between the treated layer and the layer below it, caused by volumetric reduction of the treated layer. Researchers have shown that these cracks are the starting point for other distresses due to the increased stresses and strains caused by traffic traveling over the crack *(4,15-17)*. Refining the mix design and microcracking the treated layer can improve fatigue life and reduce shrinkage crack reflection by minimizing drying shrinkage crack widths, which limits reductions in aggregate interlock and load transfer efficiency (LTE) across the crack. Limiting reductions in LTE can reduce the stresses and strains adjacent to the cracks. A revised theoretical fatigue mechanism of cement-treated layers under traffic after implementing these improvements is proposed in Figure 1.3 *(1)*.

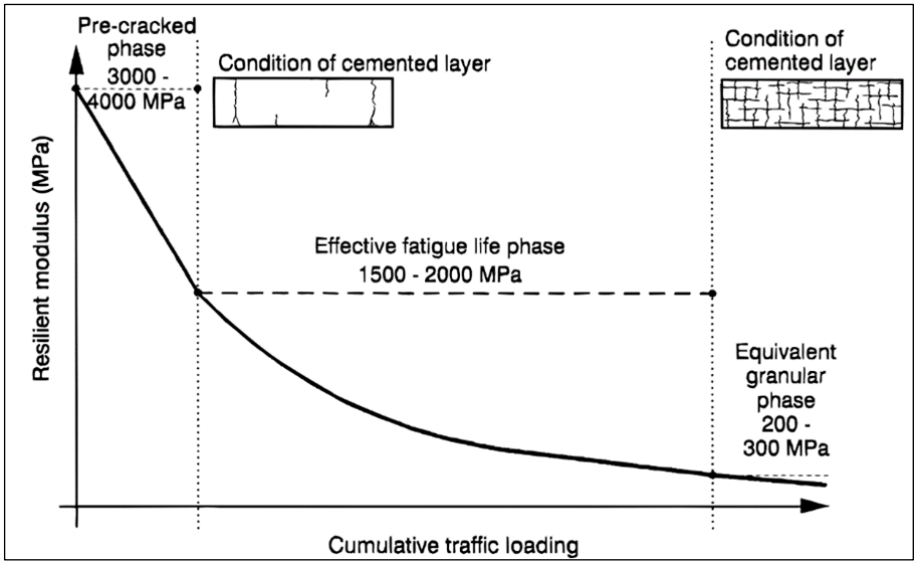

Figure 1.2: Theoretical structural life cycle of cement-treated pavement layers *(14)*.

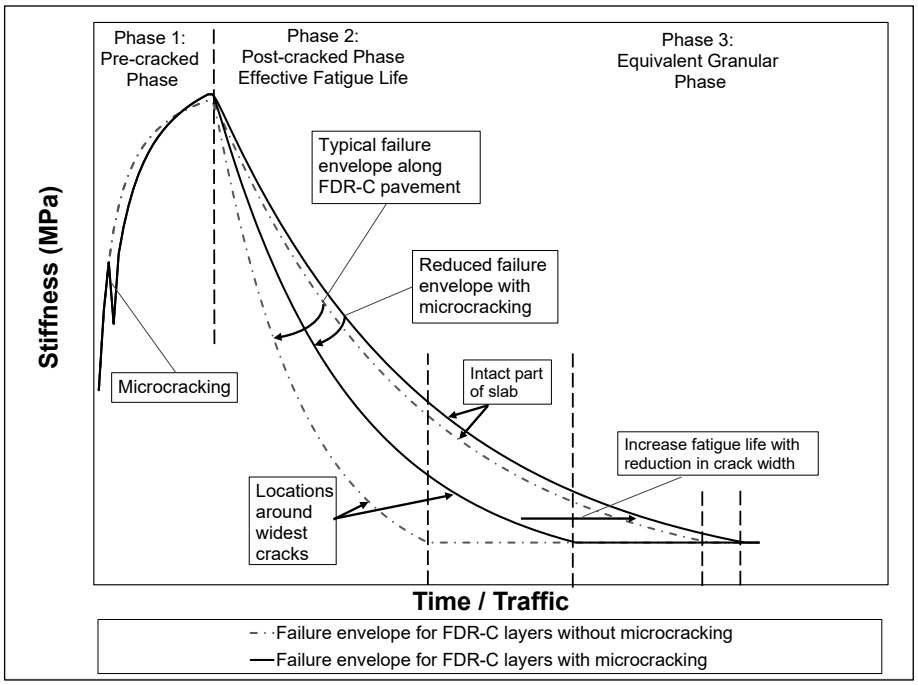

Figure 1.3: Revised theoretical structural life cycle of cement-treated pavement layers *(1)*.

1.6 Report Layout

This research report presents an overview of the work carried out in meeting the objectives of Phase 2, Task 4 of the study, and is organized as follows:

- Chapter 2 summarizes the findings from the Phase 2a study covering observations and testing on the FDR-C Test Road.
- Chapter 3 discusses refinement of the resilient modulus test for treated materials.

- Chapter 4 details development of a laboratory microcracking procedure.
- Chapter 5 summarizes the laboratory testing experimental plan.
- Chapter 6 summarizes the laboratory test results.
- Chapter 7 discusses the development of behavior models using the laboratory test results.
- Chapter 8 discusses simulations of microcracking on the FDR-C Test Road.
- Chapter 9 provides a project summary, conclusions, and preliminary recommendations.
- Appendix A provides additional plots of laboratory test results.
- Appendix B provides additional plots of modeling and simulation results.

1.7 Measurement Units

Although Caltrans has returned to the use of US standard measurement units, metric units have always been used by the UCPRC in the design and layout of test tracks and for laboratory, accelerated wheel load testing, field measurements, and data storage. In this report, both English and metric units (provided in parentheses after the English units) are provided in general discussion. In keeping with convention, metric units are used in the FDR-C Test Road and laboratory testing data analyses and reporting. A conversion table is provided on page xxv at the beginning of this report.

2 SUMMARY OF PHASE 2a REPORT

This chapter summarizes the research and conclusions documented in the Phase 2a report *(12)*, which covers Tasks 1 through 3 of the Phase 2 workplan. Chapters 6 through 8 of this report refer to observations and testing on the FDR-C Test Road documented in the Phase 2a report.

2.1 Literature Review

An extensive literature review was performed to develop an understanding of how cement-treated layers fail, how the fatigue life of cement-treated layers is modeled, why shrinkage cracks are a concern, and how shrinkage cracks can be mitigated.

2.2 Test Road Design

The construction of a test road to evaluate different microcracking variables was recommended after the conclusion of the literature review and preliminary field studies. This allowed for the inclusion of control sections where no shrinkage crack mitigation measures were implemented as well as a significantly wider factorial than could be achieved on any full-depth recycling projects with cement (FDR-C), which typically do not include control sections. The FDR-C Test Road design considered the various issues identified during the literature review, during pilot studies, and from the foundational work done in Texas. The following factors were considered in the experiment design:

- Mix design strength (2.5% and 4% cement)
- The number of curing hours between completion of construction and start of microcracking (48, 72, and 48 and 72 hours [i.e., microcracking on the same section at two different times])
- Roller weight (12-ton single drum steel roller and 10-ton double drum steel roller)
- Roller vibration amplitude (low and high settings)
- Number of roller passes (method and performance-based specifications)
- Stiffness reduction during microcracking (measured with a soil stiffness gauge and a light weight deflectometer [LWD])
- Stiffness recovery/gain after microcracking (measured with a falling weight deflectometer [FWD])
- Crack propagation and crack properties (measured during visual assessments)

2.3 Test Road Construction

The FDR-C Test Road was constructed over a two-day period (4% cement-content sections on day 1 and 2.5% cement-content sections on day 2). Construction and quality control procedures adhered to Caltrans guidance and specifications. Microcracking followed construction over a three-day period depending on the experiment factorial. A microsurfacing was applied after completion of the microcracking. All stages of construction were closely monitored, and observations and results indicated that the FDR-C Test Road was suitable for longer-term monitoring for the microcracking study.

2.4 Test Road Monitoring

Monitoring on the FDR-C Test Road included regular visual assessments focusing primarily on crack monitoring, preliminary coring to check for any indication of crushing or carbonation, and FWD deflection measurements, from which stiffness changes over time were backcalculated. Observations and findings include the following:

- Reflected cracks were observed in a limited number of cells on the 2.5% cement-content section. Cracks directly associated with instrumentation were not considered as cracks associated with microcracking and were therefore excluded from the analysis.
- Cracks reflected through the microsurfacing earlier on the 4% cement-content section compared to the 2.5% cement-content section.
- Crack density increased more rapidly on the 4% cement-content section compared to the 2.5% cement-content section.
- Microcracking reduced crack density compared to the results recorded on the control cells.
- Crack density generally reduced with an increase in the number of microcracking passes applied.
- The 2.5% cement-content cells had a lower crack density after 128 days than the 4% cement-content cells.
- The 2.5% cement-content cells did not show any observable trends in crack density with microcracking passes.
- Only the 4% cement-content cells microcracked at 72 hours showed a reduction in crack density with increased energy input (microcracking passes) using the single drum steel roller at high amplitude (1.42 kN/cm per pass).
- Microcracking the 4% cement-content cells at 48 hours resulted in a greater crack density reduction compared to microcracking at 72 hours. One pass at 48 hours was sufficient to

reduce the crack spacing significantly. The crack density continued to reduce with an increasing number of passes at 72 hours.

- The crack density results from the 10-ton double drum steel roller were inconsistent with the results from the 12-ton single steel drum roller at high amplitude. The results from the 10-ton roller showed that microcracking at 72 hours resulted in reduced cracking on both the 2.5% and 4% cement-content sections.
- Crack width was a function of microcracking effort and curing time before microcracking.
- The microcracked cells had a narrower crack-width distribution than the control cells.
- Microcracking at 48 hours resulted in narrower cracks compared to microcracking at 72 hours.
- An increase in microcracking effort (i.e., number of passes/increased energy) contributed to a further reduction in crack widths.
- The 4% cement-content control cells (i.e., no microcracking) had higher stiffnesses compared to the 2.5% cement-content control cells, as expected.
- The 2.5% cement-content cells microcracked at 48 hours had higher stiffnesses than the control cells and those cells microcracked at 72 hours.
- Increasing energy input through multiple microcracking passes reduced the long-term stiffness proportionately.

2.5 Monitoring Result Analysis

Statistical analyses of the FDR-C Test Road material testing, microcracking, crack monitoring, and backcalculated stiffness results were undertaken to better understand and explain the observations on the road. Findings include the following:

- Crack density and spacing
  - Crack density increased with increasing design strength.
  - Increased energy input (i.e., number of roller passes for a given roller weight) was most effective at reducing the crack density of the material with the higher design strength, while the lower design strength material did not show a sensitivity to energy input in terms of crack density reduction. The 2.5% cement-content material had on average one full-width reflective crack in the 49 m (≈161 ft.) long cell, regardless of the microcracking input, whereas the number of reflected cracks on the 4% cement-content cells reduced from approximately seven cracks down to three cracks with increased energy input during microcracking.
  - Increased energy input was the primary factor in reducing crack width.
  - The 2.5% cement-content material had significantly less shrinkage potential (remaining shrinkage to be incurred) after microcracking than the 4% cement-content material after

a given curing time. Shrinkage that continued after microcracking at 48 or 72 hours did not induce a sufficient number of cracks to minimize widths of the reflected cracks. The cracks that developed before microcracking thus controlled the reflective cracking. Microcracking earlier after final compaction (e.g., within 24 hours) could potentially yield more fine shrinkage cracks in the FDR-C layer and further minimize crack widths to mitigate reflective cracking.

  - The 4% cement-content material had significantly more shrinkage potential remaining after microcracking than the 2.5% cement-content material. The additional increase in the number of drying shrinkage cracks that developed with increased energy input during microcracking (resulting in lower strength) reduced the total width of cracks that developed before microcracking. Microcracking was performed sufficiently early on the 4% cement-content material to change the drying shrinkage cracking from a few wide reflective cracks to numerous thinner cracks with only a small number of them wide enough to reflect through the surface layer.
  - Microcracking should ideally be performed as early as possible to benefit from the shrinkage potential after microcracking while the material strength is still low.

- Stiffness
  - The long-term stiffness of the 4% cement-content material dropped significantly in the cells where the FDR-C layer was microcracked at 72 hours compared to stiffnesses recorded in the cells with microcracking at 48 hours.
  - The 2.5% cement-content material did not show a significant difference in long-term stiffness when microcracked at 48 or 72 hours.
  - Increasing the energy input (i.e., the number of roller passes) reduced the stiffness.
  - Low energy input during microcracking resulted in long-term stiffnesses exceeding those of the control cells for the 2.5% cement content section.
  - The original stiffness prior to microcracking was mostly recovered, and often exceeded, after microcracking on FDR-C layers with strengths at the lower end of the specified range (i.e., 2.1 MPa [≈300 psi]). Stiffness was significantly reduced on higher strength layers (i.e., >3.5 MPa [≈500 psi]) after microcracking, and it may not recover to the same stiffness measured before microcracking.
  - Higher-strength layers were more sensitive to the timing of the microcracking. The greatest reduction in long-term stiffness was associated with microcracking at 72 hours, with significantly lower stiffnesses measured compared to those measured when the layer was microcracked at 48 hours. The lower strength layers were not sensitive to the time of microcracking in the 48 to 72 hour time window.
  - The mechanistic parameters measured during microcracking (percent stiffness reduction and stiffness after microcracking) did not provide any clear explanation for the trend in the FWD-backcalculated stiffness results. This was attributed in part to stiffness

measurements being taken at the same fixed locations in each cell regardless of any surface distresses that may have influenced the results.

2.6 Conclusions

The following conclusions were drawn on completion of this phase of the research:

- Microcracking does not prevent shrinkage cracking, but it is an effective shrinkage crack mitigation procedure. Microcracking induces a network of fine cracks, which generally do not reflect through asphalt concrete surfacings as wide shrinkage cracks tend to do.
- Microcracking has limitations and will not mitigate all shrinkage cracks on all FDR-C projects. Design strength, construction procedures, curing time before microcracking, number of microcracking passes, and stiffness reduction achieved during microcracking will all influence the level of mitigation achieved.
- The original stiffness prior to microcracking is mostly recovered, and often exceeded, after microcracking on FDR-C layers with strengths at the lower end of the specified range (i.e., 2.1 MPa [≈300 psi]). Stiffness is significantly reduced on higher strength layers (i.e., >3.5 MPa [≈500 psi]) after microcracking, and it may not recover to the same stiffness measured before microcracking.
- Higher-strength layers are more sensitive to the timing of microcracking. The greatest reduction in the long-term stiffness is associated with microcracking at 72 hours, with significantly lower stiffnesses measured than those measured when the layer is microcracked at 48 hours.
- Microcracking will be most effective if the seven-day UCS falls in the range of 250 to 450 psi (1.7 to 3.1 MPa) and preferably no higher than 600 psi (4.1 MPa). Layers with design strengths greater than 600 psi will likely have shrinkage cracks forming before the road can be microcracked.
- The current Caltrans method specification for microcracking could lead to significantly different stiffness reduction results as it is currently phrased, given that 12-ton rollers from different manufacturers apply different levels of energy.

3 REFINEMENT OF THE RESILIENT MODULUS TEST FOR TREATED MATERIALS

3.1 Introduction

The AASHTO T 307 triaxial resilient modulus test has been widely used for testing FDR-C materials. The test setup, with externally mounted axial linear variable differential transformers (LVDT), and minimal consideration of preparing the specimen ends, was initially developed for testing unbound subgrade and aggregate base materials, and not stiff, treated materials. The results in Louw et al. *(11)* discussed issues related to testing treated materials with this test setup, including the following:

- Specimen ends are not smooth and parallel after compaction and do not conform to the loading platens, which leads to poor contact with the platens (Figure 3.1). Stepwise increases in the confining and contact pressure improves the contact between the specimen ends and the loading platens, which results in higher stiffnesses.
- Uneven specimen faces can be a result of saw cutting of field cores, or by smoothing the final layer during laboratory compaction. Finishing a specimen that contains coarse aggregates, using a flat steel plate after compaction in a Proctor compactor (similar to ASTM D1557), often results in a broken face. This is remediated by filling the voids with fines, which do not interlock with the specimen and often break out during handling. This results in irregular specimen ends, as shown in Figure 3.2.
- Measuring axial deflections across the full length of the specimen means that anomalies associated with non-uniform stress and strain distributions at the specimen ends are included in the result.

Figure 3.1: Inconsistent specimen ends leading to poor contact.

Figure 3.2: Broken edges due to pull out of recompacted faces.

An improved method for specimen preparation and test setup was required to address problems encountered using AASHTO T 307 during initial development of a test method to induce

microcracking in the laboratory *(11)*. The reasons for questioning the results from the initial testing were:

- Relatively low stiffnesses compared to those measured in the field: The resilient moduli measured on cement-treated material were similar to those measured by Jones et al. *(19)* who tested FDR-FA, material with 3% foamed asphalt and 1.5% cement. Several of the test sequences on the FDR-C specimens also indicated that the stiffness was equal to that of untreated materials, which is generally between 100 and 300 MPa. The resilient modulus of the FDR-C specimens was expected to be in excess of 3,000 MPa.
- Relative insensitivity to curing time: Cement-treated materials are known to rapidly increase in stiffness and strength within the first 7 to 28 days, where after the rate of stiffness increase slows. The results also showed inconsistent trends, with stiffnesses after two days of curing exceeding stiffnesses after 14 days.
- Stress-hardening behavior of cement-treated materials: This was consistent with the findings by other researchers *(20-22)* where methods similar to AASHTO T 307 were used to test cement-treated materials. However, these results do not agree with the theory developed by Lovelady and Picornell *(23)* and proven by Richart et al. *(24)*, Vinson et al. *(25)*, and Capdevila and Rinaldi *(26)* who used on-specimen mounted transducers.
- Insignificant differences between resilient modulus results of specimens prepared with the same material with 3% and 4% cement: This indicates that the test setup was insensitive to materials with different stiffnesses.

3.2 Specimen Preparation

An improved preparation procedure for preparing treated material specimens was required to address two issues:

- Improvement of the stability of the specimen on the loading platens and ensuring the specimen is in full contact with them
- Ensuring accurate and repeatable attachment of LVDT gauge points on the specimen

Specimen-end issues were first addressed by thinly capping specimens with gypsum using a vertical cylinder capper to ensure a flat, square face to ensure full contact with the platens (Figure 3.3). A strip of masking tape applied around the top and bottom edges of the specimen prevents any gypsum overflow from adhering to the sides of the specimen. Excess gypsum was carefully removed from the tape before removing the tape itself to achieve a smooth, constant-diameter specimen without dislodging any material (Figure 3.4). The gypsum used in this study had a stiffness of 15,000 MPa and a UCS of 15.3 MPa based on a 200×100 mm (8×4 in.) specimen

cured for 24 hours at 25°C. The stiffness of the gypsum was greater or close to the stiffness of the FDR-C and was unlikely to affect the results.

Figure 3.3: Preparing to apply gypsum cap.

Figure 3.4: Gypsum caps after removing tape from both ends.

LVDT gauge point mounting issues were addressed by modifying the jig provided by IPC Global for attaching gauge points to specimens for testing in an Asphalt Mixture Performance Tester (AMPT) to attach gauge points at 120-degree offsets on 200×100 mm (8×4 in.) specimens at third or quarter points (Figure 3.5).

Figure 3.5: Modified gauge point jig with gauge point holders for 200×100 mm specimens.

The jig provides a solution to the problems experienced by Hilbrich and Scullion *(27)* and allows the operator to precisely locate the gauge point positions. Each location is prepared with cyanoacrylate to provide a bonded surface on treated and unbound specimens for the two-part

epoxy used for attaching the gauge points. The cyanoacrylate binds any loose particles on the surface and polymerizes in the presence of moisture. The jig also positions the gauge points onto the specimen on the prepared locations, in the correct orientation, and holds them in place while the two-part epoxy cures.

3.3 Test Setup

Five different test setups (TS, shown in Figure 3.6) were investigated to determine an appropriate method to measure specimen deflection and deformation. The specimens used in this study were 200 mm (≈8 in.) in height by 100 mm (≈4 in.) in diameter. All tests included porous stone plates and filter paper between the specimen and the top and bottom platens (i.e., frictional specimen ends). The following are details for each of the five test setups:

- TS-1: ±0.1 mm (≈0.004 in.) LVDTs with a gauge length of 70 mm (≈2.8 in.) attached at approximately third points over the center of the specimen (the minimum gauge length for the LVDTs used was 70 mm, which is 4 mm [≈0.16 in.] longer than the gauge length required to measure at exactly third points)
- TS-2: ±0.1 mm LVDTs with a gauge length of 100 mm (≈4 in.) attached at quarter points over the center of the specimen
- TS-3: ±0.1 mm LVDTs with a gauge length of 185 mm (≈7.3 in.) attached near the ends of the specimen
- TS-4: ±1 mm LVDTs measuring the deflection between the top of the specimen and the bottom platen
- TS-5: ±1 mm LVDTs measuring the deflection between the top and bottom cap (this is the setup prescribed in AASHTO T 307)

A series of three axial cyclic stresses (93, 138, and 300 kPa) were chosen to evaluate the test setups. The lower stress was chosen based on an analysis of the mean and standard deviation of the resilient modulus following the sequences in AASHTO T 307 using each of the proposed test setups. The seating stresses used for each cyclic stress sequence were 20, 100, 180, 260, and 340 kPa. This selected seating stress range is unrealistically high compared to the stress range used in AASHTO T 307, which only ranges between 2.1 and 27.6 kPa, but was considered appropriate for assessing the sensitivity of the test setups to changes in seating stress.

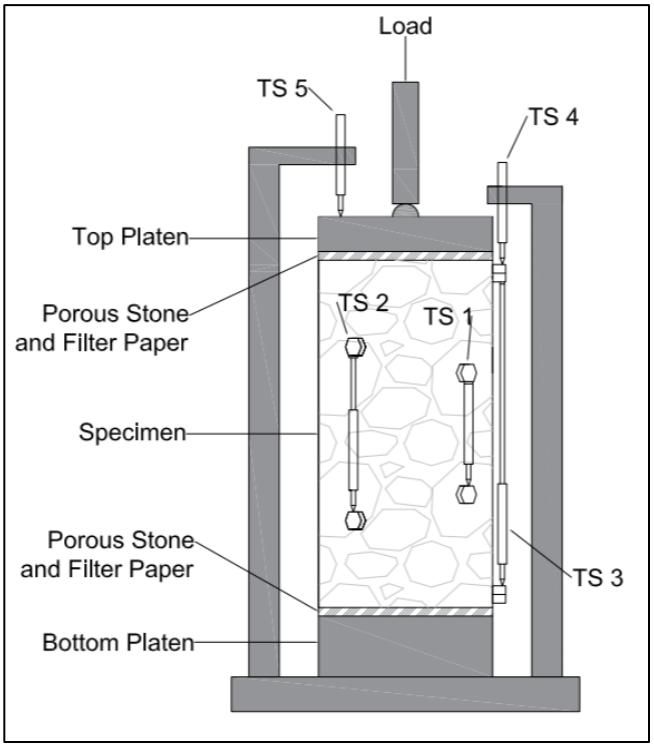

Figure 3.6: Test setups used for evaluating the proposed test method.

The tests were performed following the naming convention for the test setups (TS-1 through TS-5). The TS-1 tests were repeated at the end of the testing sequence with a 300 kPa cyclic stress to determine if the specimen had incurred any damage during the testing sequence.

The following series of tests were performed to address concerns related to the results from the initial microcracking simulation in the laboratory *(11)*:

- Mounting LVDTs at different locations on the specimen to confirm the effect of non-uniform stress distribution along the length of the specimen
- Measuring the signal-to-noise ratio (SNR) at low stresses to ensure the transducers were capable of accurately measuring the deflection of the stiff specimens
- Increasing the seating stresses during cyclic testing to simulate the effect of the confining pressures applied during AASHTO T 307 testing on the top loading platen (i.e., to overcome poor contact between specimen and loading platen)
- Increasing cyclic axial stresses to determine the stress sensitivity of the cement-treated material

The testing was done on a specimen cored from the FDR-C lane on the FDR Test Track in a location with known FWD backcalculated stiffnesses (Figure 3.7). Laboratory resilient moduli would need to be within the range of 10,000 to 20,000 MPa to match the backcalculated stiffnesses from the

FDR Test Track *(9)*, keeping in mind that the conditions between field and laboratory tests are not the same. The backcalculated results include the following:

- Confinement effect of the 60 mm (≈2.4 in.) thick asphalt concrete layer above the FDR-C layer, which should not affect the stiffness of the FDR-C layer, since it is bound
- Potentially different moisture contents, with higher moisture contents decreasing the stiffness
- Capillary suction, which should increase the stiffness of the FDR-C layer

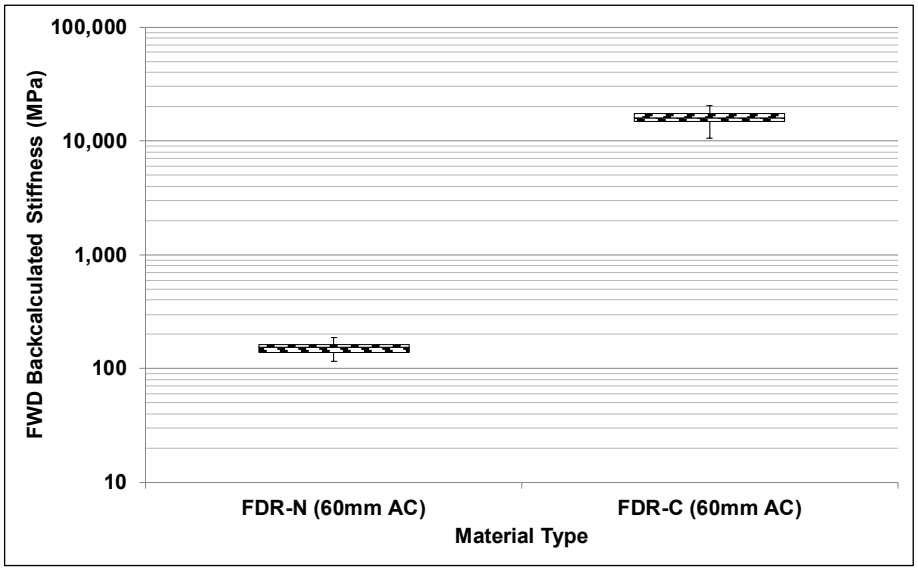

Figure 3.7: FWD-backcalculated stiffness on the FDR-N and FDR-C test track lanes.

3.4 Test Results

The average strain measurements recorded during the stiffness testing for each test setup are provided in Figure 3.8 for the case with a seating stress of 20 kPa and a cyclic stress of 300 kPa. The recorded strain results show the rapid decrease of the end effects as the measured location incrementally excludes the ends of the specimen and approaches an asymptote as the gauge length decreases over the center of the specimen (TS-5 to TS-1). Reducing the gauge length can result in non-representative strain measurements due to the representative volume element (RVE) of the specimen.

The effect of the different average strain measurements on the resilient modulus determined for each test setup at the different cyclic axial and seating stresses are shown in Figure 3.9.

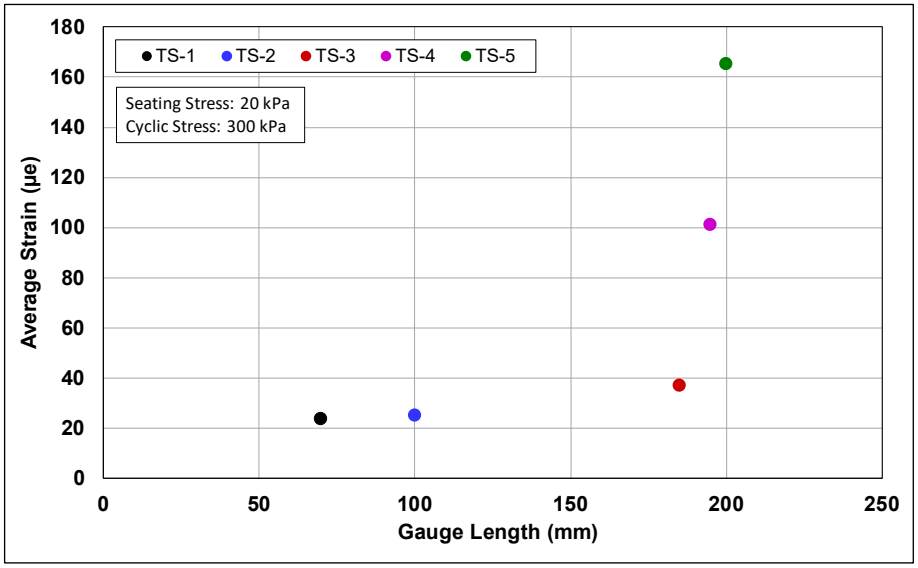

Figure 3.8: Average elastic strain for each test setup.

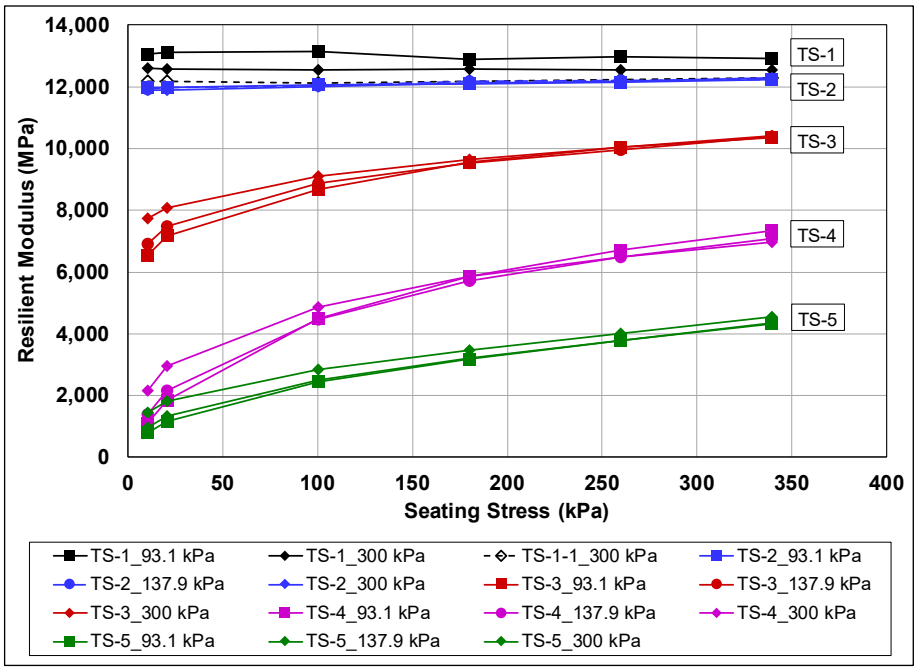

Figure 3.9: Resilient modulus results determined from all test setups.

The stiffnesses measured following AASHTO T 307 (TS-5), with LVDTs measuring the cap-to-cap strain, are clearly much lower compared to the stiffnesses measured on the specimen (TS-1 and TS-2). The stiffness increased (i.e., the strain decreased) as the measured area excluded increasingly more of the end effect as the ends were confined by the loading platens. This confirms the observation made by Peng *(28)*.

The stress-strain results for each test setup, at the 99th cycle, with a 20 kPa seating stress at each of the three cyclic stresses, are shown in Figure 3.10 through Figure 3.14. There was a notable change in the shape of the stress-strain curve from TS-1 through TS-5, which changed from a linear to a parabolic shape as end effects were increasingly included in the measured length (i.e., from TS-1 to TS-5). This agrees with the research by Peng *(28)* and confirms the effects of the confinement of the ends of the specimens caused by the loading platens.

Figure 3.15 through Figure 3.19 show the resilient moduli for each of the test setups. The y-axis scales are not constant between the graphs to emphasize the effects of increased axial cyclic stress. The cement-treated material appeared to be sensitive to both increases in cyclic and seating stresses using TS-3, TS-4, and TS-5. This indicates that the material was stress hardening, and thus differed from the theoretical model from Lovelady and Picornell *(23)*, but it was consistent with the observations from Potturi *(20)*, Puppala et al. *(21)*, and Alabaster et al. *(22)*. However, when the measured area was at quarter or third points (TS-2 or TS-1, respectively) around the specimen center, the specimen's response was largely insensitive to stress change. Minimal difference was recorded in stiffness for each of the cyclic stresses recorded for TS-2. This is likely a result of partial influence of the end effects as the gauge length increased.

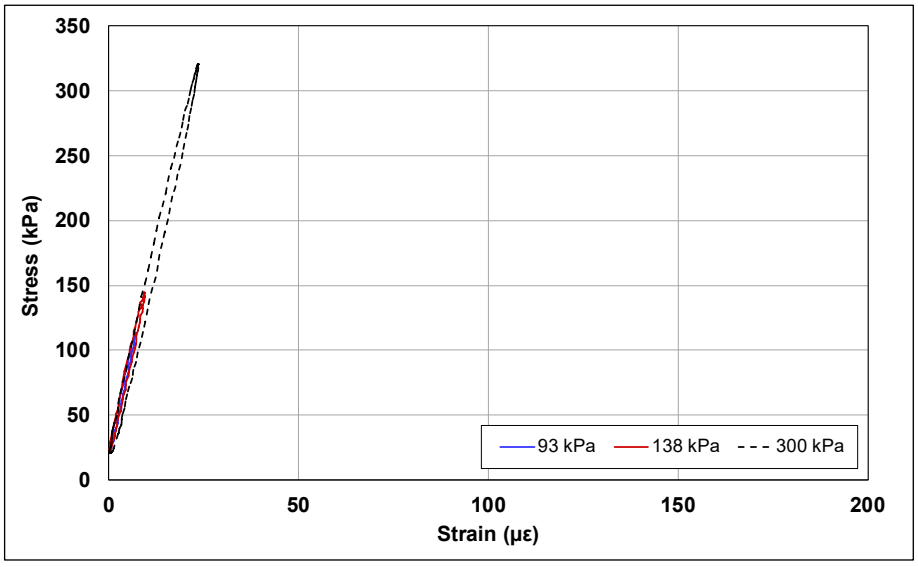

Figure 3.10: Cyclic stress-strain curve of TS-1.

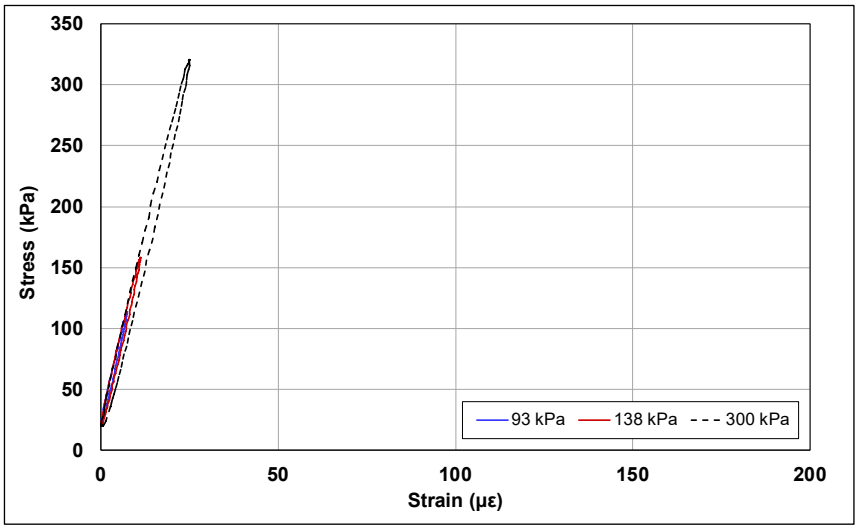

Figure 3.11: Cyclic-stress strain curve of TS-2.

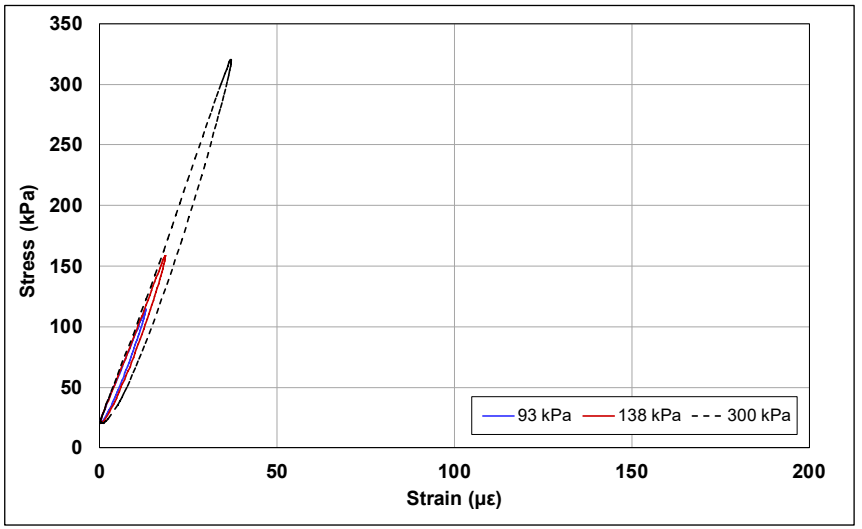

Figure 3.12: Cyclic stress-strain curve of TS-3.

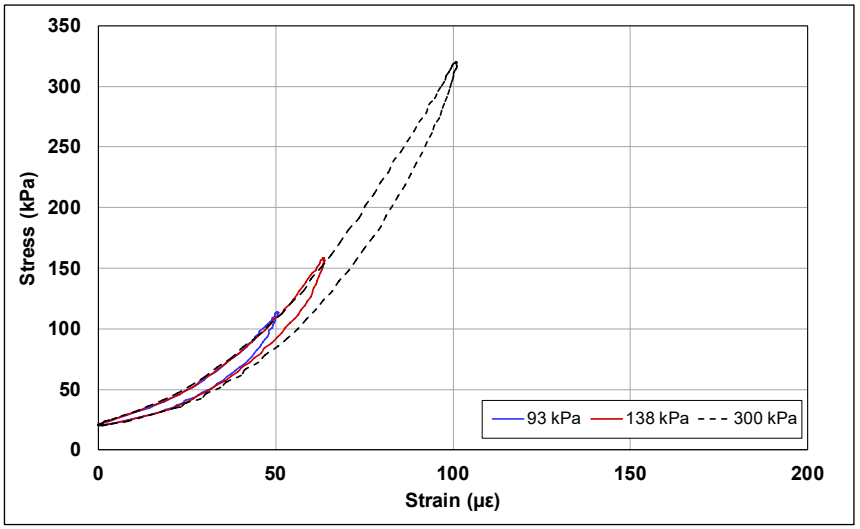

Figure 3.13: Cyclic stress-strain curve of TS-4.

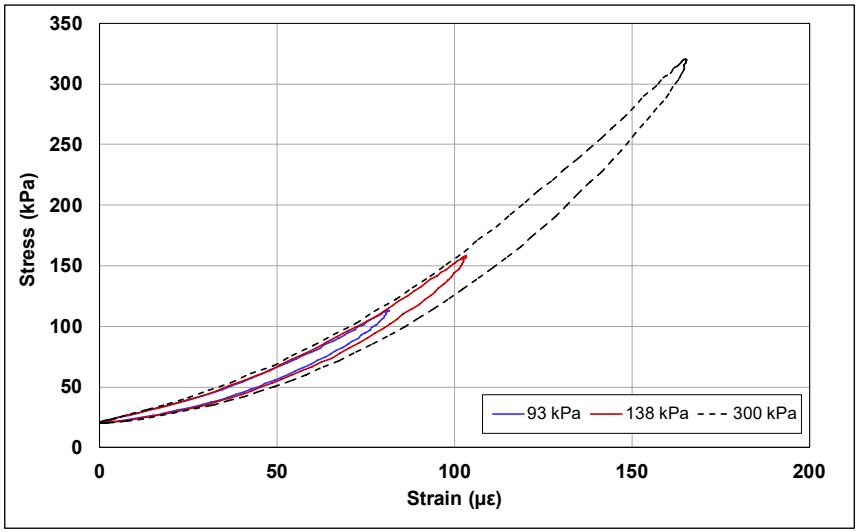

Figure 3.14: Cyclic stress-strain curve of TS-5.

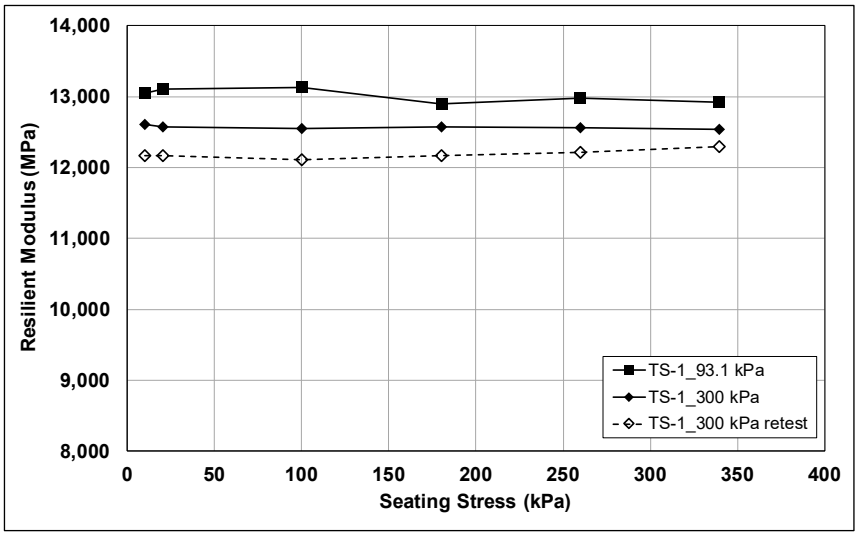

Figure 3.15: Resilient modulus determined from TS-1.

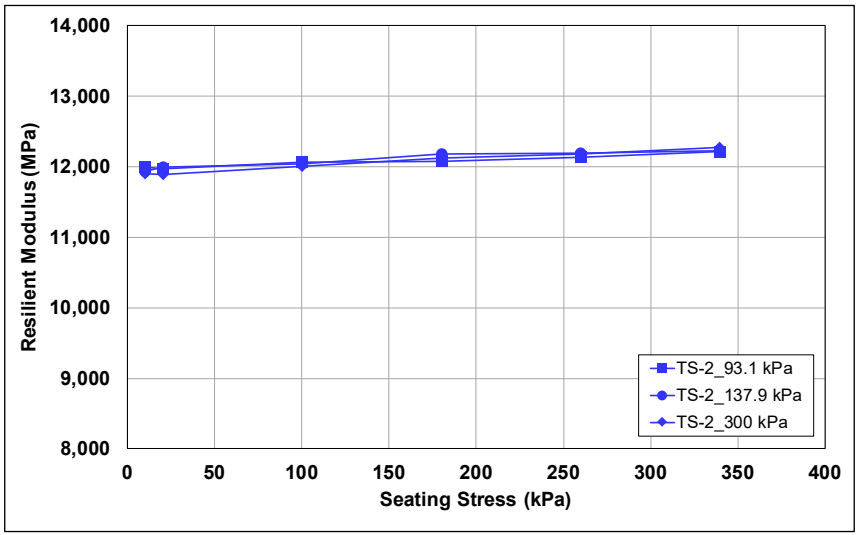

Figure 3.16: Resilient modulus determined from TS-2.

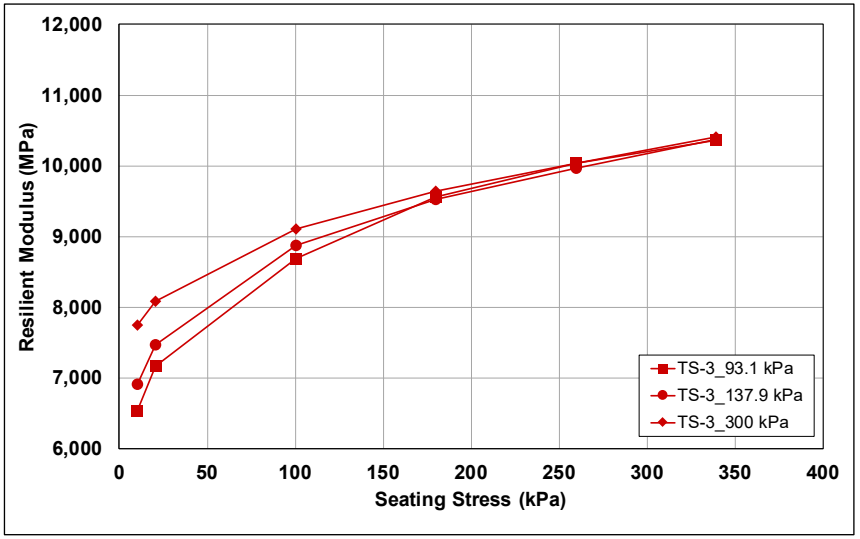

Figure 3.17: Resilient modulus determined from TS-3.

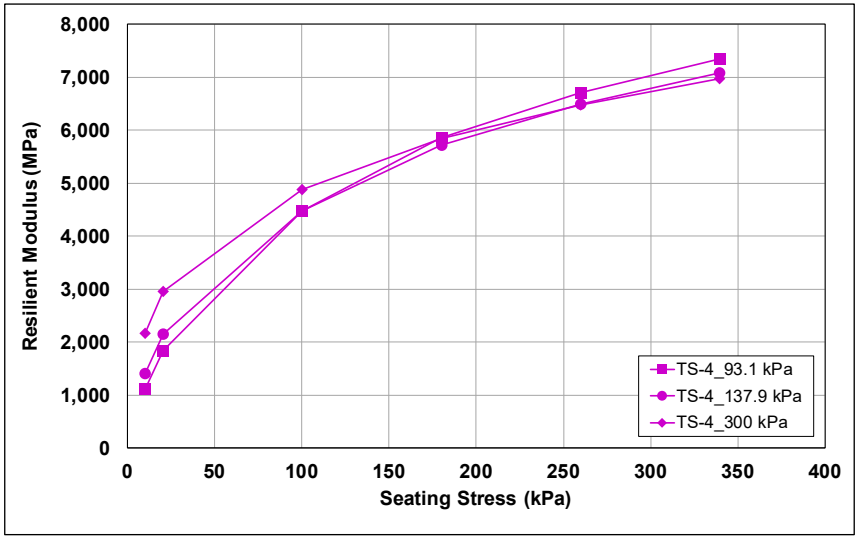

Figure 3.18: Resilient modulus determined from TS-4.

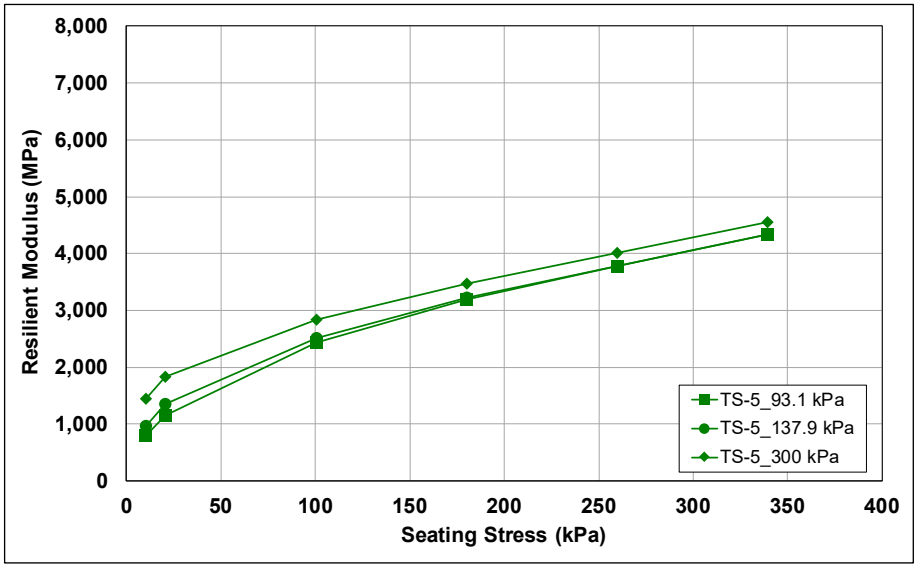

Figure 3.19: Resilient modulus determined from TS-5.

There was some variability in the stiffnesses measured using TS-1, which was attributed to a lower SNR. The stiffness was calculated using the resilient strain, which is the difference between the peak recorded strain and the strain at the end of the rest period. Since the resilient strain is calculated without a smoothing function on the strain signal, the effects of the noise are included in the resilient strain. The reduction in stiffness determined with TS-1, with increased cyclic stresses from 93.1 to 300 kPa, was possibly caused by the following:

- The cement-treated material is stress softening
- The SNR increased with increasing cyclic stress, which increased the definition of the signal, thereby measuring higher strains
- Damage was induced during the cyclic testing leading to lower stiffnesses

Stress softening is unlikely the cause of the reduction in stiffness as this effect would have also been observed during the testing with TS-2.

SNR issues likely contributed to the reduction in stiffness. The SNR for each cyclic and loading stress combination (Table 3.1) was calculated according to Figure 3.20. The possible error included in the calculation due to the SNR is also provided in Table 3.1. The error was calculated as $1/SNR \times M_r$, where M_r is the average resilient modulus calculated for each sequence. The possible error in the calculation of the resilient modulus is relatively large for TS-1 and a cyclic stress of 93.1 kPa compared to TS-2 with each of the cyclic stresses.

Damage during cyclic testing, which relates the reduction in stiffness to stress softening during testing as a result of increasing cyclic stresses, is unlikely because this effect would also have been observed during the testing of TS-2. Damage was, however, induced in the specimen after testing of all five test setups (Figure 3.9), when comparing the resilient modulus for the 300 kPa result to the 300 kPa retest result. This damage only occurred after multiple tests on the same specimen had been completed.

Table 3.1: SNR for each Test Setup and Potential Error in the Stiffness Calculation

		Signal-to-Noise Ratio					Possible Error in Calculation (MPa)				
	Test Setup	TS-1		TS-2			TS-1		TS-2		
	Cyclic Stress (kPa)	93.1	300	93.1	137.9	300	93.1	300	93.1	137.9	300
Seating Stress (kPa)	20	21	68	31	47	87	624	186	382	258	136
	100	22	68	32	45	84	606	185	382	266	143
	180	21	67	32	46	85	606	188	380	267	144
	260	21	66	32	44	87	613	190	382	276	141
	340	21	67	30	40	89	604	189	414	306	138

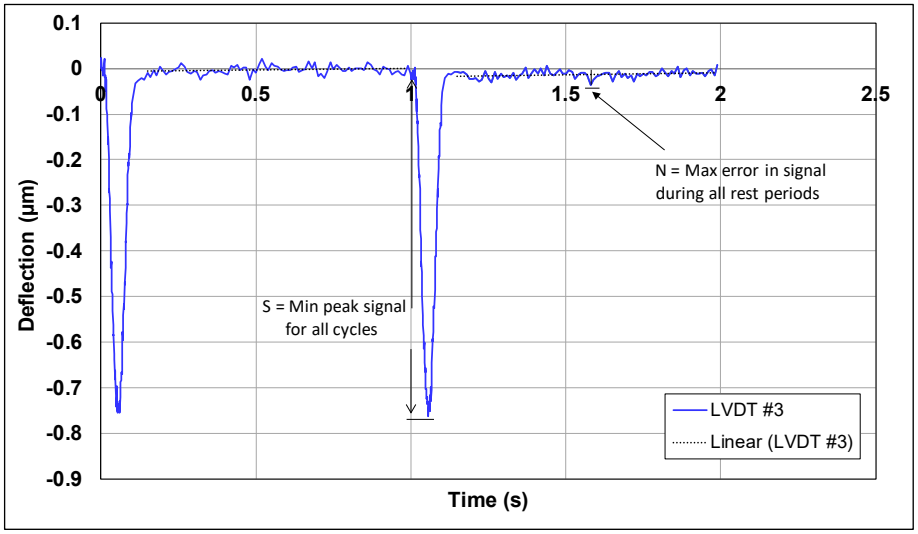

Figure 3.20: Schematic of SNR definition.

3.5 Discussion on a Feasible Test Setup

TS-1 and TS-2 both produced resilient modulus values on the same material within the expected range of backcalculated FWD stiffness. Both setups also produced results that conformed to the theory that cemented materials are not sensitive to stress changes until the cemented bonds break down *(23)*. TS-1 and TS-2 are also likely greater than the RVE due to the agreement between the results for the 19 mm (≈0.75 in.) nominal maximum aggregate size used in this study.

Potential limitations of TS-1 include the following:

- The SNR for low-stress testing was relatively low when testing stiff FDR-C specimens. The cyclic stresses used in AASHTO T 307 (maximum applied stress of 248.2 kPa) were within the lower range of vertical stresses expected in the field. Higher cyclic stresses will have a higher probability of inducing permanent damage (microcracking) during the test and will not be a measure of the material stiffness determined during a non-destructive test, but rather a destructive test similar to repeated load testing.
- The sensitivity of the LVDTs is a limiting factor. The deflection measured during testing with TS-1 with a cyclic stress of 93.1 kPa was approximately 0.3 µm. The calibrated measuring range of the LVDTs is ±0.1 mm. This testing therefore used less than 0.2% of the range of the LVDTs with signal noise at approximately 0.008% of that range. Other options for this test setup would be the use of strain gauges instead of LVDTs, but these would likely be affected by the RVE of the material and be subject to large variability given the nominal maximum aggregate size (i.e., 19 mm) used in this study.

Potential limitations of TS-2 include the following:

- The span of the ±0.25 mm LVDTs can be exceeded during microcracking and resilient modulus testing due to permanent deformation of the specimen caused by the high-stress microcracking sequences. This can lead to critical strain data not being recorded.
- The setup accommodates minor influences of the end effects caused by confinement from the loading platens. However, this effect is small compared to the results obtained for TS-3, TS-4, and TS-5.
- Test results also showed a slight stress sensitivity with increased seating stresses, but this was negligible compared to the magnitude of the average resilient modulus determined. This was confirmed by the consistency of the resilient moduli measured for each cyclic stress.

4 DEVELOPMENT OF A LABORATORY MICROCRACKING PROCEDURE

4.1 Introduction

Development of a laboratory procedure for inducing microcracking in cement-treated specimens was required for this phase of testing to provide a controlled method for reducing the stiffness of compacted specimens that would simulate the results from the FDR-C Test Road. The procedure needed to:

- Represent field conditions as closely as possible and induce microcracking within the cementitious bonds between the aggregates
- Induce microcracking to a controlled level (i.e., be able to control the level of stiffness reduction)
- Maintain specimen integrity for long-term testing
- Be highly repeatable, without complicated setup procedures
- Provide stress and strain results to determine the effort required to induce different levels of microcracking independent of the stress sequences

The procedure would be used to:

- Develop models for stiffness recovery after different levels of microcracking
- Induce microcracking in specimens for indirect tensile strength (ITS) and unconfined compressive strength (UCS) testing
- Develop a relationship between energy input and stiffness reduction in the laboratory to model the effect of roller passes on stiffness reduction in the field

Various procedures were considered, including using a handheld vibratory hammer drill, a vibrating table, and a small dual steel drum vibrating roller *(11)*. These methods were difficult to perform and difficult to control, and all of them damaged the specimen ends, which compromised the specimen for long-term testing. The level of microcracking (i.e., stiffness reduction) induced by these different microcracking procedures could not be readily quantified. Based on the findings of this initial research, use of a hydraulic load frame to induce and measure the level of microcracking through cyclic loading was explored.

The hydraulic load frame considered for this study was a universal testing machine (UTM) with a dynamic load range of up to 30 kN (UTM30) that could apply loads at frequencies of up to 70 Hz. The average 72-hour UCS of cement-treated specimens used in this part of the study, tested

according to ASTM D1633, was 3.75 MPa, which equates to approximately 30 kN of loading for a 100 mm (4 in.) diameter specimen.

The procedure applied the concept of using increasingly larger cyclic stresses to induce microcracks and ultimately fracture the specimen, similar to the submaximal modulus test used by Rashidi et al. *(18)*. This test characterizes the resilient modulus of cement-treated specimens at large strains. Cyclic stresses equivalent to 20%, 40%, and 60% of the UCS of the material are applied for 5,000 cycles at each load level to determine the resilient modulus of the material at different stress levels. The procedure developed for this study incorporated low-stress sequences after each microcracking sequence to accurately quantify the stiffness and the level of microcracking induced at a comparable stress state. This low-stress sequence was also used as the initial stress state to determine the resilient modulus prior to microcracking. This approach is similar to conducting stiffness testing during microcracking in the field, where soil stiffness gauge measurements are taken before and after each microcracking pass.

Confinement of the specimen was not considered in the procedure given that undamaged cement-treated material is typically not sensitive to confining stress. Using confinement in a triaxial cell on compacted bound and unbound aggregate specimens can increase the level of complexity of the test setup, primarily because the gauge points for the linear variable differential transformers (LVDTs) are covered by the confining membrane, which in turn affects the accuracy and sensitivity of the measurements.

Development of the UTM30-based microcracking procedure was conducted on specimens prepared with material sampled from the FDR Test Track.

4.2 Test Setup

The first round of tests used the test setup with LVDTs mounted at quarter points (TS-2 in Figure 3.6). This setup was chosen based on the higher signal-to-noise ratio (SNR) compared to LVDTs mounted at third points (TS-1). However, the span of the ±0.25 mm LVDTs was often exceeded during the test schedule due to permanent deformation of the specimen caused by the high-stress microcracking sequences, which resulted in some critical strain data not being recorded. TS-1 was therefore chosen for measuring strains during microcracking, as well as for monitoring stiffness change over time.

4.3 Load Pulse

The hardware and software of the UTM30 used only allows stress-controlled testing. A continuous haversine cyclic wave was considered for this study to simulate a vibratory roller.

The load pulse frequency was initially selected to model typical frequencies of vibratory rollers used for microcracking. However, initial tests performed at frequencies of 30 Hz proved to be unsafe because the specimen tended to resonate under the load and vibrate itself out of the center of the load path. This resulted in damage to the specimen and the potential for damage to the equipment.

Rashidi's submaximal modulus test used a frequency of only 3 Hz *(18)*. Yeo *(29)* used frequencies of 1 to 2 Hz for fatigue testing on treated materials, while Arnold et al. *(30)* did permanent deformation tests at up to 4 Hz. The test frequencies selected by these researchers were often a function of the expected test duration (Yeo increased the test frequency from 1 Hz to 2 Hz to reduce testing time). For this study, a frequency of 2 Hz was selected as it provided a reasonable test duration of up to one hour to achieve a stiffness reduction of 60%.

4.4 Stress Sequences

A deviatoric stress of 80 kPa, with a seating stress of 10 kPa, without confinement, was selected as the cyclic stress to determine the initial stiffness of the specimen and for measurement of stiffness after the microcracking sequences. This stress state is similar to what the FDR-C layer would be subjected to under typical traffic loads, and it also provided repeatable results after multiple sequences on a compacted specimen at 48 hours of curing. The degree of damage to the specimen from this stress state was negligible.

The microcracking stress sequences used during the study are provided in Table 4.1. The first sequence was used to condition the specimen and ensure good contact with the loading platens. This was followed by a measurement of the initial stiffness. The first two stiffness sequences after microcracking were for recovery from the high stresses after microcracking and the third was used to report the stiffness of the specimen. These sequences provided reasonable control over the rate of stiffness reduction. The UTM30 software did not provide an option to stop the test

after a certain stiffness reduction level was reached. This required monitoring the test and manually stopping when the desired level of stiffness reduction had been reached.

Table 4.1: Laboratory Microcracking Stress Sequences

Sequence	Deviatoric Stress (kPa)	Purpose	Sequence	Deviatoric Stress (kPa)	Purpose
1	80	Conditioning	18	80	Stiffness
2	80	Stiffness	19	1,500	Microcracking
3	160	Microcracking	20	80	Stiffness
4	80	Stiffness	21	80	Stiffness
5	80	Stiffness	22	80	Stiffness
6	80	Stiffness	23	1,880	Microcracking
7	480	Microcracking	24	80	Stiffness
8	80	Stiffness	25	80	Stiffness
9	80	Stiffness	26	80	Stiffness
10	80	Stiffness	27	2,260	Microcracking
11	800	Microcracking	28	80	Stiffness
12	80	Stiffness	29	80	Stiffness
13	80	Stiffness	30	80	Stiffness
14	80	Stiffness	31	2,580	Microcracking
15	1,120	Microcracking	32	80	Stiffness
16	80	Stiffness	33	80	Stiffness
17	80	Stiffness	34	80	Stiffness

The number of cycles in each sequence was set to 300. The equipment software, which was originally developed to perform repeated load testing, only allowed fixed cycle lengths for different sequences. A total of 300 cycles proved to be sufficient for determining the stiffness of the material at low cyclic stresses. The degree of damage at higher stresses after 300 cycles proved sufficient to produce a stiffness reduction curve with a manageable number of sequences. Fewer cycles per microcracking sequence would have required more sequences, and more cycles would have risked inducing too much damage and exceeding the desired stiffness reduction during microcracking before the damage level could be determined with a stiffness sequence.

4.5 Stiffness Determination

Equation 4.1 was used to determine the stiffness. This equation assumes a linear-elastic material response to cyclic loading, as shown in the linear backbone of the stress-strain curve (Figure 4.1 and Figure 4.2), and that induced strain is practically all recoverable. Equation 4.1 calculates the secant stiffness of the material shown in Figure 4.2.

$$M_R = \frac{\sigma_d}{\varepsilon_r} \quad \textbf{(4.1)}$$

Where: M_R = Stiffness (MPa)

σ_d = Deviatoric stress (MPa)

ε_r = Recoverable strain

4.6 Assessment of End-Effects at Large Strains

The material stress-strain response curves to the increasing microcracking stresses are shown in Figure 4.3. The subsequent stiffness sequence tests to measure the induced damage are provided in Figure 4.4 and show the cyclic stress-strain at 300 cycles. The microcracking sequence curves do not follow the assumptions of linearity, but instead have a similar nonlinear shape compared to the shapes recorded with the longer gauge-length setups (i.e., TS-3, TS-4, and TS-5) discussed in Section 3.3. This was attributed to the influence of the confinement of the end caps and the non-uniform strain distribution over the measured area at increasingly higher stresses. Stiffness under large strains cannot be calculated using Equation 4.1 since the backbone of the stress-strain curve (i.e., the slope of the stress-strain curve which represents the secant stiffness) is not linear. This supported the decision to include the low-stress stiffness sequences after the microcracking sequences.

4.7 Assessment of Preliminary Stiffness Reduction Results

The typical stiffness reduction profile during microcracking is shown in Figure 4.5. The initial conditioning and stiffness sequences were relatively stable but indicated some noise. The last 50 cycles of stiffness sequence number two were used to represent the initial stiffness of the specimen. Subsequent stiffness sequences, before the microcracking sequences, were used to indicate the level of damage induced during the previous microcracking sequence. The stiffness typically decreased significantly after the second microcracking sequence. The rate of stiffness reduction, considering the stiffness sequences, reduced with subsequent microcracking sequences.

The initial stiffness recorded during the first conditioning sequence after the first microcracking sequences was similar to the stiffness at the end of the microcracking sequence. The difference between the stiffness at the end of a microcracking sequence and the stiffness at the start of the conditioning sequence increased with subsequent microcracking sequences. There was also an increase in stiffness after the microcracking sequences.

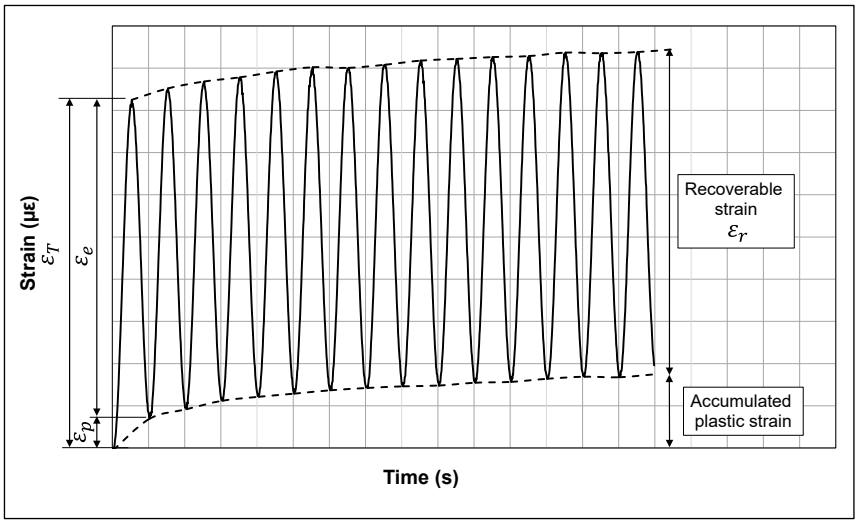

Figure 4.1: Strain response under cyclic loading.

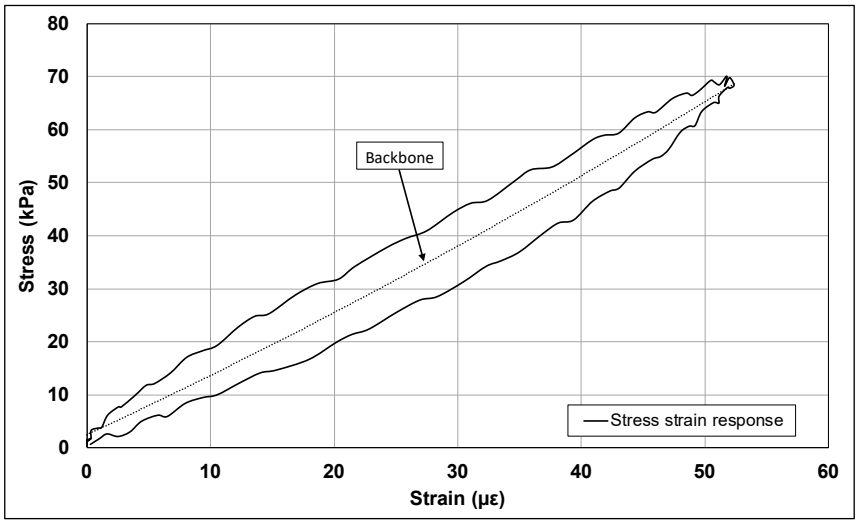

Figure 4.2: Stiffness represented by the linear backbone of the stress-strain curve.

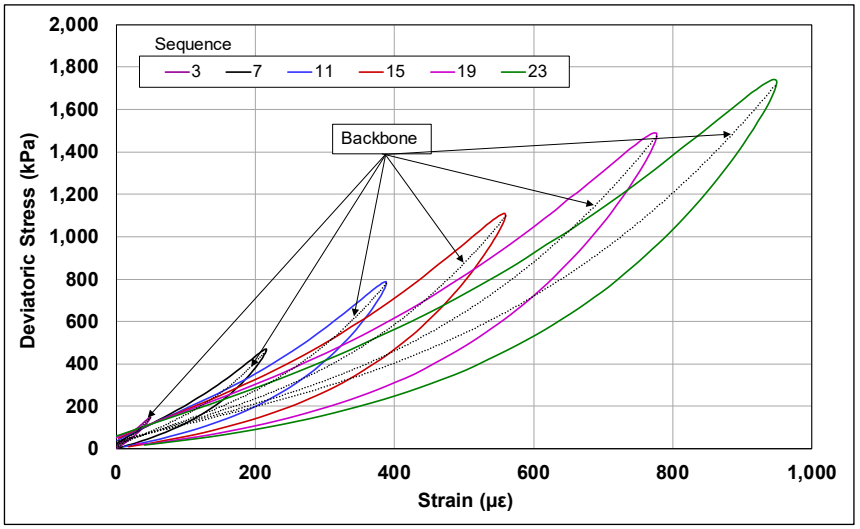

Figure 4.3: Microcracking sequences for stress-strain response curves.

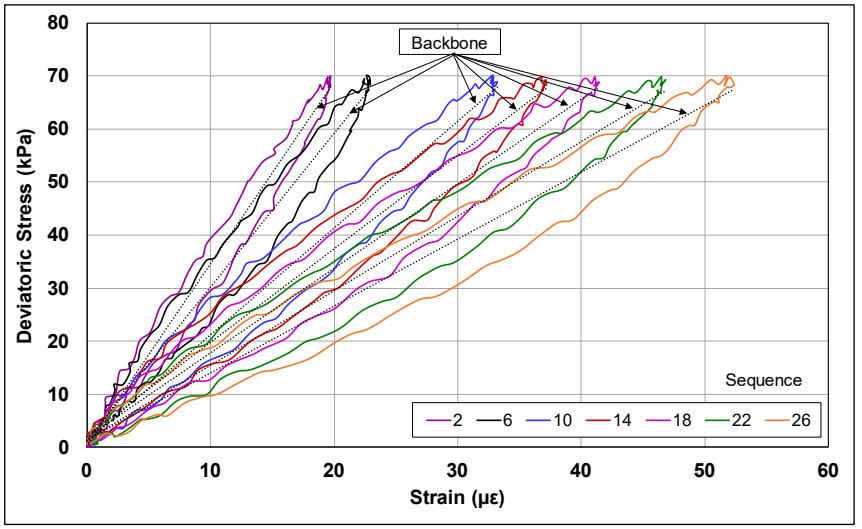

Figure 4.4: Stiffness sequences for material stress-strain response curves.

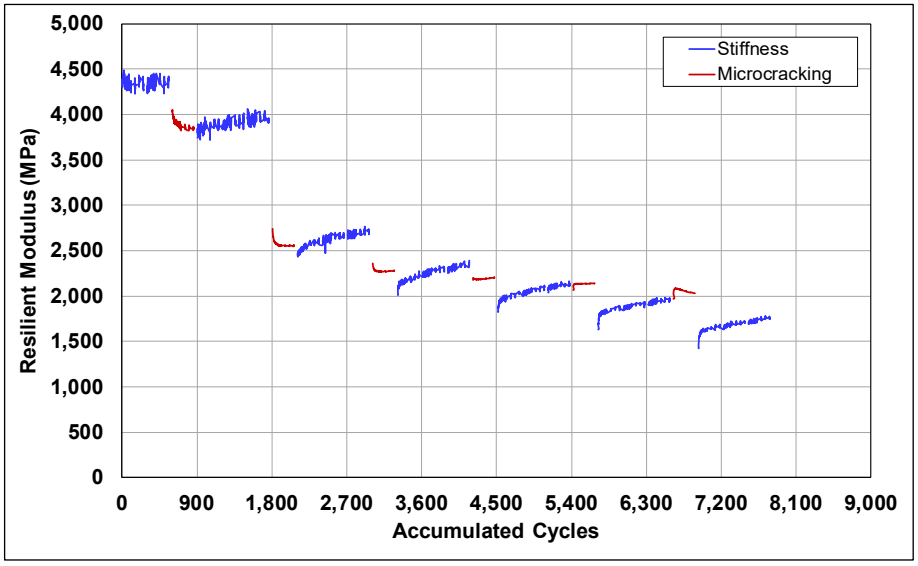

Figure 4.5: Stiffness reduction pattern during microcracking with proposed loading sequence.

The stiffness reduction curve in Figure 4.5 showed several characteristics requiring further investigation for validating the test method, including the following:

- Significant differences in the stiffness measured during the microcracking sequences compared to the stiffness sequences
- Rapid recovery of stiffness after microcracking
- Continued cement hydration during the test

4.7.1 Difference in Stiffness Between Microcracking and Stiffness Sequences

The difference in stiffness between the last 50 cycles of the microcracking sequence and the start of the stiffness sequences are shown in Figure 4.6, normalized to the initial stiffness prior to microcracking. Both the stiffness and the microcracking patterns indicate a reduction in stiffness initially due to microcracking, with the rate of reduction decreasing with later microcracking sequences. This eventually resulted in the stiffness measured during high-stress microcracking exceeding the stiffness measured during the low-stress stiffness sequence.

4.7.2 Stiffness Recovery After Microcracking

Stiffness recovery after the microcracking sequences was attributed to the creep characteristics of the material. The permanent deformation response of the microcracking test shown in Figure 4.5 is provided in Figure 4.7. These responses after microcracking show that the specimen had viscoelastic characteristics, attributed to the recycled asphalt in the specimen. A sudden elastic recovery was evident when the load was reduced after the microcracking sequences, and

creep recovery was evident during the first two stiffness sequences. The third stiffness sequence was not significantly affected by creep recovery.

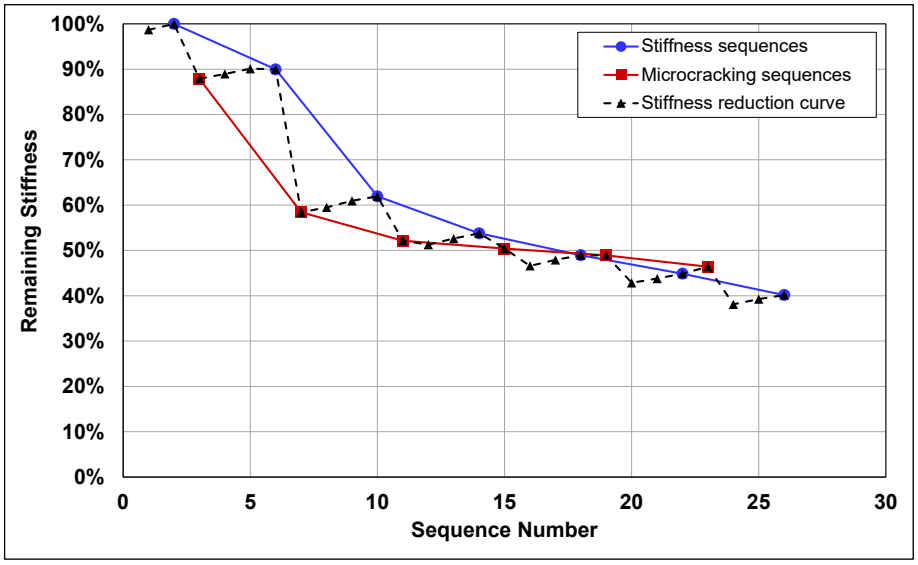

Figure 4.6: Comparison of stiffness measured during microcracking and stiffness sequences.

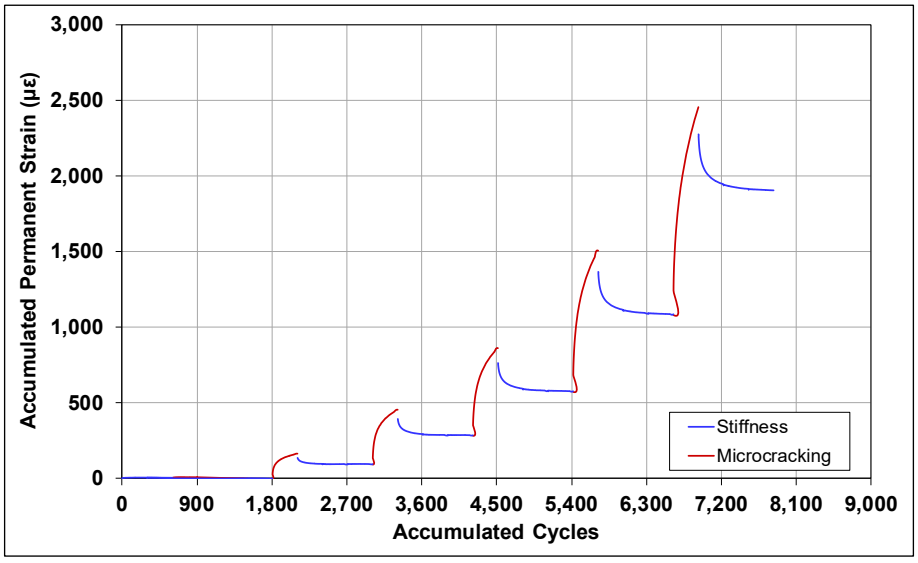

Figure 4.7: Permanent deformation pattern during microcracking with loading sequence.

4.7.3 Cement Hydration During Testing

Another factor that could contribute to the increase in stiffness during the microcracking test is continuing cement hydration. Microcracking was typically performed between 48 and 72 hours after compaction, in line with field practice. This is relatively early in the cement hydration cycle, during which hydration is still occurring at a rapid rate. The stiffness recovery curve over the first seven days, for the specimen microcracked as shown in Figure 4.5, is provided in Figure 4.8. This

specimen was tested for stiffness at 7, 24, and 48 hours, and microcracked at 72 hours, followed by further stiffness measurements at 78, 96, 120, 148, and 168 hours. Stiffness was reduced by approximately 60% during microcracking (4,360 to 1,760 MPa). The stiffness recovered by 480 MPa in the first six hours after microcracking. A point of interest in Figure 4.8 is the change in the rate of stiffness recovery after microcracking. The rate of stiffness increased significantly in the first 24 hours after microcracking and then slowed. Although the exact reason for this is not known, autogenous healing of the cemented bonds is a likely cause.

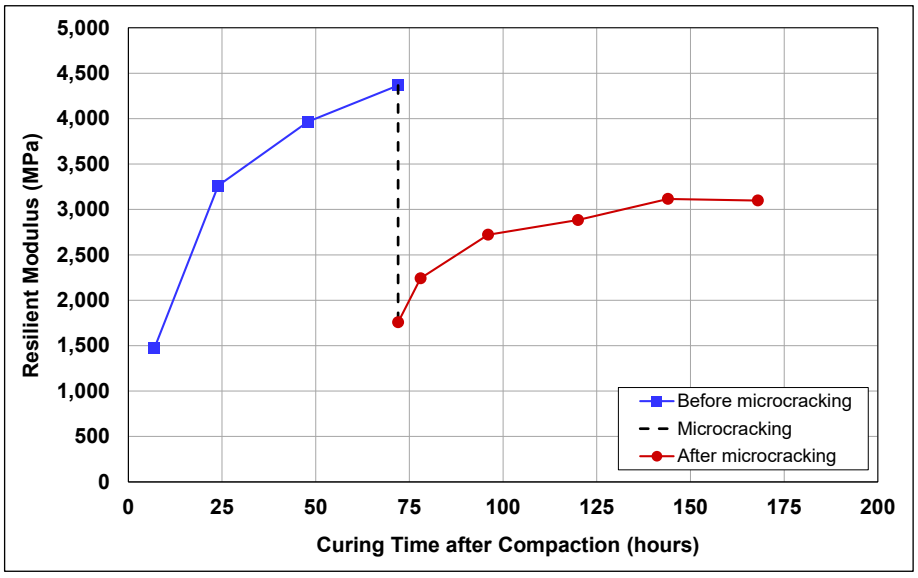

Figure 4.8: Cement hydration with microcracking.

4.8 Assessment of Curing During Testing

To investigate the effect of curing during the microcracking procedure, a specimen was prepared with 2.5% cement, compacted to field density, and sealed with wax. The specimen was cured for 48 hours at 25°C (77°F) and then tested with TS-1 using a repeated load cyclic test in the UTM30 at a constant temperature of 25°C. The test used a haversine wave, with a deviatoric stress of 80 kPa, a seating stress of 10 kPa, and a loading frequency of 2 Hz. A total of 150,000 cycles were applied. The test was run twice, once at 48 hours and once at 69 hours. The results are plotted in Figure 4.9.

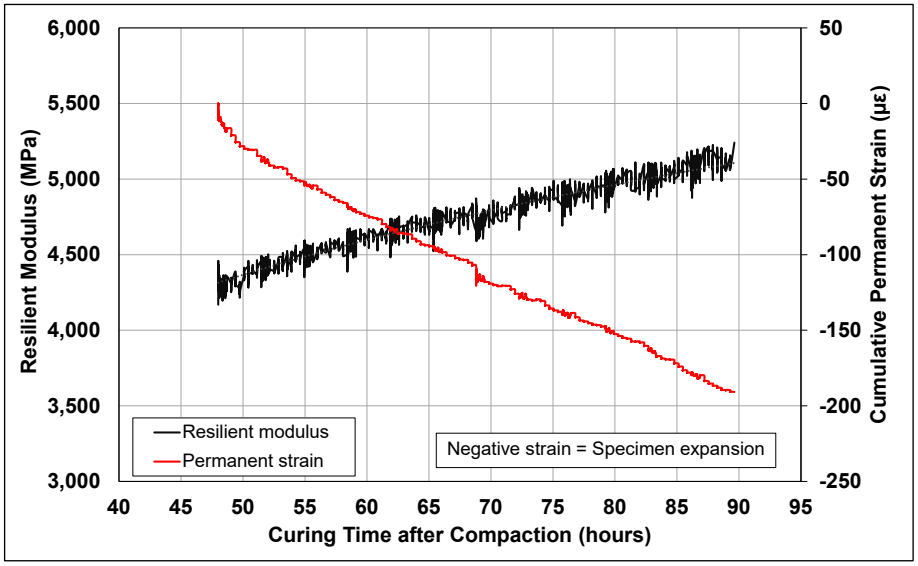

Figure 4.9: Repeated load test to measure cement hydration under load.

Figure 4.9 shows that hydration continued under the stress state used for measuring stiffness, and that stiffness continued to increase under the 80 kPa cyclic deviatoric stress. The reduction in cumulative permanent strain (i.e., expansion of the specimen) was attributed to the specimen preparation procedure, in which the wax-sealed specimen did not dry back or shrink, and to the presence of ettringite, which forms during cement hydration *(31)*.

4.9 Assessment of Creep Relaxation During Microcracking

The effects of stiffness recovery after the microcracking sequences were investigated to determine the mechanism behind the observed trends in the microcracking test data and to choose an appropriate stiffness test cycle that minimized the effect of creep on stiffness measurements. Creep tests were performed in the UTM30, using the same test setup that was used for the stiffness testing. Temperature in the environmental control chamber was maintained at 25°C (77°F) for the tests.

Two creep tests were performed on two 2.5% cement-content specimens. The first specimen was tested after 96 hours, and the second after 1,464 hours (58 days). Load sequences and results are plotted in Figure 4.10. Each load was applied for 300 seconds.

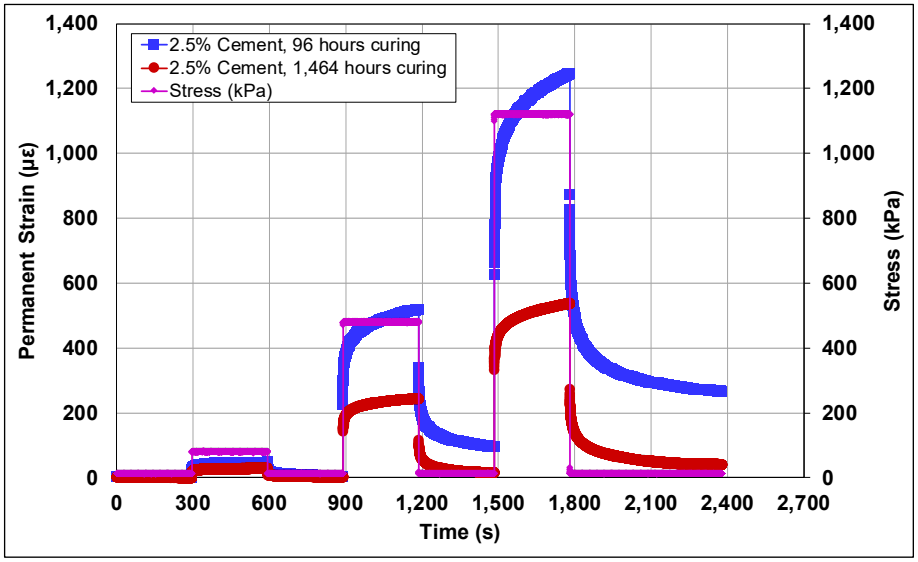

Figure 4.10: Viscoelastic creep tests after 96 and 1,464 hours.

A sudden increase in strain occurred when the load was applied, followed by creep under the sustained loads. With the load removed, the material had a partial elastic recovery, followed by creep recovery with time. The effect of curing time had a significant effect on the creep response of the material. The results show that the FDR-C material had viscoelastic properties, which supports the recommendation that stiffness of specimens should be determined near or after complete relaxation to exclude the relaxation effects, as shown in Table 4.1.

4.10 Assessment of Stiffness Reduction with Total Energy

The total energy per unit volume was considered a parameter to correlate the energy applied by the vibratory roller, per pass, to the reduction in stiffness measured in the laboratory. The total energy was also used to determine the sensitivity of the stiffness reduction curve to different loading sequences. Total energy was calculated as the area under the stress-strain curve (Figure 4.11).

Microcracking tests were performed on eight 2.5% cement-content specimens compacted to field density. These specimens were microcracked using four different microcracking sequences (Figure 4.12), where the stresses applied in the microcracking stress sequences (Table 4.1) were randomized. The stiffness results for these microcracking tests are plotted in Figure 4.13. The stiffness results were normalized to the stiffness before microcracking for each specimen and are plotted against total energy in Figure 4.14.

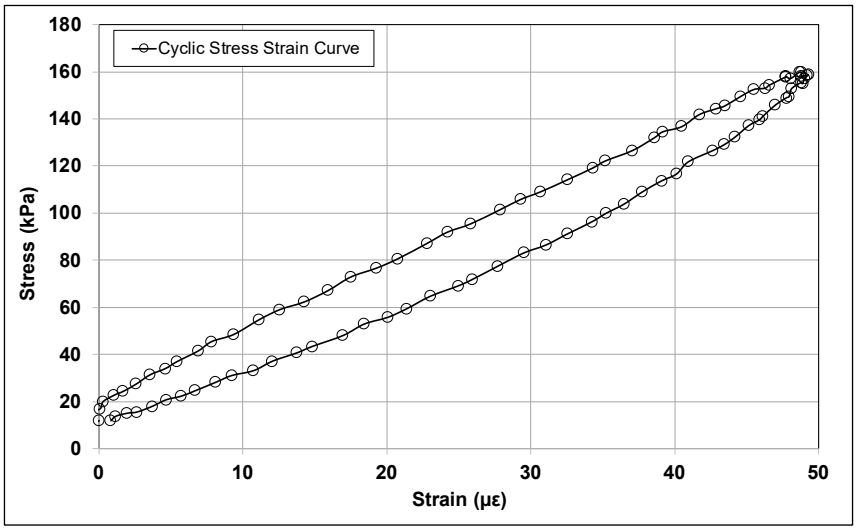

Figure 4.11: Typical stress versus strain curve using TS-1.

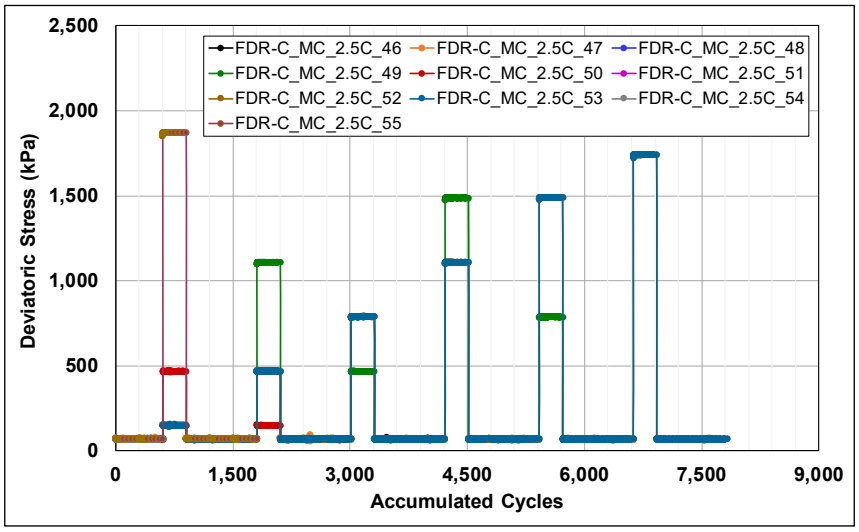

Figure 4.12: Random deviatoric stress sequences.

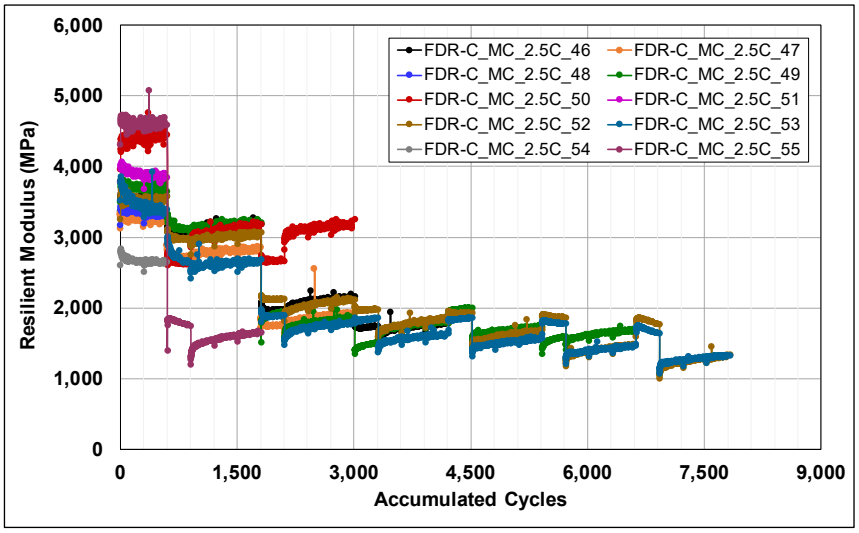

Figure 4.13: Microcracking results with random stress sequences.

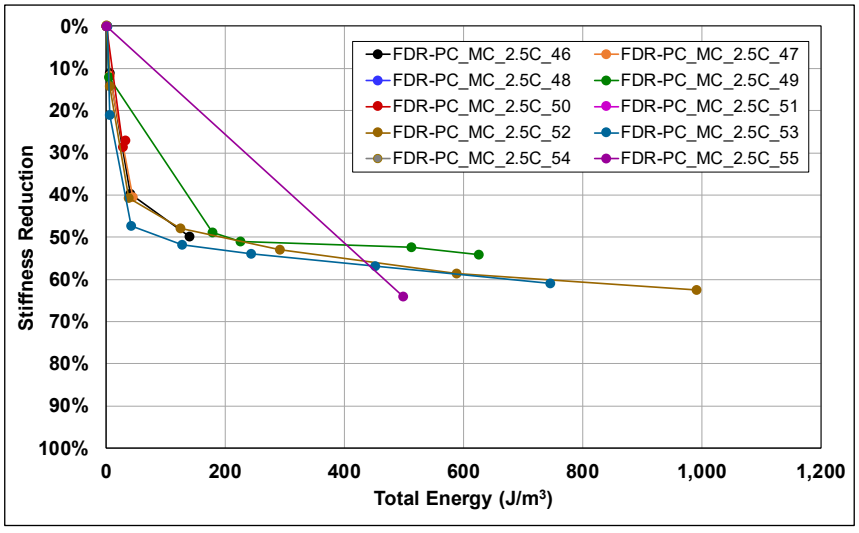

Figure 4.14: Normalized stiffness results versus energy input.

Figure 4.15 shows that the stiffness reduction reduced log-linearly with total energy and that the relationship was not influenced by the sequence in which the stress was applied.

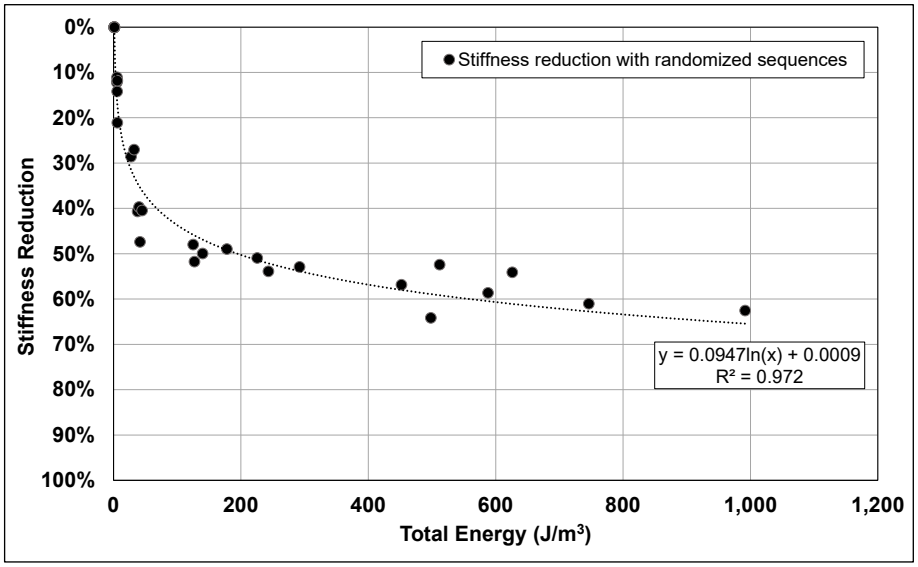

Figure 4.15: Relationship between stiffness reduction and total energy.

4.11 Final Laboratory Microcracking Method

The microcracking method used for all further testing in this study is outlined in the following discusion. Specimens were prepared following the procedure described in Section 3.2.

4.11.1 Test Setup

The TS-1 test setup, with LVDTs mounted at third points on the specimen was adopted to minimize test reset and the risk of exceeding the LVDT range. High accuracy LVDTs with a span of ±0.1 mm were used for stiffness testing and for microcracking to small stiffness reductions (i.e., <40%), while LVDTs with longer spans of ±0.25 mm were used for microcracking to levels exceeding 40% stiffness reduction.

4.11.2 Load Shape

The test was stress controlled. A cyclic haversine load shape with a frequency of 2 Hz was used for all stiffness and microcracking tests.

4.11.3 Stress Levels

The microcracking stress levels and sequences listed in Table 4.1 were used for all testing. Test sequence 1 was the conditioning sequence, and test sequence 2 was a stiffness sequence. Each

microcracking sequence was followed by two conditioning sequences and a stiffness sequence. Each sequence consisted of 300 cycles.

4.11.4 Performing the Test

Custom software developed for the UTM30 was used to run the tests and record the data. All tests were continuously monitored given that the software could not be programmed to stop the test once a certain percentage of stiffness reduction had been reached. Once the required percentage of stiffness reduction was reached, the test was manually stopped at the end of that stiffness testing sequence.

5 LABORATORY TESTING EXPERIMENTAL PLAN

5.1 Scope of Testing

The goal of the laboratory testing discussed in this phase of the study was to determine the effect of microcracking on strength and stiffness of FDR-C layers in a controlled (temperature and humidity) environment. The testing program focused on inducing controlled levels of stiffness-reduction damage, using the procedures discussed in Chapter 3 and Chapter 4, to simulate the effects of microcracking on specimens prepared with material sampled from the FDR-C Test Road prior to recycling. Tests included changes in stiffness, indirect tensile strength (ITS), unconfined compressive strength (UCS), and free-drying shrinkage tests. Additional strength and stiffness tests were performed to develop models that can estimate to what extent microcracking induces damage. Test results are discussed in Chapter 6.

Test results were loaded into a database for further analysis in conjunction with field-collected data from the FDR-C Test Road to develop performance models for microcracked FDR-C layers (discussed in Chapter 7 and Chapter 8). The following material parameters were assessed:

- Stiffness increase with time, with results used to develop hydration models for the materials used on the FDR-C Test Road: The effect of microcracking to reduce the stiffness to different levels, and after two different curing times, was also assessed.
- ITS with different microcracking levels: These tests were performed on specimens after stiffness testing to develop a relationship between ITS and stiffness. Specimens subjected to different levels of microcracking were tested for stiffness before testing their ITS. This data was used to develop models for ITS as a function of stiffness with different microcracking levels, to determine the fatigue life of FDR-C layers with microcracking using existing models, and to support input used in determining microcracking mechanisms.
- UCS increases with time: These tests were performed on both cement contents used on the FDR-C Test Road to determine the stress/strength load levels used during microcracking.
- UCS with different microcracking levels: These tests were conducted to collect data for modeling microcracking mechanisms.
- Free-drying shrinkage tests with time: These tests were conducted to collect data for developing a preliminary model for the material treated with different cement contents to model shrinkage in the pavement.

5.2 Experimental Factors

The experimental setups for the stiffness, strength, and shrinkage testing are provided in the following sections. Both short- and long-term tests were performed for strength testing. Short-term tests were performed within three days after specimen preparation, while longer-term testing was conducted 56 days after specimen preparation. Three days was selected because it match the time of microcracking, and it is also a commonly used testing interval. Although peak stiffness was expected around 28 days, 56 days was selected for the longer-term test to ensure that a representative long-term values was used in the modeling.

Target stiffness reductions for laboratory microcracking were selected to represent those measured on the FDR-C Test Road *(12)*, summarized in Table 5.1. Table 5.2 compares the laboratory and FDR-C Test Road factorials.

Table 5.1: Average Stiffness Reduction During Microcracking on the FDR-C Test Road

Cement Content (%)	Roller Type	Microcracking Pass	Microcracking Time (hours)	Stiffness Reduction (%)
2.5	12-ton SSR High vibration amplitude 1.42 kN/cm applied energy	1	48	19
		1	72	17
		2	48	33
		2	72	31
		3	48	47
		3	72	45
4.0	12-ton SSR High vibration amplitude 1.42 kN/cm applied energy	1	48	16
		1	72	14
		2	48	30
		2	72	28
		3	48	44
		3	72	42

Table 5.2: Laboratory Stiffness Reduction Factorial

Microcracking Time (hours)	Laboratory Factorial (% Reduction)	Matching FDR-C Test Road Factorial
N/A	Control	Control
48	20	1 pass with SSR at high vibration amplitude
	40	3 passes with SSR at high vibration amplitude
	60	None
72	20	1 pass with SSR at high vibration amplitude
	40	3 passes with SSR at high vibration amplitude
	60	None
48 and 72	60 on both days	Microcracking after both days

5.2.1 Stiffness Testing with Microcracking

The experimental factors for long-term stiffness monitoring tests are provided in Table 5.3 and included the following parameters:

- Cement contents: 2.5% and 4%
- Microcracking levels: 0% (control), 20%, 40%, and 60% stiffness reduction
- Microcracking intervals: 0 (controls), 48, and 72 hours after compaction
- Number of specimens: Three replicates for each combination of cement content, microcracking level, and microcracking interval
- Testing intervals (Table 5.4): An additional stiffness test was performed approximately four to eight hours after microcracking

Table 5.3: Experimental Plan for Long-Term Stiffness Testing with Microcracking

Test Parameter	Cement Contents	Microcracking Levels	Microcracking Intervals	Number of Specimens	Testing Intervals
Long-term stiffness with microcracking[a]	2	4	3	3	13
ITS testing after long-term tests	N/A	N/A	N/A	N/A	1

[a] Non-destructive test. Specimens were used for ITS test after stiffness testing.

Table 5.4: Testing Intervals for Assessing Stiffness Increase

Testing Intervals														
	Hours	7	24	48	72	96	120	144	168	336	504	672	1,176	1,344
	Days	-	1	2	3	4	5	6	7	14	21	28	49	56

5.2.2 Long-Term Indirect Tensile Strength Tests

The long-term stiffness monitoring specimens were tested for ITS after the last stiffness testing period, shown in Table 5.4.

5.2.3 Short-Term Indirect Tensile Strength Tests

The experimental factors for short-term ITS testing are provided in Table 5.5 and included the following parameters (stiffness tests were carried out on each specimen prior to ITS testing):

- Cement content: 2.5%
- Microcracking levels: 0% (controls), 20%, and 60% stiffness reduction
- Microcracking intervals: 0 (controls), 48, and 72 hours after compaction
- Number of specimens: Three replicates for each combination of cement content, microcracking level, and microcracking interval
- Testing intervals: 48 and 72 hours

Table 5.5: Experimental Plan for Short-Term ITS Testing

Test Parameter	Cement Contents	Microcracking Levels	Microcracking Intervals	Number of Specimens	Testing Intervals
Stiffness with microcracking for ITS[a]	1	3	3	3	2
ITS after long-term stiffness testing	N/A	N/A	N/A	N/A	1

[a] Non-destructive test. Specimens were used for ITS test after stiffness testing.

5.2.4 Short-Term Unconfined Compressive Strength Tests

The experimental factors for short-term UCS testing are provided in Table 5.6 and include the following parameters (stiffness tests were carried out on each specimen prior to UCS testing):

- Cement content: 2.5% and 4% for the UCS increase with time, and 2.5% for simulating the 2.5% cement-content FDR-C Test Road design
- Microcracking levels: 0% (controls), 20%, and 60% stiffness reduction
- Microcracking intervals: 0 (controls), 48, and 72 hours after compaction
- Number of specimens: Three replicates for each combination of cement content, microcracking level, and microcracking interval

Table 5.6: Experimental Plan for UCS Testing

Test Parameter	Cement Contents	Microcracking Levels	Microcracking Intervals	Number of Specimens	Testing Intervals
UCS increase with time (ASTM D1633)	2	0	0	9	3
Stiffness with microcracking for UCS[a]	1	3	3	3	1
UCS with microcracking	N/A	N/A	N/A	N/A	1

[a] Non-destructive test. Specimens were used for UCS test after stiffness testing.

5.2.5 Shrinkage Tests

The experimental factors for free-drying shrinkage testing are provided in Table 5.7 and included the following parameters:

- Cement content: 2.5% and 4%.
- Curing: Specimens were left unsealed and placed in a temperature-controlled chamber set to 25°C (77°F).
- Humidity: The chamber was set to a constant relative humidity of 80%.
- Shrinkage data was collected continuously over a period of 30 days.

Table 5.7: Experimental Plan for Free-Drying Shrinkage Testing

Test Parameter	Cement Contents	Microcracking Levels	Microcracking Intervals	Number of Specimens	Testing Intervals
Drying shrinkage	2	0	0	4	Continuous

5.3 Material Sampling

Recycled asphalt pavement (RAP) and subgrade materials used for laboratory testing were collected during construction of the FDR-C Test Road discussed in the Phase 2a report *(12)*. All materials were dried, quartered, and then blended to a ratio of 80% RAP to 20% subgrade material to simulate the composition of the recycled layer on the road. Sieve analysis (AASHTO T11 and T 27) results of the blended material are plotted in Figure 5.1.

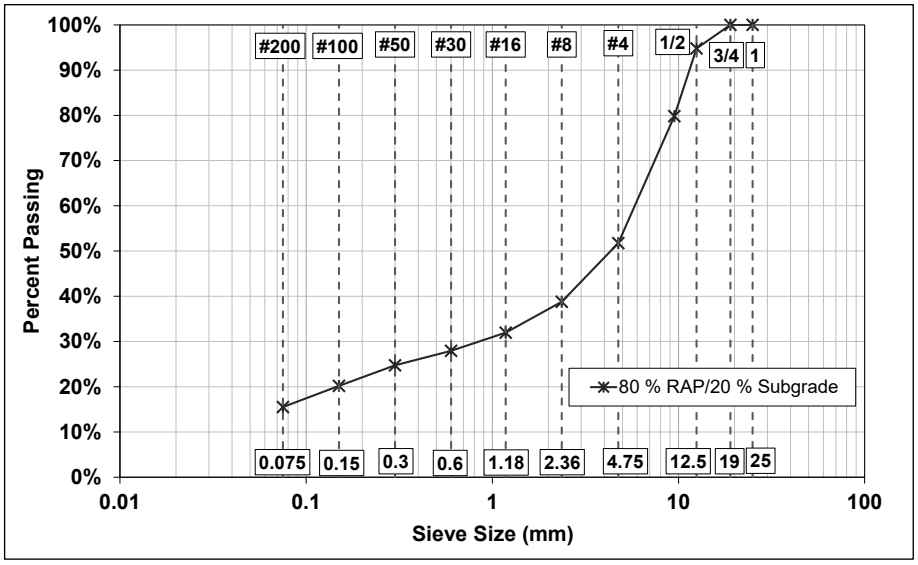

Figure 5.1: Grading envelope for 80% RAP:20% subgrade blend.

Atterberg limit (AASHTO T 89) tests indicated the following:

- The RAP was non-plastic.
- The subgrade material had a plasticity index of 18 and was classified (ASTM D2487) as lean clay.
- The combined material had a plasticity index of 13 and was classified as a clayey gravel.

The optimum compaction moisture content of the 80:20 blend was 4.9% with a maximum dry density of 2,217 kg/m^3 (138.4 lb./ft^3), determined with modified Proctor effort (AASHTO T 180). The as-built dry density on the FDR-C Test Road was 2,036 kg/m^3 (127.1 lb./ft^3), equal to 92% of the laboratory determined density. This field density was used as the target density for preparing laboratory specimens.

5.4 Specimen Preparation

5.4.1 Specimen Compaction

Specimens were compacted to the average density and moisture content determined during construction of the FDR-C Test Road. The manual vibratory compaction method listed in AASHTO T 307 was used in initial studies *(11)*, but it was found to be operator dependent and did not provide a satisfactory means of controlling the density of the specimens. After some experimentation with different methods, a computer controlled vibrating hammer was selected as the most appropriate compaction method for this phase of the study (Figure 5.2).

Figure 5.2: Vibrating hammer used for specimen compaction.

This vibratory compactor can control the density of the specimen based on user input, which includes the number of lifts required to compact the specimen. The user adds the material required for each lift to achieve the desired wet density, with the number of lifts dependent on specimen height. Lift height is measured/controlled by the compactor with a string potentiometer.

The 100 mm (≈4 in.) diameter specimens were compacted in different numbers of lifts depending on the height of the specimen. Five lifts were used for the 200 mm (≈8 in.) high stiffness and microcracking specimens, and three lifts were used for the 116 mm (≈4.6 in.) high UCS specimens.

Specimens were compacted in batches, with three 200×100 mm (≈8×4 in.) specimens or six 116×100 mm (≈4.6×4 in.) specimens compacted in each batch. Material (blended aggregate, cement, and water) for each batch was mixed in a paddle mixer (Figure 5.3) for three minutes. A representative scoop of material was taken, adjusted to the mass required per lift, and deposited in the mold. The material was compacted to the lift height, and then vigorously scoured afterwards to ensure good bonding between lifts. This sequence was continued for each lift.

A moisture content sample was taken during the compaction of the middle lift of each specimen. The production of specimens with large aggregates (i.e., passing a 0.75 in. [19 mm] sieve) typically results in variability between replicate specimens in terms of grading, moisture content, cement content, and compacted density. Following a sequential method using a mixed batch of material, with a user attempting to scoop representative material from the batch without remixing in between scoops, has the potential for segregation and a loss in moisture over time. Attempts were made to mitigate these problems by continually mixing the material, covering the bowl containing the material with a damp cloth, recording the compaction moisture for each specimen, and considering the variability during analysis of the results.

All compacted specimens were capped with gypsum (Figure 5.4) to ensure optimal platen contact during testing. Although the specimen-end finish was a significant improvement over that achieved following the AASHTO T 307 compaction method, which often results in a rough, irregular finish (the consequences of this are discussed in Section 3.2), the practice of adding the caps was continued to protect the brittle ends from damage during repeated handling and testing.

5.4.2 Specimen Curing

Compacted specimens were sealed in wax and cured at a constant temperature of 25°C (77°F). This helped to limit uncontrolled specimen variability over time. Figure 5.5 shows a capped and wax-sealed specimen. The wax at the ends of the specimen was removed before testing. After testing, the caps were sealed with plastic wrap and the edges taped, to prevent any moisture loss. Initial testing indicated that the cement-treated material continued to hydrate during this curing state and that specimens showed an increase in stiffness over time.

Figure 5.3: Paddle mixer used to mix material, cement, and water.

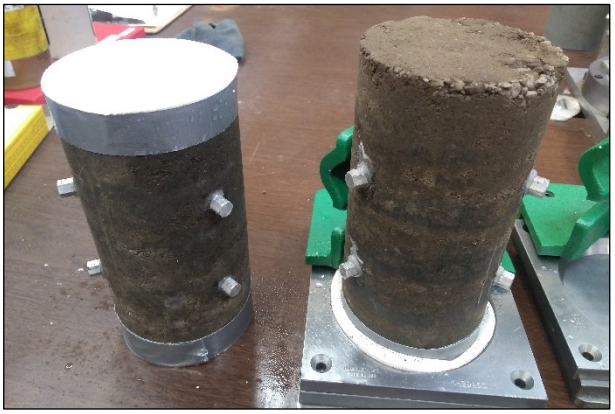

Figure 5.4: Compacted specimen being capped with gypsum.

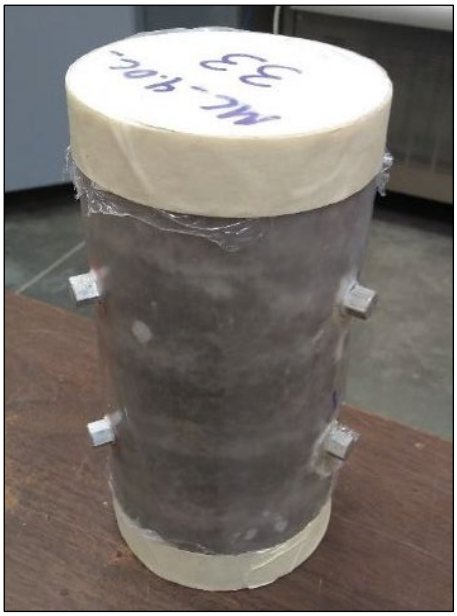

Figure 5.5: Wax-sealed specimen.

The authors recognize that this curing procedure does not represent field conditions (temperatures in the recycled layer on the FDR-C Test Road varied by up to 20°C [36°F] on any one day and ranged between 5°C and 50°C [41°F and 122°F] seasonally), but this setting was chosen to minimize the number of uncontrolled variables considered. The reasons for not curing the specimens in the more traditional 100% relative humidity environment include the following:

- Wet conditions soften the epoxy that attaches the LVDT gauge points to the specimen. Curing in moist conditions would require reapplication of the gauge points and risk exposing the specimen to a drying cycle.

- Testing specimens can take up to one hour in a dry temperature-controlled chamber. Without being sealed during the test, the specimens could dry out and potentially carbonate, which would jeopardize future testing on the specimen.
- Gypsum is soluble in water. Previous experience with using a moisture conditioning chamber showed that the specimen faces with gypsum caps would become irregular and require recapping before every test.

5.4.3 Indirect Tensile Strength Specimens

The laboratory microcracking method discussed in Chapter 4 was developed for larger specimens (i.e., 200×100 mm and 300×150 mm [≈8×4 in. and 12×6 in.]). Microcracking standard ITS specimens, which are 65 mm high and 100 mm in diameter (≈2.56×4 in.) is not possible because they do not meet the 2:1 height-to-diameter ratio required for axial stiffness tests. The method was therefore refined for ITS specimens as follows:

- Compact, cure, and microcrack larger 200×100 mm specimens as described in Sections 5.4.1 and 5.4.2.
- After microcracking, strip the wax and studs and then dry-cut the specimens to the required size using a concrete cut-off saw with compressed air-cooling.
- Conduct ITS tests on the cut specimens.
- Determine specimen moisture contents on the remains of the specimen by weighing before and after oven-drying at 60°C (140°F).

Following this method did cause some edge damage on some microcracked specimens (Figure 5.6 and Figure 5.7) and the authors acknowledge that the ITS results may have been influenced on these damaged specimens. This was considered in the analysis of the results. Damage after dry cutting was more noticeable on specimens that were:

- Microcracked at 48 hours compared to those microcracked at 72 hours, likely due to the lower strength/stiffness of the material
- Microcracked to 40% of the initial stiffness compared to those microcracked to 20% of the initial stiffness

5.4.4 Unconfined Compressive Strength Specimens

Specimens with two different sizes were prepared for UCS testing. The first set were 200×100 mm (8×4 in.) stiffness specimens that were prepared in the same way as other stiffness specimens and microcracked prior to UCS testing. The wax and gypsum cap were not removed prior to UCS testing.

Figure 5.6: ITS specimen with no damage after cutting.

Figure 5.7: ITS specimen with edge damage after cutting.

The second set were 116×100 mm (4.57×4 in.) compacted according to ASTM D1557. These were not capped since they required minimal handling over their life and there was little risk in damaging the integrity of the faces. The specimens were wrapped in at least four layers of plastic wrap, with a minimum layer thickness of 0.1 mm (4 mil) and cured in a conditioning chamber set at 25°C (77°F).

The internal moisture content of all UCS specimens was determined after testing by taking a 500 g sample and weighing it before and after drying to constant mass at 60°C (140°F).

5.4.5 Free-Drying Shrinkage

Specimens for free-drying shrinkage tests were compacted following the method described in Section 5.4.1. The specimens were not sealed. Shrinkage tests were performed using an aluminum jig designed to serve both as a stable platform for the specimen for the duration of the test and to hold an LVDT over the center of the specimen (Figure 5.8). An aluminum disc was glued to the surface of the specimen to provide a stable contact for LVDT-measured strains. Free-drying shrinkage tests were performed in an environmental chamber maintained at 25°C and 80% relative humidity. Shrinkage measured by the LVDTs was continuously recorded by a datalogger.

Figure 5.8: Free-drying shrinkage test setup.

6 LABORATORY TEST RESULTS

6.1 Introduction

First-level analysis results from the various tests are discussed in this chapter. Detailed analyses and modeling are discussed in Chapter 7 and Chapter 8.

6.2 Stiffness Reduction During Microcracking

Microcracking was performed on the specimens at the intervals outlined in Table 5.3. The loading sequences used for microcracking are provided in Table 4.1. The control specimens were subjected to stiffness tests at each interval (sequences one and two). Microcracked specimens were subjected to an additional stiffness test approximately six hours after microcracking to capture the rapid recovery of stiffness. This interval is not listed in Table 4.1 since it varied between four and eight hours and was dependent on the number of tests conducted on the days that microcracking was scheduled.

Stiffness reduction, with total energy results, for both 2.5% and 4% cement-content specimens are provided in Appendix A for the different microcracking efforts. Results are summarized in Figure 6.1. The stiffnesses in the figure were normalized to the initial stiffness before microcracking. Observations from this testing include the following:

- The stiffness reduction for the 4% cement-content cases was lower than the 2.5% cement-content cases.
- Stiffnesses reduced log-linearly with total energy for all cases, except for the 2.5% cement-content specimens microcracked at 48 hours and again at 72 hours. These specimens appear to have regained stiffness after the first round of microcracking at 48 hours.
- The reduction in stiffness with increased energy input was consistent for all cases except for the 2.5% cement-content microcracked at 48 hours and again at 72 hours.
- There was no difference in the stiffness reduction for the 2.5% cement-content cases microcracked at 48 hours or at 72 hours.
- The 4% cement-content specimens microcracked at 72 hours had a lower stiffness reduction compared to the specimens with 4% cement microcracked at 48 hours.
- The stiffness reduction for the 4% cement-content specimens microcracked at 48 hours and again at 72 hours was similar to the stiffness reduction for the specimens microcracked at 72 hours.

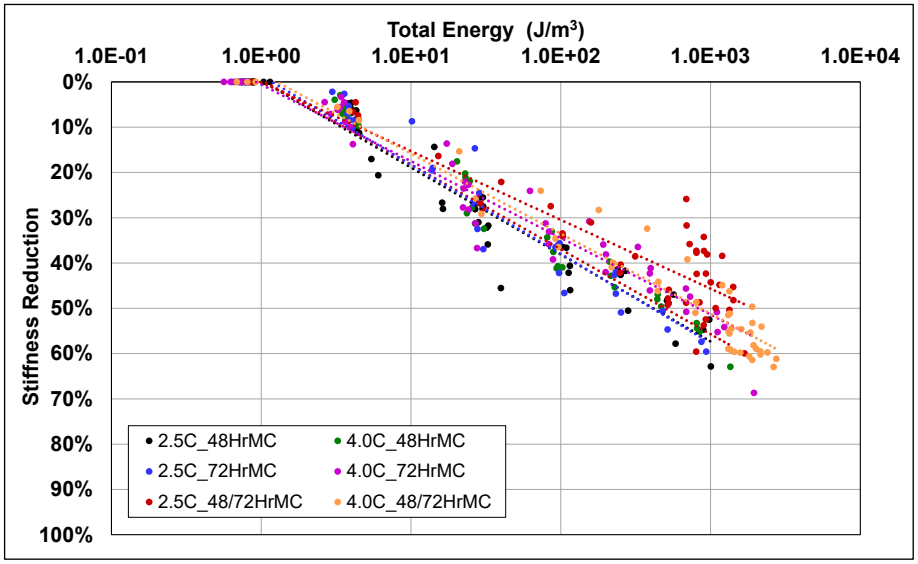

Figure 6.1: Comparison of stiffness changes with energy input during microcracking.

6.3 Long-Term Stiffness and Indirect Tensile Strength with Microcracking

Long-term stiffness monitoring tests after microcracking, and final ITS tests, were performed according to Table 5.3 and Table 5.4.

6.3.1 Specimen Production: Moisture Content and Density

Moisture content data for the specimens tested for long-term stiffness and ITS with microcracking are plotted in Figure 6.2 and Figure 6.3 for the 2.5% and 4% cement-content specimens, respectively. Error bars show the lowest and highest results for the replicates tested. The average compaction moisture content was 4.6%, which was 0.7% below the average field moisture content. A reduction in internal moisture content was recorded for both the 2.5% and 4% cement-content specimens. This moisture discrepancy was attributed to the time (approximately 30 minutes) that elapsed between demolding the specimens and sealing them in wax, when some moisture loss probably occurred. There was, however, a significant difference between the internal moisture content of the 2.5% and the 4% cement-content specimens, attributed to the higher hydration moisture demand for the higher cement content. These specimens were subjected to ITS testing 1,344 hours (56 days) after compaction.

Densities of the long-term stiffness and ITS specimens are plotted in Figure 6.4. Error bars show the lowest and highest results for the replicates tested. The overall average of both the 2.5% and 4% cement-content specimens was 2,072 kg/m^3 (129.4 lb./ft^3), approximately 40 kg/m^3

(2.5 lb./ft^3) above the target field dry density. There was some variation in the densities determined for the different batches (depicted by the error bars), attributed to the change in moisture content of the mixed material over time during compaction, and to the inevitable small amounts of segregation during material transfer from the mixing bowl to the mold.

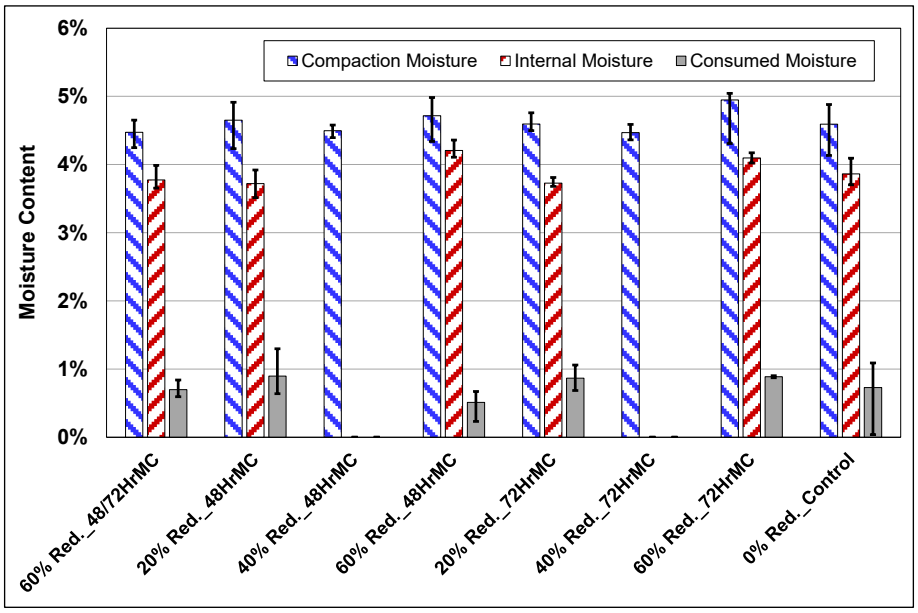

Figure 6.2: 2.5% Cement: Specimen moisture content history.

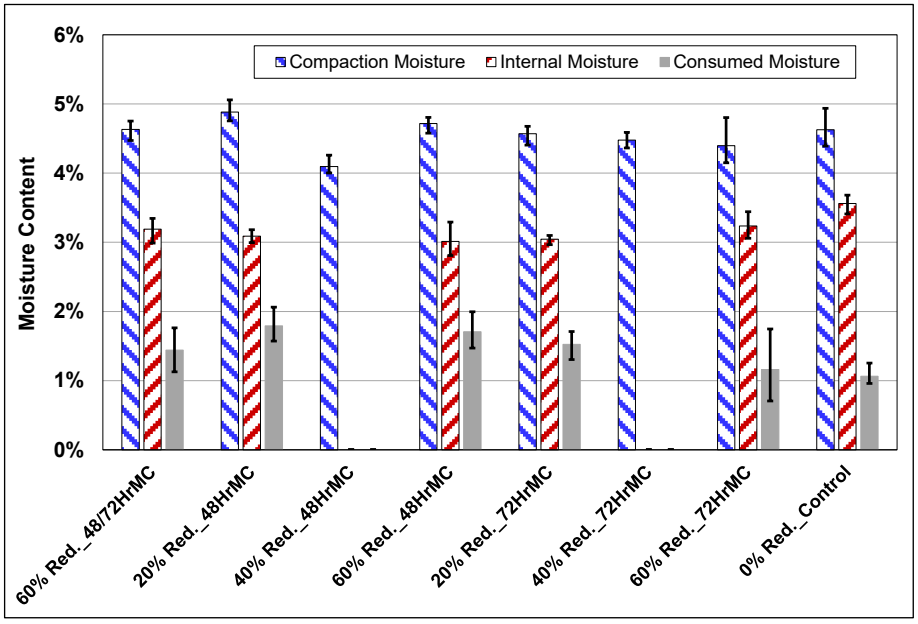

Figure 6.3: 4% Cement: Specimen moisture content history.

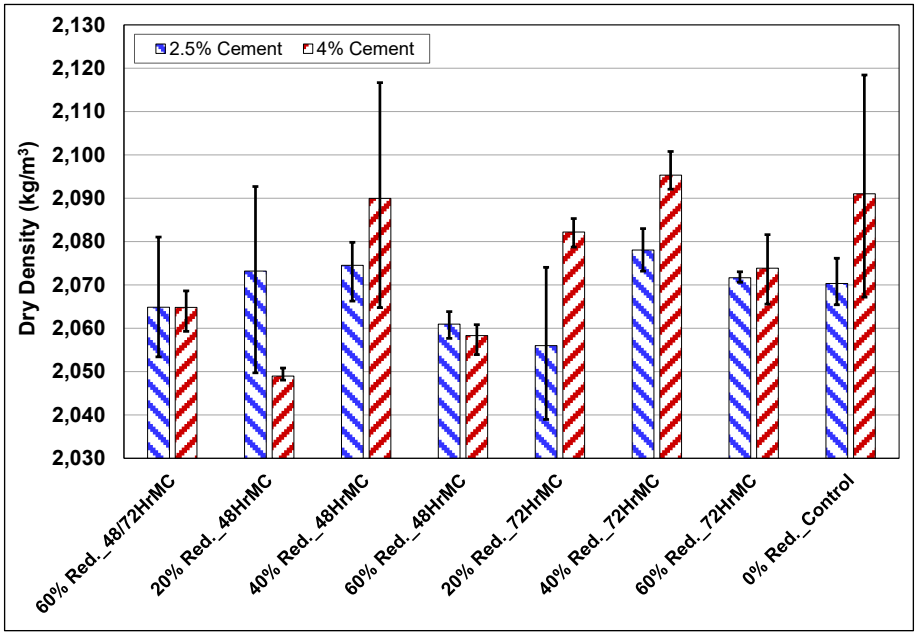

Figure 6.4: Long-term specimen density results.

6.3.2 Stiffness Change Over Time

The stiffness of each specimen was tracked for 56 days, following the experimental plan, to develop a model for stiffness recovery over time after microcracking. Stiffness recovery for the 2.5% and 4% cement-content specimens with various microcracking efforts are summarized in Figure 6.5 through Figure 6.8. The results for each specimen are provided in Appendix A. The results for the 2.5% cement-content specimens (Figure 6.5) show that:

- Stiffness recovery with time was positive for each case, regardless of the level of microcracking.
- The control case in Figure 6.5 had an initial increase in stiffness but plateaued after about 500 hours.
- The microcracked 2.5% cement-content specimens continued to gain stiffness throughout the monitoring period but did not show any consistent trends.
- The stiffness recovery rates for the different batches varied significantly, especially considering the differences between the specimens microcracked at 48 hours to 20%, 40%, and 60% of initial stiffness. The ICS test, which is used to determine the minimum cement content required to permanently stabilize a material, showed that a minimum cement content of 2% was required for the FDR-C Test Road material. However, an additional 0.5% was added for durability instead of the recommended 1% to limit the design UCS. It is hypothesized that the 2.5% cement-content specimens were sensitive to this lower-than-recommended cement content, which could explain the variations in long-term stiffnesses.

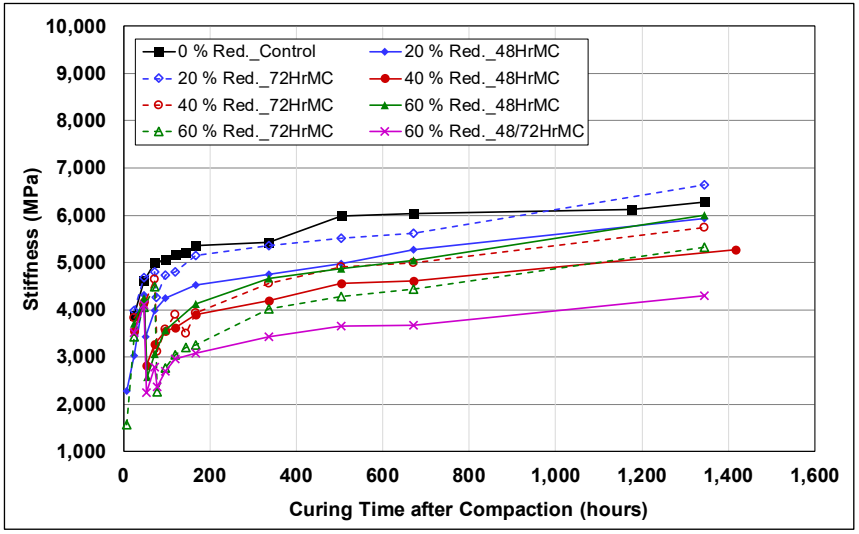

Figure 6.5: 2.5% Cement: Average stiffness recovery over time.

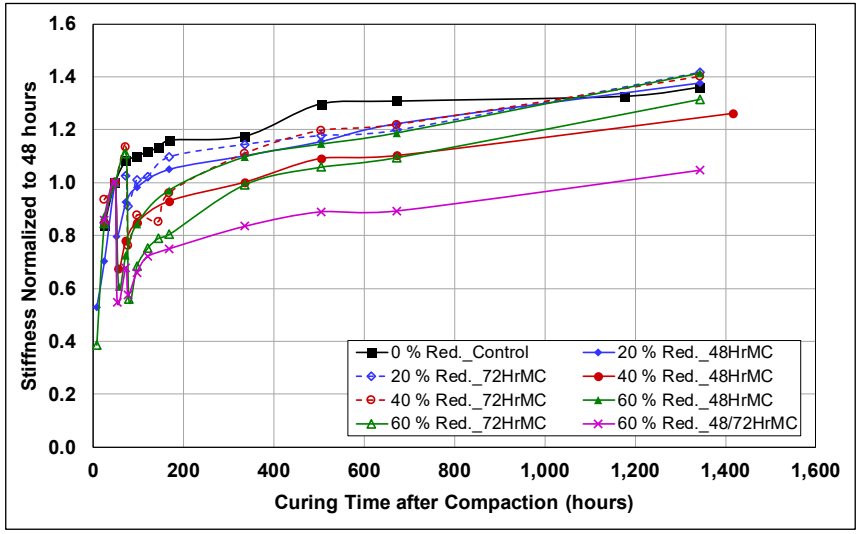

Figure 6.6: 2.5% Cement: Normalized average stiffness recovery.

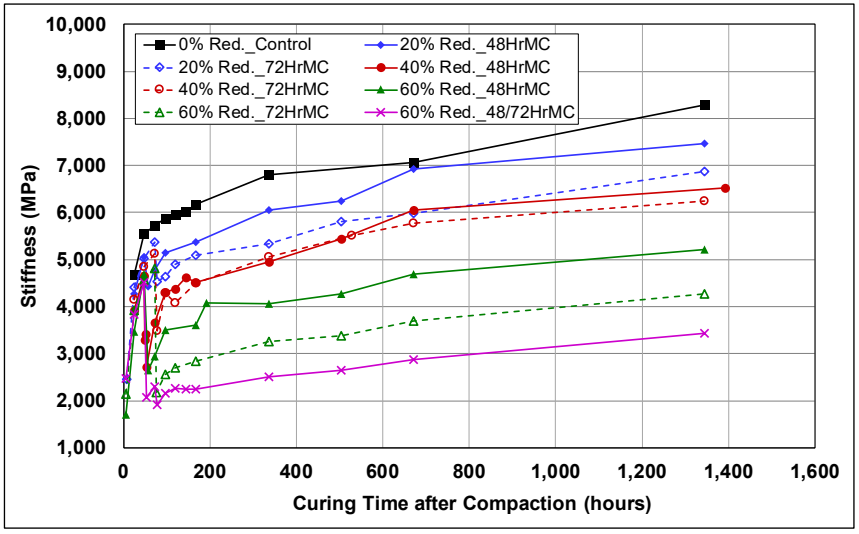

Figure 6.7: 4% Cement: Average stiffness recovery over time.

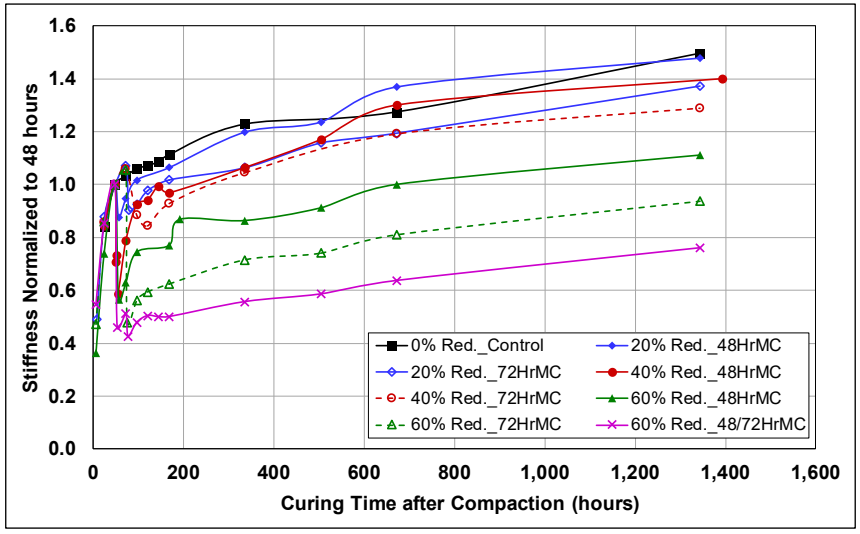

Figure 6.8: 4% Cement: Normalized average stiffness recovery.

The average stiffnesses for the 2.5% cement-content specimens, normalized to the stiffness at 48 hours, are plotted in Figure 6.6. The results show that:

- All specimens exhibited stiffness recovery and most gained strength above that recorded prior to microcracking. However, there did not appear to be a consistent trend in the rates of stiffness gain between the different experimental factors for the specimens microcracked with a single event.
- The specimens microcracked at 48 hours with 40% reduction in stiffness had a lower stiffness after 56 days than the controls and the 20% and 60% stiffness-reduction specimens.
- The specimens microcracked at 72 hours to 60% stiffness reduction had lower stiffnesses than the control and the 20% and 40% stiffness-reduction specimens.
- The specimens microcracked at 48 hours and again at 72 hours had the lowest stiffness recovery after 56 days.

The stiffness recovery and gain over time for the 4% cement-content specimens with various microcracking efforts for each specimen are provided in Appendix A. The average stiffness gain curves for each case are plotted in Figure 6.7. Observations were similar to those for the 2.5% cement-content results, except the control case did not plateau. The average stiffness results show a strong trend where the long-term stiffness is reduced with increased stiffness reduction, and with increasing time before microcracking.

The average stiffnesses for the 4% cement-content specimens, normalized to the stiffness at 48 hours, are plotted in Figure 6.8. The results show the following:

- There appears to be a significant difference in the stiffness change with time for each microcracking effort, except for the controls and the specimens microcracked to a 20% reduction of the initial stiffness at 48 hours.
- Stiffnesses decreased with increasing microcracking effort and with longer curing intervals before microcracking.
- The rate of stiffness recovery/gain after microcracking appeared to be relatively consistent regardless of the microcracking effort.

A certain level of variability in the results was apparent, which was expected due to the sampling, batching, and compaction methods used, and to the large number of specimens prepared. The overall trends in the 4% cement-content specimens were much stronger than those of the 2.5%

cement-content specimens, which was attributed in part to the more durable mix achieved with the higher cement content (i.e., ICS plus 2%).

6.3.3 Indirect Tensile Strength

Indirect tensile strength testing was performed according to ASTM D6931 in a UTM30. Tests were done at the end of the 56-day monitoring period on the specimens used for assessing stiffness recovery/gain over time with various microcracking efforts. Results are plotted in Figure 6.9 and Figure 6.10 for the 2.5% and 4% cement-content specimens, respectively. Figure 6.11 shows a direct comparison of the strengths for different microcracking efforts.

The ITS results for the 2.5% cement-content specimens show that:

- The effect of microcracking was significant even after 56 days.
- The specimens microcracked at 48 hours and again at 72 hours had the lowest ITS.
- The specimens microcracked to a stiffness reduction of 60% had a lower ITS than those with a stiffness reduction of 20%.
- The specimens microcracked at 48 hours had a higher ITS than those microcracked at 72 hours.
- The strengths of the 2.5% cement-content control specimens were lower than expected.

The ITS results for the 4% cement-content specimens had higher strengths but showed similar trends to the 2.5% cement-content specimens.

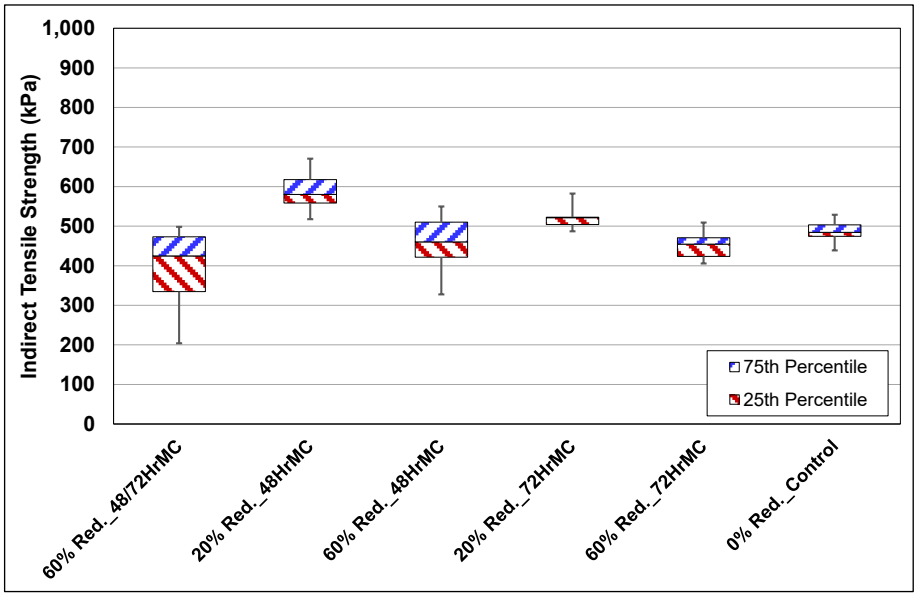

Figure 6.9: 2.5% Cement: ITS after 56 days.

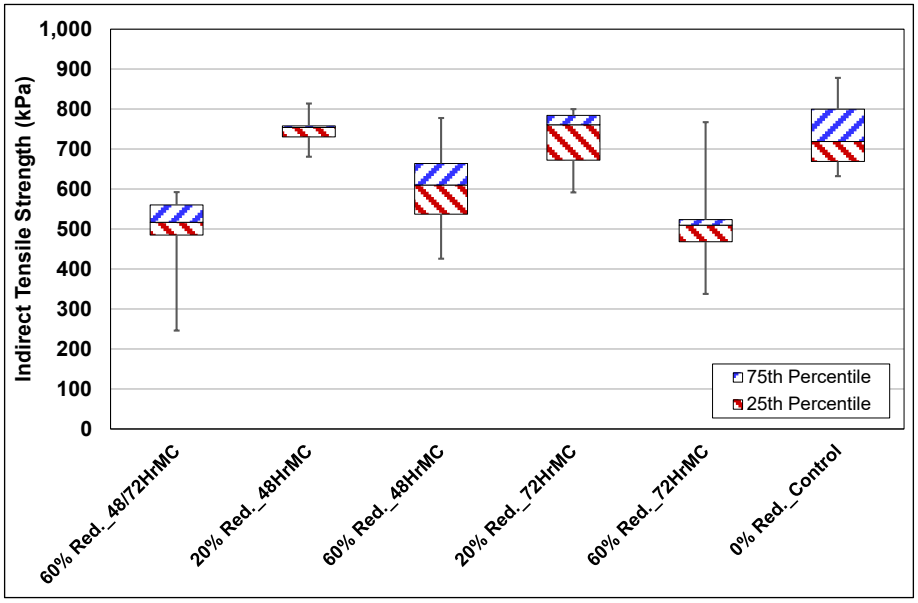

Figure 6.10: 4% Cement: ITS after 56 days.

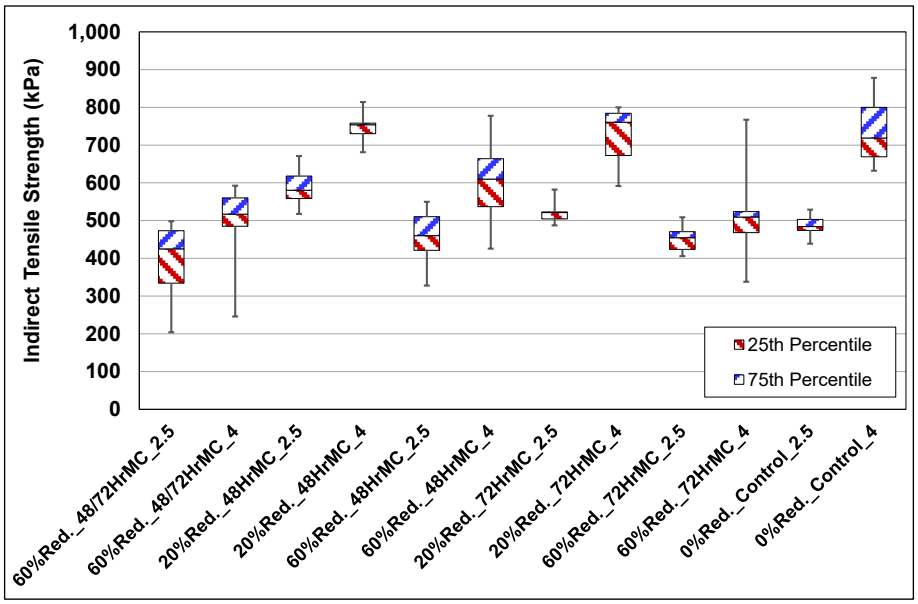

Figure 6.11: Comparison of ITS after 56 days.

The effect of damage from cutting was considered negligible on the microcracked specimens with a stiffness reduction of up to 20% since the difference between the 25th and 75th percentiles was minimal. There were also relatively small differences between the minimum and maximum strengths. The effect of saw cutting on the specimens microcracked to 60% of the initial stiffness showed greater variability, as shown by the increase in the difference between the minimum and maximum, and the difference between the 25th and 75th percentiles. This was, however,

accepted as saw cutting was the only appropriate method available at the time to obtain specimens that had been subjected to microcracking.

6.3.4 Long-Term ITS Relationship with Stiffness

The long-term ITS results are plotted against the stiffness recorded prior to ITS testing in Figure 6.12 and Figure 6.13 for the 2.5% and 4% cement-content specimens, respectively.

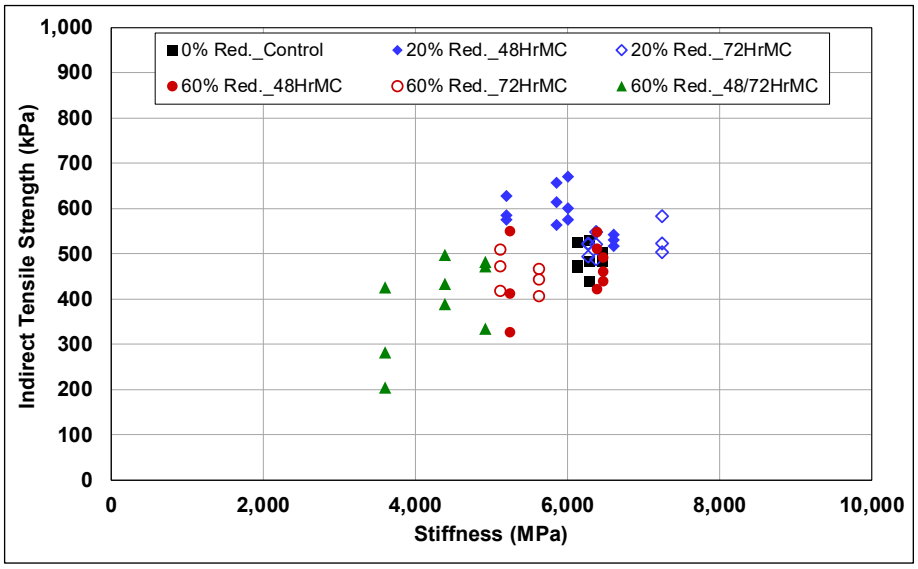

Figure 6.12: 2.5% Cement: ITS versus stiffness with different microcracking levels.

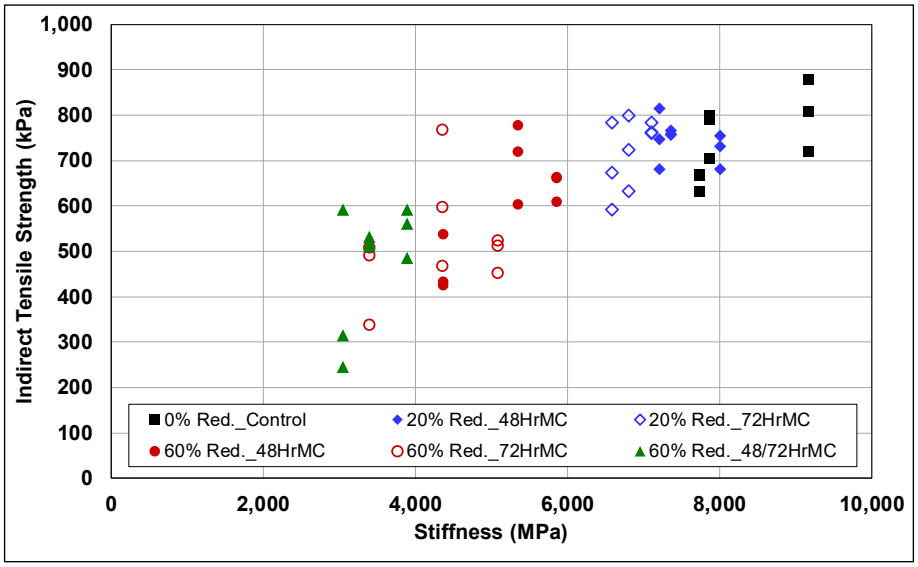

Figure 6.13: 4% Cement: ITS versus stiffness with different microcracking levels.

The ITS was strongly correlated with stiffness for both cement contents. The effects of microcracking at different ages were consistent with the observations between the long-term

stiffness tests and the ITS results. The ITS and stiffness were affected by the following microcracking efforts in order of most to least effect:

- Microcracking at 48 hours and again at 72 hours, to reduce the stiffness by 60%.
- Microcracking at 72 hours, to reduce the stiffness by 60%.
- Microcracking at 48 hours, to reduce the stiffness by 60%.
- Microcracking at 72 hours, to reduce the stiffness by 20%.
- Microcracking at 48 hours, to reduce the stiffness by 20%.
- No microcracking.

6.4 Early-Age Indirect Tensile Strength After Microcracking

Early-age ITS testing (i.e., ITS tests were done immediately after microcracking), following the experiment plan summarized in Table 5.5, was required to develop a model for the reduction in ITS with increased microcracking efforts (discussed in Section 7.3). The density and moisture content, microcracking, and ITS results are discussed below. Note that testing was only done on specimens prepared with 2.5% cement.

6.4.1 Specimen Production: Moisture Content and Density

The moisture content and dry density data for the short-term ITS specimens are provided in Figure 6.14 and Figure 6.15, respectively. Error bars show lowest and highest results for replicate specimens. The moisture content results were similar to those measured on the long-term (56-day) stiffness specimens, with the consumed moisture content consistently below 1%. Specimens were subjected to ITS testing 48 or 72 hours after compaction. The dry densities were also similar to those of the long-term stiffness specimens. However, some variation was noted, and the overall mean density was approximately 40 kg/m^3 (2.5 lb./ft^3) higher than the target field density.

6.4.2 Stiffness Reduction After Microcracking

The stiffness results for the early-age ITS specimens are provided in Figure 6.16 and Figure 6.17 for specimens microcracked after 48 and 72 hours, respectively. Two specimens, one control and one with 60% stiffness reduction, tested at 48 hours had significantly lower stiffnesses than the rest, likely due to the higher variability in the moisture content and dry density results for the 48-hour cure specimens.

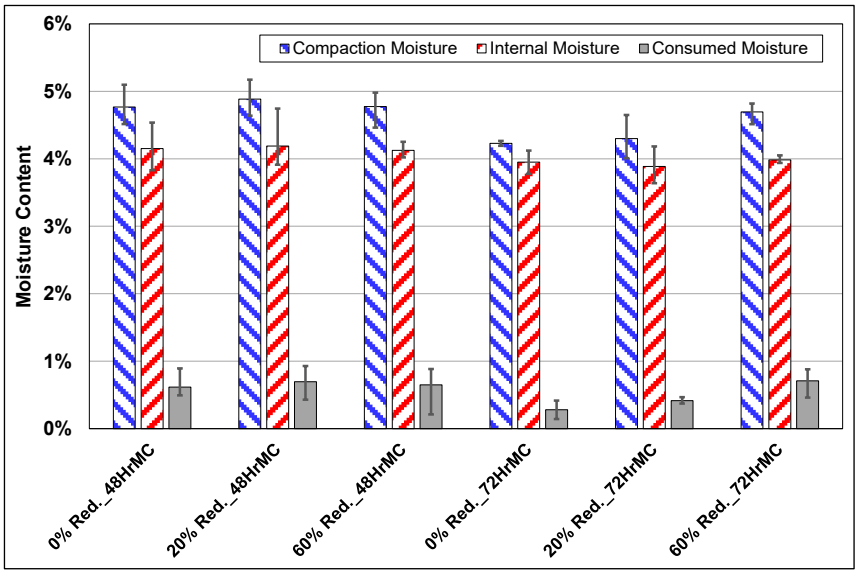

Figure 6.14: Short-term ITS specimen moisture contents.

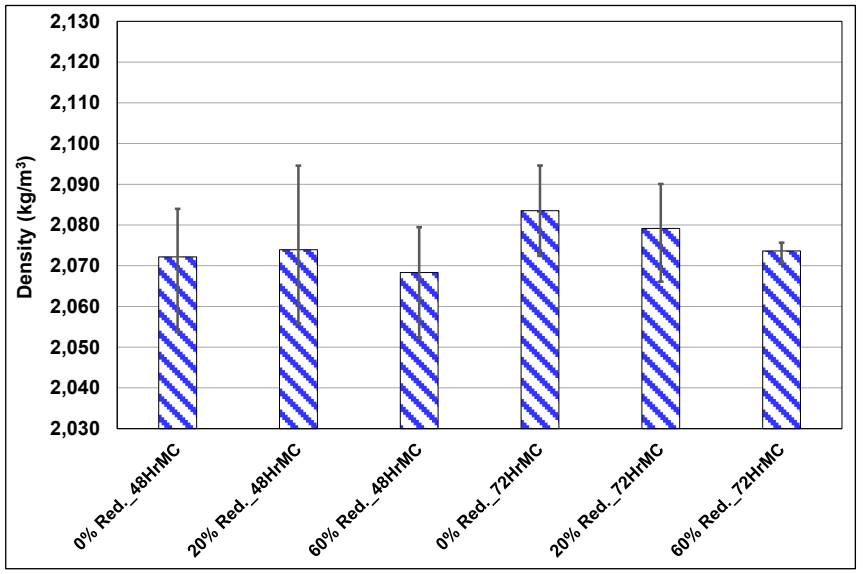

Figure 6.15: Short-term ITS specimen dry densities.

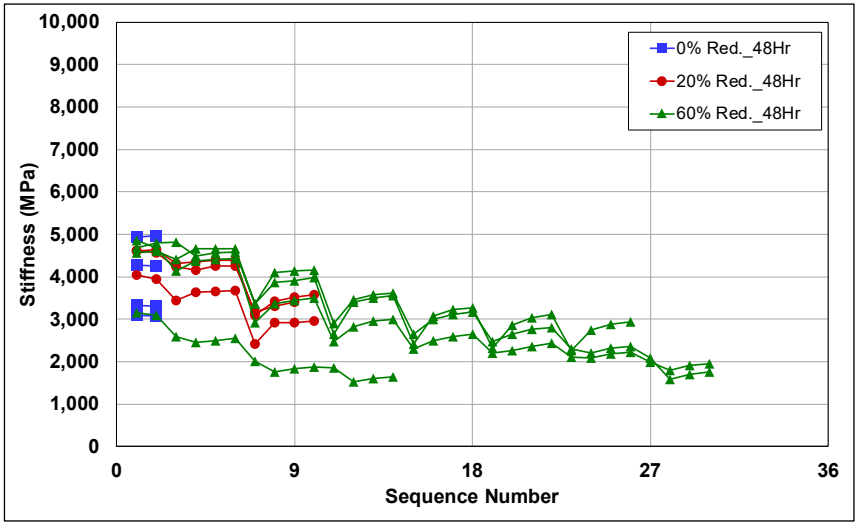

Figure 6.16: 2.5% Cement: Stiffness of ITS specimens after microcracking (48-hour cure).

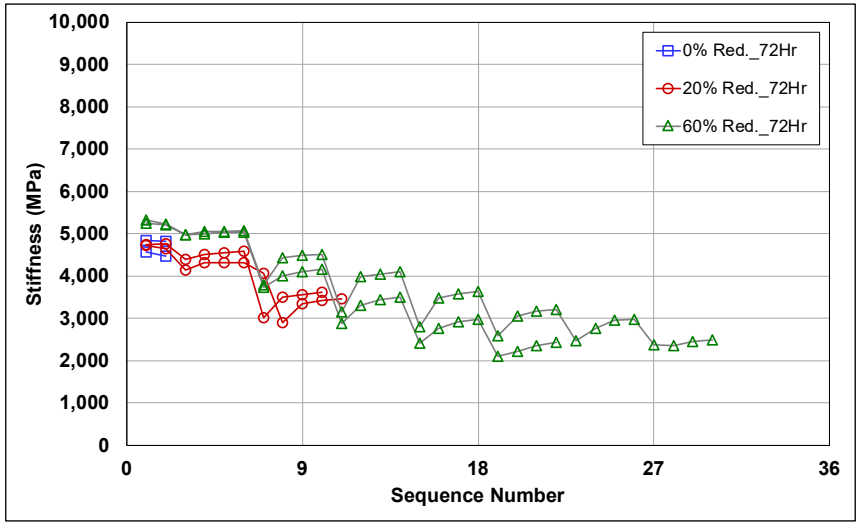

Figure 6.17: 2.5% Cement: Stiffness of ITS specimens after microcracking (72-hour cure).

The variability in the 72-hour microcracked specimens was less than in the 48-hour microcracked specimens. The dry densities and the internal moisture contents of the 60% stiffness-reduction specimens tested at 72 hours were the least variable, and the results were similar to the initial stiffnesses recorded during microcracking.

Figure 6.18 illustrates the variability in the level of stiffness reduction for the 20% and 60% stiffness-reduction microcracking tests. The largest variability was in the target 60% stiffness reduction at 48 hours. The specimen had a low initial stiffness and the test was stopped early to prevent failing the specimen during the following microcracking sequences.

6.4.3 Indirect Tensile Strength

Indirect tensile strength testing was performed according to ASTM D6931 in a UTM30 immediately after the 48- and 72-hour microcracking efforts. Results are provided in Figure 6.19. The results show relatively small differences in the mean ITS between the various microcracking efforts. The 20% target stiffness reduction at 48 hours curing had the highest ITS and the 60% target stiffness reduction at 48 hours curing had the lowest. The variation in results was consistent with the observations discussed for the other tests described previously.

6.4.4 Early Age ITS Relationship with Stiffness

The early age ITS relationship with stiffness is provided in Figure 6.20. The ITS was positively correlated with stiffness. These data were used to develop a model to describe the effect of microcracking on ITS (discussed in Section 7.4).

6.5 Early-Age Unconfined Compressive Strength After Microcracking

The goal of UCS testing was to determine the increase in UCS over seven days for the 2.5% and 4% cement-content control specimens, following the factorial in Table 5.6, to develop a model for the reduction in UCS with increased microcracking efforts (discussed in Section 7.4). These results were required to provide a measure of the stress-to-strength ratio during microcracking tests and to determine the crushing sensitivity of the material during microcracking in the field. UCS testing was performed according to ASTM D1633.

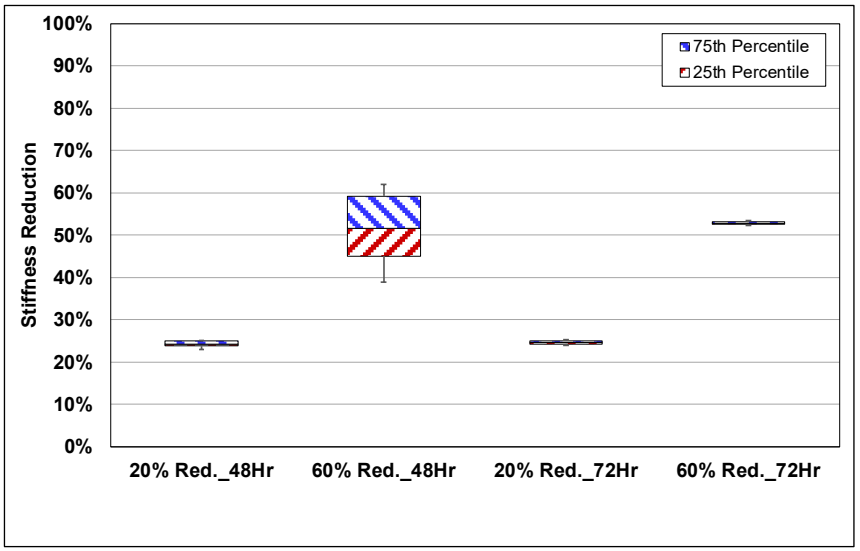

Figure 6.18: 2.5% Cement: Stiffness reduction on ITS specimens during microcracking.

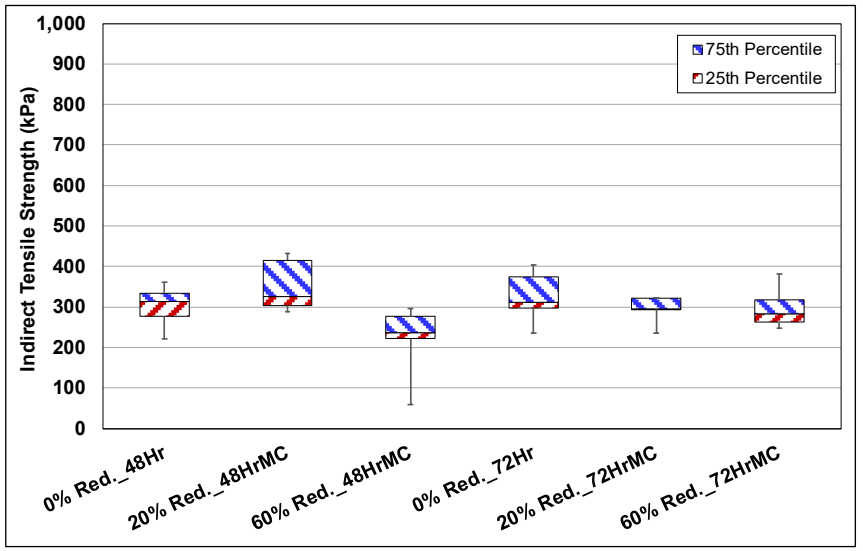

Figure 6.19: 2.5% Cement: ITS with different microcracking levels.

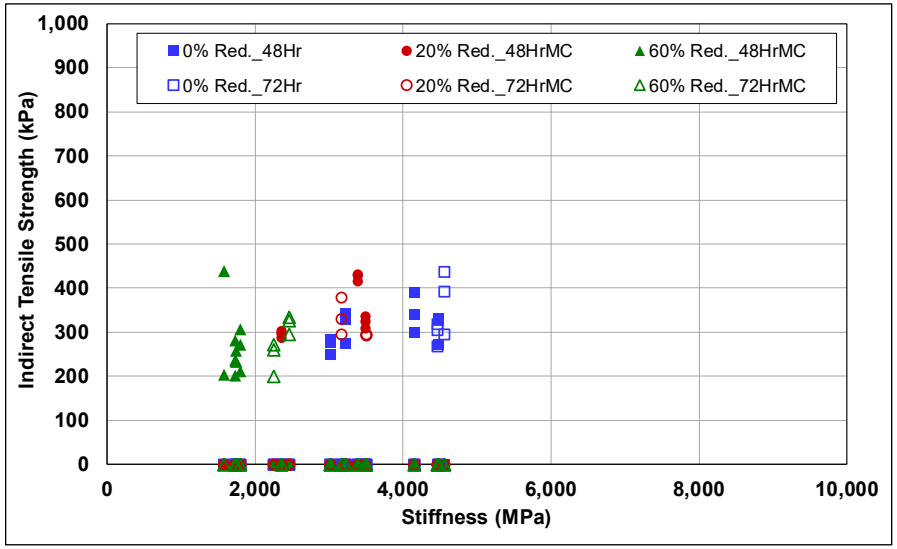

Figure 6.20: 2.5% Cement: Early age ITS versus stiffness with different microcracking levels.

6.5.1 Specimen Production: Moisture Content and Density

The average specimen compaction properties are provided in Table 6.1. Moisture contents are provided in Figure 6.21. The average dry density and internal moisture contents, which were tested at different curing ages, are provided in Figure 6.22. The dry densities were similar to those of the short-term ITS specimens, with similar variation. The overall mean density was approximately 40 kg/m^3 (2.5 lb./ft^3) higher than the target field density. The moisture contents were similar to the short-term ITS specimens with the consumed moisture content consistently below 1%. Specimens were subjected to initial UCS testing 48 hours after compaction.

Table 6.1: Specimen Compaction Properties

Curing Age (Days)	2.5% Cement			4% Cement		
	Internal Moisture Content (%)	Dry Density		Internal Moisture Content (%)	Dry Density	
		(kg/m^3)	(lb./ft^3)		(kg/m^3)	(lb./ft^3)
2	4.3	2,070	129.2	3.7	2,034	127.0
3	4.2	2,061	128.7	4.0	2,043	127.5
7	3.9	2,060	128.6	3.7	2,058	128.5

6.5.2 Stiffness Reduction After Microcracking

The stiffness reduction results for the microcracked UCS specimens are provided in Figure 6.23 and Figure 6.24. The variability recorded in the dry density after compaction is reflected in the stiffness results. The achieved stiffness reduction levels for the 20% and 60% target stiffness-reduction specimens were 34% and 55%, respectively. The microcracking efforts exceeded the stiffness reduction target for the 20% stiffness reduction specimens and were approximately within range of the 60% stiffness reduction specimens.

6.5.3 Strength Increase with Time

The UCS results after different curing periods are provided in Figure 6.25 for the 2.5% and 4% cement-content specimens, respectively. The 4% cement-content specimens had a significantly larger strength increase with time compared to the 2.5% cement-content specimens, as expected. The approximate strength-to-stress ratios used during microcracking (Table 4.1) for the 2.5% and 4% cement-content specimens are provided in Figure 6.26. Comparing the strength-to-stress ratio for each cycle to a typical stiffness reduction pattern during microcracking of an FDR-C specimen (Figure 6.27), it is clear that a significant portion of the stiffness was lost during sequence seven, where after the stiffness reduced gradually with an increase in the ratio.

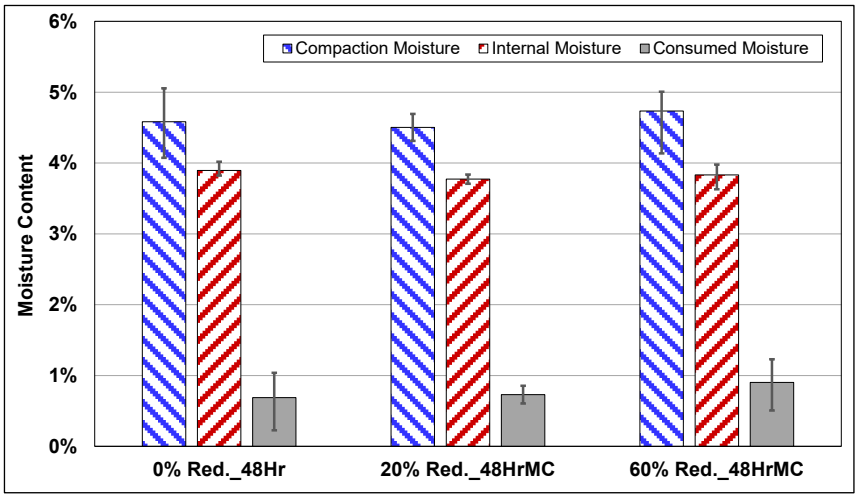

Figure 6.21: Short-term UCS specimen moisture contents.

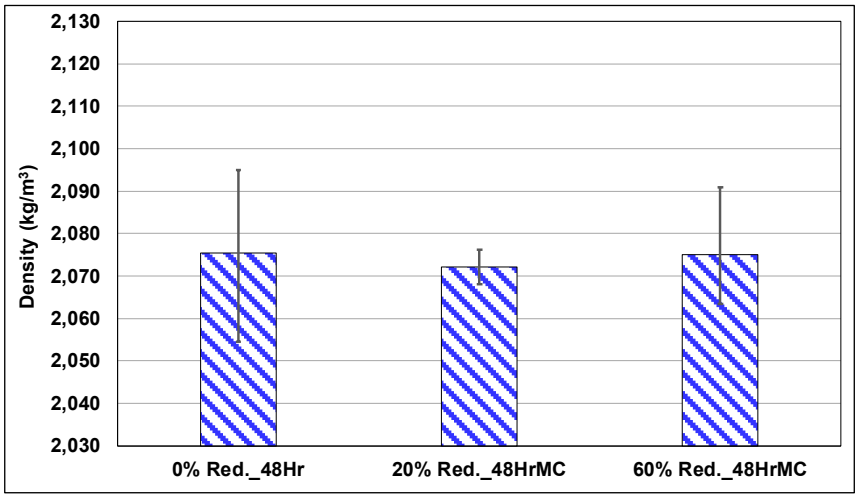

Figure 6.22: Short-term UCS specimen dry densities.

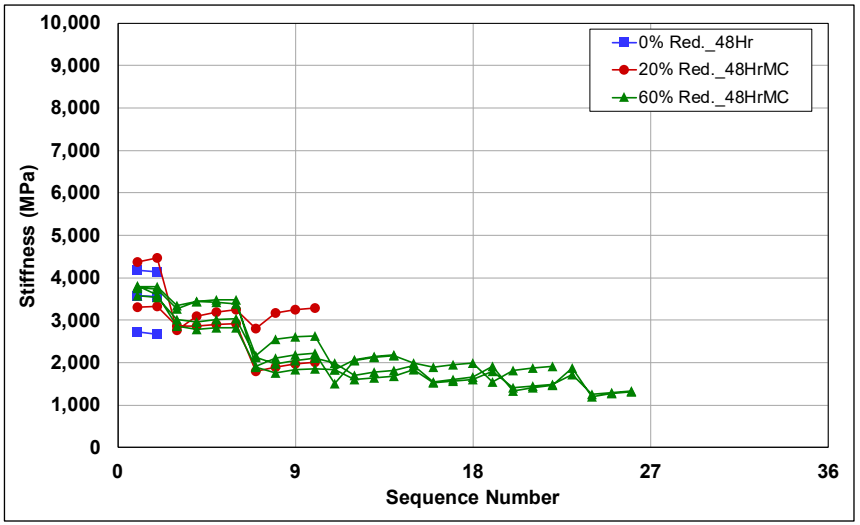

Figure 6.23: 2.5% Cement: Stiffness on UCS specimens after microcracking (48-hour cure).

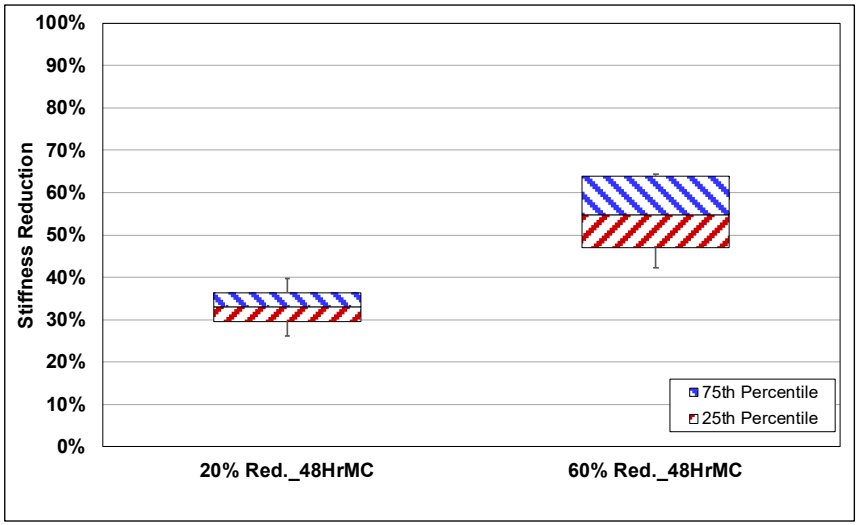

Figure 6.24: 2.5% Cement: Stiffness reduction on UCS specimens during microcracking.

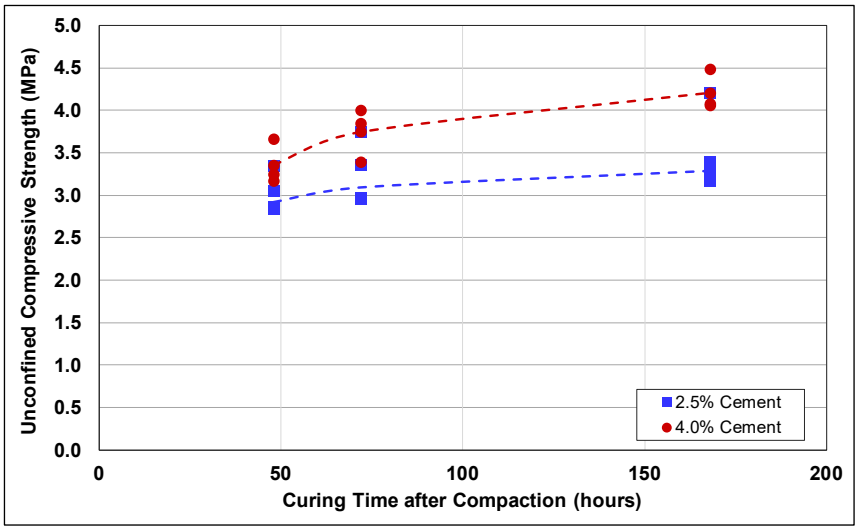

Figure 6.25: UCS versus curing time.

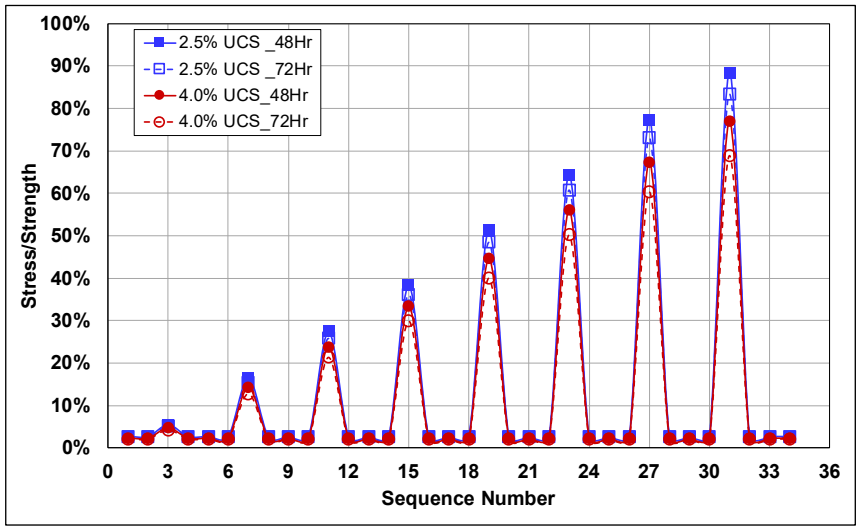

Figure 6.26: Stress/strength ratios during microcracking.

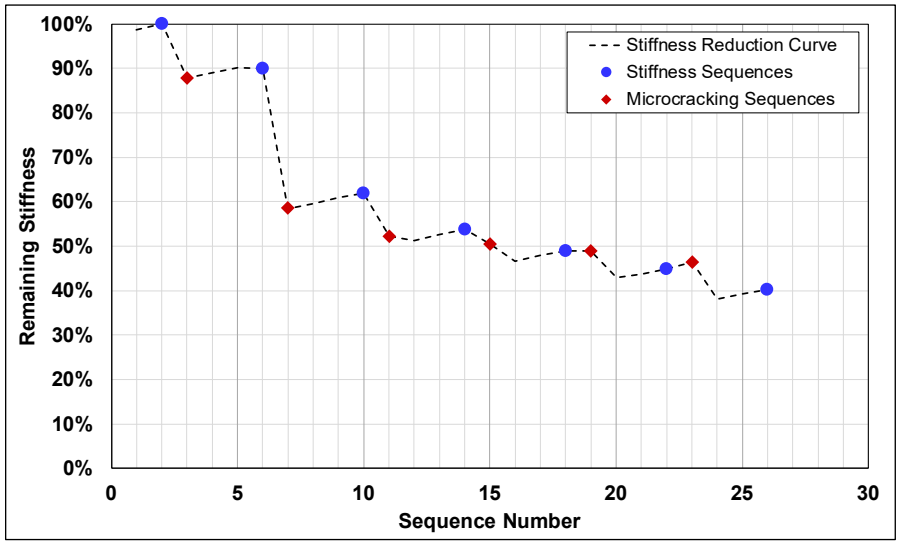

Figure 6.27: Stiffness reduction on UCS specimens during microcracking.

6.5.4 Effect of Microcracking on Unconfined Compressive Strength

The effect of microcracking on UCS was negligible, as shown in Figure 6.28, with no significant reduction in the UCS with increased microcracking effort. This was attributed to the testing procedure, where the cracks caused by microcracking are in compression and do not affect the structural properties of the specimen, unlike ITS testing where the cracks are in tension. The stiffness of the specimens was effectively reduced during microcracking, and there were no significant differences in the densities or moisture contents.

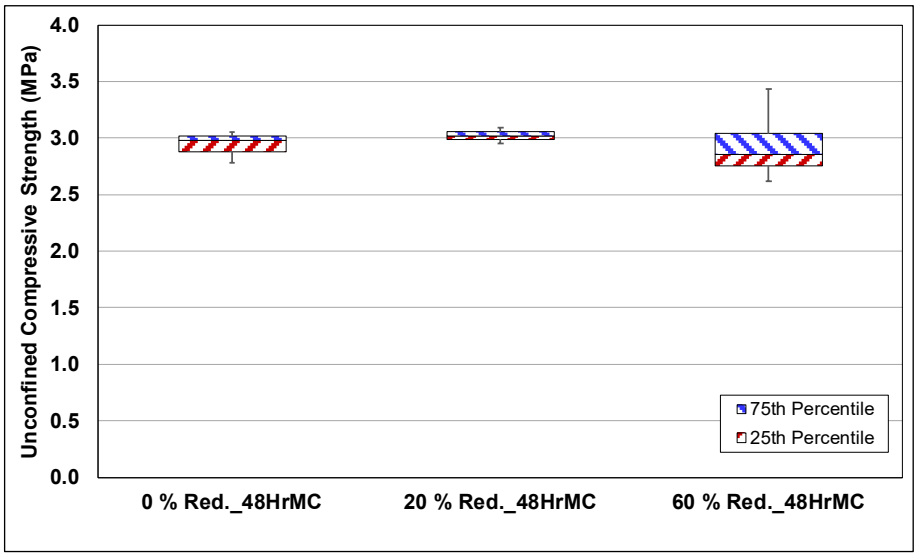

Figure 6.28: 2.5% Cement: UCS with different microcracking levels.

6.5.5 Strength and Stiffness Relationship with Microcracking

The relationship between UCS and stiffness is provided in Figure 6.29. These specimens were all tested at 48 hours of curing after compaction. There was no correlation between the stiffness after microcracking and the UCS. As noted, this was attributed to the cracks induced during microcracking being in compression during the UCS test.

6.6 Free-Drying Shrinkage

The results from the free-drying shrinkage tests are provided in Figure 6.30. The 2.5% cement-content specimens had a slightly higher shrinkage rate than the 4% cement-content specimens for the first four days, after which the 4% cement-content specimen shrinkage rate exceeded that recorded on the specimens with 2.5% cement. The shrinkage appeared to be initially exponential with time (i.e., up to 10 days), after which it continued to increase at a more linear rate.

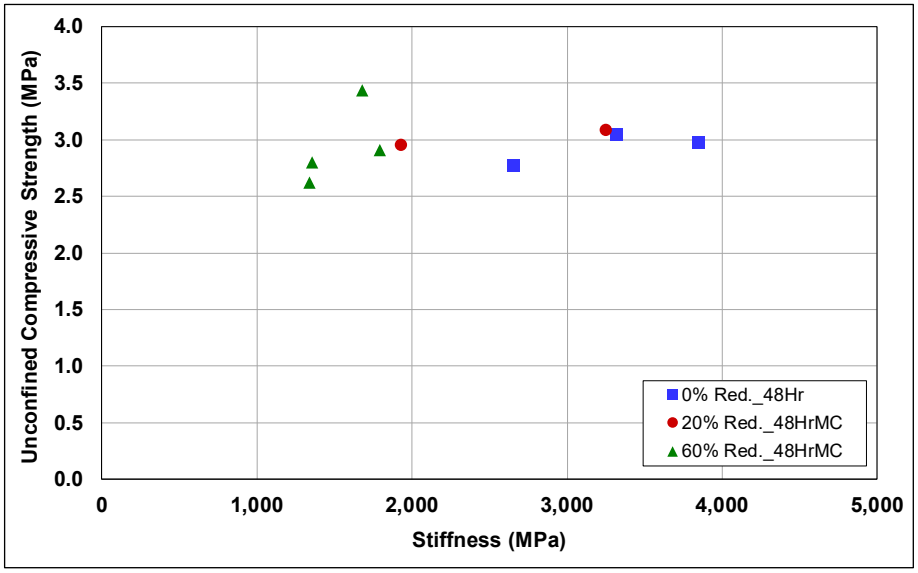

Figure 6.29: 2.5% Cement: UCS versus stiffness with different microcracking levels.

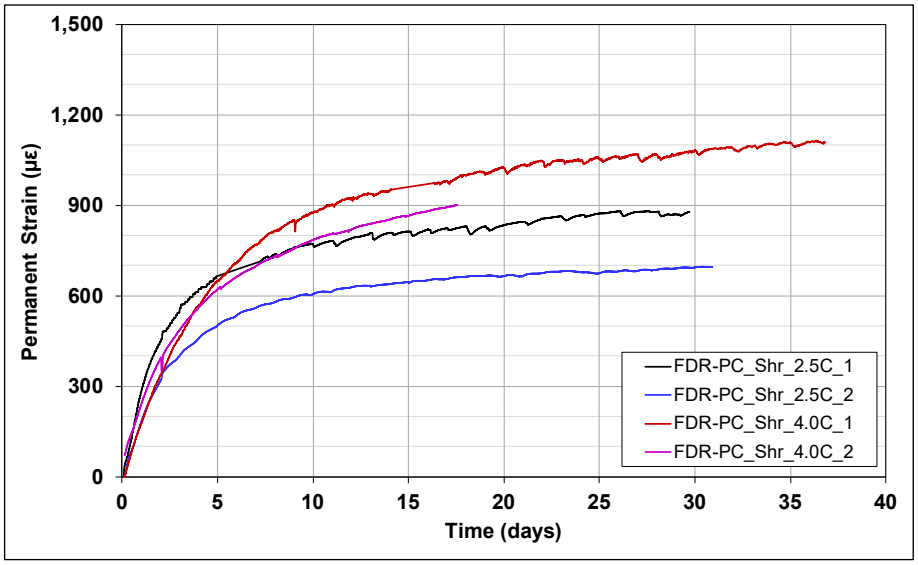

Figure 6.30: Free-drying shrinkage results.

6.7 Scanning Electron Microscopy

Scanning electron microscopy (SEM) was investigated as a technique to visually assess the cementitious reactions and the effects of microcracking on the crystalline structure of the cementitious bonds. The downside of the technique in the context of observing the internal structure of cement-treated specimens is that the specimens have to be broken to expose the internal structure where microcracking occurred. The relatively low cement contents used in the test specimens (2.5% and 4%), the early curing age of the specimens (56 days), and the relatively

high fines content, also made finding sites with visible calcium silicate hydrate (CSH) reactions difficult.

SEM was performed on fractured pieces of 2.5% and 4% cement-content long-term stiffness monitoring specimens after ITS testing. The SEM specimens, sampled from the control and microcracked ITS specimens, were sealed immediately after sampling to prevent carbonation. Specimens were mounted on an SEM stud, placed in an ultra-high vacuum degassing chamber for 30 minutes to limit outgassing during SEM scanning, and then evaluated.

The images that were collected (example in Figure 6.31) showed that there was no uniform or continuous layer of cementitious CSH between larger particles. Extensive scanning was required to locate any CSH sites. No conclusions could be reached regarding the effect of microcracking on the cementitious bonds due to the problems identified with the sampling method.

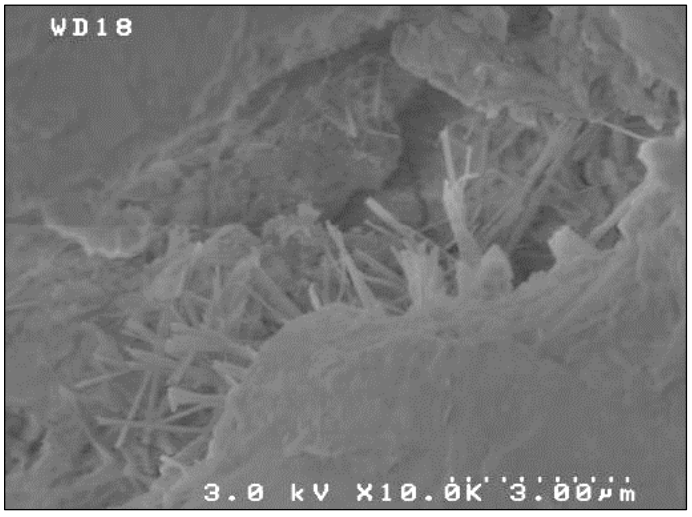

Figure 6.31: Ettringite formations.

6.8 Comparison Between Laboratory- and Field-Determined Stiffnesses

Laboratory testing to evaluate the effect of microcracking on long-term stiffness gain showed similar trends to those observed from the FWD testing on the FDR-C Test Road and discussed in the Phase 2a report *(12)*. One limitation of the comparison between laboratory and field microcracking was the inability to measure the actual energy applied by the roller during microcracking. The values used for energy input were based on the peak stress applied by the roller per unit width of the drum, and not an actual measurement of the energy applied to the layer (area below the stress-strain curve as measured on the layer).

To illustrate the relationship between field and laboratory results, Figure 6.32 and Figure 6.33 provide comparisons between laboratory-measured stiffnesses up to 56 days and FWD backcalculated stiffnesses from the FDR-C Test Road, as follows:

- Figure 6.32 compares laboratory stiffness change for the 2.5% cement content specimens microcracked at 48 hours to a target stiffness reduction of 40% with Cell S17 on the Test Road (2.5% cement, microcracked with three roller passes at 48 hours).
- Figure 6.33 compares laboratory stiffness change for the 4% cement content specimens microcracked at 72 hours to a target stiffness reduction of 40% shows results with Cell S15 on the Test Road (4% cement, microcracked with three roller passes at 72 hours).

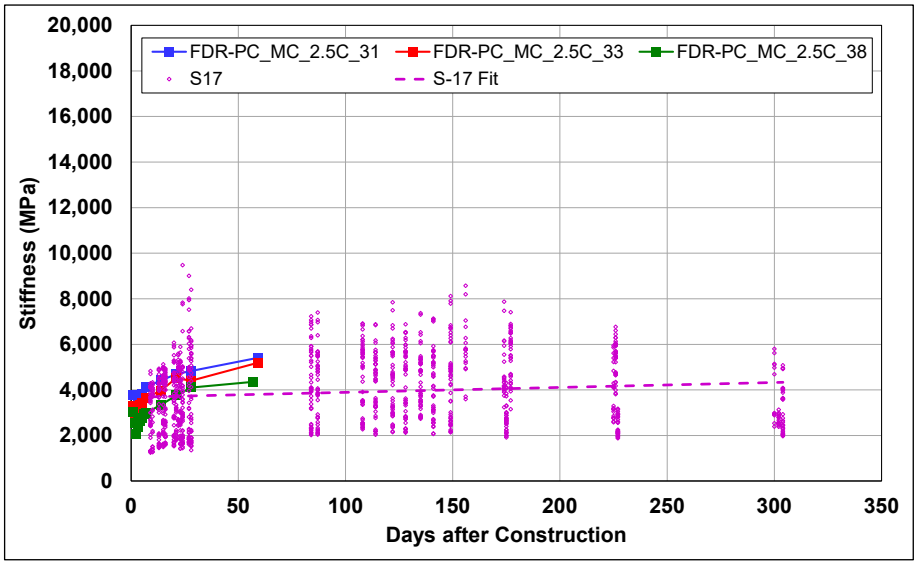

Figure 6.32: 2.5% Cement: Comparison between laboratory- and field-measured stiffness.

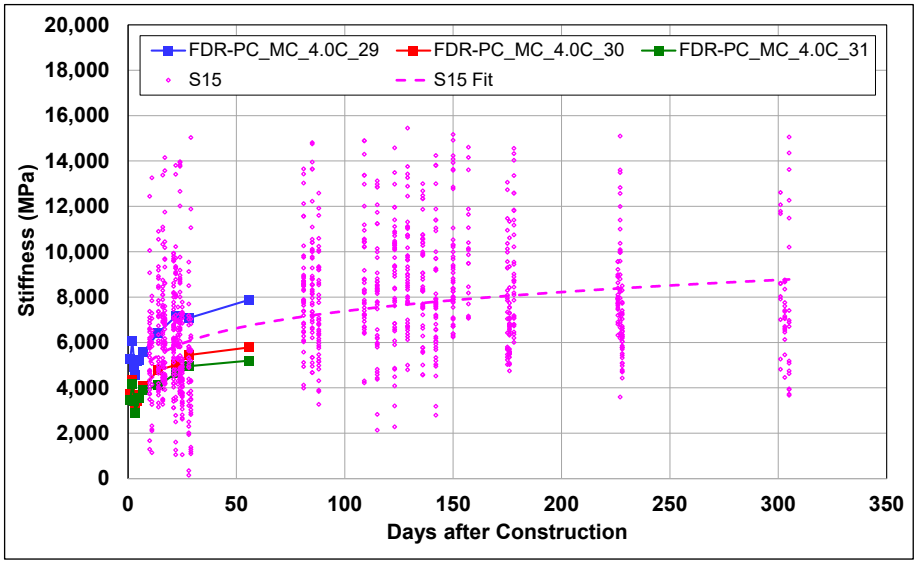

Figure 6.33: 4% Cement: Comparison between laboratory- and field-measured stiffness.

Observations include the following:

- The FDR-C Test Road and laboratory results showed similar trends in stiffness change after microcracking.
- The laboratory results showed similar trends to the FWD results, but in some scenarios tended toward the upper percentiles of the FWD results. This was attributed to less variation in the laboratory results compared to the FDR-C Test Road, which was expected given the controlled conditions under which the laboratory testing was performed.
- There was a large variation in FWD backcalculated stiffness results within and between sections, attributed to inherent variability in the materials and to the testing procedure that required testing in the same position each time regardless of any distresses in the drop- and geophone-contact zones.

The satisfactory agreement between the laboratory- and field-measured stiffnesses and the observed similar behavior between the two methods provided a strong validation for the test method to simulate microcracking in the laboratory.

6.9 Discussion

This chapter provides the first-level analyses of the laboratory test results to simulate microcracking in the laboratory. The laboratory microcracking test results were consistent with the backcalculated stiffness results from the FDR-C Test Road in terms of the range of stiffnesses measured and the trends among the different applied energies. The main findings from this part of the study include the following:

- Stiffness Change
  - The laboratory microcracking procedure effectively simulated microcracking in the field, with results showing similar trends between laboratory- and field-measured stiffnesses.
  - The stiffness of the 2.5% cement-content specimens after microcracking recovered through autogenous healing to equal or exceed the stiffness of the control specimens at the same age.
  - The 4% cement-content specimens after microcracking had a significant long-term reduction in stiffness with microcracking effort and curing time before microcracking.
  - Microcracking resulted in damage to the specimens in the form of internal microcracks that led to stiffness reduction.
  - The critical factor affecting differences in stiffness behavior was the difference in the water-to-cement-for-cementation ratio (w/c_c) for the two cement contents, with the 2.5% cement-content material having a w/c_c of 9.8 and the 4% cement-content material

having a w/c_c of just 2.45. As a result, the 2.5% cement-content specimens had significantly more free water available for rehydration after microcracking.

  - The long-term effect of microcracking on stiffness was also dependent on the w/c_c ratio, with microcracked material with higher w/c_c ratios recovering stiffness more effectively than material with a lower w/c_c. These materials also achieved stiffness levels similar to, and greater than, specimens/pavement layers that were not microcracked, depending on energy input. Microcracked material with lower w/c_c ratios had levels of recovery that were dependent on curing time after compaction and applied energy input. Longer curing times and increased energy input reduced the level of stiffness recovery.
  - Microcracking facilitated the movement of moisture through the induced microcracks due to increased permeability, allowing access to any unhydrated cement. The higher cement content specimens did not have the same free water available for this later hydration, which in turn limited stiffness recovery after microcracking. Compaction of FDR-C materials in the field is typically performed at or close to the optimum moisture content (OMC) of the material. In order to benefit from the ability of the material to gain stiffness after microcracking, the w/c_c should be optimized. However, increasing the moisture content above the OMC to increase the w/c_c can result in a mix that will have a lower density, reduced strength and stiffness, and increased shrinkage cracking. This supports selection of cement contents for FDR-C that meet the minimum strength requirements (i.e., 300 to 450 psi [≈2.1 to 3.1 MPa]) while still meeting the ICS plus 1% cement requirement.
  - Stiffness reduction was log-linearly correlated with energy input, and independent of the number of cycles or the order of stress sequences.
  - The rate of stiffness reduction with energy input was similar for the different cement contents and microcracking times, except for the 4% cement-content specimens microcracked at 72 hours, which had the lowest rate of stiffness reduction due to the increased strength of the material.

- Indirect Tensile Strength and Stiffness
  - The ITS of the specimens was shown to be linearly correlated with stiffness. It is thus expected that reducing the ITS by microcracking will result in shorter crack spacings and lowering the stiffness will reduce the crack widths. This was, however, not observed in the first four months of FDR-C Test Road crack monitoring. It is hypothesized that the cracks existed, but due to their frequency, they were not visible or had not reflected through the microsurfacing four months after construction.
- Unconfined Compressive Strength with Different Microcracking Efforts
  - Unconfined compressive strength was not significantly affected by the reduction in stiffness due to microcracking. This is likely due to the mechanics of the test method, which applies an axial load on the specimen and compresses the microcracks to their

original state before the specimen fails in shear. The UCS was also poorly correlated with the stiffness after different microcracking efforts.

- Effect of Microcracking on Strength (UCS and ITS)
  - Microcracking at 48 and/or 72 hours effectively reduced the ITS in both the short (i.e., after microcracking) and longer term (i.e., after 56 days). The UCS, tested two days after microcracking, was not significantly affected by microcracking.
  - The stiffness of both the 2.5% and 4% cement-content specimens were linearly correlated with ITS.

7 DEVELOPMENT OF BEHAVIOR MODELS FROM LABORATORY TEST RESULTS

7.1 Introduction

This chapter discusses using the laboratory results presented in Chapter 6, together with the stiffness changes recorded during microcracking on the FDR-C Test Road with a soil stiffness gauge (SSG), to model the effects of curing time and microcracking effort on stiffness, indirect tensile strength (ITS), unconfined compressive strength (UCS), and drying shrinkage. The following models were developed to simulate the effects of microcracking on crack-width and crack-spacing, discussed in Chapter 8:

- A model to predict the stiffness change over time after microcracking with different curing times and efforts
- A model to predict the reduction in stiffness with total energy input
- A generic model for determining the UCS at different time intervals
- A model to determine the effect of microcracking on ITS and UCS
- A model to predict drying shrinkage results

Since the laboratory tests were performed at a single temperature, moisture content, and material gradation, the parameters could only be described within the different cement contents, curing times, and microcracking efforts listed in Table 7.1.

Table 7.1: Microcracking Parameters

Descriptor	Cement Contents (%)	Curing Time before Microcracking (hrs)	Target Stiffness Reduction (%)
Controls	2.5, 4.0	0	0
Microcracked	2.5, 4.0	48, 72, 48 and 72	0, 20, 40, and 60

7.2 Determining Stiffness with Different Microcracking Intervals and Efforts

7.2.1 Introduction

These models were developed to determine the effects of different cement contents, curing time before microcracking, and microcracking effort on the laboratory-measured stiffness of the materials used in the FDR-C Test Road. The long-term stiffness tests discussed in Chapter 6 and summarized in Figure 7.1 and Figure 7.2 for the 2.5% and 4% cement-content specimens, respectively, showed that the material had a certain curing rate, and curing potential, for different cement contents.

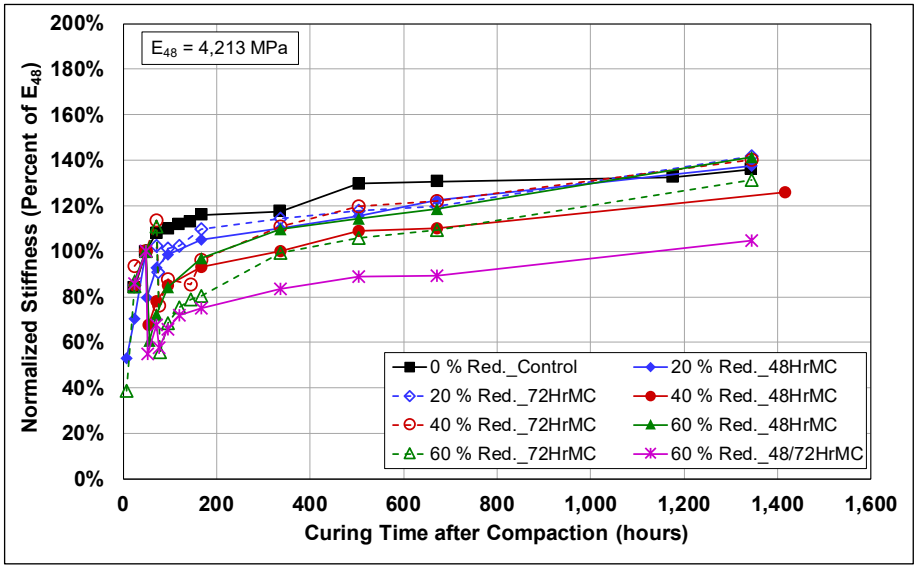

Figure 7.1: 2.5% Cement: Stiffness history of specimens before and after microcracking.

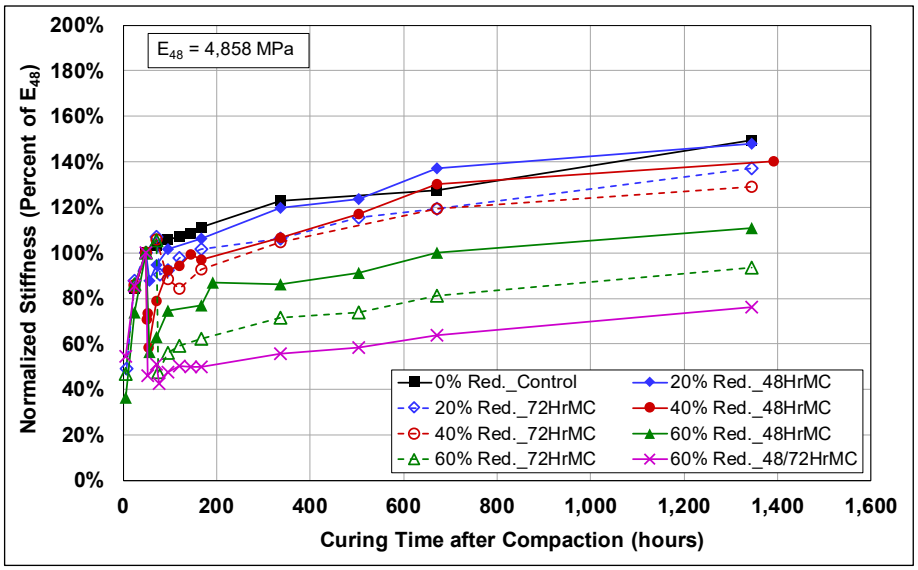

Figure 7.2: 4% Cement: Stiffness history of specimens before and after microcracking.

Microcracking had the following effects on the specimens:

- Microcracking induced damaged and reduced the stiffness.
- The long-term stiffness of the 2.5% cement was less sensitive to the damage induced during microcracking, and showed a greater potential to recover stiffness, compared to the 4% cement-content specimens. The microcracking efforts with lower energy inputs during microcracking also showed the potential to exceed the stiffness of the control specimens.
- The long-term stiffness of the 4% cement materials decreased with increased energy inputs and curing time before microcracking. The 4% cement-content specimens did not recover stiffness as effectively as the 2.5% cement-content specimens.

7.2.2 Model Designs

Nonlinear regression was used to develop a model to describe the average stiffness gain over time of the control specimens (no microcracking) from the laboratory testing. An exponential growth function (Equation 7.1) with parameters including initial stiffness (E_0), cementation potential (A_0) (discussed below), and curing rate (B_0) provided a satisfactory model to effectively describe the stiffness gain of the control specimens.

$$E(t) = E_0 + A_0\left(1 - e^{\left(-1*B_0*10^{-6}*t\right)}\right) \quad \textbf{(7.1)}$$

Where: $E(t)$ = Stiffness over time (MPa)
E_0 = Initial stiffness at t = 0 (MPa)
t = Curing time after compaction (hours)
A_0 = Coefficients determining the maximum increase in stiffness (MPa)
B_0 = Rate of change of stiffness without microcracking

Results from field projects and first-level analyses of the long-term stiffness results with microcracking were used to develop a model that describes stiffness history with microcracking. The results from the field and laboratory testing showed that:

- Stiffness increase was nonlinear. The rate of increase was initially high and then reduced with time.
- The rate of stiffness increase for the 2.5% cement-content material was initially higher than that of the 4% cement-content material. However, the period over which the initially higher rates were observed was longer for the higher cement-content material.
- The initial stiffnesses of the 4% cement-content materials were greater than those with 2.5% cement.
- Microcracking reduced the stiffness, but the stiffness recovered in most instances, attributed to recementation of damaged bonds and hydration of initially unhydrated cement as a result of locally available free water movement through induced microcracks inside the specimen.
- The level of stiffness reduction during microcracking varied among specimens, resulting in differences in stiffness after microcracking, stiffness after 56 days, and continued curing times after microcracking.
- The level of recovery depended on the percent stiffness reduction during microcracking.
- The stiffness of the 4% cement-content materials after microcracking depended on the curing time before microcracking. The 2.5% cement-content material was less sensitive to curing time before microcracking.

- Microcracking at 48 hours and again at 72 hours resulted in the greatest reduction in stiffness.
- Scanning electron microscopy (SEM) results showed sites of cement hydration, but the material was not continuously cemented.

The above statements were considered to support the following roles of primary and secondary cementation in the development of a nonlinear model to describe stiffness history with microcracking:

- Primary cementation is the stiffness increase over time resulting from the cementitious bonds that have hydrated since mixing during construction. This includes the stiffness contribution after microcracking of the portion of the cementitious bonds not damaged during microcracking.
- Secondary cementation is the stiffness increase over time after microcracking, resulting from recementation of damaged, interrupted bonds and hydration of previously unhydrated cement.

The models in Equation 7.2 through Equation 7.4 are proposed to describe stiffness history over time with and without microcracking, using the concepts of primary and secondary cementation, to determine total cementation (stiffness gain over time). The control results, without microcracking, were best described by the exponential growth function in Equation 7.2. With microcracking (Equation 7.3. and Equation 7.4), the growth function was replaced at the time of microcracking with three exponential growth functions to describe the increase in stiffness after microcracking as a result of:

- Continued cementation of undamaged bonds
- Recementation of damaged bonds that were interrupted during microcracking
- Hydration of previously unhydrated cement

This model assumes the following:

- The hydration of the cement is continuous until available water for cementation has reduced below the level required for hydration to continue.
- Unhydrated cement is present in the layer at the time of microcracking.
- Microcracking induces internal microcracks that allow available free water to reach unhydrated cement.
- Some cementitious bonds are interrupted during microcracking, but these recement and continue hydrating thereafter.

The assumptions for the microcracking model are illustrated in Figure 7.3.

$$\frac{E(t)}{E_{48}} = \frac{1}{E_{48}}\left(E_0 + A_0\left(1 - e^{\left(-1*B_0*10^{-3}*t\right)}\right)\right) \quad \textbf{(7.2)}$$

$$\frac{E(t_1 \leq t)}{E_{48}} = \frac{1}{E_{48}}\left((\alpha_1)\{E_0 + A_0[1 - e^{\left(-1*B_0*10^{-3}*t\right)}]\} + (1-\alpha_1)\{A_1[1 - e^{\left(-1*B_1*10^{-3}*t_1\right)}]\} + \{A_{11}[1 - e^{\left(-1*B_{11}*10^{-3}*t_1\right)}]\}\right) \quad \textbf{(7.3)}$$

$$\frac{E(t_2 \leq t)}{E_{48}} = \frac{1}{E_{48}}\left((\alpha_2)\left((\alpha_1)\{E_0 + A_0[1 - e^{\left(-1*B_0*10^{-3}*t\right)}]\} + (1-\alpha_1)\{A_1[1 - e^{\left(-1*B_1*10^{-3}*t_1\right)}]\} + \{A_{11}[1 - e^{\left(-1*B_{11}*10^{-3}*t_1\right)}]\}\right) + (1-\alpha_2)\{A_2[1 - e^{\left(-1*B_2*10^{-3}*t_2\right)}]\} + \{A_{22}[1 - e^{\left(-1*B_{22}*10^{-3}*t_2\right)}]\}\right) \quad \textbf{(7.4)}$$

Where: $E(t)$ = Stiffness over time (MPa)

E_{48} = Stiffness at 48 hours (MPa)

E_0 = Initial relative stiffness at $t = 0$

t = Curing time after compaction (hours)

t_1 = Time after 1st microcracking event, with t_1 = 0 at the time of microcracking (hours)

t_2 = Time after 2nd microcracking event, with t_2 = 0 at the time of microcracking (hours)

A_0 = Primary cementation parameter

A_1, A_2, A_{11}, A_{22} = Secondary cementation parameter

B_0 = Rate of change of stiffness without microcracking

B_1, B_2 = Recementation rate of interrupted cementitious bonds after microcracking

B_{11}, B_{22} = Stiffness gain rate of hydrated cement after microcracking

α_1, α_2 = Portion of the cementitious bonds not damaged due to microcracking

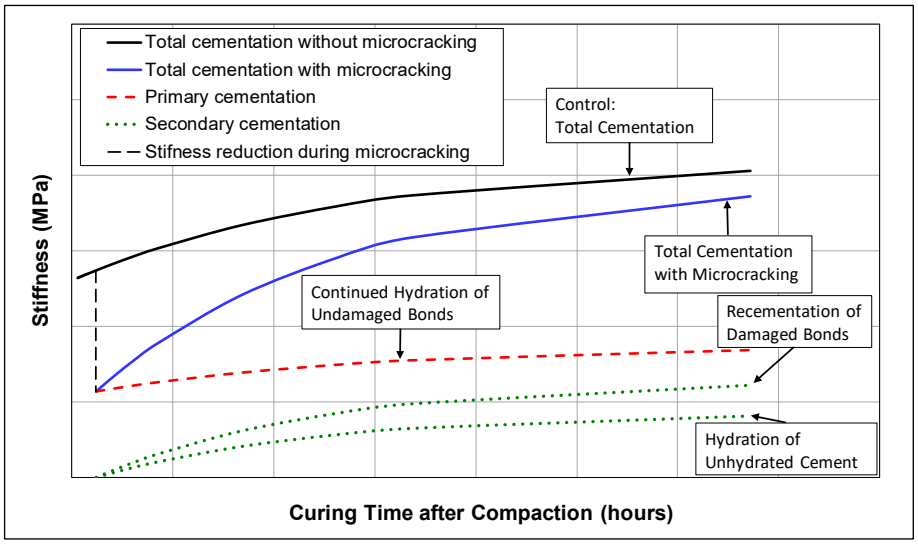

Figure 7.3: Illustration of different mechanisms contributing to stiffness after microcracking.

The concept of primary and secondary cementation potentials was employed to compare their relative contributions to the stiffness at 48 hours of curing for the two cement contents assuming

that the total cementation potential, or final stiffness, normalized to the stiffness at 48 hours, is the sum of the primary and secondary cementation potentials after a duration long enough (t approaches infinity) for the stiffness to plateau. The model coefficients A_0, A_1, A_{11}, A_2 and A_{22}, together with E_0, determine the maximum relative stiffness that can be reached.

Due to the limited scope of the factorial, with only one parent material type and two cement contents, and without being able to provide sufficient constraints on the coefficients, the models proposed in Equation 7.3 and Equation 7.4 could not be fitted without overfitting during the regression analyses. To address this, the secondary cementation components were grouped into a single exponential function to account for recementation of the interrupted bonds, as well as hydration of the previously unhydrated cement. The modified equation for stiffness with a single microcracking effort is provided in Equation 7.5 and for two microcracking efforts in Equation 7.6. Figure 7.4 illustrates the final model parameters.

$$\frac{E(t_1 \leq t)}{E_{48}} = \frac{1}{E_{48}}\left(\left(\frac{\alpha_1}{100}\right)\left\{E_0 + A_0\left[1 - e^{\left(-1*B_0*10^{-3}*t\right)}\right]\right\} + \left(1 - \frac{\alpha_1}{100}\right)\left\{A_1\left[1 - e^{\left(-1*B_1*10^{-3}*t_1\right)}\right]\right\}\right) \quad \textbf{(7.5)}$$

$$\frac{E(t_2 \leq t)}{E_{48}} = \frac{1}{E_{48}}\left(\left(\frac{\alpha_2}{100}\right)\left(\left(\frac{\alpha_1}{100}\right)\left\{E_0 + A_0\left[1 - e^{\left(-1*B_0*10^{-3}*t\right)}\right]\right\} + \left(1 - \frac{\alpha_1}{100}\right)\left\{A_1\left[1 - e^{\left(-1*B_1*10^{-3}*t_1\right)}\right]\right\}\right) + \left(1 - \frac{\alpha_2}{100}\right)\left\{A_2\left[1 - e^{\left(-1*B_2*10^{-3}*t_2\right)}\right]\right\}\right) \quad \textbf{(7.6)}$$

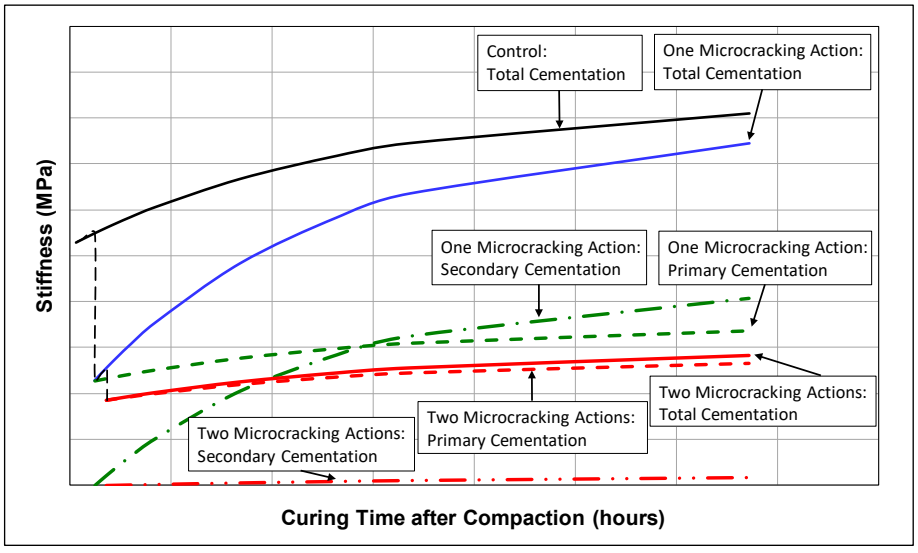

Figure 7.4: Schematic of stiffness model after different microcracking actions.

The total cementation potential, consisting of the primary and secondary cement potentials (Equation 7.7), can be calculated using Equation 7.2, Equation 7.5, and Equation 7.6 for the case

with no microcracking, a single microcracking event, and two microcracking events, respectively, with t of infinity, to obtain Equation 7.8, Equation 7.11, and Equation 7.14. The latter three equations can be further reduced to the primary and secondary cementation potentials for the different microcracking efforts as provided in the following equations:

- Equation 7.9: primary cementation potential without microcracking
- Equation 7.10: secondary cementation potential without microcracking
- Equation 7.12: primary cementation potential with one microcracking effort
- Equation 7.13: secondary cementation potential with one microcracking effort
- Equation 7.15: primary cementation potential with two microcracking efforts
- Equation 7.16: secondary cementation potential with two microcracking efforts

$$CP_{T,i} = CP_{P,i} + CP_{S,i} \quad \textbf{(7.7)}$$

Where: $CP_{T,i}$ = Total cementation potential with i microcracking events
$CP_{P,i}$ = Primary cementation potential with i microcracking events
$CP_{S,i}$ = Secondary cementation potential with i microcracking events
i = 0, 1 or 2 microcracking events.

$$CP_{T,0} = (E_0 + A_0) \quad \textbf{(7.8)}$$

$$CP_{T,0} = CP_{P,0}$$

Where:

$$CP_{P,0} = E_0 + A_0 \quad \textbf{(7.9)}$$

$$CP_{S,0} = 0 \quad \textbf{(7.10)}$$

$$CP_{T,1} = \left(\left(\frac{\alpha_1}{100}\right)\{E_0 + A_0\} + \left(1 - \frac{\alpha_1}{100}\right)\{A_1\}\right) \quad \textbf{(7.11)}$$

$$CP_{T,1} = \left(\left(\frac{\alpha_1}{100}\right) CP_{P,0} + \left(1 - \frac{\alpha_1}{100}\right)\{A_1\}\right)$$

$$CP_{T,1} = \left(CP_{P,1} + CP_{S,1}\right)$$

Where:

$$CP_{P,1} = \left(\frac{\alpha_1}{100}\right) CP_{P,O} \quad \textbf{(7.12)}$$

$$CP_{S,1} = \left(1 - \frac{\alpha_1}{100}\right)\{A_1\} \quad \textbf{(7.13)}$$

$$CP_{T,2} = \left(\left(\frac{\alpha_2}{100}\right)\left(\left(\frac{\alpha_1}{100}\right)\{E_0 + A_0\}\right) + \left(\frac{\alpha_2}{100}\right)\left(1 - \frac{\alpha_1}{100}\right)\{A_1\} + \left(1 - \frac{\alpha_2}{100}\right)\{A_2\}\right) \quad \textbf{(7.14)}$$

$$CP_{T,2} = \left(\left(\frac{\alpha_2}{100} \right) CP_{P,1} + \left(\frac{\alpha_2}{100} \right) CP_{S,1} + \left(1 - \frac{\alpha_2}{100} \right) \{A_2\} \right)$$

$$CP_{T,2} = \left(CP_{P,2} + CP_{S,2} \right)$$

Where:

$$CP_{P,2} = \left(\frac{\alpha_2}{100} \right) \left(\frac{\alpha_1}{100} \right) \{E_0 + A_0\} \quad \textbf{(7.15)}$$

$$CP_{S,2} = \left(\frac{\alpha_2}{100} \right) \left(1 - \frac{\alpha_1}{100} \right) \{A_1\} + \left(1 - \frac{\alpha_2}{100} \right) \{A_2\} \quad \textbf{(7.16)}$$

7.2.3 Analysis Methodology

The analysis was performed using the following steps:

1. Fit Equation 7.2 to the control specimens to quantify A_0, B_0, and E_0 for different cement contents using nonlinear regression.
2. Fit Equation 7.5 to the specimens microcracked at 48 and 72 hours using nonlinear regression with random effects while using A_0, B_0, and E_0 as previously defined. Determine the functional relationships of A_1, B_1, and α_1 with energy input, microcracking intervals, and the water-to-cement-for-cementation ratio (w/c_c).
3. Fit Equation 7.6 to the specimens microcracked at 48 hours and again at 72 hours for the different cement contents to determine A_2, B_2, and α_2 using nonlinear regression with random effects with the parameters A_0, B_0, and E_0 and the functional relationships for A_1, B_1, and α_1.

Random effects in the regression models were considered to determine the effect the difference in energy input during microcracking had on the stiffness recovery of each specimen.

7.2.4 Stiffness Gain with No Microcracking

Nonlinear regression was used to fit Equation 7.2 to the stiffness results for the control specimens with no microcracking, with the stiffness normalized to the stiffness results at 48 hours (results are provided in Appendix B). The coefficients for the fit are provided in Table 7.2 and the fitted results are plotted in Figure 7.5. The R^2 of the fit for each specimen's stiffness at 48 hours was 0.84 for the 2.5% cement-content specimens and 0.81 for the 4% cement-content specimens.

Table 7.2: Fitting Coefficients for Equation 7.2

Coefficient	2.5% Cement	4% Cement
E_0	0.815	0.914
A_0	0.494	0.526
B_0	7.893	2.774

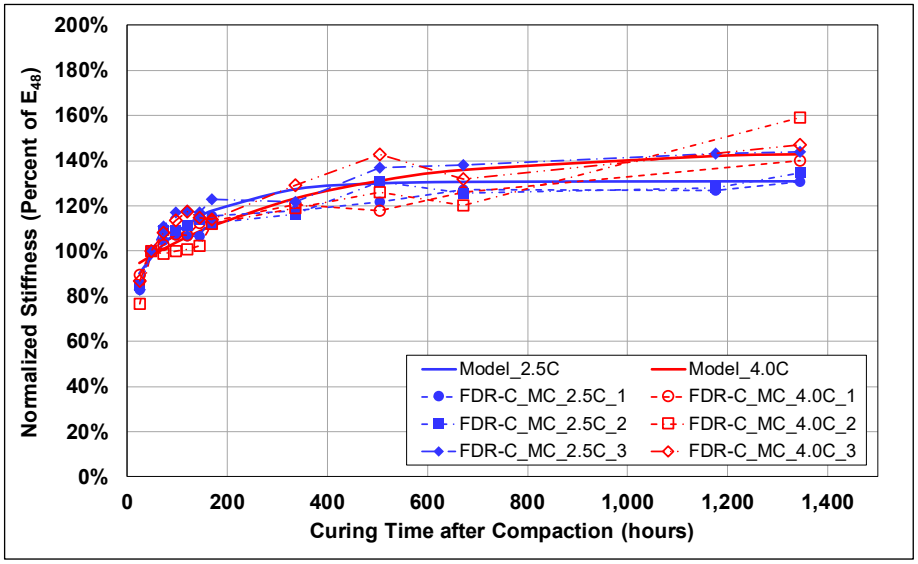

Figure 7.5: Fitted model with no microcracking (normalized to stiffness at 48 hours).

The following inferences can be made about the fit and fitting coefficients for Equation 7.2:

- The cementation rate for the 2.5% cement-content materials was initially fast and thus reached the effective cementation potential relatively early. This was attributed to the high w/c_c providing sufficient moisture for the available cement to hydrate, but, with lower cement content, the reaction time was shorter compared to the 4% cement-content materials.
- The cementation rate for the 4% cement-content materials, although slower than that of the 2.5% cement-content materials, continued over a longer period to reach a higher cementation potential. With the increased cement available, but less water, this reaction was slower, but achieved a higher stiffness.

7.2.5 Stiffness Gain After a Single Microcracking Effort

Modeling of stiffness history with a single microcracking event was completed in two steps:

1. Use nonlinear regression with random effects to fit Equation 7.5 to the stiffness results with a single microcracking effort for each cement content.
2. Determine the effect of energy input, curing time before microcracking, and w/c_c on the fitted parameters for the two cement contents.

Nonlinear Regression with Random Effects

Nonlinear regression with random effects was used to fit Equation 7.5 to the stiffness results with microcracking at 48 and 72 hours for both cement contents to determine the secondary cementation parameter (A_1), the recementation rate after microcracking (B_1), and the portion of

cementitious bonds not damaged during microcracking (α_1). The results are summarized in Appendix B. Observations from microcracking in the laboratory showed that:

- The 2.5% cement-content specimens did not show a consistent trend in the recementation after microcracking for different microcracking efforts (Figure 7.1). Recementation appeared to recover the stiffness to the level of the control specimens, except for the 40% stiffness reduction at 48 hours (40% Red._48HrMC) and 60% stiffness reduction at 72 hours (60% Red._72HrMC). There was no apparent reason for this inconsistency and all results were therefore included in the nonlinear regression.
- A consistent trend was observed in the 4% cement-content specimens (Figure 7.2), indicating that the stiffness recovery after microcracking decreased with increased stiffness reduction and microcracking time.
- Different levels of stiffness reduction were induced for the same microcracking effort (stress sequences) in the laboratory on different specimens.

A random-effects nonlinear fit was used to account for the differences in the percent stiffness reduction for the different microcracking efforts and the variability in the stiffness gain rate and recementation levels. The initial parameters determined from the control specimens (E_0, A_0, and B_0) were used as the initial parameters for each of the different sets. The coefficients for the 2.5% and 4% cement-content specimens are provided in Table 7.3 and Table 7.4, respectively. The initial R^2 values, before providing explanatory variables for the coefficients, were 0.87 and 0.80 for the 2.5% and 4% cement-content results, respectively.

Regression analyses were performed on the coefficients of the different microcracked specimens to determine the relationship of the secondary cementation parameter (A_1), the recementation rate (B_1), and the portion of undamaged bonds (α_1) with energy input, time to microcracking, and w/c_c. The correlation matrix in Figure 7.6 shows that:

- The regression coefficient for A_1 was negatively correlated with microcracking time (*MCTime*) and total energy (*TotalEnergy*), and positively correlated with w/c_c (*wcc*).
- The regression coefficient for recementation rate after microcracking (B_1) was negatively correlated with microcracking time and w/c_c. The total energy during microcracking was not correlated with B_1.
- The regression coefficient for the portion of bonds not damaged during microcracking (α_1) was negatively correlated with total energy.

Table 7.3: 2.5% Cement: Fitted Coefficients for Equation 7.3

Specimen Name	Factorial	A_0	B_0	E_0	A_1	B_1	α_1
FDR-C_MC_2.5C_19	20% Red_48HrMC	0.494	7.893	0.815	1.719	1.436	89.054
FDR-C_MC_2.5C_20	20% Red_48HrMC	0.494	7.893	0.815	1.468	1.430	76.615
FDR-C_MC_2.5C_21	20% Red_48HrMC	0.494	7.893	0.815	1.379	1.428	80.013
FDR-C_MC_2.5C_4	20% Red_48HrMC	0.494	7.893	0.815	2.016	1.443	78.810
FDR-C_MC_2.5C_31	40% Red_48HrMC	0.494	7.893	0.815	1.315	1.428	70.972
FDR-C_MC_2.5C_33	40% Red_48HrMC	0.494	7.893	0.815	1.443	1.429	70.372
FDR-C_MC_2.5C_38	40% Red_48HrMC	0.494	7.893	0.815	1.492	1.432	65.615
FDR-C_MC_2.5C_10	60% Red_48HrMC	0.494	7.893	0.815	1.893	1.444	68.948
FDR-C_MC_2.5C_11	60% Red_48HrMC	0.494	7.893	0.815	2.190	1.453	71.167
FDR-C_MC_2.5C_12	60% Red_48HrMC	0.494	7.893	0.815	1.413	1.433	58.059
FDR-C_MC_2.5C_16	20% Red_72HrMC	0.494	7.893	0.815	1.896	1.033	87.209
FDR-C_MC_2.5C_17	20% Red_72HrMC	0.494	7.893	0.815	2.289	1.037	83.161
FDR-C_MC_2.5C_18	20% Red_72HrMC	0.494	7.893	0.815	2.482	1.041	86.026
FDR-C_MC_2.5C_34	40% Red_72HrMC	0.494	7.893	0.815	3.742	1.073	77.843
FDR-C_MC_2.5C_35	40% Red_72HrMC	0.494	7.893	0.815	1.668	1.032	69.963
FDR-C_MC_2.5C_36	40% Red_72HrMC	0.494	7.893	0.815	1.820	1.039	76.254
FDR-C_MC_2.5C_13	60% Red_72HrMC	0.494	7.893	0.815	1.724	1.035	59.504
FDR-C_MC_2.5C_14	60% Red_72HrMC	0.494	7.893	0.815	1.966	1.036	61.271

Table 7.4: 4% Cement: Fitted Coefficients for Equation 7.3

Specimen Name	Factorial	A_0	B_0	E_0	A_1	B_1	α_1
FDR-C_MC_4.0C_16	20% Red_48HrMC	0.526	2.774	0.914	0.930	21.034	84.315
FDR-C_MC_4.0C_17	20% Red_48HrMC	0.526	2.774	0.914	0.922	21.037	89.745
FDR-C_MC_4.0C_18	20% Red_48HrMC	0.526	2.774	0.914	0.890	21.034	82.596
FDR-C_MC_4.0C_28	40% Red_48HrMC	0.526	2.774	0.914	0.764	21.020	68.622
FDR-C_MC_4.0C_32	40% Red_48HrMC	0.526	2.774	0.914	0.999	20.990	66.417
FDR-C_MC_4.0C_33	40% Red_48HrMC	0.526	2.774	0.914	0.962	21.036	67.371
FDR-C_MC_4.0C_10	60% Red_48HrMC	0.526	2.774	0.914	0.505	21.015	42.536
FDR-C_MC_4.0C_11	60% Red_48HrMC	0.526	2.774	0.914	0.748	21.060	58.128
FDR-C_MC_4.0C_12	60% Red_48HrMC	0.526	2.774	0.914	0.658	21.009	51.477
FDR-C_MC_4.0C_13	20% Red_72HrMC	0.526	2.774	0.914	0.473	3.264	87.101
FDR-C_MC_4.0C_14	20% Red_72HrMC	0.526	2.774	0.914	0.488	3.269	87.764
FDR-C_MC_4.0C_15	20% Red_72HrMC	0.526	2.774	0.914	0.494	3.261	86.176
FDR-C_MC_4.0C_29	40% Red_72HrMC	0.526	2.774	0.914	0.515	3.391	78.626
FDR-C_MC_4.0C_30	40% Red_72HrMC	0.526	2.774	0.914	0.538	3.454	77.316
FDR-C_MC_4.0C_31	40% Red_72HrMC	0.526	2.774	0.914	0.518	3.392	76.113
FDR-C_MC_4.0C_7	60% Red_72HrMC	0.526	2.774	0.914	0.380	2.905	36.907
FDR-C_MC_4.0C_8	60% Red_72HrMC	0.526	2.774	0.914	0.441	3.124	55.234
FDR-C_MC_4.0C_9	60% Red_72HrMC	0.526	2.774	0.914	0.492	3.175	57.880

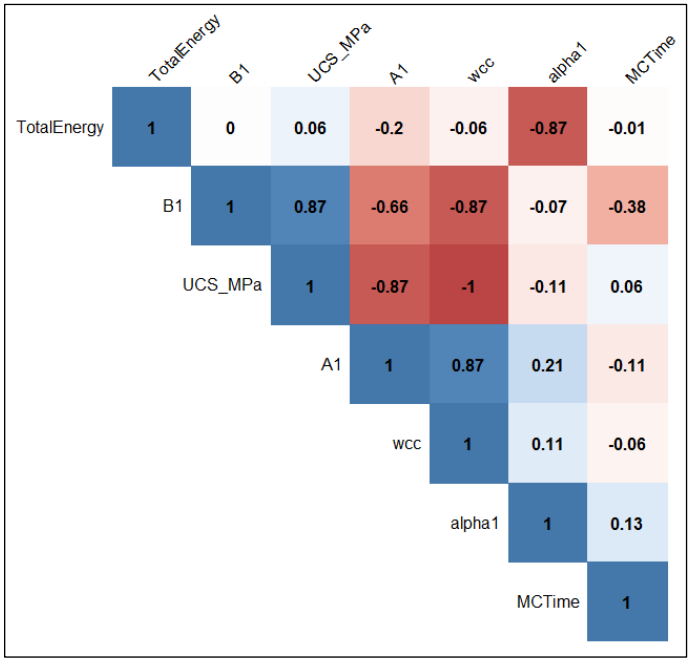

Figure 7.6: Correlation matrix for regression coefficients model (one microcracking event).

Fitting Explanatory Variables to the Secondary Cementation Parameter

The secondary cementation parameter, A_1, was negatively correlated with microcracking time and energy input, and positively correlated with w/c_c. The A_1 values were fitted to Equation 7.17 to determine the relationship between the three parameters. The regression coefficients for the fit, which had an R^2 of 0.70, are provided in Table 7.5.

$$A_1 = \beta_0 + \beta_1 \times MC + \beta_2 \times wcc + \beta_3 \times Energy_T + \beta_4 \times MC \times wcc \quad \textbf{(7.17)}$$

Where: $Energy_T$ = Total energy (Joules/m^3)
wcc = Water-to-cement-for-cementation ratio
MC = Microcracking time (hours)
$\beta_0 - \beta_4$ = Regression coefficients

Table 7.5: Regression Coefficients for Equation 7.17

Term	Coefficient	Estimate	Std. Error	t-value	Pr(>|t|)
(Intercept)	β_0	1.83	0.61	2.99	5.46E-03
MC	β_1	-2.58E-02	1.01E-02	-2.57	1.52E-02
wcc	β_2	-1.31E-01	8.51E-02	-1.54	0.13
$Energy_T$	β_3	-9.34E-05	1.26E-04	-0.74	0.46
$MC \times wcc$	β_4	5.03E-03	1.41E-03	3.57	1.20E-03

To determine whether any of the variables were significant, a t-test was performed with a null hypothesis of β_0 =…= β_3 = 0, and an alternative hypothesis that β_0 … $\beta_3 \neq 0$. The t-value at a 95% confidence interval was t(0.975, 32) = 2.037. The t-value for the interaction between

microcracking time and the interaction between microcracking time and w/c_c exceeded the t-statistic. The t-value for total energy was significantly less than the t-statistic, indicating that it did not provide any significance to explain A_1.

The data for A_1 were fitted to Equation 7.18, which excludes total energy input. The final coefficients for Equation 7.18 are provided in Table 7.6. The R^2 for the fit was 0.78. Figure 7.7 illustrates the relationship between A_1 and microcracking time for the two w/c_c values. The results show that:

- The secondary cementation parameter was greater for the higher w/c_c associated with the 2.5% cement-content mix design when compared to the secondary cementation potential for the lower w/c_c for the mix design with 4% cement. This was attributed to the increased water available for recementation and hydration of the remaining unhydrated cement.
- The secondary cementation parameter increased with curing time before microcracking for the 2.5% cement-content material but decreased for the material with 4% cement. This was attributed to the higher w/c_c of the 2.5% cement-content material.

$$A_1 = \beta_0 + \beta_1 \times MC + \beta_2 \times wcc + \beta_3 \times MC \times wcc \quad \textbf{(7.18)}$$

Table 7.6: Regression Coefficients for Equation 7.18

Term	Coefficient	Estimate	Std. Error	t-value	Pr(>|t|)
(Intercept)	β_0	1.83	0.61	3.01	5.05E-03
MC	β_1	-2.66E-02	9.93E-03	-2.38	1.15E-02
wcc	β_2	-0.14	8.44E-02	-1.60	0.12
$MC \times wcc$	β_3	5.12E-03	1.39E-03	3.68	8.64E-04

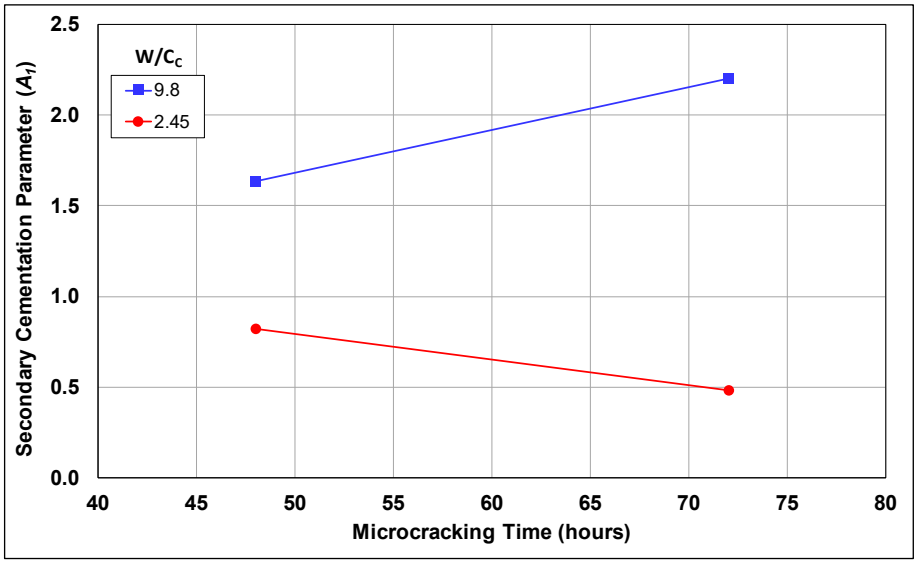

Figure 7.7: Relationship between A_1 and microcracking time for two w/c_c values.

Fitting Explanatory Variables to the Recementation Rate After Microcracking

The recementation rate after microcracking parameter (B_1) was negatively correlated with microcracking time and w/c_c. Equation 7.19 was proposed to determine the effect of microcracking time and w/c_c on B_1.

$$B_1 = \beta_0 + \beta_1 \times MC + \beta_2 \times wcc + \beta_3 \times MC \times wcc \quad \textbf{(7.19)}$$

Where: β_0, β_1 = Regression coefficients

Linear regression was used to fit Equation 7.19 to the B_1 coefficients for all the fitted results. The regression coefficients are provided in Table 7.7. The R^2 for the fit was 0.99.

Table 7.7: Regression Coefficients for Equation 7.19

Term	Coefficient	Estimate	Std. Error	t-value	Pr(>|t|)
(Intercept)	β_0	74.70	0.14	536.40	<2e-16
MC	β_1	-9.82E-01	2.28E-03	-431.00	<2e-16
wcc	β_2	-7.40	1.94E-02	-381.90	<2e-16
$MC \times wcc$	β_3	9.85E-02	3.20E-04	308.00	<2e-16

To determine whether microcracking time and w/c_c were significant, a t-test was performed with a null hypothesis that $\beta_0 \ldots \beta_3 = 0$ and an alternative hypothesis that $\beta_0 \ldots \beta_3 \neq 0$. The t-value at a 95% confidence interval was t(0.975,31) = 2.04. The null hypothesis was rejected since the absolute value of the t-value for all the coefficients was greater than 2.04. The relationships between B_1 and the different microcracking times and w/c_c are provided in Figure 7.8.

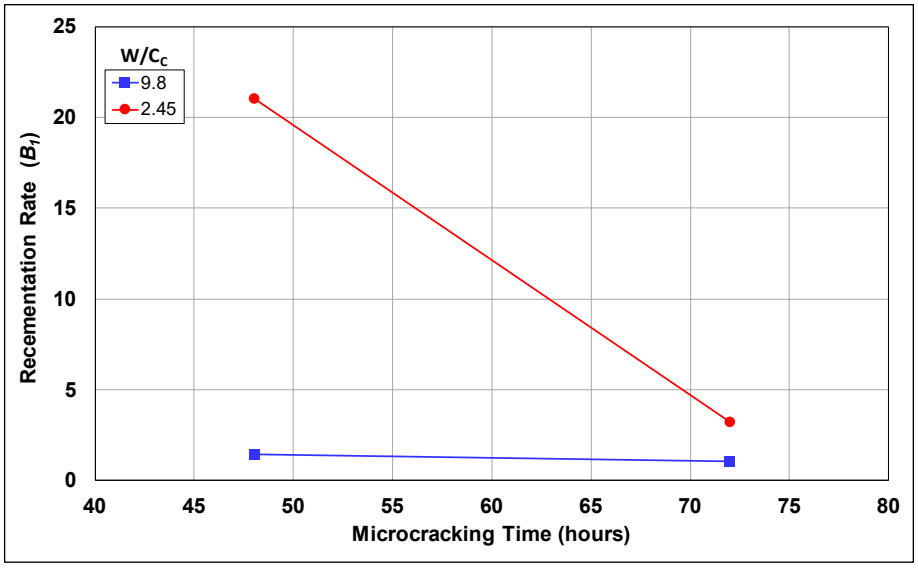

Figure 7.8: Relationships between B_1 and different microcracking times and w/c_c.

The results show that:

- The recementation rate for the 4% cement-content material, with a w/c_c of 2.45, was faster than that of the 2.5% cement-content material. This was attributed to the higher percentage of available unhydrated cement, which had access to free water after microcracking. However, with less free water available, this faster rate would only be sustained for a short period. The reduction in the recementation rate with curing time before microcracking was attributed to the reduced free water available after the additional 24 hours of curing.
- The recementation rate of the 2.5% cement-content material with a w/c_c of 9.8 was lower than the 4% cement-content material and unaffected by the longer curing time before microcracking. This was attributed to the reduced unhydrated cement available, but with sufficient free water available to achieve similar recementation rates after the two microcracking times.

Fitting Explanatory Variables to the Coefficient for Undamaged Bonds

The α_1 parameter, which represents the portion of the cementitious bonds not damaged during the first microcracking event, was negatively correlated to the total energy applied during microcracking. Using linear regression, Equation 7.20 was fitted to the α_1 coefficients for all specimens subjected to a single microcracking event. The regression coefficients are provided in Table 7.8. The R^2 for the fit was 0.74. A t-test was performed with a null hypothesis of $\beta_0 ... \beta_1 = 0$, and an alternative hypothesis that $\beta_0 ... \beta_1 \neq 0$, to determine whether the total energy input was significant. The t-value at a 95% confidence interval was t(0.975,35) = 2.03. The null hypothesis was therefore rejected given that the absolute value of the t-value for β_0 and β_1 was greater than 2.03, confirming that α_1 reduces with increased energy input.

$$\alpha_1 = \beta_0 + \beta_1 \log(Energy_T) \quad \textbf{(7.20)}$$

Where: β_0, β_1 = Regression coefficients

Table 7.8: Regression Coefficients for Equation 7.20

Term	Coefficient	Estimate	Std. Error	t-value	Pr(>|t|)
(Intercept)	β_0	103.94	3.50	29.66	<2e-16
$\log(Energy_T)$	β_1	-6.72	0.69	-9.71	2.46E-11

Regression Analyses of the Stiffness Reduction During Microcracking

The relationship between the amounts of energy input required to reduce stiffness to a desired level was investigated during laboratory testing (Section 6.2). The results showed that:

- Stiffness reduced log-linearly with energy input.

- There was no significant difference in the stiffness reduction between 48- and 72-hour microcracking times for the 2.5% cement-content specimens.
- The stiffness reduction of the 4% cement-content specimens was lower than the 2.5% cement-content specimens.
- The stiffness reduction for microcracking at 72 hours was lower than the rate at 48 hours for the 4% cement-content specimens.

The regression model in Equation 7.21 was proposed for determining the effect of total energy, cement content, and curing time before microcracking on stiffness. The interaction between cement content and energy input, and between curing time before microcracking and energy input, were also considered. Linear regression was used to fit Equation 7.21 to the stiffness reduction results recorded during microcracking. The model coefficients are provided in Table 7.9. The R^2 of the fit was 0.88.

$$E_{Red} = \beta_0 + \beta_1 \times \log(Energy_T) + \beta_2 \times MC + \beta_3 \times UCS \quad \textbf{(7.21)}$$

Where: E_{Red} = Percent stiffness reduction during microcracking
β_0, β_1 = Regression coefficients

Table 7.9: Regression Coefficients for Stiffness Versus Energy Input in Equation 7.21

Term	Coefficient	Estimate	Std. Error	t-value	Pr(>|t|)
(Intercept)	β_0	0.04	0.09	0.42	6.78E-01
$\log(Energy_T)$	β_1	8.68E-02	5.64E-03	15.40	2.38E-16
MC	β_2	0.00	7.85E-04	-0.85	0.40
UCS	β_3	-6.34E-03	1.82E-02	-0.35	7.30E-01

A t-test was conducted to determine the significance of the different predictor variables on stiffness reduction during microcracking. The t-test had a null hypothesis of $\beta_0 ... \beta_3 = 0$, and an alternative hypothesis that $\beta_0 ... \beta_3 \neq 0$. The t-value at a 95% confidence interval was t(0.975, 32) = 2.04. The null hypothesis was rejected since the absolute value of the t-values for β_2 and β_3 were less than 2.04, confirming that the percent stiffness reduction during microcracking was not significantly affected by design strength, cement content, or the additional 24-hour cure time from 48 hours to 72 hours, even though a small difference was observed in the results.

Considering the results from the regression analysis of Equation 7.21, a final model for the relationship between microcracking effort and stiffness reduction is proposed in Equation 7.22. The coefficients for the equation are provided in Table 7.10. The R^2 of the fit was 0.88.

$$E_{Red} = \beta_0 + \beta_1 \times \log(Energy_T) \quad \textbf{(7.22)}$$

Where: β_0, β_1 = Regression coefficients

Table 7.10: Regression Coefficients for Stiffness versus Energy Input in Equation 7.22

Term	Coefficient	Estimate	Std. Error	t-value	Pr(>|t|)
(Intercept)	β_0	-2.73E-02	2.80E-02	-0.98	3.36E-01
$\log(Energy_T)$	β_1	8.66E-02	5.54E-03	15.65	<2e-16

7.2.6 Final Microcracking Model for a Single Microcracking Event

The final model for determining stiffness change over time with a single microcracking event, with different stiffness reduction levels, is provided in Equation 7.23. The initial coefficients (E_0, A_0, and B_0) for the two cement contents are provided in Table 7.2. The average stiffness at 48 hours for the 2.5% and 4% cement-content materials before microcracking were 4,213 and 4,858 MPa, respectively. Using the equations for the fitted parameters, the R^2 of the fit for the single microcracking event specimens was 0.74.

$$\frac{E(t_1 \le t)}{E_{48}} = \left(\left(\frac{\alpha_1}{100}\right)\left\{E_0 + A_0\left[1 - e^{\left(-1 * B_0 * 10^{-6} * t\right)}\right]\right\} + \left(1 - \frac{\alpha_1}{100}\right)\left\{A_1\left[1 - e^{\left(-1 * B_1 * 10^{-6} t_1\right)}\right]\right\}\right) \quad \textbf{(7.23)}$$

Where: $A_1 = 1.836 - 0.026 \times MC - 0.135 \times wcc + 0.005 \times MC \times wcc$

$B_1 = 74.7 - 0.982 \times MC - 7.395 \times wcc + 0.099 \times MC \times wcc$

$\alpha_1 = 103.94 - 6.72 \times \log(Energy_{Total})$

$E_{Red} = -0.027 + 0.087 \times \log(Energy_{Total})$

The fitted results to the average normalized stiffness are provided in:

- Figure 7.9 for the 2.5% cement-content specimens with microcracking at 48 hours
- Figure 7.10 for the 2.5% cement-content specimens with microcracking at 72 hours
- Figure 7.11 for the 4% cement-content specimens with microcracking at 48 hours
- Figure 7.12 for the 4% cement-content specimens with microcracking at 72 hours

Discussion

The total, primary and secondary cementation potentials were calculated to compare the effect of microcracking of the cementation potentials for the following:

- No microcracking
- 20%, 40%, and 60% stiffness reduction with microcracking at 48 hours
- 20%, 40%, and 60% stiffness reduction with microcracking at 72 hours

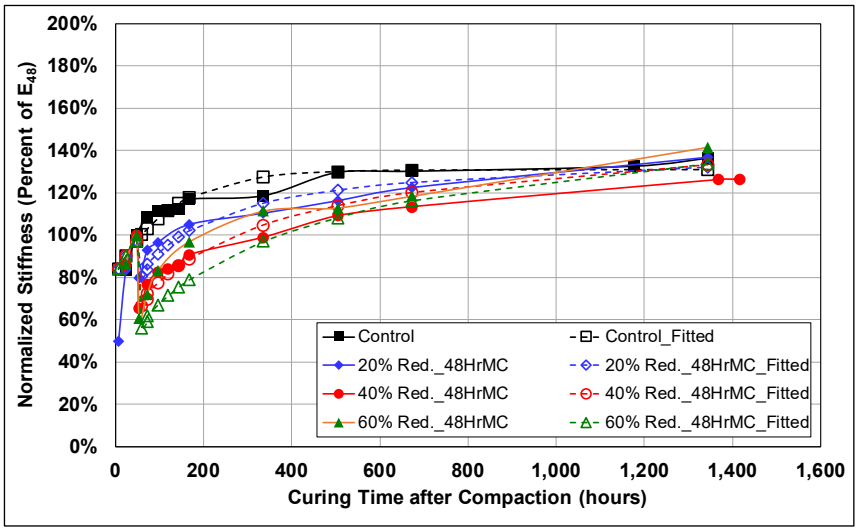

Figure 7.9: 2.5% Cement: Fitted versus average normalized stiffness (48-hour cure).

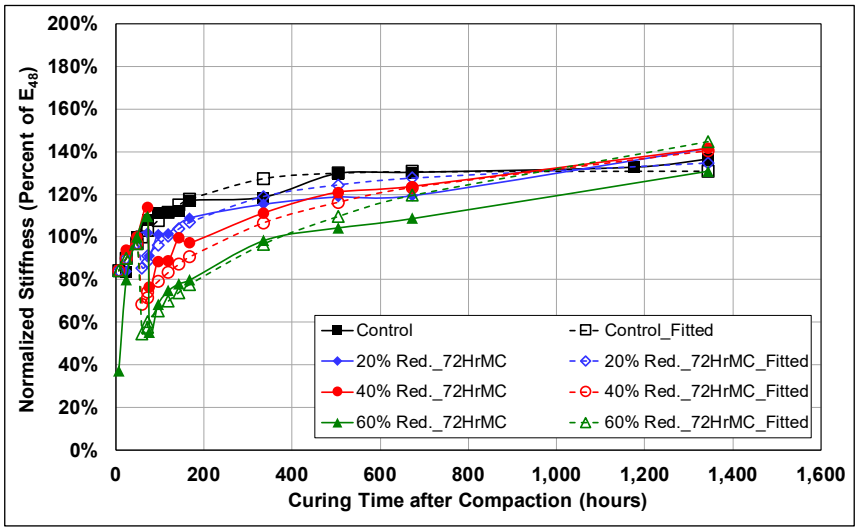

Figure 7.10: 2.5% Cement: Fitted versus average normalized stiffness (72-hour cure).

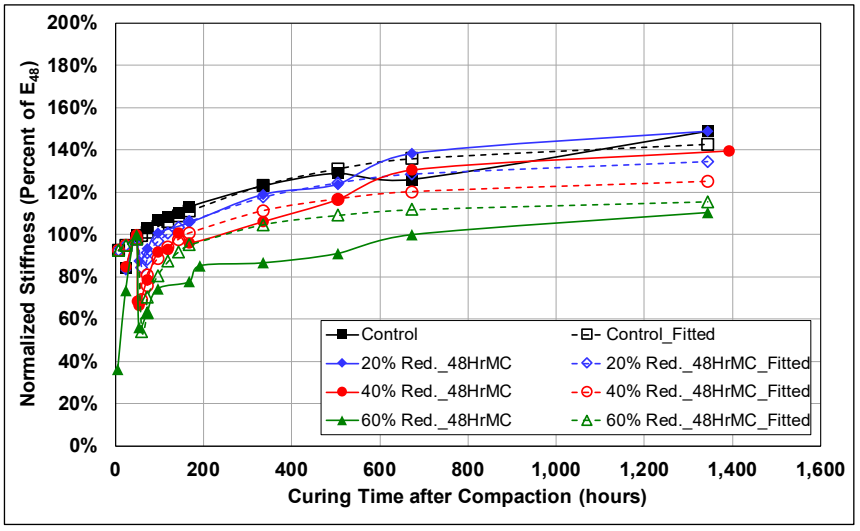

Figure 7.11: 4% Cement: Fitted versus average normalized stiffness (48-hour cure).

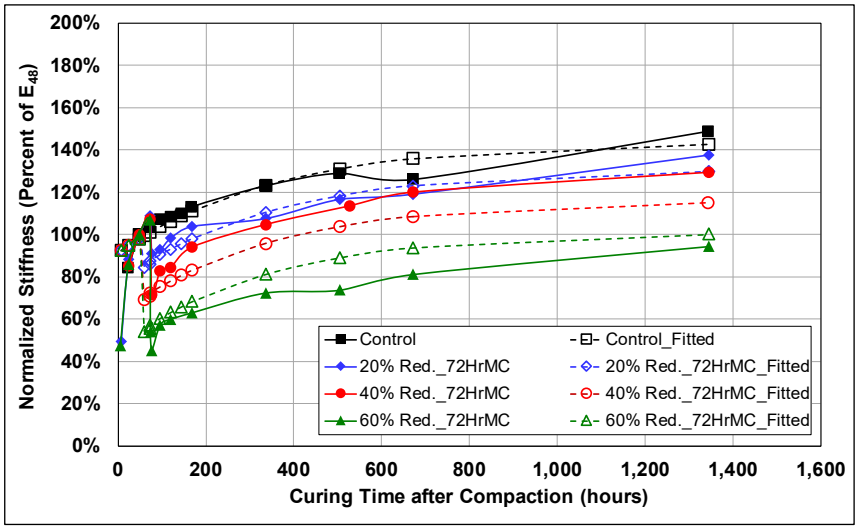

Figure 7.12: 4% Cement: Fitted versus average normalized stiffness (72-hour cure).

The calculated cementation potentials for the 2.5% and 4% cement-content materials are provided in Figure 7.13 and Figure 7.14, respectively, and compared in Figure 7.15. The results show that:

- For the 2.5% cement-content material:
  - The total cementation potential increased with increased microcracking (additional energy input) and curing time before microcracking.
  - The primary cementation potential reduced as the portion of bonds not damaged during microcracking (α_1), decreased.
  - The secondary cementation potential increased with increased stiffness reduction and curing time before microcracking.
- For the 4% cement-content material:
  - The total cementation potential decreased with increased microcracking and curing time before microcracking.
  - The secondary cementation potential increased with increased microcracking but decreased with increased curing time before microcracking.

The comparison of the cementation potentials in Figure 7.15 shows the mechanisms that contributed to the behavior noted in the 2.5% and 4% cement-content specimen results in Figure 7.13 and Figure 7.14, respectively. The following observations were made:

- With the portion of the bonds not damaged during microcracking only being a function of total energy input, the reduction in primary cementation potential was similar for both cement contents and microcracking times.
- The secondary cementation potential of the 2.5% cement-content material contributed sufficiently to the total cementation potential for the microcracked material to exceed the cementation potential of the material without microcracking.
- The secondary cementation potential of the material with 4% cement showed a reduction in cementation potential with increased microcracking effort, attributed to the difference in the w/c_c ratios. It was initially proposed in the development of the stiffness model with microcracking that the secondary cementation covered two mechanisms, namely the recementation of damaged bonds and the hydration of previously unhydrated cement, both of which require water to occur and to sustain the action of contributing to the strength and stiffness of the matrix. It is clear from the results that increasing the cement content did not contribute to increased secondary cementation potential, while increasing the w/c_c did. This shows the benefit of maximizing the w/c_c as part of the mix design when microcracking is specified by optimizing the cement content required for a specific material using a combination of initial consumption of stabilizer (ICS) and UCS tests.

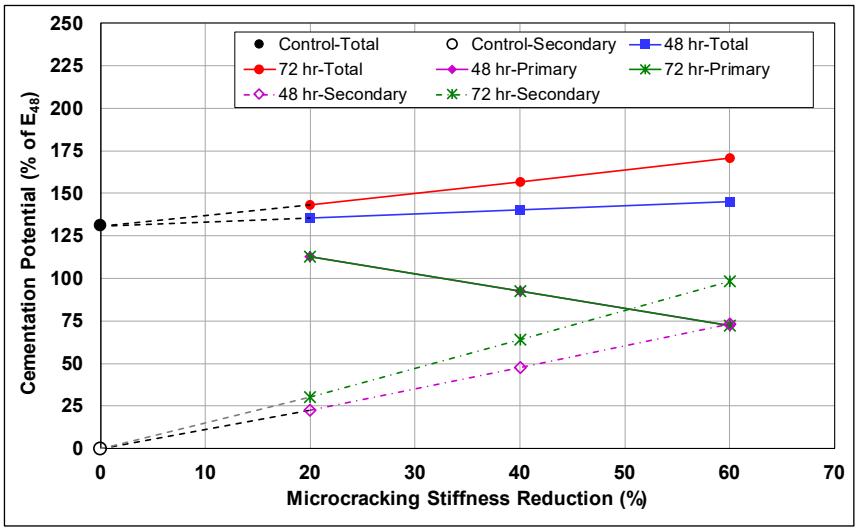

Figure 7.13: 2.5% Cement: Calculated cementation potential (one microcracking event).

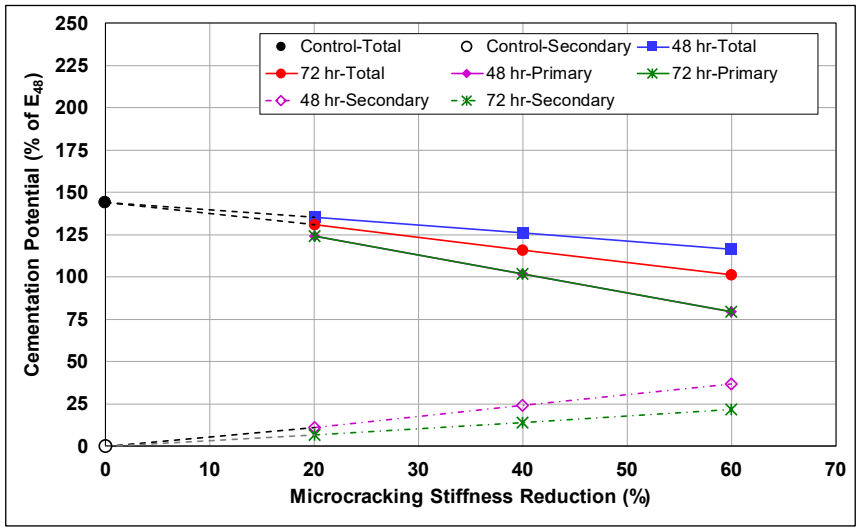

Figure 7.14: 4% Cement: Calculated cementation potential (one microcracking event).

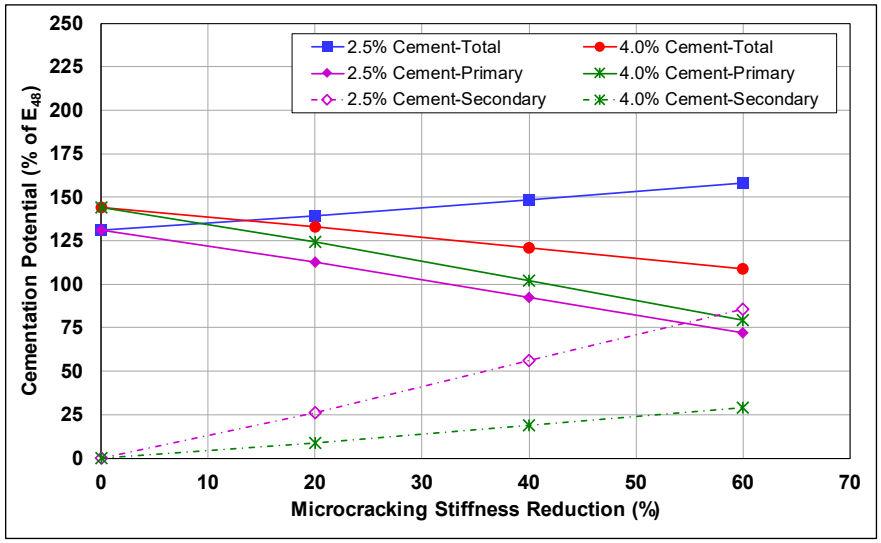

Figure 7.15: Comparison of 2.5% and 4% cementation potentials (one microcracking event).

- The increased cementation potential in the 2.5% cement-content material when microcracked at 72 hours compared to microcracking at 48 hours was attributed to the increased bonds that developed over the additional 24-hour curing period before microcracking. Microcracking damaged a larger number of bonds in the 72-hour curing specimens, and the available water allowed the damaged bonds to rehydrate thereby increasing the cementation potential.

The final calculated stiffnesses for the two cement contents, with the different microcracking efforts, are provided in Figure 7.16. The total cementation potentials were multiplied by the average stiffness at 48 hours for the different cement contents to determine the final asymptotic stiffness. The results show that the material with 4% cement with no microcracking had a higher stiffness than the material with 2.5% cement, as expected, but that with microcracking, the stiffness of the material with 2.5% cement quickly exceeded that of the 4% cement-content material.

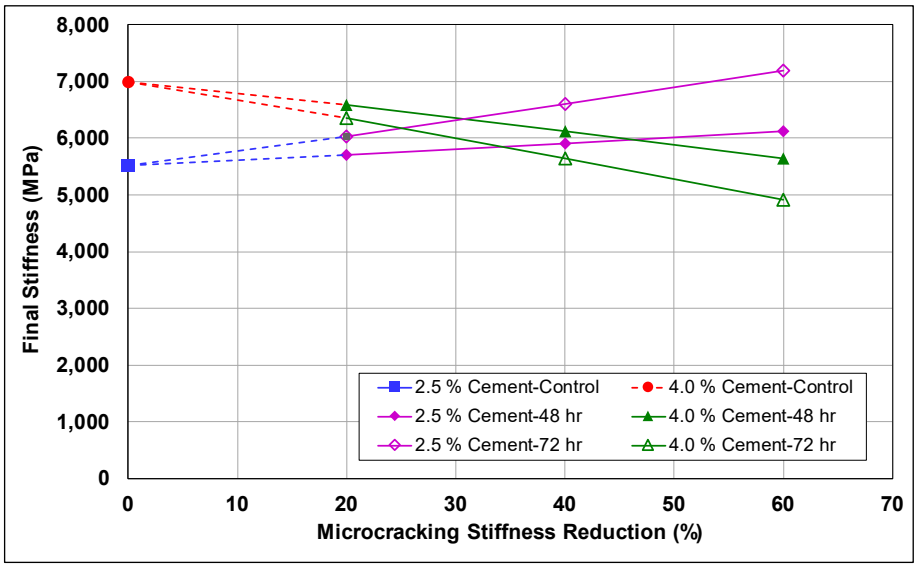

Figure 7.16: Calculated final stiffness (one microcracking event).

7.2.7 Stiffness Gain After a Second Microcracking Effort

The model for predicting stiffness gain after a second microcracking effort required the models for both the unmicrocracked controls (Equation 7.2) and for a single microcracking event with the fitted regression coefficients (Equation 7.23). Equation 7.6 was fitted to the stiffness gain results for the microcracking efforts at 48 hours and again at 72 hours for the two cement contents. A random-effects nonlinear fit was used to account for the differences in the percent stiffness

reduction during the second microcracking event, and the variability in recementation rates and secondary cementation levels. Stiffness data were grouped by cement content. The R^2 fit for the 2.5% and 4% cement-content results were 0.89 and 0.71, respectively. The fitted coefficients for A_2, B_2, and α_2 are provided in Table 7.12 and Table 7.13 for the 2.5% and 4% cement-content specimens, respectively.

Table 7.11: 2.5% Cement: Fitted Coefficients for Equation 7.6

Specimen Name	Factorial	A_1	B_1	α_1	A_2	B_2	α_2
FDR-C_MC_2.5C_7	60%Red_48/72HrMC	1.633	1.436	60.037	0.383	1.119	68.226
FDR-C_MC_2.5C_8	60%Red_48/72HrMC	1.633	1.436	64.573	0.383	1.118	47.536
FDR-C_MC_2.5C_9	60%Red_48/72HrMC	1.633	1.436	64.285	0.383	1.119	57.866

Table 7.12: 4% Cement: Fitted Coefficients for Equation 7.6

Specimen Name	Factorial	A_1	B_1	α_1	A_2	B_2	α_2
FDR-C_MC_4.0C_4	60%Red_48/72HrMC	0.820	21.026	53.201	0.434	0.478	40.633
FDR-C_MC_4.0C_5	60%Red_48/72HrMC	0.820	21.026	64.573	0.434	0.479	44.796
FDR-C_MC_4.0C_6	60%Red_48/72HrMC	0.820	21.026	64.285	0.434	0.477	39.316

Figure 7.17 shows the correlation between the fitted parameters and explanatory variables. The strong multicollinearity between the predictor variables and the coefficients was attributed to the small factorial. The explanatory variables were thus not fitted to the coefficients as no useful generalized model could be developed with the limited data.

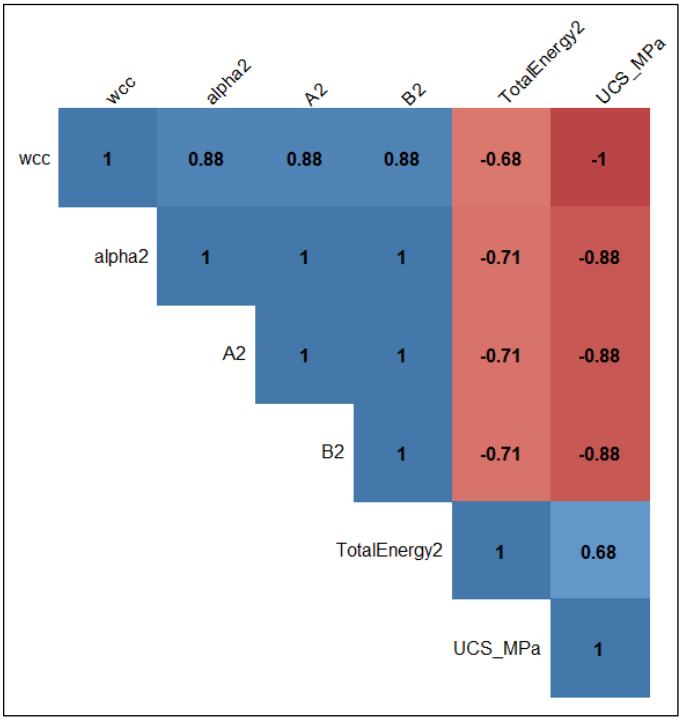

Figure 7.17: Correlation matrix for regression coefficients model (two microcracking events).

Discussion

Models for A_2, B_2, and α_2 were not developed due to the limited dataset for microcracking at 48 hours and again at 72 hours. The initial goal was to reduce the stiffness by 60% at 48 hours, allow stiffness to recover over a 24-hour period, and then reduce it by 60% again during the second 72-hour microcracking event. The target reduction of 60% was achieved at 48 hours, but only a 20% reduction was achieved after the second microcracking event for both cement contents. The same microcracking sequences were used during the 72-hour microcracking event, but the energy input was insufficient to reduce the stiffness to the desired level.

Figure 7.18 illustrates the cementation potentials for the double microcracking event for both the 2.5% and 4% cement-content specimens, calculated using Equation 7.14 and Equation 7.15. The cementation potential results for both cement contents at 48 and 72 hours, with 60% stiffness reduction, are included for reference.

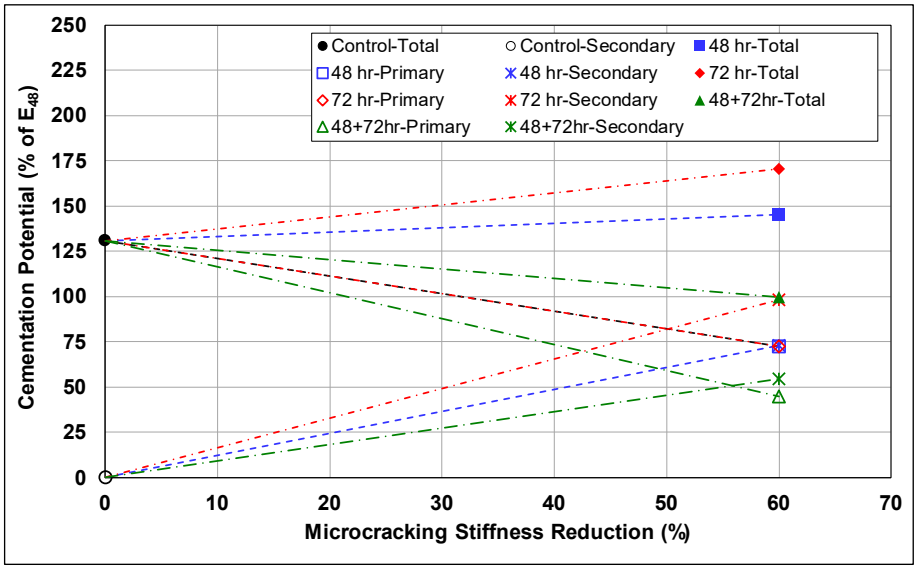

Figure 7.18: 2.5% Cement: Calculated cementation potential (two microcracking events).

The results for the 2.5% cement-content specimens with microcracking at 48 hours and again at 72 hours show that:

- The total cementation potential reduced to a level below that of the specimens with no microcracking.
- The primary cementation potential reduced after the second microcracking effort.
- The additional damage induced by the second microcracking effort could not be recovered through recementation and hydration.

- The second microcracking effort damaged the secondary cementation that had developed after the first microcracking effort and caused additional damage to the primary cementation.
- The secondary cementation potential contribution decreased after the second microcracking effort and was lower than expected considering the increased potential for free water availability for unhydrated cement and damaged bonds. It is likely that either the free water availability was reduced sufficiently to limit the potential for secondary cementation, or that the available 0.5% cement for cementation was fully consumed after the first microcracking effort, leaving no additional cement for additional hydration.
- The benefit (increased stiffness) observed with microcracking on the 2.5% cement-content materials can be lost with excessive energy input.

The results for the 4% cement-content material with microcracking at 48 hours and again at 72 hours are plotted in Figure 7.19.

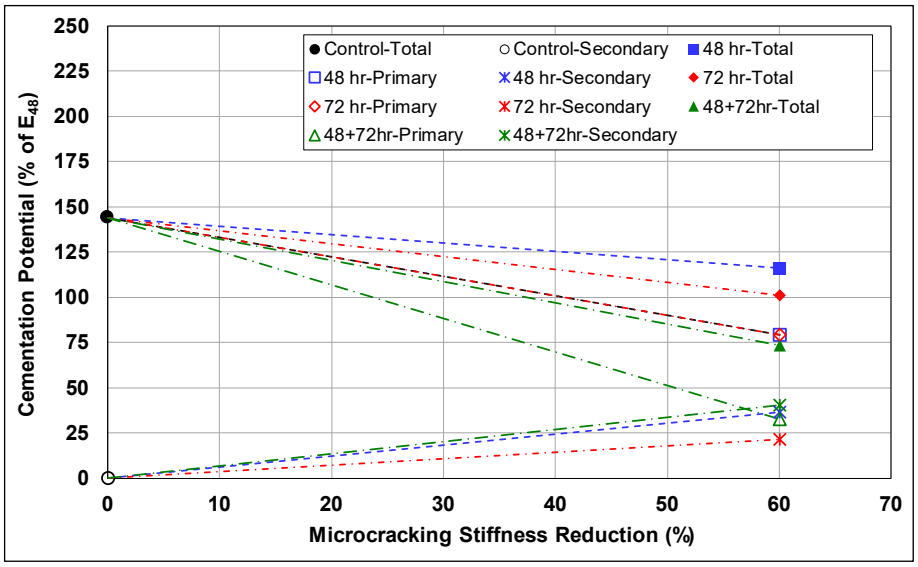

Figure 7.19: 4% Cement: Calculated cementation potential (two microcracking events).

The results show that:

- Similar trends to those of the 2.5% cement-content specimens, except for the contribution of the secondary cementation, were observed.
- The total cementation potential reduced significantly after the additional microcracking effort.
- The primary cementation potential reduced after the second microcracking effort.
- The secondary cementation potential contribution did not change significantly when compared to that of the specimens microcracked at 72 hours to 60% of the stiffness at

48 hours, indicating that the additional damage from the microcracking initiated recovery through recementation of existing bonds and hydration of unhydrated cement.

- The rate of stiffness recovery decreased with increased energy input.

7.2.8 Field and Laboratory Stiffness Reduction Comparison

The stiffness reduction model developed using the SSG data in the field and discussed in the Phase 2a report (Equation 7.6 in Section 7.4) *(12)* used the linear total force applied by the roller as energy input to determine the stiffness reduction per pass. No data were available from the roller or instrumentation to determine the pavement response to calculate the induced energy during microcracking. The laboratory-measured stiffness reduction with total energy input (Equation 7.24) was therefore used to calibrate the field-determined model to calculate a shift factor for the linear total force to approximate an equivalent total energy input.

$$E_{Red} = \beta_0 + \beta_1 \times k \times Energy_{T_{Field}} + \beta_2 \times UCS + \beta_3 \times MCTime \quad \textbf{(7.24)}$$

Where: $Energy_{T_{Field}}$ = Total applied force during microcracking

k = Shift factor for equivalent total energy applied in the laboratory

The field- and laboratory-stiffness reduction models are plotted in Figure 7.20. Linear regression models with a zero intercept were calculated for each model to determine the slope of the energy reduction curves. The slopes of the two models were used to calculate a shift factor of 1.26 between laboratory- and field-measured stiffness reductions. Applying this shift factor to the linear total energy calculated for the rollers provides an equivalent total energy input that can be used to calculate the stiffness reduction during microcracking (Figure 7.21).

7.3 Effect of Microcracking on Long-Term Indirect Tensile Strength

The relationship between long-term stiffness and ITS is required to determine the effect of microcracking on ITS and, from this, the effect of microcracking on crack-width and crack-spacing based on the models by Zhang and Li *(32)*. The long-term stiffness versus ITS results are discussed in Section 6.3. The analyses of the long-term stiffness versus ITS results indicated that ITS increased with increased stiffness and cement content. Regression analyses were performed on the results to determine the relationship between stiffness and strength, and if it is dependent on the cement content.

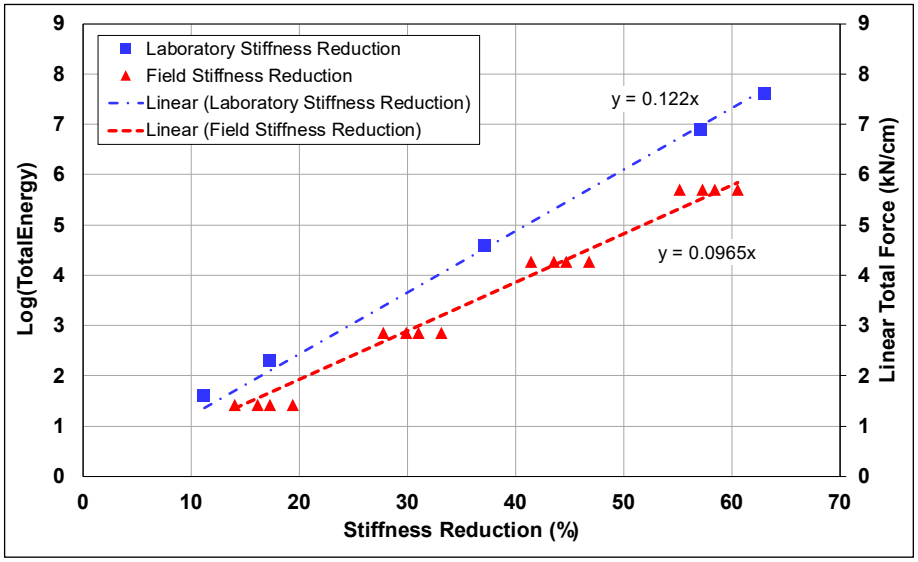

Figure 7.20: Field and laboratory stiffness reduction with linear total force and energy input.

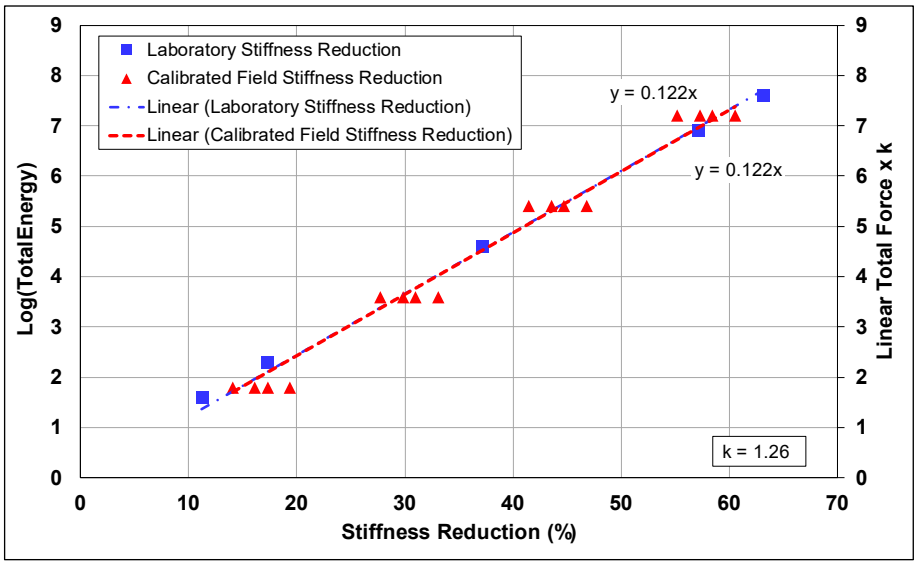

Figure 7.21: Calibrated field stiffness reduction compared to laboratory stiffness reduction.

Based on the analysis of the long-term stiffness and ITS results, Equation 7.25 was proposed to determine the relationship between the mean ITS and stiffness for different cement contents using linear regression. The model coefficients are provided in Table 7.13. The R^2 of the fit was 0.66.

$$ITS = \beta_0 + \beta_1 \times E + \beta_2 \times X_1 \times E \quad \textbf{(7.25)}$$

Where: *ITS* = Indirect tensile strength (kPa)

E = Shift factor for equivalent total energy applied in the laboratory

$\beta_0, \beta_1, \beta_2$ = Regression coefficients

X_1 = Indicator variable; 0 = 2.5% cement, 1 = 4% cement

Table 7.13: Regression Coefficients for ITS Versus Time in Equation 7.25

Term	Coefficient	Estimate	Std. Error	t-value	Pr(>|t|)
(Intercept)	β_0	258.9	33.66	7.69	8.30E-12
E	β_1	0.040	0.01	6.75	8.41E-10
$X_1 \times E$	β_2	0.023	0.00	8.66	6.24E-14

A t-test was performed to determine the effect of cement content on the rate of ITS increase with stiffness. The null hypothesis was $\beta_2 = 0$, and the alternative hypothesis was $\beta_2 \neq 0$. The t-value at a 95% confidence interval was t(0.975, 105) = 1.98, which is less than 8.66, indicating that the null hypothesis can be rejected. Thus, the ITS increase with stiffness was greater for the 4% cement-content specimens than the 2.5% cement-content specimens.

The final relationship for ITS versus stiffness is provided in Equation 7.26, which shows that the ITS increased at a faster rate for the 4% cement-content specimens compared to the 2.5% cement-content specimens.

$$ITS = \beta_0 + \beta_1 \times E \quad \textbf{(7.26)}$$

Where: β_0 = 258.5 kPa

β_1 = 0.04 for 2.5% cement, 0.063 for 4% cement

7.4 Effect of Microcracking on Indirect Tensile and Unconfined Compressive Strengths

The effect of microcracking on the ITS and UCS of the 2.5% cement-content specimens was required for finite element modeling. The ITS and UCS results are discussed in Section 6.4 and Section 6.5, respectively. An analysis of the test results showed that:

- ITS was linearly correlated with stiffness decrease after microcracking.
- UCS was poorly correlated with stiffness decrease after microcracking, and no model could be fitted.

The effect of microcracking on strength parameters can therefore be observed as the relationship between stiffness and ITS after different microcracking efforts. Based on the analysis of the initial results, Equation 7.27 was proposed to evaluate the effect of stiffness after microcracking on strength.

$$Strength = \beta_0 + \beta_1 \times E \quad \textbf{(7.27)}$$

Where: $Strength$ = ITS (MPa)

β_0, β_1 = Regression coefficients

The regression model in Equation 7.27 was fitted to the ITS versus stiffness results using linear regression. Regression coefficients for the relationship are provided in Table 7.14. The R^2 of the fit was 0.48.

Table 7.14: Regression Coefficients for ITS Versus Stiffness in Equation 7.27

Term	Coefficient	Estimate	Std. Error	t-value	Pr(>|t|)
(Intercept)	β_0	199.7	22.96	8.70	2.37E-11
E	β_1	0.03	0.01	4.73	2.06E-05

The effect of stiffness reduction after microcracking on ITS was evaluated using a t-test, with a null hypothesis of $\beta_1 = 0$, and alternative hypothesis that $\beta_1 \neq 0$. Since t(0.975, 47) = 2.01, which is less than 4.73, the null hypothesis was rejected, indicating that microcracking, which reduces stiffness, also reduces the ITS. This relationship is only applicable for microcracking at 48 hours of curing. The final relationship is provided in Equation 7.28.

$$Strength = 199.7 + 0.03 \times E \quad \textbf{(7.28)}$$

7.5 Effect of Shrinkage Over Time

Models for drying shrinkage were required for input to crack-width and crack-spacing models developed by Zhang and Li *(32)*, George *(33)*, and Wang *(34)* to predict crack-density and crack-width.

The shrinkage model proposed by Wang *(34)* in Equation 7.29 was initially considered for fitting the drying shrinkage results. However, this model does not consider different cement contents, which is a critical determinant of the amount of shrinkage, nor does it consider different material properties. The drying shrinkage results near the surface of the layer predicted using Wang's model are provided in Figure 7.22, along with the laboratory free-drying shrinkage results. Wang's shrinkage model underestimated shrinkage with the difference increasing with increasing cement contents. The model predicted similar ultimate drying shrinkage levels for the two different cement contents, which did not correspond with the test results.

$$\varepsilon_g(t) = \varepsilon_{su}\left[1 - \left(\frac{RH_c}{100}\right)^{a_6}\right] \quad \textbf{(7.29)}$$

Where: $\varepsilon_g(t)$ = Drying shrinkage strain with moisture gradient at *t* days after construction (μstrain)
RH_c = Calculated relative humidity (%)

Where: $RH_c = RH + (100 - RH)f(t)^{a_5}$
RH = Atmospheric relative humidity (%)

$$f(t) = 1/\left(1+\frac{t}{b}\right)$$

Where: t = Time since construction (days)

$b = a_1(d+a_2)^{a_3}\left(\frac{w}{c}\right)^{a_4}$

d = Depth from evaporation surface (ft.)

$\frac{w}{c}$ = Water/calcium ratio in mass

a_i = Regression coefficients

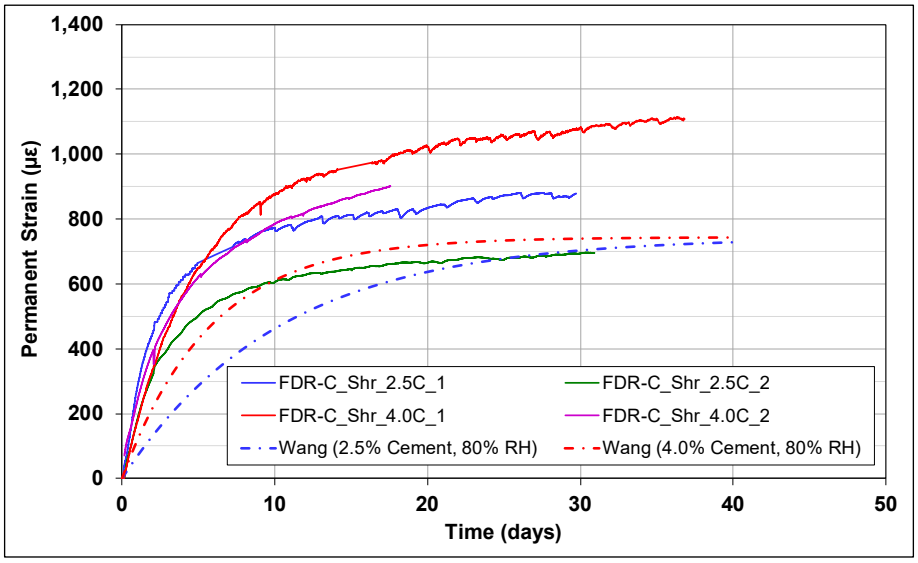

Figure 7.22: Measured drying shrinkage results compared to Wang's *(34)* model.

The nonlinear model in Equation 7.30 was proposed for obtaining a better estimate of the free-drying shrinkage from laboratory test results (discussed in Section 6.6) for the FDR-C Test Road material. This model was based on the observed exponential growth in shrinkage during the early part of hydration and incorporates continued shrinkage over time, while not allowing the shrinkage to asymptote at large values for t.

$$\varepsilon(t) = (\beta_0 + t \times \beta_1)\left(1 - e^{(-1 \times B \times t)}\right) \quad \textbf{(7.30)}$$

Where: $\varepsilon(t)$ = Drying shrinkage strain at time t (strain)

β_0, β_1 = Fitting coefficient

t = Time (days)

B = Initial rate of increase in drying shrinkage strain

Nonlinear regression was used to fit Equation 7.30 to the free-drying shrinkage results in Figure 7.23. The results for specimen FDR-C_Shr_4.0C_2 was limited to only 17 days due to technical problems that caused the LVDT to stop recording. This resulted in the drying shrinkage model overestimating the drying shrinkage result for the 4% cement-content data when fitted to

the average shrinkage of the two specimens. The fit appears more reasonable when the results for the FDR-C_Shr_4.0C_2 specimen are removed, with a slightly elevated shrinkage rate after the initial exponential growth.

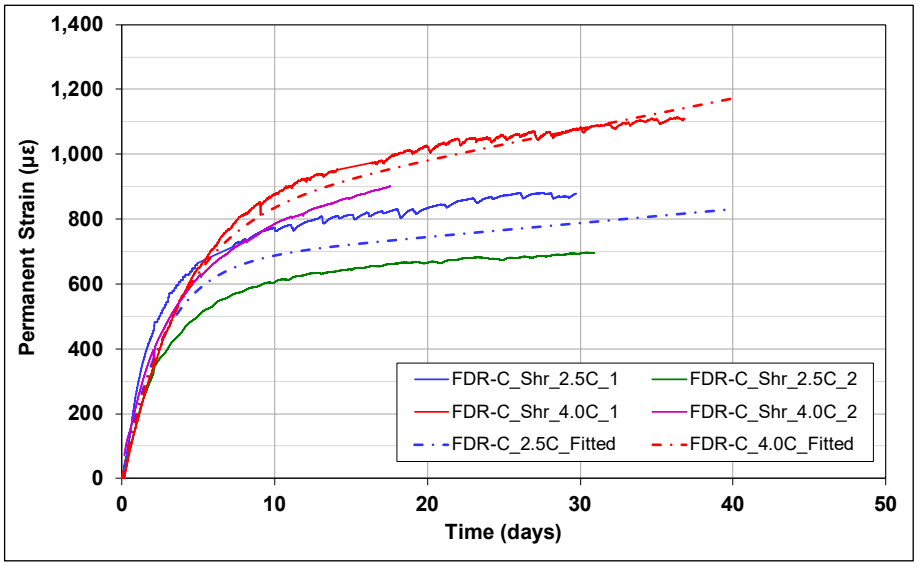

Figure 7.23: Fitted free-drying shrinkage results.

The regression coefficients for Equation 7.30 are provided in Table 7.15. The R^2 for the 2.5% and 4% cement-content results was 0.86 and 0.99, respectively. The fitted results are provided in Figure 7.24 together with the raw data used for the fit.

Table 7.15: Fitting Coefficients for Equation 7.30

Coefficient	2.5% Cement	4% Cement
β_0	6.57E-04	9.30E-04
β_1	4.62E-06	4.97E-06
B	4.08E-01	2.25E-01

The model in Equation 7.30, together with the coefficients in Table 7.15 were considered appropriate as input for the crack-width and crack-spacing models developed by Zhang and Li *(32)* for the material used in the FDR-C Test Road.

7.6 Summary

A series of models was developed for predicting the effects of microcracking on stiffness (Equation 7.23). The 2.5% cement-content material was less sensitive to microcracking efforts than the 4% cement-content material. This was attributed to the higher water-to-cement-for-cementation ratio and increased free water of the 2.5% cement-content material, which

contributed to rehydration of the broken cement bonds after microcracking as well as hydration of previously unhydrated cement.

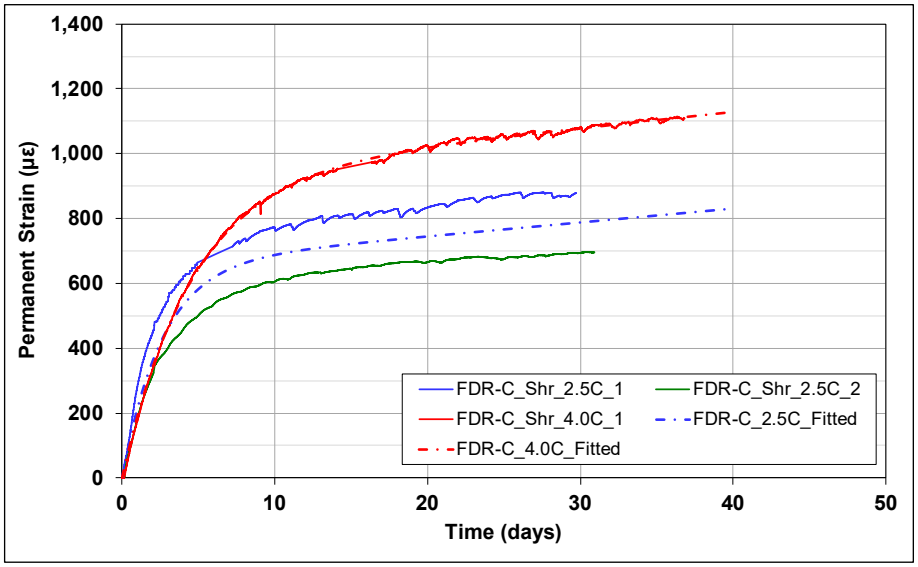

Figure 7.24: Final drying shrinkage results.

8 SIMULATING MICROCRACKING ON THE FDR-C TEST ROAD

8.1 Introduction

The effect of microcracking on crack width and crack density was studied on the FDR-C Test Road and is discussed in the Phase 2a report *(12)*. Results from the FDR-C Test Road showed that microcracking reduced the number of cracks that reflected through to the road surface, reduced the width of those reflected cracks, and influenced the stiffness.

Vibratory rollers apply large compressive stresses on the road surface and large tensile stresses at the bottom of the FDR-C layer. If these stresses exceed the strength of the layer, the layer could fail in compression (crushing of the surface) and/or tension (bending resulting in bottom up fatigue cracks). These effects were modeled using the finite element method (FEM) to determine changes in the effective intact layer thickness after microcracking and effects on shrinkage cracking. Severely distressed material on the top or bottom of an FDR-C layer does not contribute to the structural capacity of that layer, and therefore, based on the assumption that microcracking temporarily reduces the stiffness and hence the carrying capacity of the FDR-C layer, the effect will be equivalent to a temporary thickness reduction of the layer until the stiffness recovers. The alternative case of no effective thickness reduction was also considered to compare changes in the predicted results. The different analyses were then compared against the field results to further determine which mechanisms predominantly influenced the reduction in reflective cracking.

8.2 Scope of the Simulation

The simulation was considered in four parts:

- FEM modeling to determine the types of distresses induced during microcracking and their effect on the effective thickness of an FDR-C layer.
- Simulation of microcracking using the FDR-C Test Road microcracking factorial and the crack-width and crack-spacing models derived by Zhang and Li *(32)* to validate the models and develop a better understanding of reflective cracking.
- Simulation of earlier microcracking (e.g., after 24 hours) to determine changes in expected crack widths if microcracking is applied after a shorter than typical curing period (e.g., at 24 hours instead of 48 hours).

- Simulation of crack development with no microcracking and reduced levels of shrinkage development over time if a low-shrinkage cement is used, to determine changes in expected cracking development.

8.2.1 Effect of Microcracking on Effective Layer Thickness

The effect that microcracking has on effective intact layer thickness was modeled with FEM using the *Abaqus* software program. The model considered a pavement structure similar to that of the FDR-C Test Road, with the FDR-C and subgrade layers modeled as elastic layers, with no plastic deformation.

8.2.2 Crack-Width and Crack-Spacing Simulation

The scope of the crack-width and crack-spacing modeling was limited to the FDR-C Test Road factorials and included the following:

- Shrinkage due to hydration: Shrinkage due to thermal contraction and expansion was not considered.
- Stiffness, strength, and shrinkage models: The models were determined for the 2.5% and 4% cement-content materials.
- Stiffness reduction: The reduction was equivalent to what was measured for one, two, and three microcracking passes using a 12-ton vibratory roller with total linear load per unit width of 1.42 kN/cm.
- Curing times before microcracking of 48 and 72 hours: An additional case was considered for a curing time of 24 hours to address the observation from the FDR-C Test Road that indicated the potential for further reducing reflective cracking if this option was pursued.

8.3 Microcracking Effect on the FDR-C Layer Effective Thickness

8.3.1 Finite Element Model

An FEM model was developed to model the stresses in the FDR-C layer during microcracking (Figure 8.1 and Figure 8.2). A 10×3.6 m (≈33×12 ft.) slab was modeled over a 4 m (≈13 ft.) thick elastic subgrade to represent the FDR-C Test Road. The roller drum was considered to be rigid, with dimensions based on the 12-ton single steel drum roller used on the FDR-C Test Road. The mesh detail below the roller drum, shown in Figure 8.3, represents the mesh design that was considered for modeling the stresses in the region below the drum.

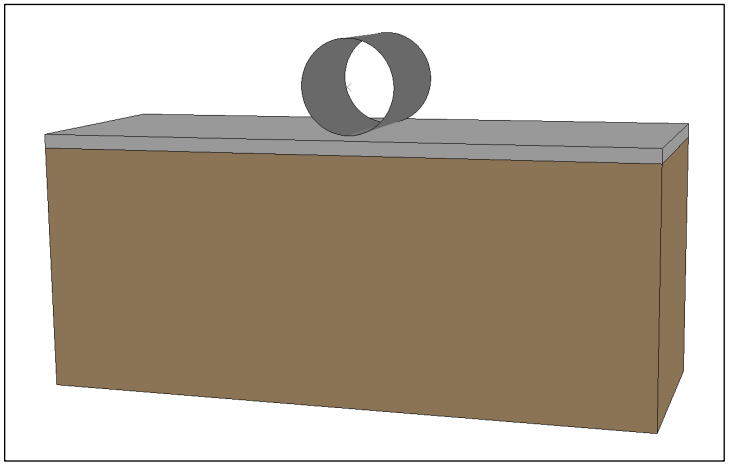

Figure 8.1: FEM microcracking model illustration.

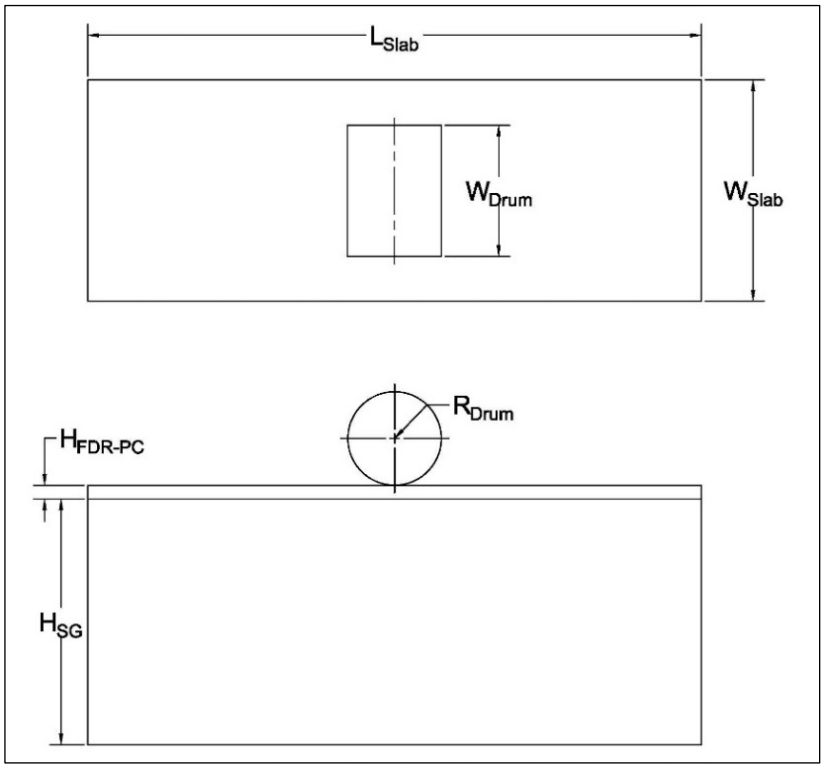

Figure 8.2: FEM model dimensions.

The assumptions made for this modeling include the following:

- The roller drum was assumed to be rigid and constrained in the lateral and longitudinal directions.
- Friction was considered between the drum and the pavement.
- Both the longitudinal and lateral directions of the pavement were constrained.
- The FDR-C layer was considered to be elastic.
- The subgrade was modeled as an elastic layer.

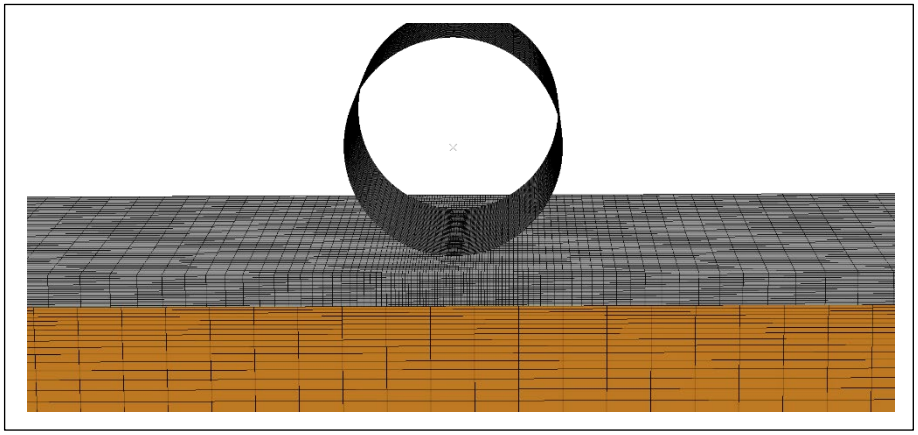

Figure 8.3: FEM mesh design below roller drum.

Roller speed was not considered in this analysis. It was assumed that the roller would not be stationary when the drum vibration is turned on, which is standard construction practice. The standard frequency of the roller used on the FDR-C Test Road was 30.5 Hz. The roller speed recommended during microcracking is 3 to 5 km/h (2 to 3 mph), which equates to a distance between peak load applications of 27 and 46 mm (1.06 and 1.81 in.) for the two speeds, respectively.

The mechanisms of stiffness reduction considered in the FEM model included fatigue failure of the cementitious bonds due to cyclic loading, crushing failure, and bending failure.

Fatigue Failure of the Cementitious Bonds due to Cyclic Loading

The two hypotheses of fatigue failure due to cyclic loading are *(35)*:

1. The progressive deterioration of the cementitious bonds between the aggregate and matrix
2. The coalescence of preexisting microcracks in the interfacial zones resulting in localized macrocracks

The load levels during cyclic loading in the case of fatigue failures are not sufficient to cause failures under static loading *(35)*. The effect of fatigue failure in this analysis was assumed based on the stiffness reduction results measured during microcracking in the field, as well as in the laboratory.

Crushing Failure

Crushing of the FDR-C layer during microcracking would result in a partially bound surface, which could ravel under vehicular traffic before placing the asphalt concrete surfacing. It also does not provide a bound layer for the asphalt concrete to bond to, which will increase the strain at the

bottom of the asphalt concrete layer under traffic, leading to early fatigue failure in that layer. The concept of crushing in this report is based on the work by De Beer *(14)* who concluded that thick cement-treated layers fail predominantly in compression (crushing) in the upper portion of the layer, which is manifested at the surface as permanent deformation. This was prevalent on roads with thick cement-treated layers that had thin surface seals and carried high volumes of heavy traffic loads with high contact stresses. De Beer further developed the concept of the "crushing life" of a cement-treated layer (i.e., the number of load repetitions before crushing initiates down to a depth of 2 mm [0.08 in.]). He also developed a model for the number of repetitions to reach advanced crushing, where the crushed layer extends to a depth of 10 mm (0.4 in.). The model is provided in Equation 8.1, with the fitting parameters listed in Table 8.1 for different design reliabilities of road categories in southern Africa.

$$N_{C_{i/a}} = 10^{k_1\left(1-\frac{\sigma_v}{k_2 UCS}\right)} \quad \textbf{(8.1)}$$

Where: N_{C_i} = Number of cycles to crush initiation, with approximately 2 mm deformation on top of the layer

N_{C_a} = Number of cycles to advanced crushing, with approximately 10 mm deformation on top of the layer

k_1, k_2 = Fitting parameters

σ_v = Vertical compressive stress at the top of the cement-treated layer (kPa)

UCS = Unconfined compressive strength

Table 8.1: Parameters for Cement-Treated Layer Crushing Functions

Road Category	Design Reliability (%)	Crush Initiation (N_{Ci})		Advanced Crushing (N_{Ca})	
		k_1	k_2	k_1	k_2
A	95	7.386	1.09	8.064	1.19
B	90	7.506	1.10	8.184	1.20
C	80	7.706	1.13	8.384	1.23
D	50	8.516	1.21	8.894	1.31

Based on De Beer's description of crushing, it was considered appropriate to compare the vertical compressive stresses induced by the vibratory roller during microcracking to the UCS of the material. Using Equation 8.1, the number of load repetitions can be calculated if the vertical stress is equal to the UCS of the material. For a Category A road, which requires the highest design reliability, the layer can withstand four load repetitions when the vertical stress at the top of the layer is equal to the UCS of the material. This does not assume any structural changes due to bending or fatigue failure of the microstructure due to microcracking. For a single pass to initiate

crushing, σ_v should equal 1.1 to 1.2 times the UCS. Advanced crushing requires 19 passes with σ_v/UCS equal to one, or one pass with a vertical stress equal to 1.2 to 1.3 times the UCS.

Bending Failure

Bending failure occurs when the tensile stress exceeds the flexural strength of the material, which results in tensile cracks initiating at the bottom of the layer. It was assumed that the length of the cracks would only extend through the depth of the layer over which the maximum principal stress exceeded the indirect tensile strength (ITS) of the material. The thickness of the layer was assumed to be fully cracked (i.e., in an equivalent granular phase) and was modeled with similar properties as the subgrade for subsequent microcracking passes. The tensile strength derived from the ITS testing was used as a measure of the flexural strength for this simulation.

8.3.2 Experiment Plan

The experiment plan for FEM modeling included element convergence testing, where a range of element sizes was considered to determine the appropriate element size in the FEM model to ensure that the tensile stresses at the bottom of the layer and the compressive stresses below the roller drum converged. The pavement structure and the soil stiffness gauge (SSG) results from the FDR-C Test Road were used for this scenario. Three roller passes, with no crushing, were modeled using the stiffness reduction recorded during microcracking.

8.3.3 Vibratory Roller Loading Characteristics

The magnitude of the force applied by the roller and the size of the contact area are two important parameters required to investigate the mechanism of microcracking using a vibratory roller. For this simulation, the 12-ton roller used on the FDR-C Test Road was considered. The roller loading properties, as calculated using Equation 8.2, are provided in Table 8.2.

$$F_s = F_{ev}\cos(\Omega t) + (m_f + m_d)g - m_d\ddot{z}_d - m_f\ddot{z}_f \quad \textbf{(8.2)}$$

Where: F_s = Force transmitted to layer (N)
m_d, m_f = Mass of drum and frame, respectively (kg)
g = Acceleration of gravity (m/s^2)
$\ddot{z}_d$, $\ddot{z}_f$ = Drum and frame accelerations, respectively (m/s^2)

Table 8.2: 12-Ton Vibratory Roller Properties with High Vibration Amplitude

Project	Drum Width (cm)	Drum Diameter (cm)	Static Load (kg/cm)	Total Force (kN)	Linear Total Force (kN/cm)
Test Road	213	153	33.4	304	1.42

In terms of contact area between the roller and the FDR-C layer, it was assumed that the interaction between the roller drum and the surface layer was elastic due to the relatively high stiffness of the FDR-C layer prior to microcracking. Figure 8.4 shows that the roller drum did not cause any visual plastic deformation during microcracking that would increase the contact area, create ruts, or cause shear deformation in the surface due to densification. The width of the contact area was thus determined using Equation 8.3, which was originally developed for calculating the contact area of two parallel elastic cylinders.

Figure 8.4: Checks for deformation between drum and FDR-C layer during microcracking.
(Note vibration ripples on water.)

$$B = \sqrt{\frac{4F\left[\frac{1-\nu_1^2}{E_1}+\frac{1-\nu_2^2}{E_2}\right]}{\pi L\left[\frac{1}{R_1}+\frac{1}{R_2}\right]}} \quad \textbf{(8.3)}$$

Where: B = Half width of contact area (mm)
F = Force perpendicular to contact area (N)
ν_1, ν_2 = Poisson's ratio of cylinder one and two, respectively
E_1, E_2 = Young's modulus of cylinder one and two, respectively (MPa)
R_1, R_2 = Radius of cylinder one and two, respectively (mm)

By setting the radius of cylinder two (R_2) to approach infinity, $1/R_2$ would equate to zero. This equation can then be used to calculate the width of the contact area of the roller drum on a flat surface. Figure 8.5 shows the sensitivity of the contact area width, as calculated using Equation 8.2, for the 12-ton roller using the peak total load at high vibration amplitude. The contact width increases exponentially with a decrease in stiffness of the layer directly below the drum.

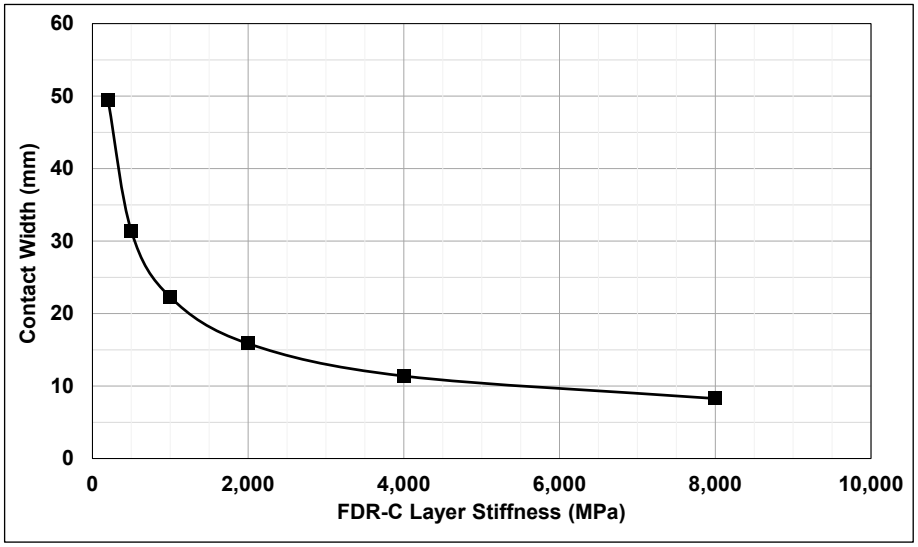

Figure 8.5: Sensitivity of roller contact width to change in stiffness.

8.3.4 Material Properties

The material properties required for the FEM model were FDR-C layer stiffness and strength.

Stiffness

Two options for FDR-C layer stiffness were available at the time of microcracking:

- SSG stiffnesses, fitted to the FWD backcalculated stiffness, from the 2.5% cement-content cells on the FDR-C Test Road, discussed in the Phase 2a report *(12)*.
- The laboratory-determined stiffnesses on the same material discussed in Section 7.2.

The field determined stiffness on the 2.5% cement-content material using the SSG-FWD relationship was compared against the laboratory-measured stiffness for the 2.5% and 4% cement-content materials (Equation 7.22) in Figure 8.6. The adjusted stiffness reduction relationship for each roller pass was used to calculate the percent stiffness reduction measured with the SSG. The results show that the field-measured stiffnesses were lower than the laboratory-measured stiffnesses. Although the laboratory-prepared material closely simulated the field conditions, there are multiple factors that could have affected the field measurements, ranging from inherent variability in construction to limitations of the instruments. The decision was therefore made to use the laboratory-measured stiffnesses for the stiffness reduction in the modeling of microcracking since these models were also used as the stiffness history for these simulations.

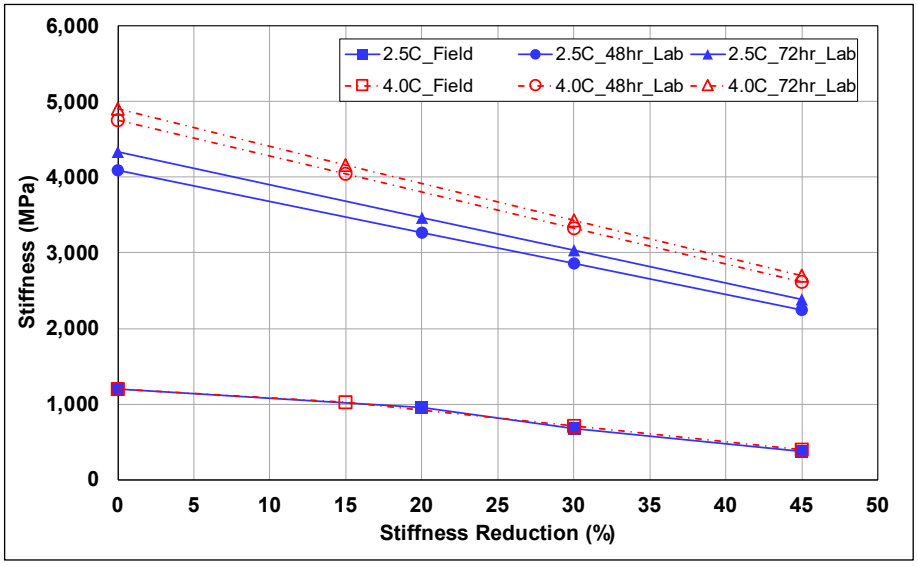

Figure 8.6: Comparison between field- and laboratory-measured stiffness reductions.

The energy input using the 12-ton roller at high vibration amplitude for the three passes was calculated using Equation 8.2 to determine the stiffness reduction using Equation 7.23. Table 8.3 provides a summary of the energy input and the stiffness before and after microcracking for the different cement contents and microcracking times used on the FDR-C Test Road.

Table 8.3: Material Properties with Energy Input during Microcracking

Cement Content (%)	Microcrack Time (hr)	Stiffness Reduction (%)	Total Force (kN/cm)	Total Energy Input (Joule/m^3)	Stiffness (MPa)	ITS (kPa)
2.5	48	0	0	0	4,089	422
		20	1.42	13.6	3,271	389
		30	2.84	42.9	2,862	373
		45	4.26	240.5	2,249	348
	72	0	0	0	4,335	432
		20	1.42	13.6	3,468	397
		30	2.84	42.9	3,034	380
		45	4.26	240.5	2,384	354
4.0	48	0	0	0	4,759	558
		15	1.42	7.6	4,045	513
		30	2.84	42.9	3,331	468
		45	4.26	240.5	2,617	423
	72	0	0	0	4,903	567
		15	1.42	7.6	4,167	521
		30	2.84	42.9	3,432	475
		45	4.26	240.5	2,696	428

Strength

The UCS and ITS of the FDR-C layer material are required to compare against the minor (σ_1) and major (σ_3) principal stress outputs from the FEM analyses, respectively. The FDR-C Test Road UCS

results (3.5 and 4.5 MPa for the 2.5% and 4% cement-content sections, respectively) were fitted to the US Air Force UCS model *(36)* in Equation 8.4 to backcalculate UCS values at the time of microcracking. Figure 8.7 shows the calculated UCS strength gain curves over the first seven days. The ITS values in Table 8.3 were calculated using Equation 7.25.

$$UCS(t) = UCS(t_0) + K \times \log(\frac{t}{t_0}) \quad \textbf{(8.4)}$$

Where: $UCS(t)$ = UCS at time t (days)
$UCS(t_0)$ = UCS of a material after t_0 days
K = 70×C for cement
t = Curing time (days)
C = Stabilizer content (%)

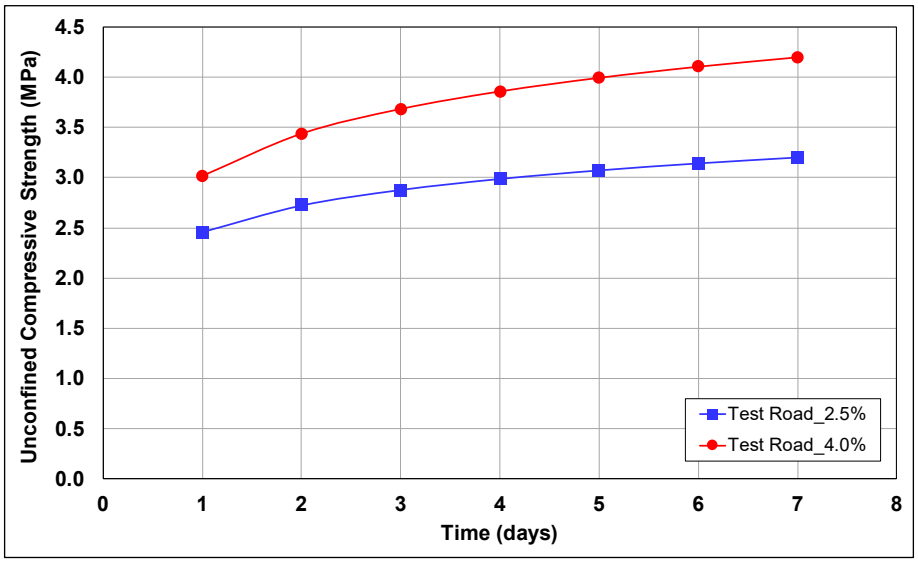

Figure 8.7: Predicted UCS curing curves for FDR-C Test Road.

8.3.5 Pavement Structure

The actual FDR-C Test Road pavement structure (250 mm FDR-C layer over subgrade) was used in the general case analysis, along with the initial FDR-C and subgrade layer stiffnesses of 2,000 MPa and 110 MPa, backcalculated from the FWD deflections measured on the FDR-C Test Road prior to microcracking. Poisson's ratio was kept constant at 0.35 for the FDR-C layer and subgrade material.

8.3.6 Mesh Convergence Study

The FEM model discussed in Section 8.3.2 required refinement to determine an appropriate mesh size to produce converging stresses for different mesh sizes. The vibratory drum was modeled for mesh sizes ranging from 2 to 10 mm to calculate the following:

- Minor principal stress at the surface below the roller drum
- Major principal stress at the bottom of the FDR-C layer below the roller drum

Minor Principal Stresses

The minor principal stresses in the longitudinal direction at the surface of the FDR-C layer are plotted in Figure 8.8 for the different mesh sizes. The stresses below the roller drum continued to increase as the mesh size reduced, which is indicative of a singularity. To address this issue, the minor principal stresses were averaged in the longitudinal direction to compare them for the different mesh sizes. Figure 8.8 shows that, within the range of the expected contact width of 1.5 to 20 mm, a mesh size of 2 mm provided convergent results.

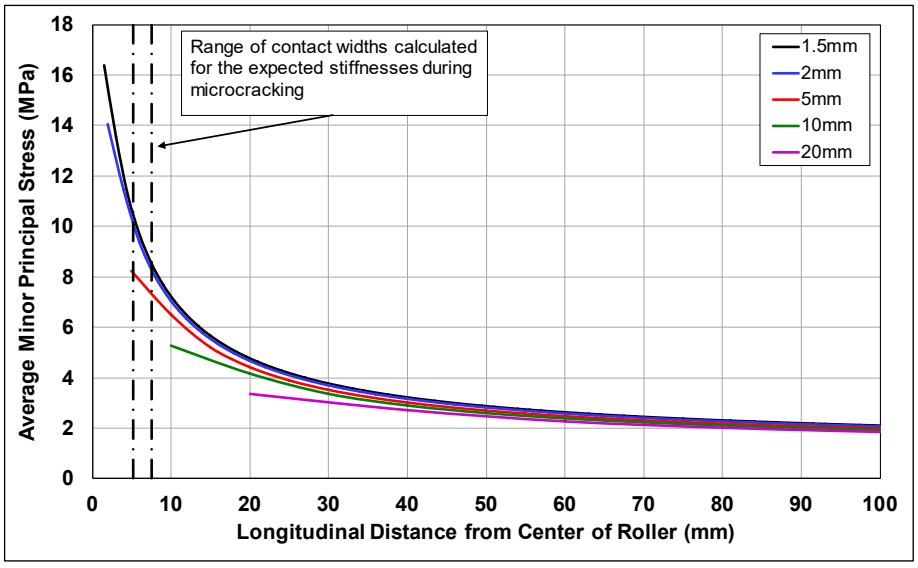

Figure 8.8: Average minor principal stress on FDR-C layer surface below roller.

The average minor principal stress below the roller drum determined with the FEM model was 10.1 MPa. The calculated average stress based on the area calculated using Equation 8.2 was 10.2 MPa. The results indicate that the two methods used to calculate the stress directly below the drum provided similar compressive stresses. The calculated stresses significantly exceeded the UCS of the FDR-C material at the time of microcracking (3.7 MPa), which should have caused the surface of the FDR-C layer to crush during microcracking. Based on field observations after

microcracking, as well as from cores that were cut from the FDR-C layers, no signs of crushing were observed except in areas where the layer was not appropriately cured after final compaction and showed signs of carbonation. For the purpose of this simulation, and without sufficient data to properly calibrate the FEM model, the effect of crushing was not considered, and it was assumed that the layer was appropriately cured.

Major Principal Stress

The major principal stresses at the bottom of the FDR-C layer (250 mm below the surface) below the roller drum are provided in Table 8.4 for the different mesh sizes. The results show that the stress converges for mesh sizes 20 mm and less, as shown by the relative change in the stress. A 20 mm mesh size was therefore selected to optimize computing time.

Table 8.4: Maximum Principle Stress at the Bottom of the FDR-C Layer

Mesh Size	20 mm	10 mm	5 mm	2 mm	1.5 mm
Maximum principal stress (MPa)	1.35	1.35	1.35	1.39	1.41
Relative change (%)	-	0	1	3	2

For the purpose of this study, it was assumed that the depth of the FDR-C layer over which the major principal stress exceeded the tensile strength failed in tension (with bottom up cracks). No cores were cut immediately after microcracking to validate this observation, but cores extracted 18 months after construction showed that the layer was fully intact. This was attributed to the confinement provided by the intact part of the FDR-C layer over the failed thickness of the layer after microcracking, which provided the necessary compression to facilitate recementation.

8.3.7 Stiffness and Strength Reduction During Microcracking

The strength properties (ITS and UCS) from the 2.5% cement-content material from the FDR-C Test Road were also used in this analysis. The results showed that only the tensile strength, as measured by the ITS, was a function of stiffness reduction during microcracking. This was considered for subsequent microcracking passes to reduce the effective intact thickness of the FDR-C layer.

8.3.8 Effective Layer Thickness Reduction During Microcracking

The pavement structure and pavement properties used for microcracking are provided in Table 8.5. The pavement structure was based on the FDR-C Test Road, and the stiffness was based on the results recorded during microcracking (Table 8.3).

Table 8.5: Effective FDR-C Thickness Reduction with Microcracking

Microcrack Time (hours)	Cement Content (%)	Microcrack Pass	Total Force Applied (kN/cm)	Stiffness Reduction (%)	Stiffness Before Microcracking (MPa)	Effective Thickness Before Microcracking (mm)
48	2.5	0	0.00	0	4,089	250
		1	1.42	20	3,271	175
		2	2.84	30	2,862	113
		3	4.26	45	2,249	67
	4.0	0	0.00	0	4,759	250
		1	1.42	15	4,045	186
		2	2.84	30	3,331	126
		3	4.26	45	2,617	78
72	2.5	0	0.00	0	4,335	250
		1	1.42	20	3,468	175
		2	2.84	30	3,034	113
		3	4.26	45	2,384	67
	4.0	0	0.00	0	4,903	250
		1	1.42	15	4,167	186
		2	2.84	30	3,432	126
		3	4.26	45	2,696	78
48+72	2.5	4	5.68	60	1,622	37
	4.0	4	5.68	57	2,042	44

Two different mechanisms were investigated in the modeling of microcracking, namely internal fatigue failure of the cementitious bonds and bending failure. These mechanisms were accounted for as follows:

- For fatigue failure of the internal structure (i.e., microcracking), the stiffness of the intact FDR-C layer was reduced based on the stiffness results collected during microcracking (Table 8.3).
- For bending failure, the effective thickness of the FDR-C layer was reduced by the depth over which the major principal stress exceeded the ITS of the material (i.e., from 250 mm to 225 mm). For simplicity, the stiffness of the failed thickness was set at 110 MPa to be the same as the subgrade.

8.3.9 Results

Figure 8.9 illustrates the effective layer thickness reduction for the 2.5% cement-content case microcracked at 48 hours. The results for all cases are provided in Appendix B. The major principal stress was compared with the calculated ITS of the material to determine the remaining intact layer thickness where the strength was greater than the stress. The remaining intact thickness was then used as input for the FDR-C layer thickness in a subsequent FEM model for the next microcracking pass, together with the appropriate stiffness provided in Table 8.3.

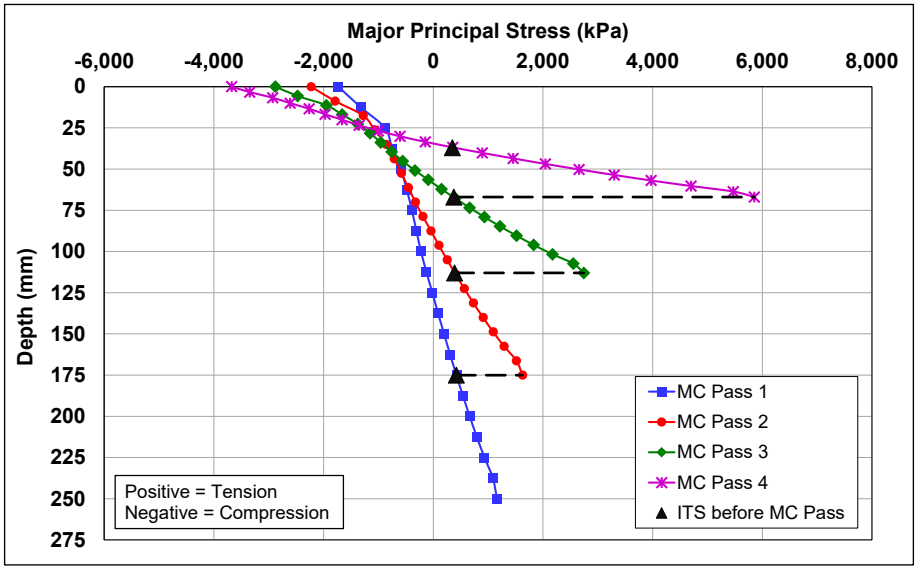

Figure 8.9: 2.5% cement with microcracking at 48 hours: Effect on effective layer thickness.

The effective intact FDR-C layers for the different cases in Table 8.3 are provided in Table 8.5. The results show that the tensile strength of the layer was exceeded during microcracking due to the layer bending under the weight of the roller. This bending induced large tensile stresses at the bottom of the layer, causing the layer to fail in tension. These results were used as input for the crack-width and crack-spacing simulation.

8.4 Crack-Width and Crack-Spacing Simulation on the FDR-C Test Road

8.4.1 Methodology

Tensile stresses develop in FDR-C layers as they shrink, which results in drying shrinkage cracks when the stress exceeds the strength. Drying shrinkage cracks also develop due to friction between the FDR-C layer and the underlying unbound layers (e.g. subgrade). These cracks restrict contraction as drying shrinkage increases and/or temperatures decrease.

The shrinkage crack spacing and displacement models for determining deformation for crack-width estimation, developed by Zhang and Li *(32)*, were considered appropriate for modeling shrinkage crack spacing and width in FDR-C layers, with and without microcracking. A half-length of a slab was considered since the slab is stationary at the center. A schematic of the pavement geometry used in the model is provided in Figure 8.10.

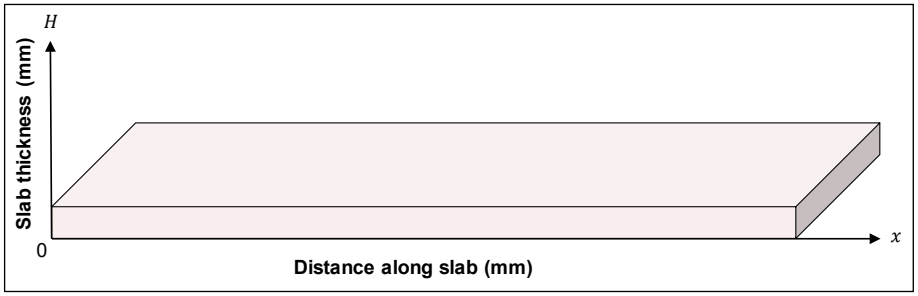

Figure 8.10: Slab geometry.

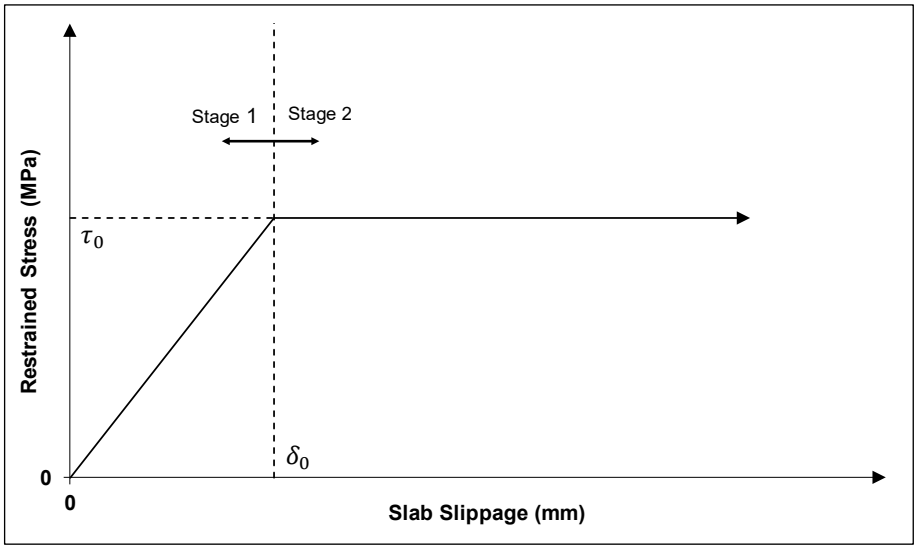

Figure 8.11: Bilinear relation between slab displacement and restraint stress.

The following two stages were considered for the shrinkage displacement (Figure 8.11):

- Stage 1 is the displacement due to shrinkage ($|u| \leq \delta_0$). Restrained stress increases with increasing strain.
- Stage 2 is the displacement due to shrinkage ($|u| > \delta_0$). Restrained stress is constant with increasing strain.

The closed form solutions for each stage are provided below. It was assumed that the stresses at the edge of the slab (i.e., σ_{c0}) caused by thermal contraction and expansion, were equal to zero *(32)*.

- The closed-form solutions for Stage 1 are:
  - Maximum displacement (Equation 8.5)
  - Restrained stress along the slab (Equation 8.6)
  - Maximum restrained stress (Equation 8.7)
- The closed-form solutions for Stage 2 are:
  - Maximum displacement (Equation 8.8)

- Restrained stress along the slab (Equation 8.9)
- Maximum restrained stress (Equation 8.10)

In order to determine if the slab slippage progressed to Stage 2, Equation 8.11 was solved to calculate x_0. If $x_0 < \delta_0$, slab slippage is in Stage 1; otherwise it is in Stage 2.

$$u_m = -\frac{1}{\beta}\varepsilon_c \tanh \beta \frac{L}{2} \quad \textbf{(8.5)}$$

$$\sigma_c = -E_c\varepsilon_c\left(1 - \frac{\cosh \beta\left(\frac{L}{2}-x\right)}{\cosh \beta\frac{L}{2}}\right) \quad \textbf{(8.6)}$$

$$\sigma_{cm} = -E_c\varepsilon_c\left(1 - \frac{1}{\cosh \beta\frac{L}{2}}\right) \quad \textbf{(8.7)}$$

$$u_m = \delta_0\left(1 - \frac{1}{2}\beta^2 x_0^2\right) - \varepsilon_c x_0 \quad \textbf{(8.8)}$$

$$\sigma_c = -E_c\varepsilon_c\left(1 - \frac{\cosh \beta\left(\frac{L}{2}-x\right)}{\cosh \beta\left(\frac{L}{2}-x_0\right)}\right) + (E_c\beta^2\delta_0 x_0)\frac{\cosh \beta\left(\frac{L}{2}-x\right)}{\cosh \beta\left(\frac{L}{2}-x_0\right)} \quad \textbf{(8.9)}$$

$$\sigma_{cm} = -E_c\varepsilon_c\left(1 - \frac{1}{\cosh \beta\left(\frac{L}{2}-x_0\right)}\right) + (E_c\beta^2\delta_0 x_0)\frac{1}{\left(\cosh \beta\left(\frac{L}{2}-x_0\right)\right)} \quad \textbf{(8.10)}$$

$$\delta_0 = -\frac{1}{\beta}\left(\beta^2\delta_0 x_0 + \frac{\sigma_{c0}}{E_c} + \varepsilon_c\right)\tanh \beta\left(\frac{L}{2} - x_0\right) \quad \textbf{(8.11)}$$

Where: σ_c = Average axial stress (MPa)
u_m = Maximum shrinkage displacement (mm)
σ_{cm} = Maximum shrinkage stress at the middle of the slab (MPa)
σ_{c0} = Average axial stress at the edge of the slab (MPa)
β = $\sqrt{\tau_0/(E_c H \delta_0)}$
τ_0 = Steady state frictional stress (MPa)
H = Slab thickness (mm)
δ_0 = Slippage up to steady state (mm)
E_c = Young's modulus (MPa)
ε_c = Drying shrinkage strain (%)
L = Length of slab (mm)
x_0 = Length of slab over which shrinkage stresses are fully developed (mm)
x = Distance along length of the slab (mm)

Based on the above equations, slab length, or crack spacing, can be calculated using Equation 8.12.

$$L = \frac{1}{\left[\frac{\beta}{2}\left(\cosh\left(\frac{\sigma_c}{E_c\varepsilon_c}+1\right)\right)\right]} \quad \textbf{(8.12)}$$

Shrinkage cracks develop once the shrinkage stress from drying, autogenous, and/or thermal shrinkage exceeds the strength of the material. Models used to understand the behavior include the following:

- The stiffness model with microcracking in Equation 7.22 was used to model the stiffness gain of the material over time with different microcracking efforts.
- The ITS versus stiffness model in Equation 7.25 provided a relationship to determine the change in ITS over time using the curing model for stiffness (Equation 7.22) as input.
- The drying shrinkage model in Equation 7.28 provided a measure of the drying shrinkage strain over time.

A slab was initially modeled with a length longer than the expected primary crack spacing, which was determined by computing the restrained stress along the slab, using either Equation 8.6 or Equation 8.9, depending on the stage. The location along the slab where the first occurrence of a crack event, or where the stress exceeded the strength, was defined as the primary crack spacing. With the primary crack spacing determined, additional crack spacings were calculated by computing the maximum restraint stress in the center of the subsequent slabs and comparing it to the strength of the slab for each subsequent timestep. If the restraint stress exceeded the strength, a crack developed, and the slab was split into two. This process was repeated for a period of 56 days, with hourly steps. The process is illustrated in Figure 8.12, where L_1 is primary crack spacing, L_2 is secondary crack spacing, L_3 is tertiary crack spacing, and L_x describes further lower-order crack development.

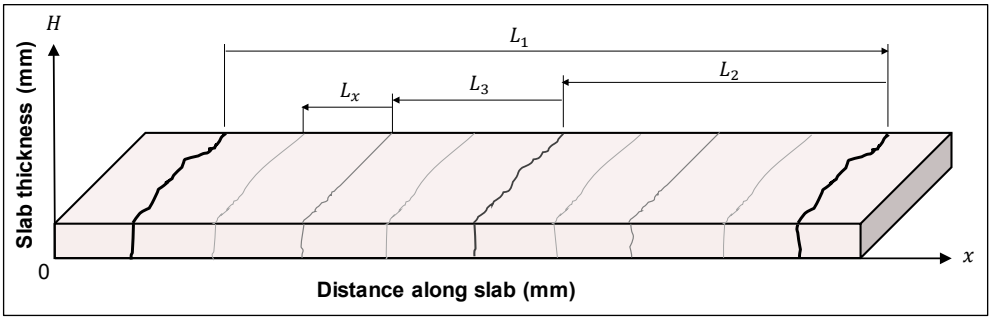

Figure 8.12: Crack development in a slab (not to scale).

8.4.2 Model Mechanics

The range of inputs considered for each model variable are provided in Table 8.6. Only Stage 1 shrinkage is assumed to illustrate the model mechanics. To determine the effect of each variable, only the variable in question is changed while the remaining variables are fixed to the values in Table 8.6. An ultimate drying shrinkage of 500 με was assumed for this comparison. The crack width and slab length were calculated with Equation 8.5 and Equation 8.12, respectively.

Table 8.6: Inputs to Evaluate Model Sensitivity

Parameter	Slab Thickness (H) (mm)	Stiffness (E_c) (MPa)	Tensile Strength (σ_c) (MPa)
Range	50 to 350	2,000 to 10,000	0.39 to 0.48
Fixed	300	4,000	0.45

Effect of Slab Thickness

The effect of slab thickness on crack spacing and crack width are shown in Figure 8.13. Both increased significantly with increasing FDR-C layer thickness. The increase in crack spacing was a result of the increased area of the slab that required a longer length to accrue a restraint stress to break the slab. This result is supported by the observations of George *(37)*.

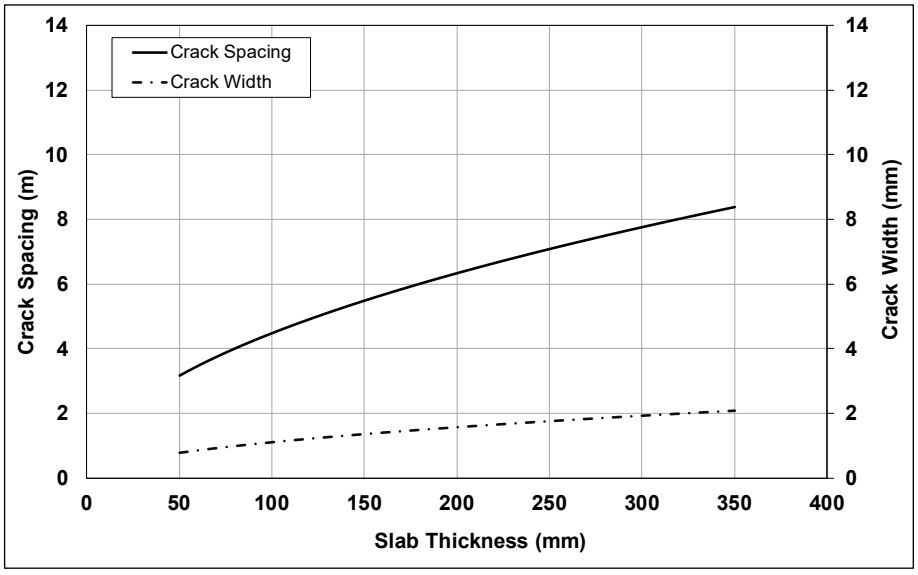

Figure 8.13: Calculated crack width and spacing sensitivity to FDR-C layer thickness.

Effect of FDR-C Layer Stiffness

The effect of FDR-C layer stiffness on crack spacing and crack width are shown in Figure 8.14. Both increased significantly with increasing FDR-C layer stiffness. This supports the model behavior described by George *(33)*, as well George's discussion on the effect of strength on crack spacing *(37)*. These results also support the reasoning for targeting lower design strengths, following George's discussion on design philosophy *(4)*. Reducing crack spacing reduces crack width, which maximizes aggregate interlock and load transfer efficiency (LTE) across the crack. It also reduces the rate of crack reflection by reducing shear stresses in the asphalt concrete layer above the crack.

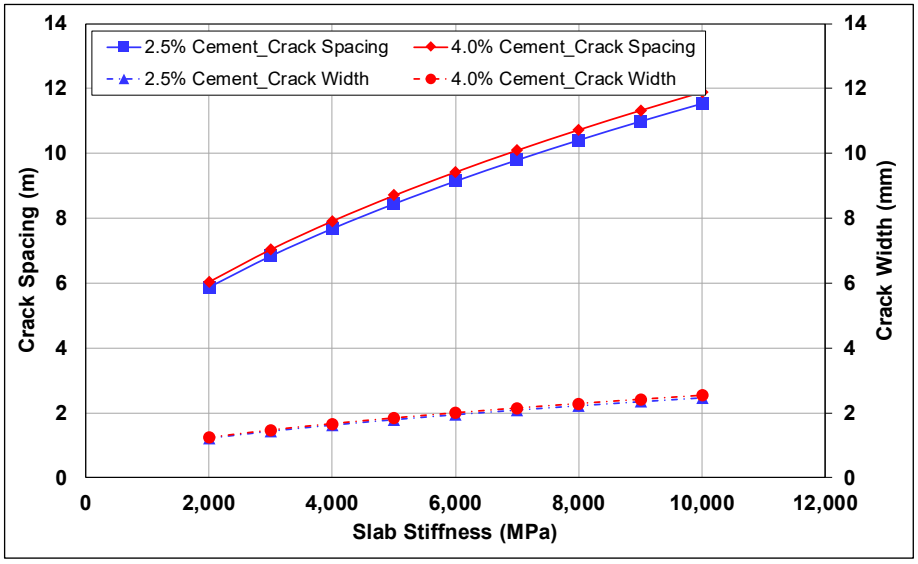

Figure 8.14: Calculated crack-width and crack-spacing sensitivity to material stiffness.

8.4.3 Model Inputs

The different input parameters for the crack model were:

- Supporting base material type
- FDR-C layer thickness
- FDR-C layer stiffness
- Material strength
- Drying shrinkage model

Supporting Material Below FDR-C Layer

The frictional restraint characteristics, required for the model, include the steady state frictional stress (τ_0) and the slippage up to the steady state (δ_0) of the material below the FDR-C layer. The material most likely below an FDR layer would be an unbound granular layer or the subgrade. The frictional restraint characteristic of an unbound granular layer suggested by Zhang and Li *(32)* was used in this analysis (τ_0 = 0.023 MPa and δ_0 = 0.5 mm).

FDR-C Layer Thickness with each Microcracking Pass

Two scenarios were considered with regards to the FDR-C layer thickness:

- Account for the bending failure resulting in effective intact layer thickness reduction as discussed in Section 8.3.9, as well as stiffness reduction.
- Keep the FDR-C layer thickness constant assuming the only damage to the layer was the stiffness reduction.

FDR-C Layer Stiffness with Time

The models developed in Chapter 7 for predicting stiffness change after microcracking were used to provide the stiffness input for determining crack spacing and crack width. The modeled stiffness results, with different microcracking efforts, are plotted in Figure 8.15 and Figure 8.16 for the 2.5% and 4% cement-content materials, respectively.

Strength with Time

The change in ITS over time determined from the relationship between stiffness and strength (discussed in Section 7.4) is plotted in Figure 8.17 and Figure 8.18 for the 2.5% and 4% cement-content specimens, respectively. The ITS was used as the strength at which a crack develops if the restraint stress exceeds the strength.

Shrinkage with Time

The drying shrinkage strains from the drying shrinkage tests (discussed in Section 7.5) were used as input for determining the crack width and crack spacing (Figure 8.19). This did not accurately represent the conditions in the field but provided input for models to compare the effect of different cement contents and microcracking efforts. The drying shrinkage in the field would depend on the curing method, humidity, and ambient conditions. FDR-C layers are typically surfaced with an asphalt concrete overlay between three and seven days after construction, which will further retard the drying shrinkage rate.

8.4.4 Crack Width and Spacing Results with Effective Layer Thickness Reduction

The modeling results for the microcracking simulation case that considered both stiffness reduction and thickness reduction are discussed below. The material inputs are provided in Table 8.3, and the layer thicknesses for the different cases are provided in Table 8.5.

Crack Development Time

The calculated times at which the shrinkage strain exceeded the tensile strength of the FDR-C layer, for the different cases, are provided in Figure 8.20. Note that Crack Event #1 is the edge of the slab and is considered to have occurred at 0 hours.

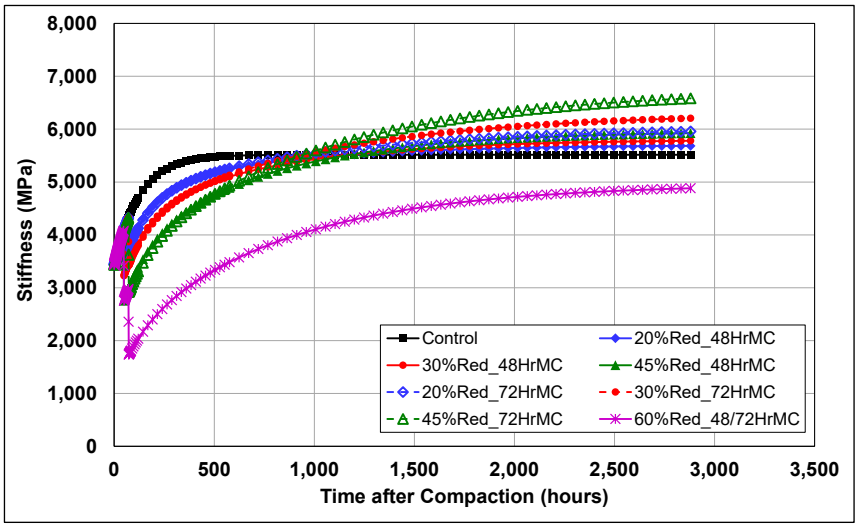

Figure 8.15: 2.5% Cement: Stiffness input.

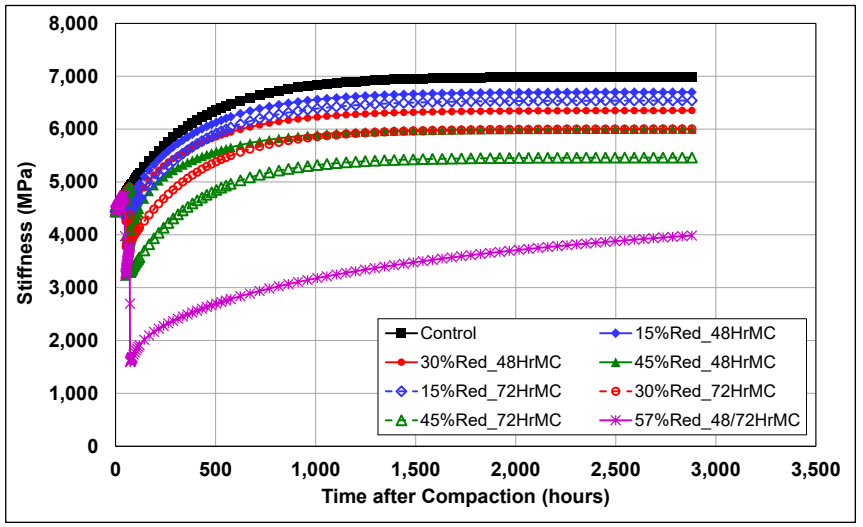

Figure 8.16: 4% Cement: Stiffness input.

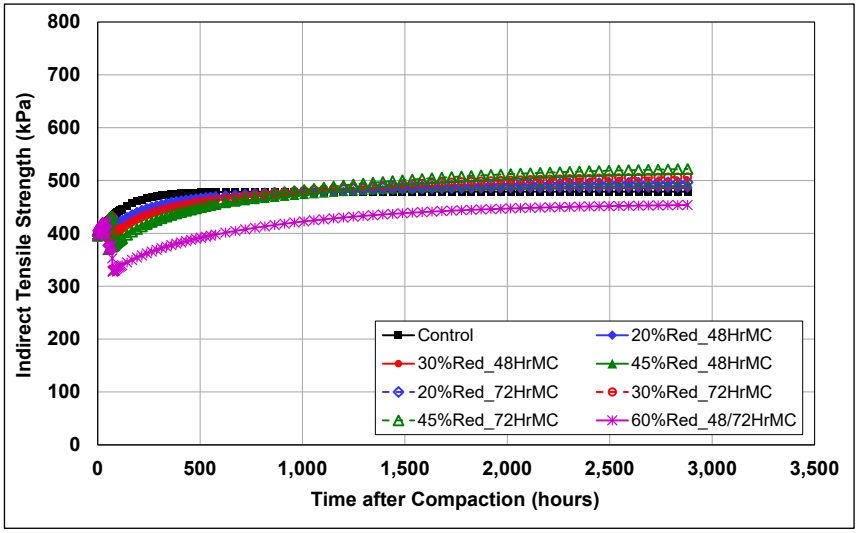

Figure 8.17: 2.5% Cement: Indirect tensile strength input.

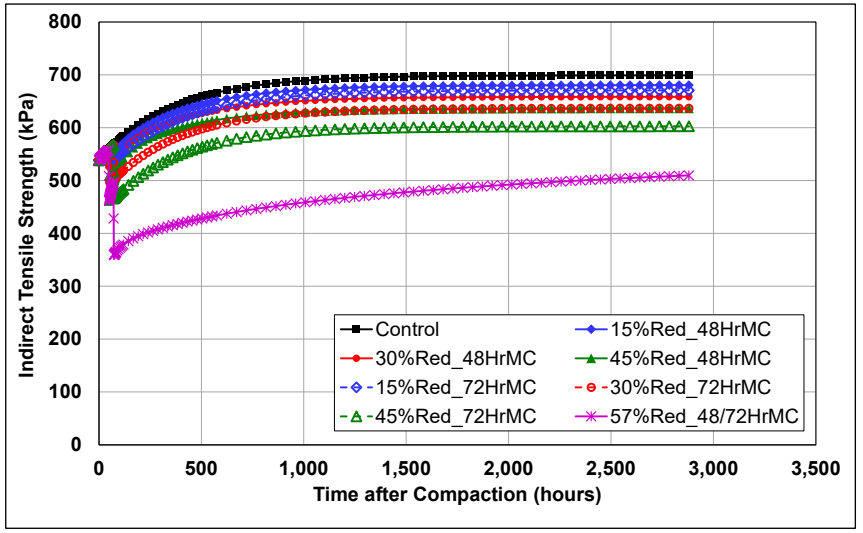

Figure 8.18: 4% Cement: Indirect tensile strength input.

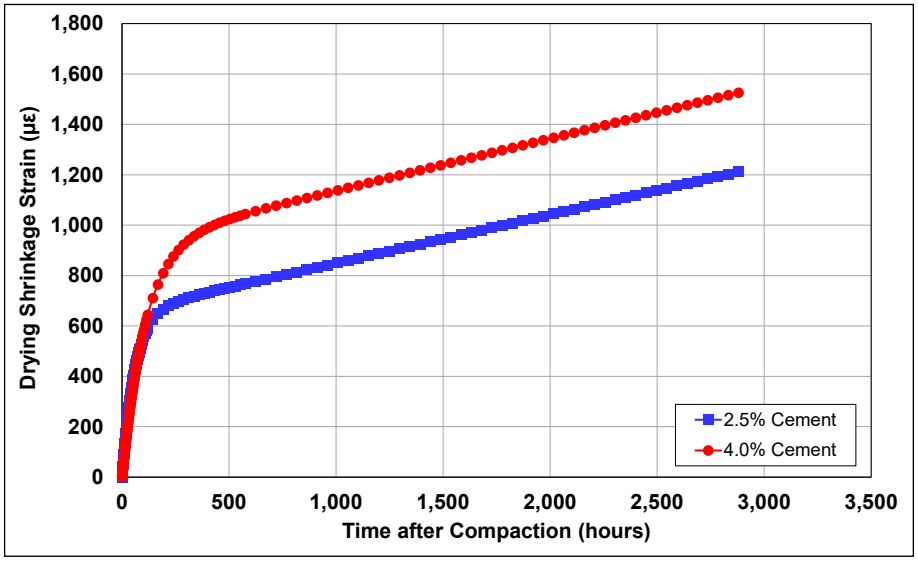

Figure 8.19: Drying shrinkage strain input.

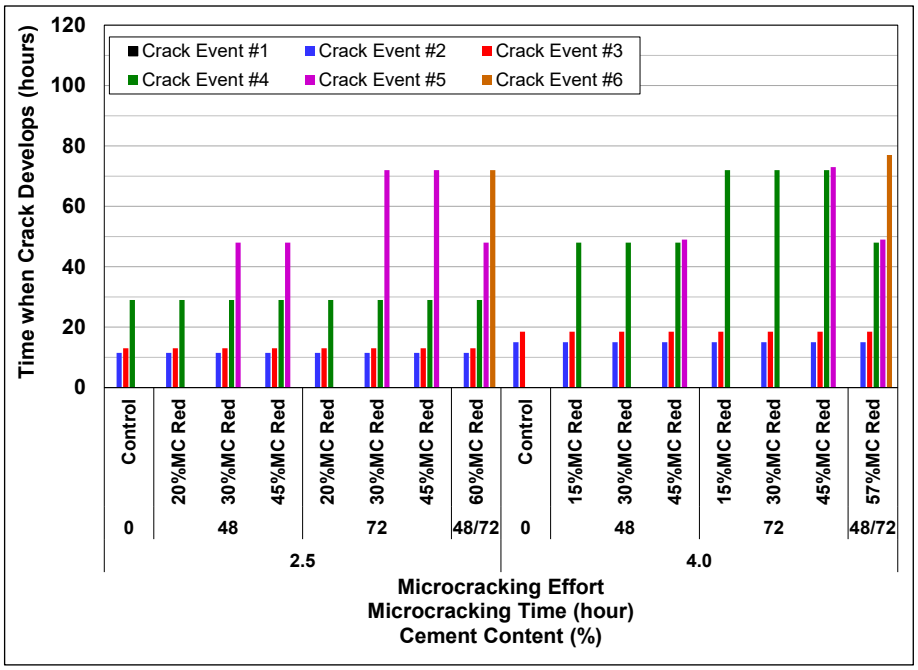

Figure 8.20: Cracking event time with effective thickness reduction during microcracking.

The results show that:

- The difference in crack development before the first microcracking effort at 48 hours for both cement contents was the number of cracking events. The 2.5% cement-content material had four cracking events, compared to three events for the 4% cement-content material. This implies that the crack spacing of the 2.5% cement-content material was half that of the 4% cement-content material before microcracking.

- The effect of microcracking, through stiffness (and strength) reduction, as well as the increase in restraint stress due to the reduction in cross sectional area of the layer caused additional cracking events depending on the microcracking effort.

Strength and Stress Development

The simulated strength and restraint stress development with time for the 2.5% cement-content material, microcracked at 48 hours and again at 72 hours, are plotted in Figure 8.21. The times at which cracking and microcracking events occurred are also provided. The results illustrate how the restraint stress changed with time.

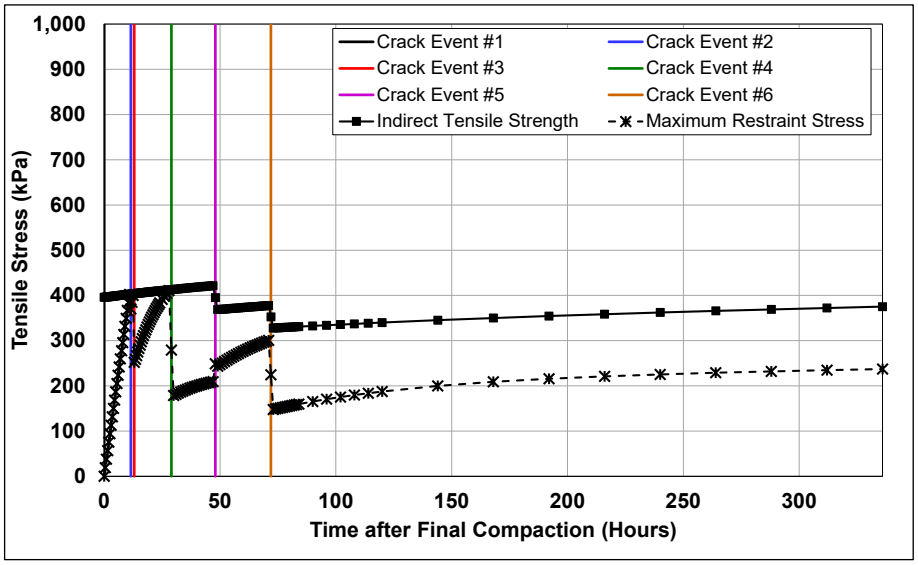

Figure 8.21: Stress and crack development over time with effective thickness reduction.

Crack Spacing and Crack Width

The simulated crack spacings after four months are plotted in Figure 8.22. The number of cracks calculated accordingly, are plotted in Figure 8.23. The results show that:

- With no microcracking, the crack spacing was the longest between cracks
- Crack spacing reduced between cracks with increased microcracking input
- The shortest distance between cracks was achieved at high energy input levels with three microcracking passes

The number of expected drying shrinkage cracks in the FDR-C layer increased with increasing energy input. The higher strength of the 4% cement-content material resulted in either equal or fewer expected cracks for the same energy input compared to the 2.5% cement-content material.

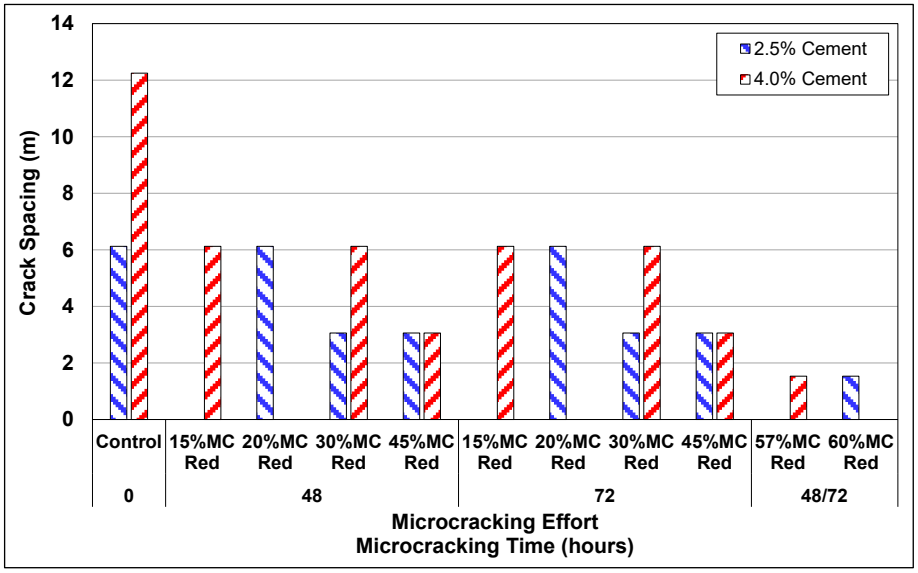

Figure 8.22: Crack spacing with effective thickness reduction.

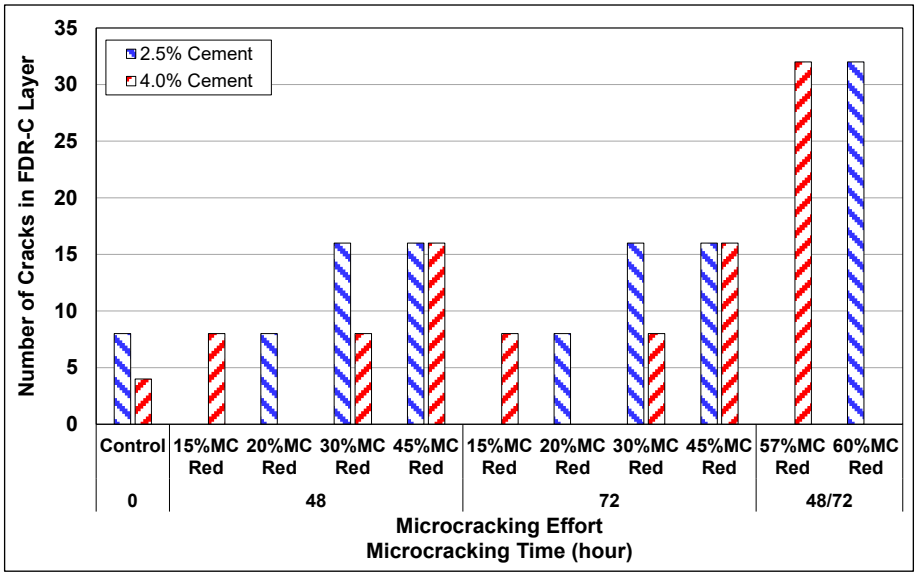

Figure 8.23: Crack density with effective thickness reduction.

The crack width results plotted in Figure 8.24 show the simulated normalized crack widths for the different cases after four months. The simulated crack widths, which ranged between 0.5 and 4.2 mm, and between 0.8 and 9.2 mm for the 2.5% and 4% cement-content materials, respectively, were significantly wider than the measured crack widths on the FDR-C Test Road *(12)*. This was attributed to the shrinkage model used for this simulation, which did not plateau like the model developed by Wang *(34)* (discussed in Section 7.5), but rather continued to shrink with time after the initial rapid shrinkage after approximately five days. Since all the simulated cracks had developed before the five-day (130-hour) mark, the constant increase in shrinkage

resulted in wider cracks rather than adding new cracks. Although the simulated crack widths were wider, there are a number of observations that can be made from the trends in the results, and therefore the crack width results were normalized to the crack width of the primary crack (Crack Event #1) of the 2.5% cement-content material without microcracking. The results from this simulation showed that:

- Without microcracking, the higher strength of the 4% cement-content FDR-C layer would lead to crack widths greater than twice the width of those in the 2.5% cement-content FDR-C layer.
- Increasing energy input during microcracking reduced crack widths accordingly.
- Crack widths in the 2.5% cement-content FDR-C layer were generally narrower than those in the 4% cement-content layer.

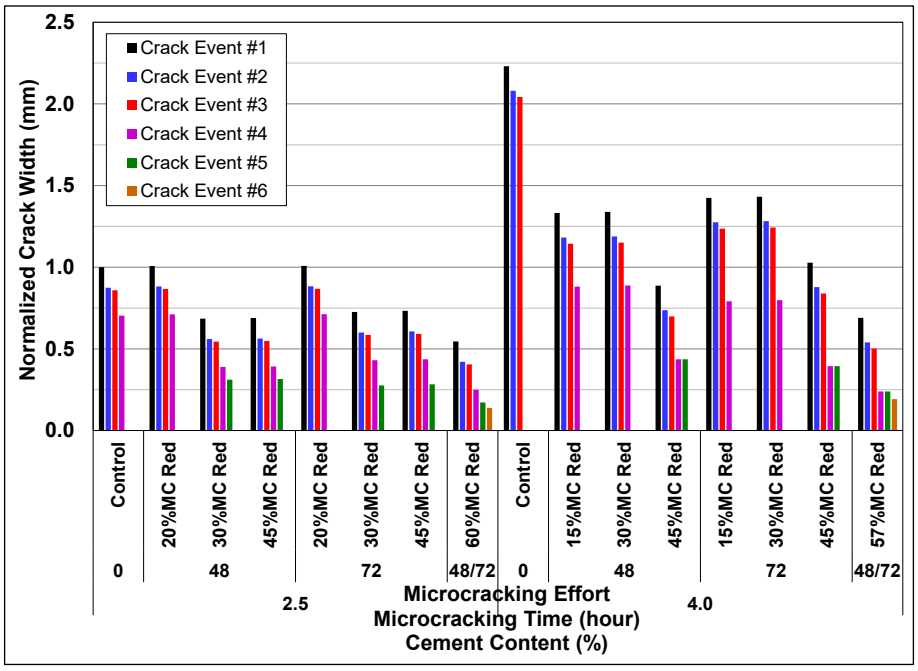

Figure 8.24: Normalized crack widths with effective thickness reduction.

8.4.5 Crack Width and Spacing Results with Constant FDR-C Layer Thickness

The simulation results without including effective layer thickness reduction damage component are discussed in this section. The material inputs are listed in Table 8.3, and the FDR-C layer thickness was kept constant at 250 mm for the entire simulation. These results showed little to no sensitivity to microcracking but are provided to illustrate the case of not considering the damage component that reduces the effective layer thickness.

Crack Development Time

The times of crack development for the different cases are plotted in Figure 8.25. Note that for the purposes of the analysis, Crack Event #1 is the edge of the slab and is considered to have occurred at 0 hours. The results show that:

- Fewer cracks developed compared to the case with effective layer thickness reduction (Figure 8.20).
- The 2.5% cement-content material results did not have any additional crack development after 29 hours, even with microcracking.
- The 4% cement-content material results showed the potential for an additional crack to develop after microcracking (at 48 hours or 72 hours).

Stress and Strength Development

The simulated strength and restraint stress development with time for the 2.5% cement-content material, microcracked at 48 hours and again at 72 hours, are plotted in Figure 8.26. In contrast to the case discussed in Section 8.4.4 where effective layer thickness reduction was considered, microcracking did not cause additional crack development. It is clear that the stress did not increase sufficiently, or that the strength decreased sufficiently with microcracking, to induce further shrinkage cracking.

Crack Density

The simulated crack spacings after four months are plotted in Figure 8.27. The number of cracks calculated accordingly, are plotted in Figure 8.28. In contrast to the crack spacing results shown in Figure 8.22, there was no change in the crack spacing with microcracking for the 2.5% cement-content material. The 4% cement-content material did develop an additional crack with microcracking, however. The number of cracks shown in Figure 8.28 and the crack widths shown in Figure 8.29 similarly show the insignificant effect of microcracking on the crack development if effective thickness is not considered.

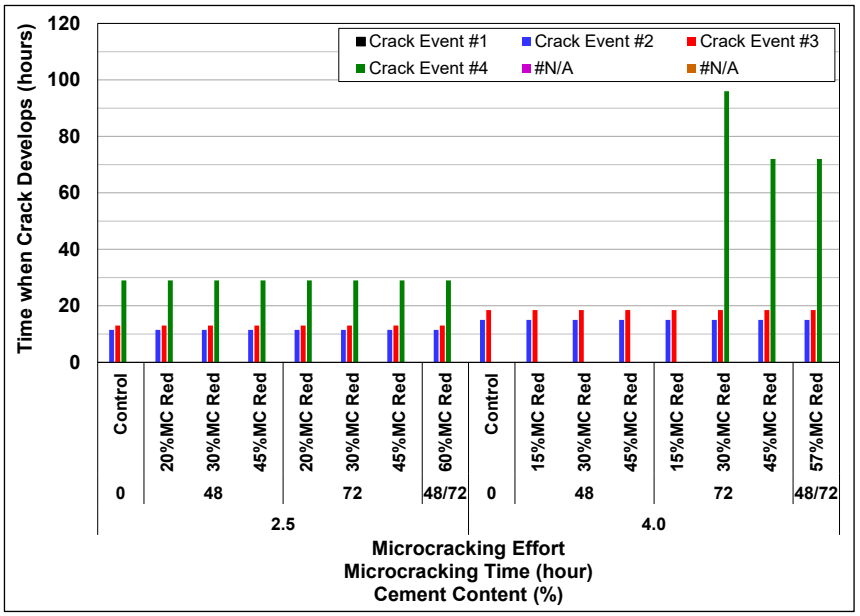

Figure 8.25: Cracking event time with no thickness reduction.

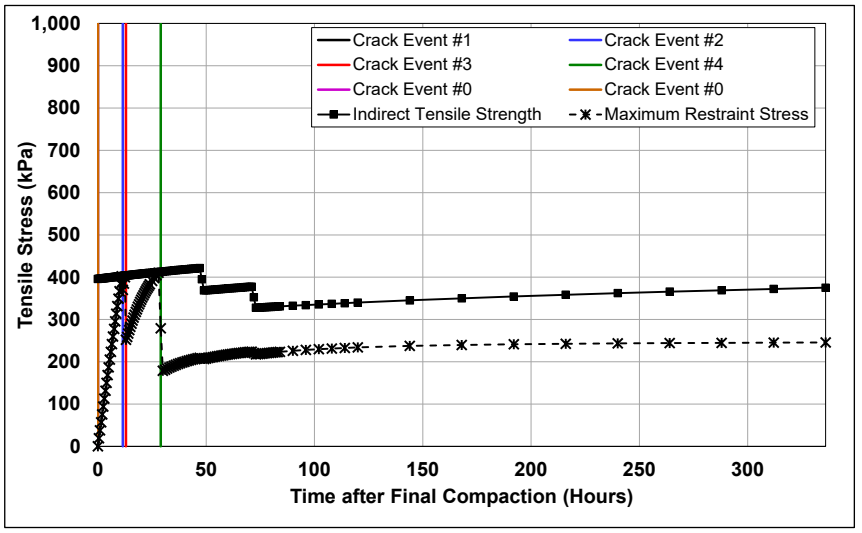

Figure 8.26: Stress and crack development with no thickness reduction.

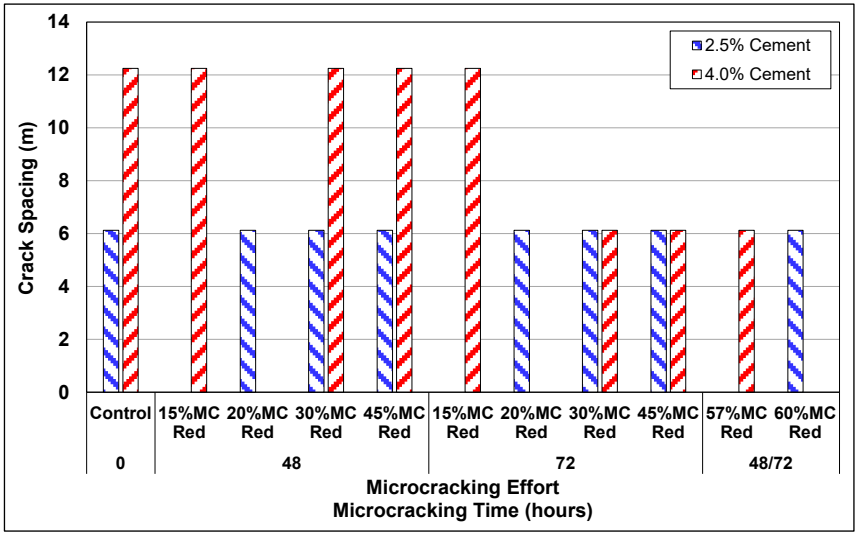

Figure 8.27: Crack spacing with no thickness reduction.

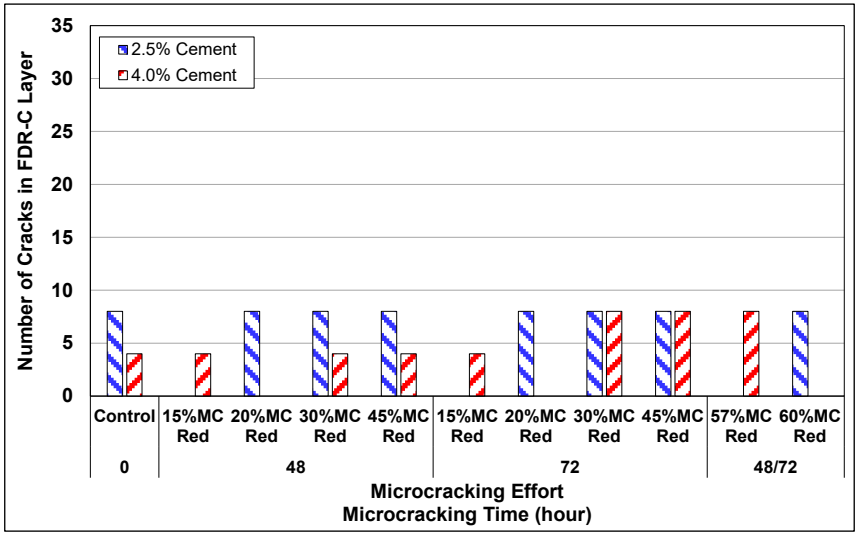

Figure 8.28: Crack density with no thickness reduction.

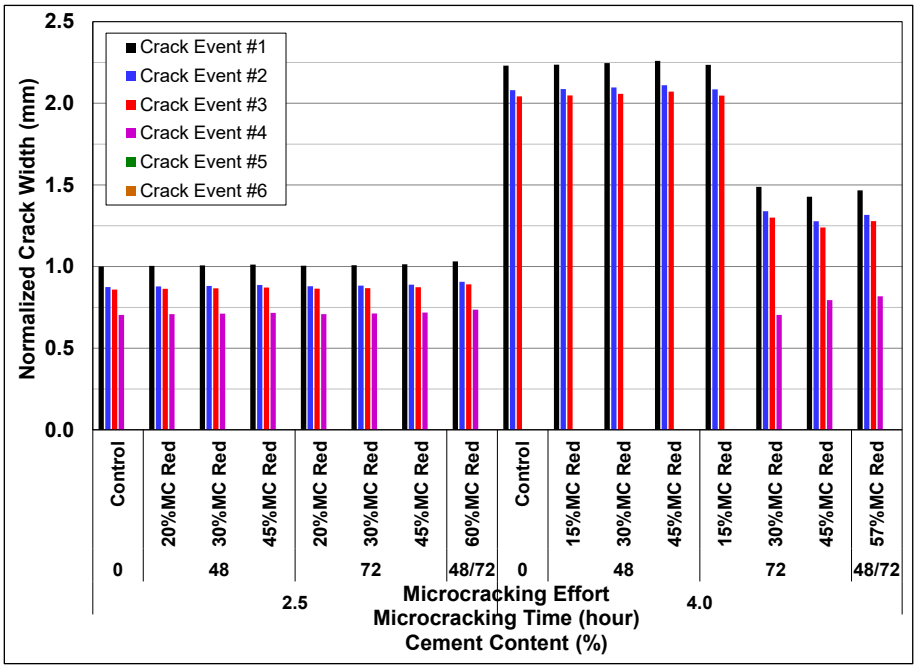

Figure 8.29: Normalized crack widths with no thickness reduction.

8.4.6 Comparison Between Modeling, Simulation and the FDR-C Test Road

Crack Development

Crack observations from the FDR-C Test Road *(12)* showed that drying shrinkage cracks, with a spacing between 10 and 20 m (≈33 and 66 ft.) were visible on the FDR-C layer between 48 and 72 hours after construction on the 4% cement-content material and before any microcracking was applied. This supports the simulations, which indicated that shrinkage cracks can develop soon after construction.

Crack Density

The field results showed a significant decrease in the number of reflected cracks for the lower cement content material. Reflective cracking also decreased with increased energy input during microcracking *(12)*. The simulated results that most closely reflected this behavior was the case that included the damage component reducing the effective thickness of the FDR-C layer after microcracking. To validate the results that included the effective layer thickness reduction, crack density on the FDR-C layer was compared to the measured reflected crack density on the microsurfacing on the FDR-C Test Road. Crack density was calculated using the assumption that every crack that developed was a full-width crack. The simulated section was 49 m long and 5.2 m wide, similar to one FDR-C Test Road experiment cell. The number of cracks associated with each

crack development phase is shown in Table 8.7. For each scenario, the number of crack events are known. If all the cracks that developed with each crack event reflected through the microsurfacing, as illustrated in Figure 8.30, it would mean that:

- The crack density of the simulated results would exceed the measured crack density.
- The reflected crack density would increase with microcracking, which is inconsistent with the FDR-C Test Road results.
- Increasing the design strength would decrease the number of reflected cracks.

Table 8.7: Inputs to Evaluate Model Sensitivity

Crack Event	Number of Full-Width FDR-C Cracks	Accumulated Number of Cracks
1	1	1
2	2	3
3	4	7
4	8	15
5	16	31
6	32	63

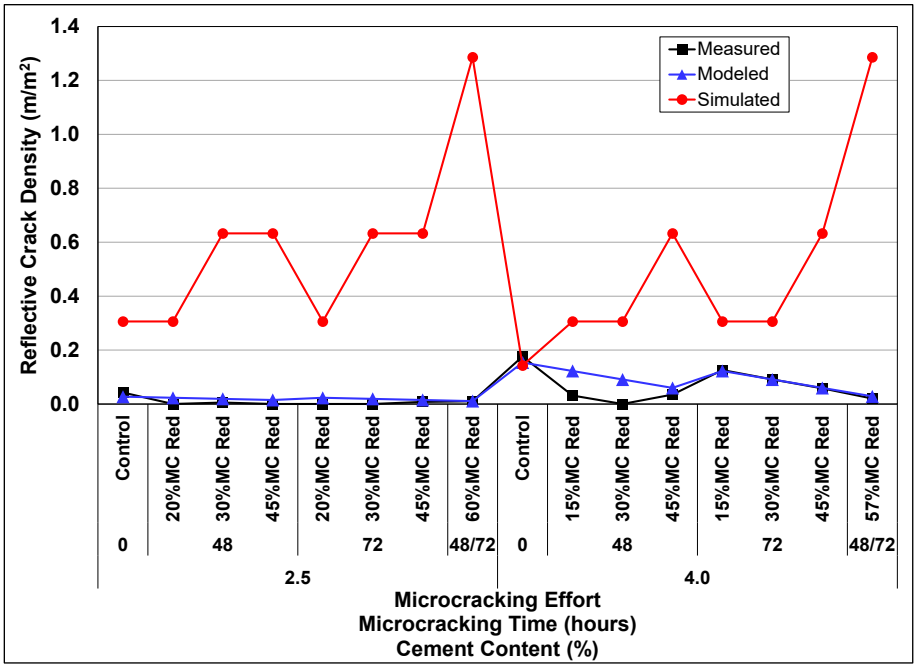

Figure 8.30: 128-day crack densities with threshold crack width.

The FDR-C Test Road results showed that microcracking and reducing the strength of the FDR-C layer reduced the number of reflective cracks. The forensic investigation on the FDR-C accelerated wheel-load test sections *(12)* also showed that not all the drying shrinkage cracks in an FDR-C layer will reflect through the asphalt concrete layer. A threshold crack width below which the drying shrinkage cracks in the FDR-C layer do not have sufficient energy to reflect through the

asphalt concrete layer should therefore exist. This threshold crack width was calculated by determining the minimum crack width that reduced the error between the simulated and modeled crack density. This was achieved by minimizing the sum of the square of the error (SSE) between the modeled results and the simulated crack densities for the effective layer thickness reduction case. The normalized crack width that minimized the SSE between the simulated and modeled reflective crack densities was 0.99. Since the crack widths calculated by the simulation overestimated the crack widths observed on the FDR-C Test Road, and since the trend in the observation is of more importance than the actual crack width, the crack width was presented as a percentage of the crack width normalized to the primary crack width of the 2.5% cement-content material, without microcracking, after four months.

Figure 8.31 shows the reflected crack density of the simulated results, which considered effective thickness reduction, together with the modeled and measured reflected crack densities with the threshold crack width incorporated. The simulated results were able to predict the reduction in crack density with increased microcracking for both cement contents.

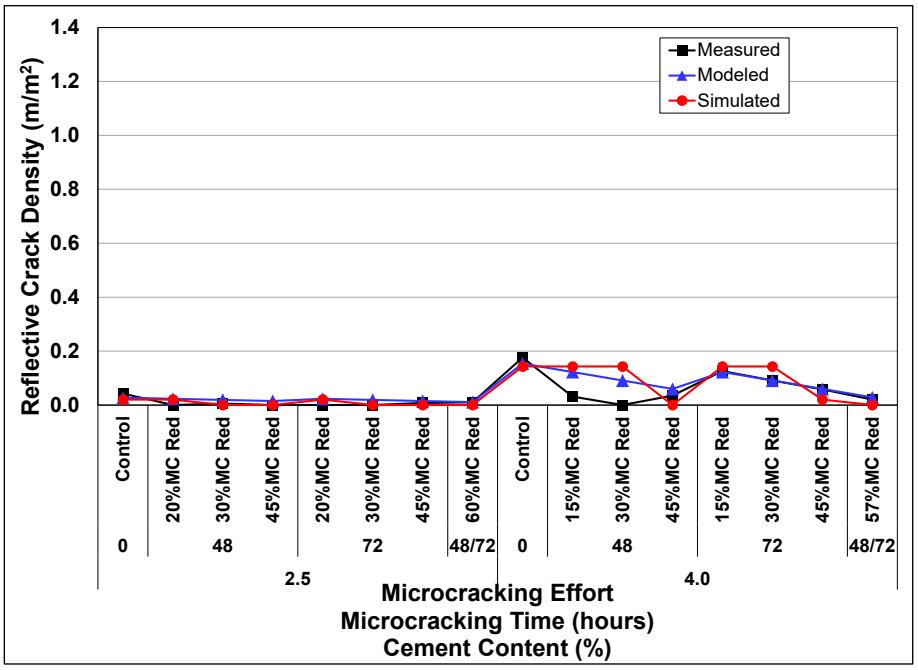

Figure 8.31: 128-day crack densities with threshold crack width and thickness reduction.

Linear regression was used to determine an R^2 value between the simulated results and the modeled results (0.83), and between the simulated and measured results (0.52), which are plotted in Figure 8.32.

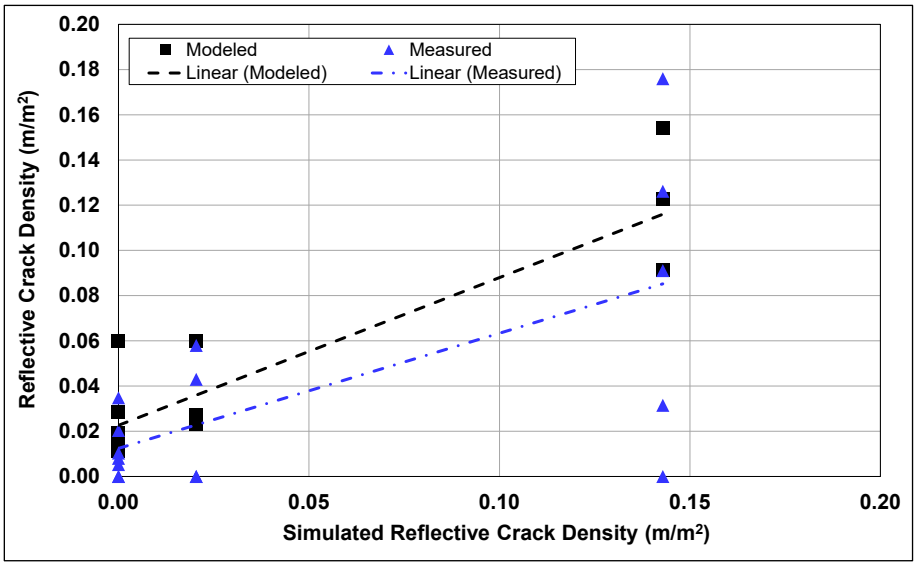

Figure 8.32: Correlation between simulated, modeled, and measured crack densities.

Figure 8.33 shows the normalized crack widths of the different cracking stages relative to the threshold crack width to develop reflective cracking. This confirms that not all the drying shrinkage cracks in an FDR-C layer reflect, but also shows how increasing the microcracking effort can introduce a buffer between the expected crack widths and the threshold crack width required to reflect through the surface layer to allow for future drying shrinkage.

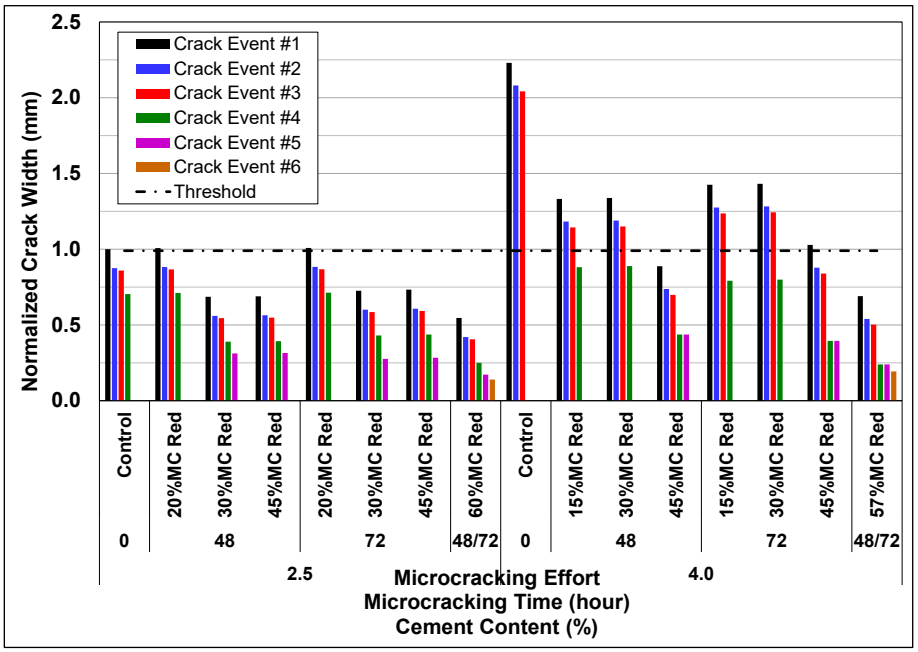

Figure 8.33: Normalized crack widths with threshold crack width.

Considering the threshold crack width calculated for the case without thickness reduction (Figure 8.34), it is clear that the simulated results do not show a reduction in crack density with increased microcracking, as expected. Using the same methodology to determine the threshold crack width without thickness reduction, a normalized crack width of 1.32 mm was calculated, which resulted in an R^2 between the simulated and modeled results of 0.79, and an R^2 of 0.75 between the simulated and the measured results.

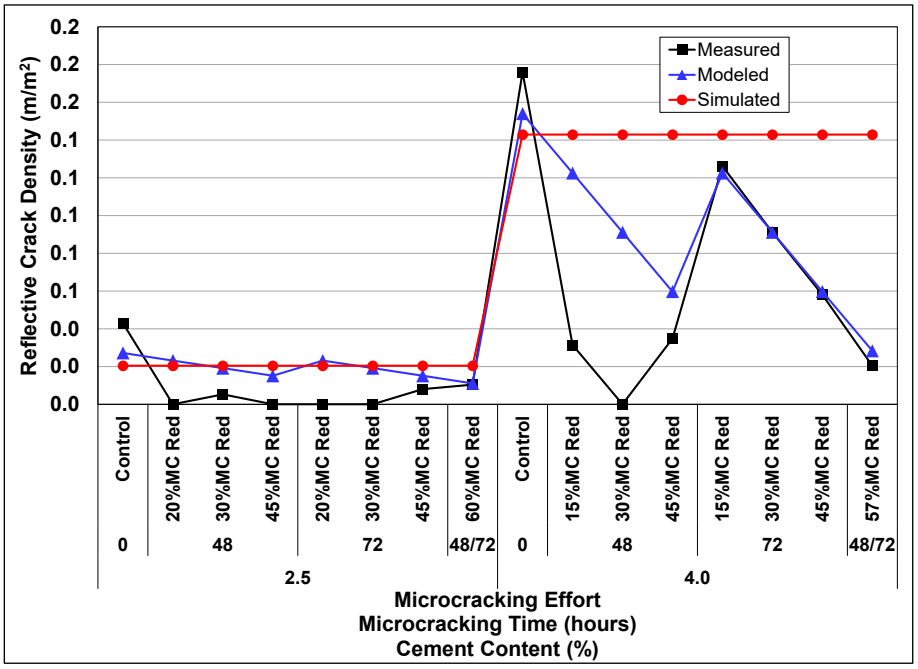

Figure 8.34: 128-day-crack densities with no threshold crack width or thickness reduction.

The reflected crack width results for the simulated case without effective thickness reduction, together with the modeled and measured crack results, are plotted in Figure 8.35. The results show that the simulation with no consideration for effective thickness reduction was unable to predict the trend in the reflected drying shrinkage cracks for the 2.5% cement-content results, but it did simulate the reduction in crack density for the 4% cement-content material results.

The case considering effective layer thickness provided a closer simulation of the effect of microcracking and design strength on reflected crack density. It can thus be concluded that microcracking does have some effect on effective layer thickness and was therefore included in subsequent analyses. This is, however, worth investigating further to better understand the observed field observations by:

- Coring before and after microcracking to compare material properties and test to assess intact effective layer thickness reduction.
- Investigating the effect of confinement on FDR-C materials during microcracking to determine if crushing occurs.
- Developing an FEM model that more accurately determines the stresses below the roller through field calibration.

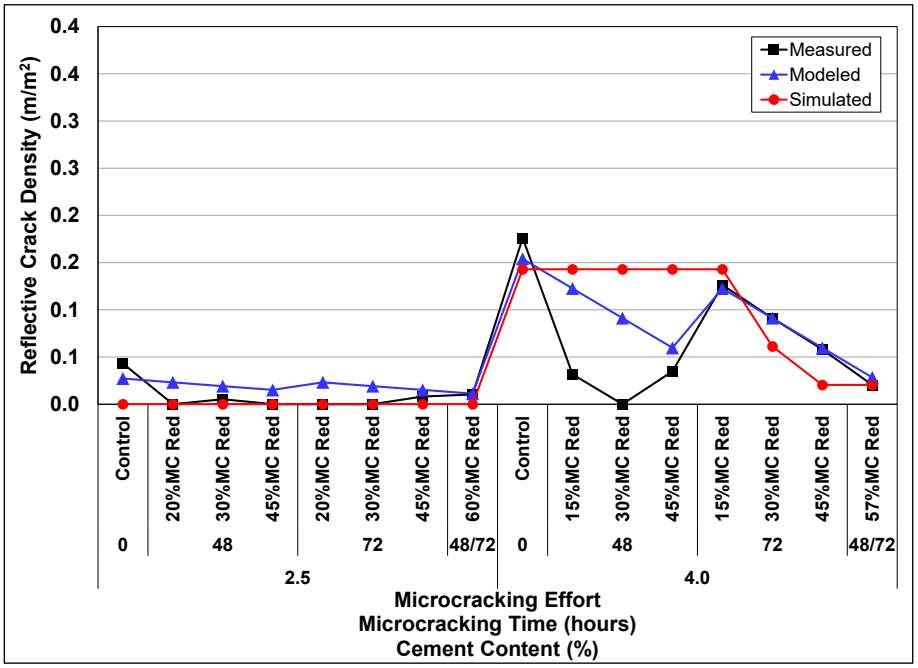

Figure 8.35: 128-day crack densities with threshold crack width and no thickness reduction.

8.4.7 Comparing the Effects of Early Microcracking

Microcracking at 24 hours was simulated to quantify the effect of earlier microcracking on crack density and crack spacing. By microcracking earlier, crack spacing and the associated slab lengths, could be reduced. With reduced slab length and increased number of cracks at an early stage in the shrinkage development, the successive shrinkage strain can be distributed over more cracks to minimize the accumulation of crack widths over individual cracks. This simulation was performed considering effective layer thickness reduction, with layer thicknesses determined from FEM analyses after each microcracking event listed in Table 8.8.

Crack Development Time

The effect of microcracking at 24, 48, and 72 hours on crack development time is plotted in Figure 8.36 for the different cement contents and stiffness reduction levels used on the FDR-C

Test Road (note that Crack #1 is the edge of the slab and is considered to have occurred at 0 hours and that microcracking at 48 hours and again at 72 hours was not included in this simulation).

Table 8.8: Effective FDR-C Thickness Reduction with Microcracking at 24 Hours

Cement Content (%)	Microcracking Time (hr)	Stiffness Reduction (%)	Total Force (kN/cm)	Total Energy Input (Joule/m^3)	Stiffness (MPa)	ITS (kPa)
2.5	24	0	0	0	3,791	410
		20	1.42	13.6	3,033	380
		30	2.84	42.9	2,654	365
		45	4.26	240.5	2,085	342
4.0	24	0	0	0	4,372	534
		15	1.42	7.6	3,716	493
		30	2.84	42.9	3,060	451
		45	4.26	240.5	2,405	410

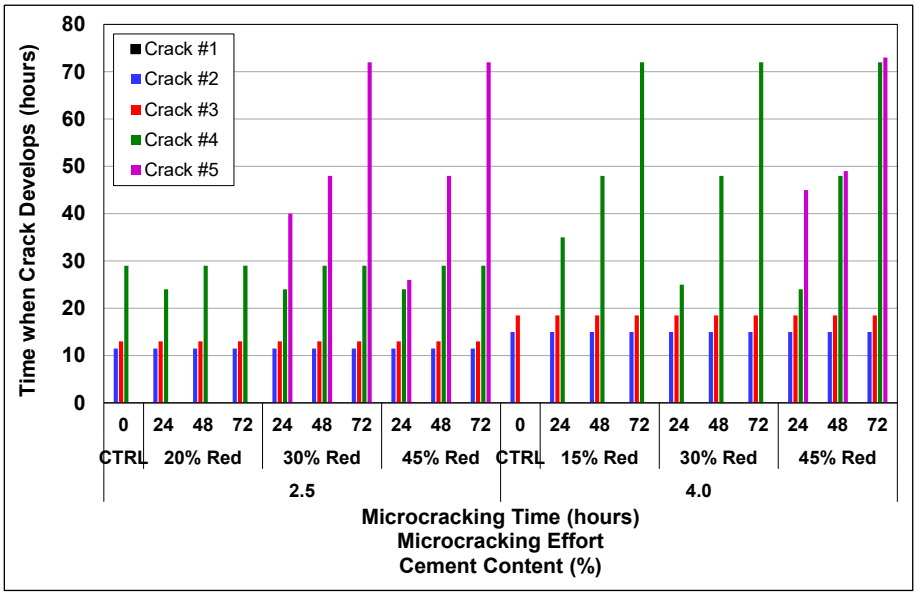

Figure 8.36: Cracking event time comparison between microcracking at 24, 48, and 72 hrs.

Additional cracks developed either during or after the microcracking event as the effective layer thickness was reduced during microcracking due to the increased restrained stress over the reduced cross section. This implies that:

- Increasing the curing time before microcracking generally lengthens the time before cracks develop.
- Increasing the energy input, or stiffness reduction, results in an increase in the number of cracking events.

Crack Width

The effects of microcracking at either 24, 48, or 72 hours are plotted in Figure 8.37. The threshold crack widths determined for the simulations with effective thickness reduction are also provided to illustrate the change in the number of reflected cracks.

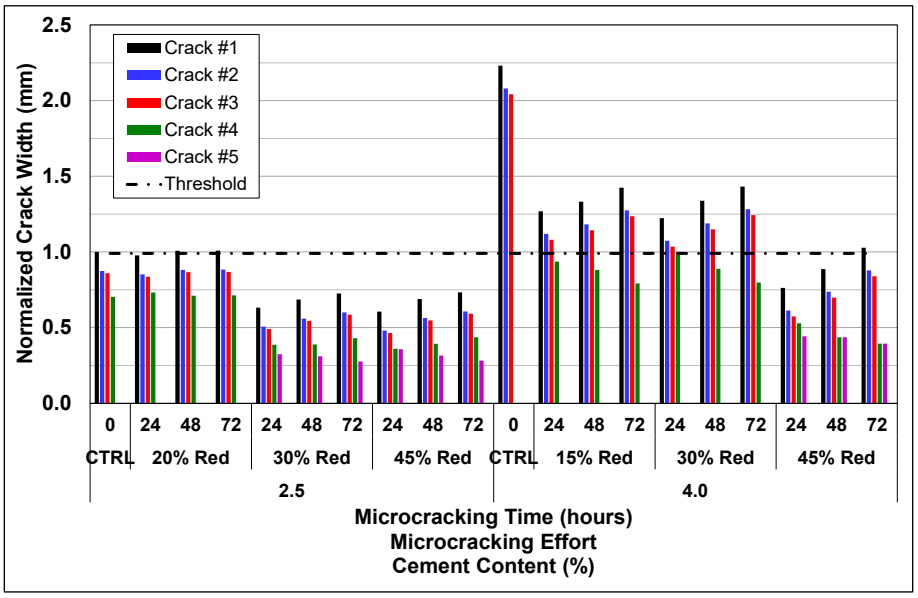

Figure 8.37: Normalized crack widths at 24, 48, and 72 hrs.

The crack-width results show that:

- Increasing the curing time before microcracking increases the widths of the cracks that develop before the microcracking event. This is due to the number of available cracks over which the shrinkage strain can be distributed before the cracks, after microcracking, have developed.
- Increasing the curing time before microcracking increases the difference in the simulated crack widths of the different cracks that develop (Crack Events #1 through #5). This is a result of the remaining shrinkage potential after the cracks have developed. If all the cracks develop in short succession, the remaining shrinkage strain will be equally distributed across all the cracks. If the period over which cracks develop is longer, a greater portion of the shrinkage strain will be applied to the cracks that occur soon after construction compared to the cracks that develop later.

For the 2.5% cement-content material with lower shrinkage potential, earlier microcracking can be beneficial to reduce the difference between the crack widths of the different cracking events. With reduced deterioration rates, localized failures associated with wide reflected cracks can be mitigated, with the pavement deteriorating more uniformly at each crack.

The risk of microcracking too early is evident for the 4% cement-content simulations (Figure 8.38), with microcracking at 24 hours and stiffness reductions of 15% and 30%. Even though the number of cracks that developed are the same for the cases microcracked at 48 and 72 hours, there is a risk that all of the cracks that had developed would reflect through the surface layer, thereby increasing the reflected crack density. Microcracking at 24 hours with three microcracking passes and a total energy input of 4.26 kN/cm resulting in 45% stiffness reduction, does show a potential case for higher strength materials. By forcing the drying shrinkage cracks to develop at a very early stage, the shrinkage strain is effectively distributed over all of the cracks, thus minimizing the crack widths to the point where none are expected to reflect through the surface layer.

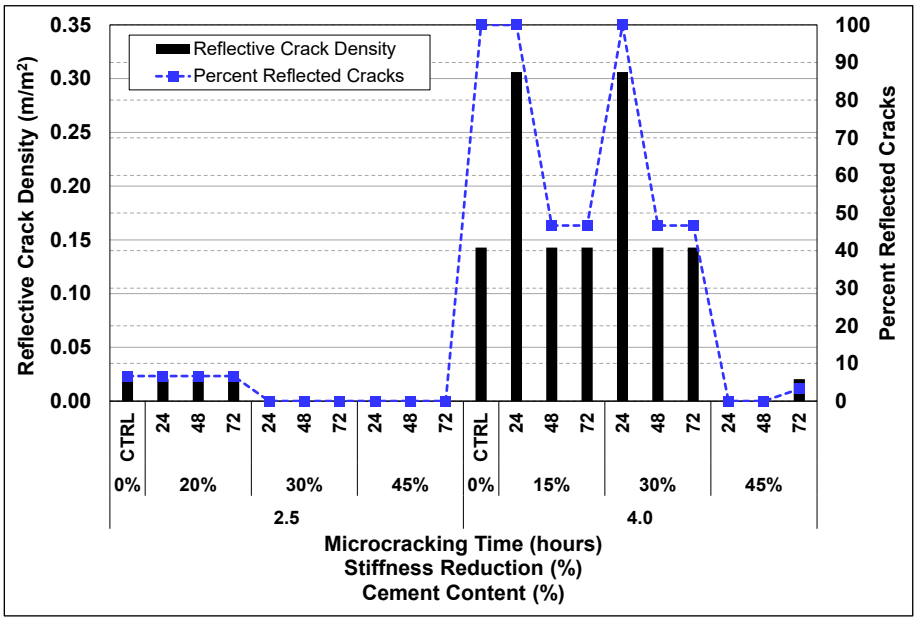

Figure 8.38: Reflective crack density and percent reflected cracks comparison.

8.4.8 Effect of Reduced Shrinkage Rates on Crack Development

A minor case that included the 2.5% and 4% cement-content materials without microcracking was simulated with different scaling factors, ranging from 20% to 100%, on the respective shrinkage development for the two cement contents, to consider the effect on crack development when using a stabilizer with reduced shrinkage potential.

Crack Development Time

The simulated crack development time for the two cement contents and the different shrinkage scaling factors are plotted in Figure 8.39. Note that Crack #1 is the edge of the slab and is

considered to have occurred at 0 hours. The results show how the expected time of crack development increases as the shrinkage rate decreases.

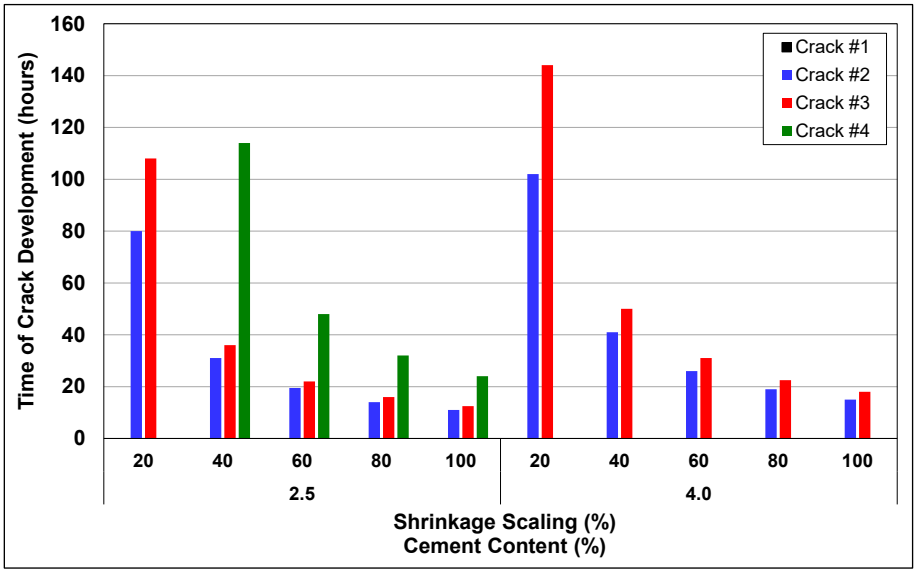

Figure 8.39: Cracking event time for different shrinkage scaling factors.

Crack Width

The effects of reduced shrinkage on simulated crack widths are plotted in Figure 8.40. The results show that the expected simulated crack widths reduce proportionally to the reduction in shrinkage, attributed to restraint stresses that develop in the layer as a function of slab length or an intact layer.

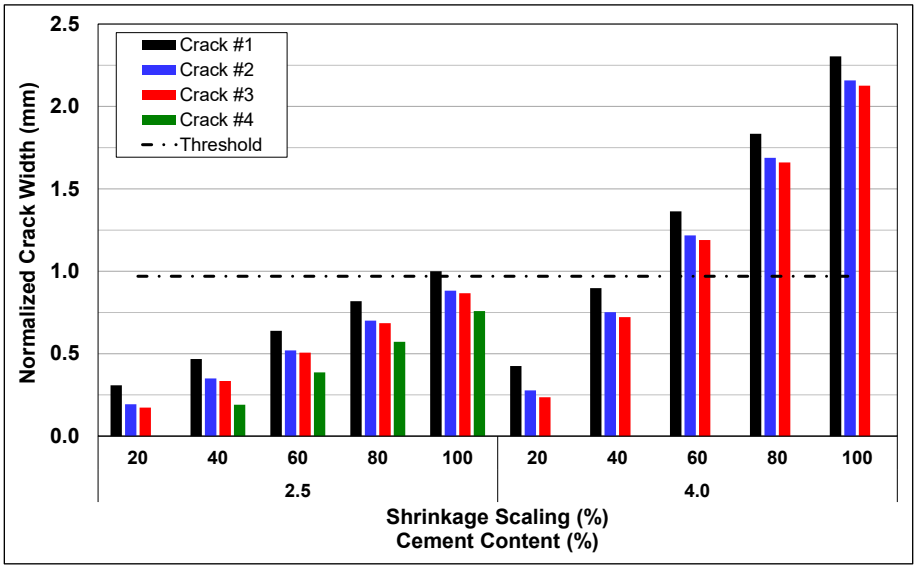

Figure 8.40: Normalized crack width with scaled shrinkage development, no microcracking.

8.5 Discussion

8.5.1 Microcracking Mechanism

Microcracking has been described as a mechanism that creates a fine network of hairline cracks in an FDR-C layer to minimize major shrinkage cracks *(38)*. The research discussed in this chapter builds on initial findings and shows that the "fine network" of cracks results in a reduction in stiffness, and consequently the strength of the layer as a result of fatigue damage of the cementitious bonds under cyclic loading. The reduction in strength during microcracking causes additional "major cracks" to develop due to the development of restraint stress. This increased number of drying shrinkage cracks in the layer also increases the number of cracks over which the shrinkage strain is distributed. Reduction in crack widths with microcracking reduces the number of cracks that are likely to reflect through the surface layer. This can be perceived as a reduction in major cracks in the FDR-C layer, which is contrary to what is actually happening in the FDR-C layer. FEM modeling has also shown that there is potentially an effective layer thickness reduction as a result of microcracking.

Tensile stresses induced during microcracking greatly exceed the tensile strength at the bottom of the FDR-C layer. Given that cement-treated material is weak in tension, it was assumed that the effective intact FDR-C layer thickness would reduce by the depth over which the tensile stress exceeded the tensile strength. This was not validated with coring before and after microcracking on the FDR-C Test Road, and a limited number of cores extracted 18 months after construction of the FDR-C Test Road indicated that the layer was fully intact. Since field and laboratory observations have shown that recementation can occur as long as moisture is present and simulation results suggest that considering effective layer thickness reduction produces trends similar to field observations, it is likely that some degree of effective layer thickness reduction occurs during microcracking.

8.5.2 Reflective Drying Shrinkage Cracks

The simulations discussed in this chapter support the forensic investigations on the FDR Test Track (accelerated wheel load testing), which showed that not all drying shrinkage cracks in the FDR-C layer reflected through the asphalt concrete surfacing. Controlling the width of drying shrinkage cracks is therefore critical to minimize the number of reflected drying shrinkage cracks. This simulation showed that this can be achieved by increasing the number of cracks, and

subsequently reducing the slab lengths between cracks, to evenly distribute the total shrinkage of the FDR-C layer and minimize accumulation of shrinkage strain at each crack.

8.5.3 Effect of Curing Time Before Microcracking on Crack Density

The effect of curing time before microcracking on crack width and crack density depends on the strength and shrinkage potential of the FDR-C layer (Figure 8.36). In the simulations, several cracks developed before 24 hours for both cement contents. Each cracking event increased the number of cracks in the base by a factor of two, based on the number of cracks that had developed in the previous cracking event. By reducing the curing time before microcracking, the shrinkage strain is distributed over more cracks sooner, reducing the widths of cracks that developed prior to microcracking.

8.5.4 Optimum Microcracking Effort

Observations from the FDR-C Test Road led to the optimum microcracking effort being defined as the curing time before microcracking and the number of microcracking passes that results in the highest long-term stiffness (or lowest reduction in stiffness) to maximize fatigue life and that reduces the crack density to minimize failures associated with drying shrinkage cracks. The FDR-C Test Road results *(12)* showed that:

- The optimum microcracking benefit on the 2.5% cement-content material with a design strength of 3.5 MPa was achieved between 48 and 72 hours of curing, with an energy input of 4.26 kN/cm, or three passes of a 12-ton roller with a peak linear total force of 1.42 kN/cm.
- The optimum microcracking benefit on the 4% cement-content material with a design strength of 4.5 MPa was achieved at 48 hours of curing with an energy input of at least 3.0 kN/cm.

The simulated reflected crack density and stiffness development, four months after microcracking at either 24, 48, or 72 hours of curing for the 2.5% and 4% cement-content materials are plotted in Figure 8.41 and Figure 8.42, respectively. The simulated results agree closely with the observed field results in that the optimum microcracking effort (between 48 and 72 hours after construction with a total energy input of between 2.82 to 4.26 kN/cm) for the two cement contents was similar.

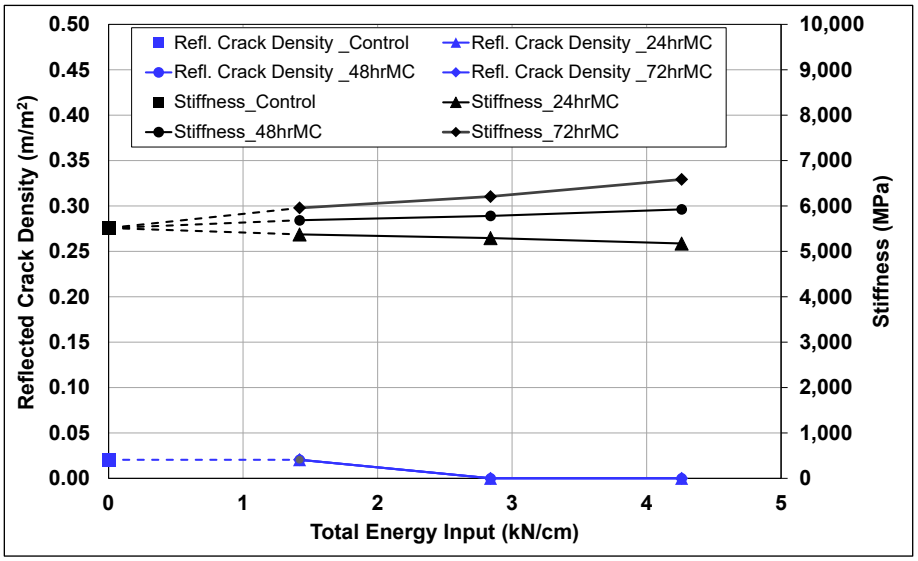

Figure 8.41: 2.5% Cement: Simulated reflected crack density and stiffness comparison.

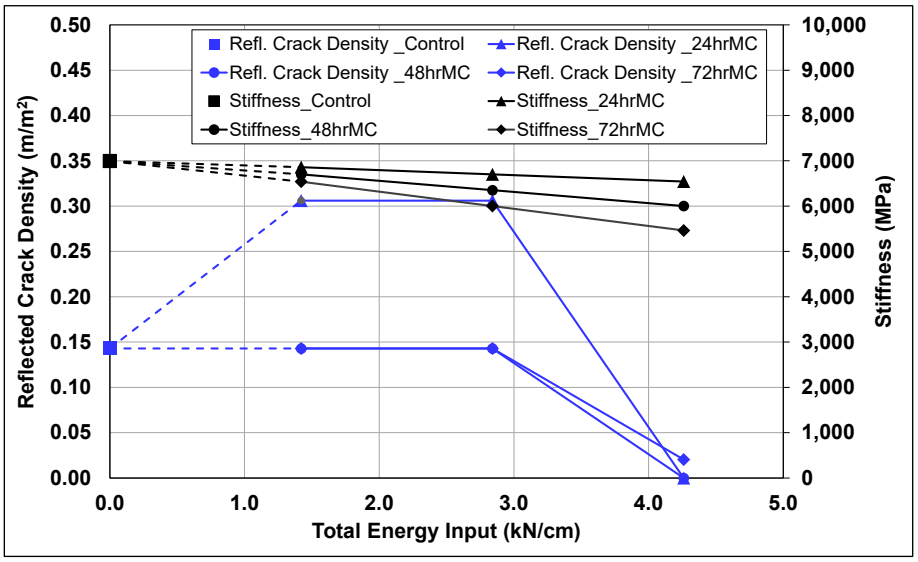

Figure 8.42: 4% Cement: Simulated reflected crack density and stiffness comparison.

The simulation results do suggest that microcracking at 24 hours, with a total energy input of 4.26 kN/cm, could effectively eliminate reflective cracking in materials with a high water-to-cement-for-cementation (w/c_c) ratio. This option warrants further investigation.

8.5.5 Effect of Strength on Shrinkage Crack Development

The 2.5% and 4% cement-content materials used in these simulations had seven-day design strengths of 3.5 and 4.5 MPa (500 and 650 psi), respectively. The simulated crack development of the two materials with no microcracking is plotted in Figure 8.43 and Figure 8.44 for the two

cement contents, respectively, to illustrate the effect of the increased resistance to cracking associated with higher strengths.

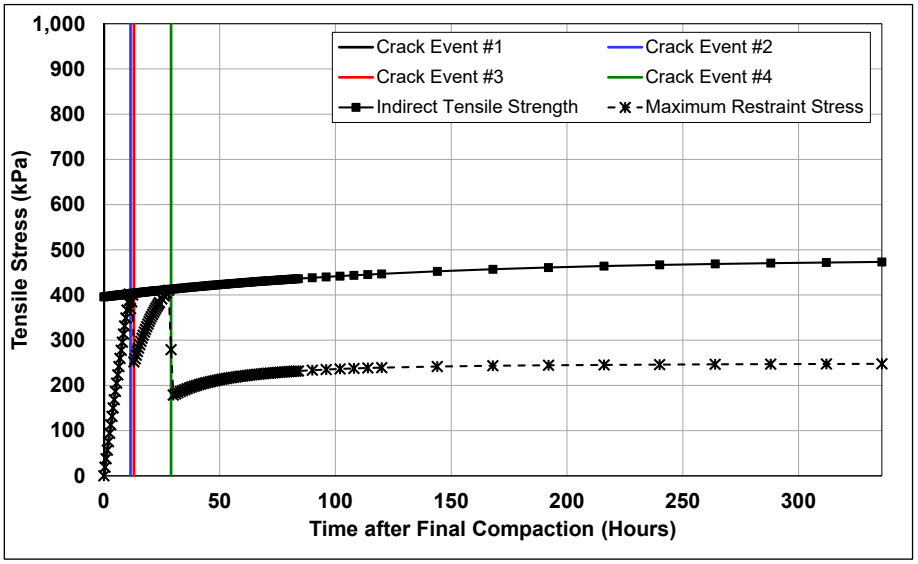

Figure 8.43: 2.5% Cement: Stress and strength history with shrinkage crack development.

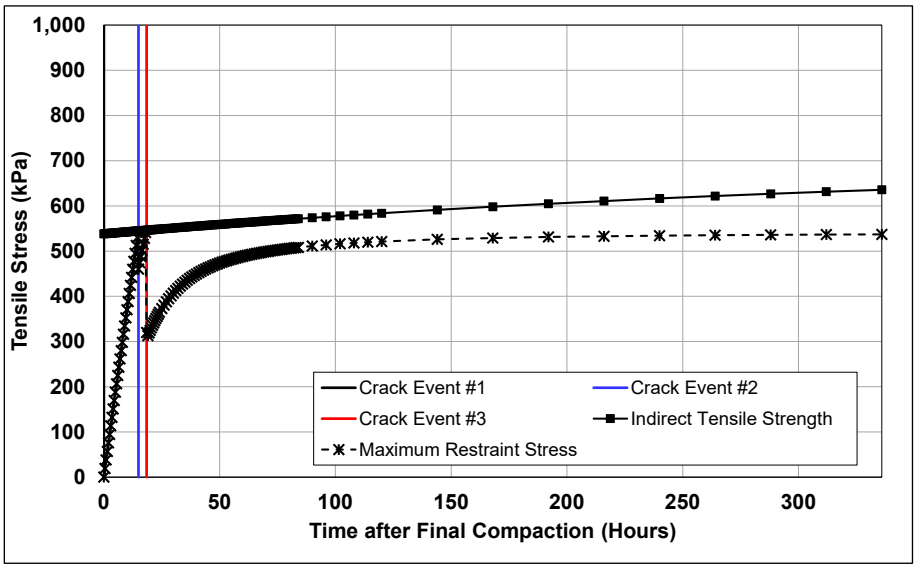

Figure 8.44: 4% Cement: Stress and strength history with shrinkage crack development.

The higher strength of the 4% cement-content material exceeded the restraint stress after the third cracking event and prevented the additional eight cracks from developing in a fourth cracking event. This resulted in fewer, but wider cracks compared to the 2.5% cement-content material. The simulated reflected crack widths in Figure 8.31 also shows the increased reflected crack density for the 4% cement-content material with no microcracking. These results agree with the results presented by George *(4)*, who showed how reflective crack density observed on

different projects correlated strongly with design strength. Although a minimum strength is a desirable property for resisting fatigue failure, very high strengths can adversely affect the fatigue life because it prevents the development of multiple shrinkage cracks, resulting in fewer, wider cracks.

The Caltrans specified mix design strength range for FDR-C layers at the time of conducting this study was 2.1 to 4.2 MPa (300 to 600 psi). This research has shown how reducing the strength of the material can reduce crack widths and reflective cracking. Several researchers *(4,16,39)* have advocated for reducing the design strength to address problems associated with high strength cement-treated layers. Luhr et al. *(39)* recommended a design strength range of 2.1 to 2.8 MPa (300 to 400 psi), which has also been adopted by the Portland Cement Association *(7)*. Given the significant reduction in reflective cracking observed in the simulations by reducing the design strength from 4.5 to 3.5 MPa (650 to 500 psi), reducing the specified maximum design strength range to 2.1 to 2.8 MPa (300 to 400 psi) or 2.1 to 3.1 MPa (300 to 450°psi) could further reduce the risk of reflective cracking and increase the fatigue life of FDR-C layers.

8.6 Conclusions

The microcracking simulation in this chapter using the laboratory-determined material models, field observations, and crack width and crack spacing models by Zhang and Li *(32)* provided understanding and information to further describe the development of shrinkage cracks in FDR-C layers for different microcracking efforts and showed the importance of distributing the shrinkage strain over several cracks to minimize crack widths in order to mitigate reflective drying shrinkage cracking. Important findings from this part of the study include the following:

- Microcracking Time and Effort
  - Microcracking is a drying shrinkage crack-control method that reduces strength and effective layer thickness to promote additional shrinkage crack development.
  - Microcracking induces high compressive stresses under the roller drum and high tensile stresses at the bottom of an FDR-C layer. This can lead to crushing on carbonated layers and/or bottom-up cracking from bending failure, which could lead to an effective layer-thickness reduction in terms of design stiffness/traffic carrying capacity.
  - The timing of microcracking can affect the crack width based on the remaining shrinkage potential after microcracking. Early microcracking can minimize the difference in crack widths among the different cracks but could result in increased reflective cracking in

some cases on layers with higher strengths and where stiffness was reduced by up to 30%.

- Shrinkage Crack Development
  - Increasing the number of drying shrinkage cracks in an FDR-C layer to reduce slab lengths between the cracks minimizes the accumulation of shrinkage strain over individual cracks and increases the number of cracks over which the shrinkage strain can be distributed.
  - Reducing the widths of drying shrinkage cracks in an FDR-C layer can reduce the number of reflected cracks in the surface layer.
- Design Strength
  - Stronger is not better. Increasing the cement content to increase the strength and stiffness in anticipation of better fatigue performance of the "intact layer" can adversely affect shrinkage crack widths because the resistance to shrinkage cracking increases. A minimum acceptable design strength should be considered for the mix design of FDR-C layers that satisfies the durability requirement (UCS at ICS-determined cement content plus 1% cement) and falls within an appropriate design strength range specified by the transportation agency.

9 CONCLUSIONS AND RECOMMENDATIONS

Cement-treated layers, including full-depth recycled layers using cement as a stabilizer (FDR-C), are prone to cracking. This is, and has been, a concern for using cement to improve the strength and stiffness properties of recycled materials that have limited amounts of fine materials and/or plasticity. The research discussed in this and a companion report, which focused on identifying and understanding appropriate shrinkage crack mitigation procedures for recycled pavement layers treated with cement, builds on previous work by the Texas Transportation Institute and others on microcracking as a shrinkage crack mitigation measure. The process involves a combination of optimum curing times before microcracking and number of roller passes at maximum vibration and amplitude, or a target stiffness reduction, to minimize drying shrinkage crack width, which will maximize long-term stiffness and fatigue life.

Studies by the Texas Transportation Institute and other organizations agreed that microcracking is a potentially effective shrinkage crack mitigation study. However, gaps in the knowledge were identified, specifically a full understanding of microcracking mechanisms, influence of cement content/design strength, optimal timing of microcracking, and roller type. This study addressed these gaps primarily through continued long-term monitoring of pilot studies, the construction and monitoring of a 37-cell FDR-C Test Road (Phase 2a), comprehensive laboratory testing, and then development of an understanding of the processes and layer behavior through modeling and simulation (Phase 2b).

9.1 Summary of Phase 2b Research

9.1.1 Refinement of the Resilient Modulus Test for Treated Materials

The AASHTO T 307 method for testing resilient modulus was originally developed for unbound materials and has been found to significantly underestimate the stiffness of treated materials. Research was conducted to assess four alternative linear variable differential transformer (LVDT) placements to determine whether more realistic stiffness values could be collected. Based on the results, the method was modified to collect on-specimen measurements using three equally spaced LVDTs, instead of the single externally mounted LVDT used in the standard method. Laboratory results using the new setup corresponded to backcalculated falling weight deflectometer (FWD) results collected on roads with FDR layers.

9.1.2 Development of a Laboratory Microcracking Procedure

A laboratory procedure for inducing microcracking in cement-treated specimens, based on the refinements to the resilient modulus test, was developed to provide a controlled method for reducing the stiffness of compacted specimens that would simulate the results from the FDR-C Test Road.

9.1.3 Laboratory Testing

Laboratory testing on specimens produced with material sampled during construction of the FDR-C Test Road included stiffness testing with microcracking, long-term indirect tensile strength (ITS) tests, short-term ITS tests, short-term unconfined compressive strength (UCS) tests, and drying shrinkage tests. The laboratory microcracking test results were consistent with the backcalculated stiffness results from the FDR-C Test Road in terms of the range of stiffnesses measured and the trends among the different applied energies. The main findings from this part of the study include the following:

- Stiffness Change
  - The laboratory microcracking procedure effectively simulated microcracking in the field, with results showing similar trends between laboratory- and field-measured stiffnesses.
  - The stiffness of the 2.5% cement-content specimens after microcracking recovered through autogenous healing to equal or exceed the stiffness of the control specimens at the same age.
  - The 4% cement-content specimens after microcracking had a significant long-term reduction in stiffness with microcracking effort and curing time before microcracking.
  - Microcracking resulted in damage to the specimens in the form of internal cracks that led to stiffness reduction.
  - The critical factor effecting differences in stiffness behavior was the difference in water-to-cement-for-cementation ratio (w/c_c) for the two cement contents, with the 2.5% cement-content material having a w/c_c of 9.8 and the 4% cement-content material having a w/c_c of just 2.5. As a result, the 2.5% cement-content specimens had significantly more free water available for rehydration of cement after microcracking.
  - The long-term effect of microcracking on stiffness was also dependent on the w/c_c ratio, with microcracked material with higher w/c_c ratios recovering stiffness more effectively than material with a lower w/c_c. Materials with higher w/c_c ratios also achieved stiffness levels similar to or greater than, specimens/pavement layers that were not microcracked, depending on energy input. Microcracked material with lower w/c_c ratios had levels of recovery that were dependent on curing time after compaction and energy

input from the roller. Longer curing times and increased energy input reduced the level of stiffness recovery.

  - Microcracking facilitated the movement of moisture through the induced cracks due to increased permeability, allowing access to any unhydrated cement. The higher cement content specimens did not have the same free water available for this later hydration, which in turn limited stiffness recovery after microcracking. Compaction of FDR-C layers in the field is typically performed at or close to the optimum moisture content (OMC) of the material. In order to benefit from the ability of the material to gain stiffness after microcracking, the w/c_c should be optimized. However, increasing the moisture content above the OMC to increase the w/c_c can result in a mix that will have a lower density, reduced strength and stiffness, and increased shrinkage cracking. This supports selection of cement contents for FDR-C layers that meet the minimum recommended target strength requirements (i.e., 300 to 450 psi [≈2.1 to 3.1 MPa]) while still meeting the initial consumption of stabilizer (ICS) plus 1% cement durability requirement.
  - Stiffness reduction was log-linearly correlated with energy input, and independent of the number of cycles or the order of stress sequences.
  - The rate of stiffness reduction with energy input was similar for the different cement contents and microcracking times, except for the 4% cement-content specimens microcracked at 72 hours, which had the lowest rate of stiffness reduction due to the increased strength of the material.

- Indirect Tensile Strength and Stiffness
  - The ITS of the specimens was shown to be linearly correlated with stiffness. It is thus expected that reducing the ITS by microcracking will result in shorter crack spacings, while lowering the stiffness will reduce crack widths. This was, however, not observed in the first four months of crack monitoring on the FDR-C Test Road. It is hypothesized that the cracks existed, but due to their frequency, they were not visible or had not reflected through the microsurfacing four months after construction.
- Unconfined Compressive Strength with Different Microcracking Efforts
  - Unconfined compressive strength (UCS) was not significantly affected by the reduction in stiffness due to microcracking. This is likely due to the mechanics of the test method, which applies an axial load on the specimen and compresses the cracks to their original state before the specimen fails in shear. The UCS was also poorly correlated with the stiffness after different microcracking efforts.
- Effect of Microcracking on Strength (UCS and ITS)
  - Microcracking at 72 hours, and at 48 hours and again at 72 hours (i.e., two microcracking actions), effectively reduced the ITS in both the short-term (i.e., after microcracking) and longer-term (i.e., after 56 days). The UCS, tested two days after microcracking, was not significantly affected by microcracking.

- The stiffness of both the 2.5% and 4% cement-content specimens were linearly correlated with the ITS.

9.1.4 Development of Behavior Models from Laboratory Test Results

A series of models using data from the FDR-C Test Road and laboratory testing was developed for predicting the effects of microcracking on stiffness. Key factors influencing model prediction trends were cement content and water-to-cement-for-cementation ratio.

9.1.5 Simulating Microcracking on the FDR-C Test Road

Microcracking simulations using the laboratory-determined material models, field observations, and published crack width and crack spacing models provided an understanding of and information to further describe the development of shrinkage cracks in FDR-C layers for different microcracking efforts. The results showed the importance of distributing the shrinkage strain over several cracks to minimize crack widths in order to mitigate reflective drying shrinkage cracking. Important findings from this part of the study include the following:

- Microcracking Time and Effort
  - Microcracking is a drying shrinkage crack-control method that reduces strength and effective layer thickness to promote additional shrinkage crack development.
  - Microcracking induces high compressive stresses under the roller drum and high tensile stresses at the bottom of an FDR-C layer. This can lead to crushing on carbonated layers and/or bottom-up cracking from bending failure, which could lead to an effective layer-thickness reduction in terms of stiffness/traffic carrying capacity.
  - The timing of microcracking can affect the crack width based on the remaining shrinkage potential after microcracking. Early microcracking can minimize the difference in crack widths among the different cracks, but it could result in increased reflective cracking in some cases.
- Shrinkage Crack Development
  - Increasing the number of drying shrinkage cracks in an FDR-C layer to reduce slab lengths between the cracks minimizes the accumulation of shrinkage strain over individual cracks and increases the number of cracks over which the shrinkage strain can be distributed.
  - Reducing the widths of drying shrinkage cracks in an FDR-C layer can reduce the number of reflected cracks in the asphalt concrete surface layer. Not all drying shrinkage cracks in an FDR-C layer will reflect through the asphalt concrete layer.

- Design Strength
  - Increasing the cement content to increase the strength and stiffness in anticipation of better fatigue performance of the "intact layer" can adversely affect shrinkage crack widths because the resistance to shrinkage cracking increases. A minimum acceptable design strength should be considered for the mix design of FDR-C layers that satisfies both the durability requirement (UCS at ICS-determined cement content plus 1% cement), as well as an appropriate minimum design strength specified by the transportation agency.
- Fatigue Life
  - Microcracking can increase the effective fatigue life in pavements with FDR-C layers, since the location that controls fatigue life is the area in the vicinity of wide, reflected shrinkage cracks.

9.2 Conclusions

The conclusions drawn after completion of the Phase 2a research were further supported by the results from the work completed in this phase of the study. Revised conclusions based on the research conducted in both Phase 2a and Phase 2b (this report) include the following:

- Microcracking of FDR-C layers does not prevent shrinkage cracking, but it is an effective shrinkage crack mitigation procedure. Microcracking induces a network of fine cracks, which generally do not reflect through asphalt concrete surfacings as wide shrinkage cracks tend to do.
- Microcracking has limitations and will not mitigate all shrinkage cracks on all FDR-C projects. Design strength, construction procedures, curing time before microcracking, number of microcracking passes, and stiffness reduction achieved during microcracking will all influence the level of mitigation achieved.
- The original stiffness prior to microcracking is mostly recovered, and often exceeded, after microcracking on FDR-C layers with strengths at the lower end of the specified target range (i.e., 300 psi [≈2.1 MPa]). Stiffness is significantly reduced on higher strength layers (i.e., >600 psi [≈4.1 MPa]) after microcracking, and it may not recover to the same stiffness measured before microcracking.
- Microcracking will be most effective if the seven-day UCS of the treated material falls in the range of 250 to 450 psi (1.7 to 3.1 MPa) and preferably no higher than 600 psi (4.1 MPa). Layers with design strengths greater than 600 psi will likely have shrinkage cracks forming before the road can be microcracked.
- Higher-strength FDR-C layers are more sensitive to the timing of microcracking. The greatest reduction in the long-term stiffness is associated with microcracking at 72 hours, with significantly lower stiffnesses measured than those measured when the layer is

microcracked between 48 and 56 hours of curing. Statistical modeling on a small data set indicated that microcracking as soon as 24 hours after final compaction may be beneficial on higher strength layers.

- Microcracking can increase the fatigue life of FDR-C layers by reducing crack widths. Given that failure in pavements with cement-treated layers initiates in the vicinity of wide reflected shrinkage cracks, reducing crack widths by forcing the development of additional cracks in the FDR-C layer will reduce the likelihood of early failures around the cracks and therefore increase fatigue life through improved load transfer efficiency (LTE) and aggregate interlock. This in turn reduces stresses and strains adjacent to the cracks at the bottom of the layer. The hypothesis proposed early in the study that microcracking would increase the fatigue life of pavements with cement-treated layers, illustrated in Figure 9.1, was therefore confirmed.

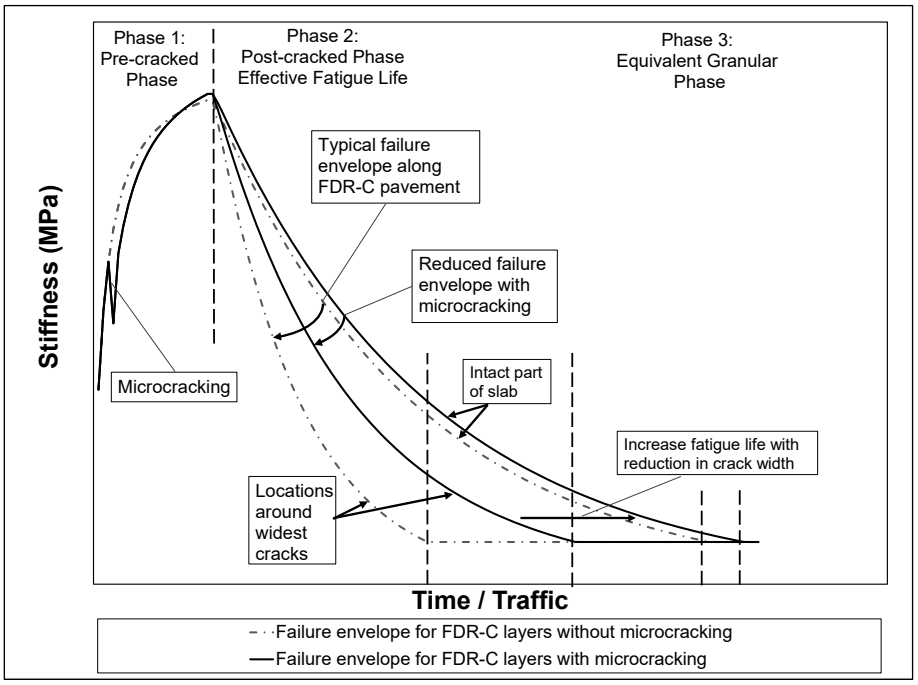

Figure 9.1: Revised theoretical structural life cycle of cement-treated pavement layers.

- Microcracking can increase the long-term stiffness of FDR-C layers, which in turn also increases the effective fatigue life of the pavement for comparable conditions. Adjusting mix designs to maximize the water-to-cement-for-cementation ratio, together with applying the appropriate energy input during microcracking, will maximize stiffness in the post-cracked phase in the form of secondary cementation and hydration of unhydrated cement through the mobilization of free water through induced microcracks.
- The current Caltrans method specification for microcracking of FDR-C layers, as it is currently phrased, could lead to significantly different stiffness reduction results given that 12-ton rollers from different manufacturers apply different levels of energy.

9.3 Recommendations

The recommendations made after completion of the Phase 2a research were further supported by the results from the work completed in this phase of the study. Revised recommendations based on the research conducted in both Phase 2a and Phase 2b (this report) include the following:

- The mix design procedure for FDR-C layers should include an ICS test to ensure an optimum cement content that will result in a durable layer is selected. The starting cement content in mix design tests should be the ICS plus 1%. If this results in a seven-day UCS higher than 450 psi (3.1 MPa), the pavement design and or choice of stabilizer/recycling agent should be reviewed.
- Microcracking of FDR-C layers will be most effective if the seven-day UCS falls in the range of 250 to 450 psi (1.7 to 3.1 MPa) and preferably no higher than 600 psi (4.1 MPa).
- Microcracking of FDR-C layers should be done as close as possible to 48 hours after final compaction, especially if design strengths exceed 450 psi (3.1 MPa). Further investigation into microcracking higher strength FDR-C layers at 24 hours is warranted.
- The Caltrans method specification language for microcracking should be changed to the following (the energy requirement will encourage contractors to check the ratings of their rollers):
  - During the period from 48 to 56 hours after compaction, microcrack the surface by applying 2 to 3 single passes, equivalent to 2.8 to 4.3 kN/cm^2 (4,060 to 6,235 psi) of energy, using a 12-ton vibratory steel drum roller at maximum vibration amplitude (centrifugal force of 200 to 300 kN [≈45,000 to 67,500 lb.]) traveling from 2 to 3 mph.
  - Note that one pass is considered to be the roller movement in one direction only (i.e., three passes would be 1) start to end, 2) end to start, and 3) start to end.
- If a performance specification is considered, then a maximum stiffness reduction of 40%, measured with a soil stiffness gauge is recommended (i.e., initial measurement before the first roller pass and then measurements after each roller pass until a 40% reduction in stiffness is achieved).
- The research cited in the literature review and testing in this study assessed microcracking on cement-treated layers between 10 and 12 in. (250 and 300 mm) thick. Research on layers thinner than 10 in. should continue to determine if microcracking effort needs to be reduced on thinner layers to prevent permanent damage (i.e., loss of stiffness) to the layer. Research on layers thicker than 12 in. should also continue to assess whether uniform compaction and effective microcracking can be achieved over the full depth of the layer, especially on weak subgrades, and the implications on shrinkage and fatigue cracking if it cannot.

- Although the soil stiffness gauge is considered an appropriate instrument for measuring stiffness reduction during microcracking, testing procedures will need to be refined and precision and bias statements prepared to ensure that reasonable quality control and quality assurance procedures are followed.
- Based on the research findings to date, further research on the following topics, in addition to those noted above, is warranted:
  - Interaction between the water-to-cement-for-cementation ratio and energy input to determine if these can be optimized to maximize stiffness recovery after microcracking, while still ensuring durability of the mix.
  - Quantification of the relationship between crack width, load transfer efficiency, and stress and strain at the bottom of the FDR-C layer adjacent to drying shrinkage cracks, to develop appropriate factors to increase the tensile stress and strain as determined from layer elastic theory for pavement design.

REFERENCES

1. Louw, S. 2020. *Models and Validation of Mechanisms and Mitigation of Early Age Shrinkage Cracking in Cement Stabilized Bases*. PhD Dissertation. Davis, CA: University of California, Davis.
2. Leoci, R. 2014. *Animal By-Products (ABPs): Origins, Uses, and European Regulations.* Mantova, Italy: Universitas Studiorum.
3. Louw, S., and Jones, D. 2015. *Pavement Recycling: Literature Review on Shrinkage Crack Mitigation in Cement-Stabilized Pavement Layers*, Technical Memorandum: UCPRC-TM-2015-02, Davis and Berkeley, CA: University of California Pavement Research Center.
4. George, K.P. 2002. *Minimizing Cracking in Cement-treated Materials for Improved Performance.* Skokie, IL: Portland Cement Association.
5. Adaska, W.S., and Luhr, D.R. 2004. Control of Reflective Cracking in Cement Stabilized Pavements. *Cracking in Pavements: Mitigation, Risk Assessment and Prevention.* Proceedings of the 5th International RILEM Conference. Bagneux, France: RILEM Publications.
6. Sebesta, S. 2005. *Continued Evaluation of Microcracking in Texas,* Report 0-4502-2. College Station, TX: Texas Transportation Institute.
7. Reeder, G.D., Harrington, D.S., Ayers, M.E., and Adaska, W. 2019. *Guide to Full-Depth Reclamation (FDR) with Cement*, Report SR1006P, Skokie, IL: Portland Cement Association.
8. Steyn, W. and Jones, D. 2005. *Technical Memorandum: HVS Testing of N12-19 East Section 2*, Contract Report CR-2005/51, Pretoria, South Africa: Council for Scientific and Industrial Research.
9. Jones, D., Louw, S., and Wu, R. 2016. *Full-Depth Recycling Study: Test Track Construction and First-Level Analysis of Phase 1 and Phase 2 HVS Testing, Forensic Investigation, and Phase 1 Laboratory Testing*, Research Report: UCPRC-RR-2015-02, Davis and Berkeley, CA: University of California Pavement Research Center.
10. Jones, D., Louw, S., Buscheck, J., and Harvey, J. 2018. *Pavement Recycling: Workplan for Continued Development of Guidelines for Shrinkage Crack Mitigation in Cement-Treated Layers*, Research Report: UCPRC-WP-2017-10.3, Davis and Berkeley, CA: University of California Pavement Research Center.
11. Louw, S., Jones, D., and Hammack, J. 2016. *Pavement Recycling: Shrinkage Crack Mitigation in Cement-Treated Pavement Layers — Phase 1 Laboratory Testing,* Research Report: UCPRC-RR-2016-07. Davis and Berkeley, CA: University of California Pavement Research Center.
12. Louw, S., Jones, D. Hammack, J., and Harvey, J. 2020. *Pavement Recycling: Shrinkage Crack Mitigation in Cement-Treated Pavement Layers — Phase 2a Literature Review and FDR-C Test Road Construction and Monitoring*, Research Report: UCPRC-RR-2019-05. Davis and Berkeley, CA: University of California Pavement Research Center.

13. Jones, D., Louw, S., and Harvey, J. 2020. *Guide for Partial- and Full-Depth Pavement Recycling in California*, Guideline: UCPRC-GL-2020-01. Davis and Berkeley, CA: University of California Pavement Research Center.
14. De Beer, M. 1990. *Aspects of the Design and Behaviour of Road Structures Incorporating Lightly Cementitious Layers.* PhD Thesis, Pretoria, South Africa: University of Pretoria.
15. Kadar, P., Baran, E. and Gordon, R.G. 1989. *The Performance of CTB Pavements under Accelerated Loading: The Beerburrum (Queensland) ALF Trial, 1986/87*. Victoria, Australia: ARRB Group LTD.
16. Kota, P.B., Scullion, T., and Little, D.N. 1995. Investigation of Performance of Heavily Stabilized Bases in Houston, Texas, District. *Transportation Research Record: Journal of the Transportation Research Board,* 1486. Washington, D.C.: Transportation Research Board. pp. 68-76.
17. Little, D.N., Scullion, T., Kota, P.B.V.S., and Bhuiyan, J. 1995. *Guidelines for Mixture Design of Stabilized Bases and Subgrades,* Report FHWA/TX-45/1287-3 F. College Station, TX: Texas Transportation Institute.
18. Rashidi, M., Ashtiani, R.S., Si, J.S., Richard, P.I., and McDaniel, M. 2018. A Practical Approach for the Estimation of Strength and Resilient Properties of Cementitious Materials. *Transportation Research Record: Journal of the Transportation Research Board,* 2672 (52), Washington, D.C.: Transportation Research Board. pp. 152-163.
19. Jones, D., Fu, P., Harvey, J., and Halles, F. 2008. *Full-Depth Pavement Reclamation with Foamed Asphalt: Final Report*, Research Report UCPRC-RR-2008. Davis and Berkeley, CA: University of California Pavement Research Center.
20. Potturi, A.K. 2006. *Evaluation of Resilient Modulus of Cement and Cement-Fiber Treated Reclaimed Asphalt Pavement (RAP) Aggregates using Repeated Load Triaxial Test*. Master of Science in Civil Engineering, University of Texas at Arlington.
21. Puppala, A.J., Hoyos, L.R., and Potturi, A.K. 2011. Resilient Moduli Response of Moderately Cement-treated Reclaimed Asphalt Pavement Aggregates, *Journal of Materials in Civil Engineering*, 23 (7), pp. 990-998.
22. Alabaster, D., Patrick, J., Arampamoorthya, H. and Gonzalez, A. 2013. *The Design of Stabilised Pavements in New Zealand*, Research Report: 498, Auckland, New Zealand: New Zealand Transport Agency.
23. Lovelady, P.L., and Picornell, M. 1990. Sample Coupling in Resonant Column Testing of Cemented Soils. *Dynamic Elastic Modulus Measurements in Materials*. West Conshohocken, PA: ASTM International.
24. Richart, F.E., Brandtzaeg, A., and Brown, R.L. 1928. *A Study of the Failure of Concrete under Combined Compressive Stresses*. Urbana-Champaign: IL: University of Illinois.

25. Vinson, T., Wilson, C., and Bolander, P. 1983. Dynamic Properties of Naturally Frozen Silt. *In Proceedings of 4th International Conference on Permafrost*. Washington D.C.: National Academy Press, pp.469-481.
26. Capdevila, J.A., and Rinaldi, V.A. 2015. Stress-Strain Behavior of a Heterogeneous and Lightly Cemented Soil under Triaxial Compression Test. *Journal of Geotechnical Engineering*, 20 (591), pp. 6,745-6,760.
27. Hilbrich, S.L., and Scullion, T. 2007. Rapid Alternative for Laboratory Determination of Resilient Modulus Input Values on Stabilized Materials for AASHTO Mechanistic-Empirical Design Guide. *Transportation Research Record: Journal of the Transportation Research Board*, 2026, Washington, D.C.: Transportation Research Board, pp 63-69.
28. Peng, S.D. 1971. Stresses Within Elastic Circular Cylinders Loaded Uniaxially and Triaxially. *International Journal of Rock Mechanics and Mining Sciences and Geomechanics Abstracts*, 8 (5), pp. 399-432.
29. Yeo, R. 2008. *The Development and Evaluation of Protocols for the Laboratory Characterisation of Cemented Materials*. Sydney, Australia: Austroads.
30. Arnold, G., Werkmeister, S. and Morkel, C. 2010. *Development of a Basecourse/Sub-Base Design Criterion*. Research Report 498. Auckland, New Zealand: New Zealand Transport Agency.
31. Min, D., and Mingshu, T. 1994. Formation and Expansion of Ettringite Crystals. *Cement and Concrete Research*, 24 (1), pp. 119-126.
32. Zhang, J., and Li, V.C. 2001. Influence of Supporting Base Characteristics on Shrinkage-Induced Stresses in Concrete Pavements. *Journal of Transportation Engineering,* 27 (6), pp. 455-462.
33. George, K.P. 1968. Cracking in Pavements Influenced by Visoelastic Properties of Soil-Cement, *Highway Research Record*, 263, pp. 49-59.
34. Wang, J. 2013. *Characterization and Modeling of Shrinkage Cracking of Cementitiously Stabilized Layers in Pavement*. PhD Dissertation, Washington State University.
35. Meyer, M., Watson, L., Walton, C., Skinner, R., Pedersen, N., and Norman, M. 2006. Control of Cracking in Concrete, State of the Art. *Transportation Research Circular. No. E-C107*. Washington D.C.: Transportation Research Board.
36. Air Force Manual 88-6. 1982. *Soil Stabilization for Roadways and Airfields*. Department of the Air Force.
37. George, K.P. 1973. Mechanism of Shrinkage Cracking of Soil-Cement Bases. *In Proceedings 52nd Annual Meeting of the Highway Research Board,* 442, Washington, DC: Highway Research Board. pp 1-10.
38. Scullion, T. 2002. Field Investigation: Pre-Cracking of Soil-Cement Bases to Reduce Reflection Cracking. *Transportation Research Record: Journal of the Transportation Research Board,* 1787. Washington, DC: Transportation Research Board. pp. 22-30.

39. Luhr, D.R., Adaska, W.S., and Halsted, G.E. 2008. *Guide to Full-Depth Reclamation (FDR) with Cement*. Skokie, IL: Portland Cement Association.

APPENDIX A: LABORATORY TEST RESULTS

This appendix presents additional laboratory results to supplement the results provided in Chapter 6. Plots include the following:

- Stiffness reduction during microcracking for the microcracking tests on specimens with 2.5% and 4% cement contents.
- Stiffness increase with time for both cement contents.

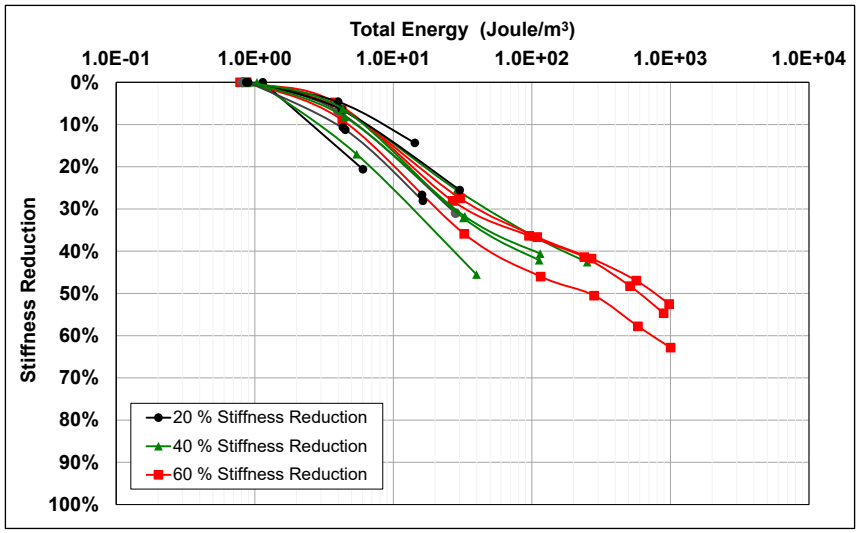

Figure A.1: 2.5% Cement: Retained stiffness versus energy input at 48 hours of curing.

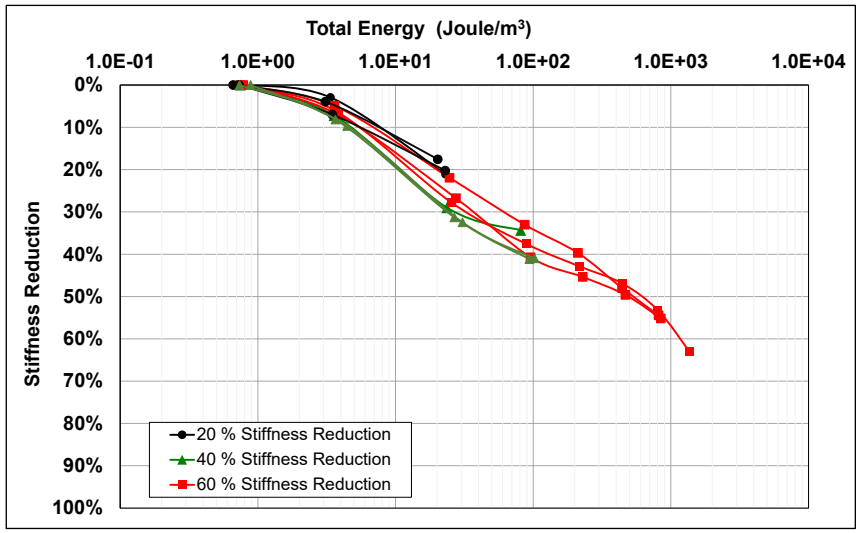

Figure A.2: 4% Cement: Retained stiffness versus energy input at 48 hours of curing.

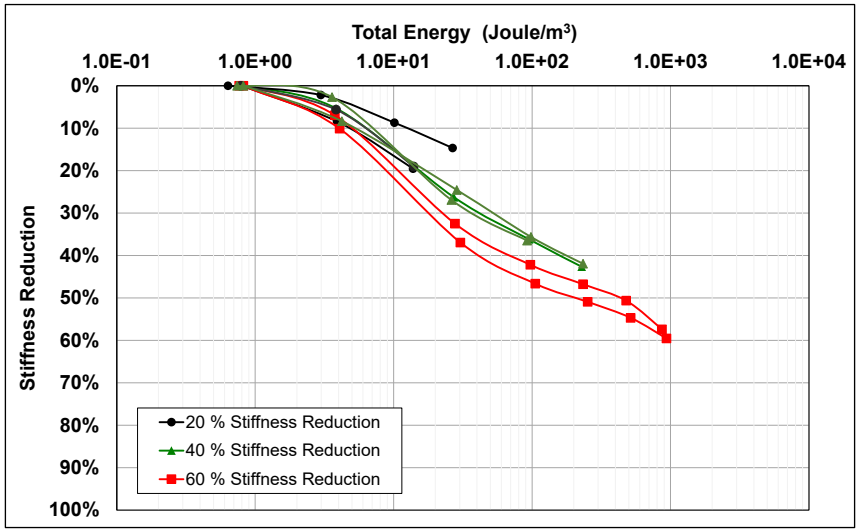

Figure A.3: 2.5% Cement: Retained stiffness versus energy input at 72 hours of curing.

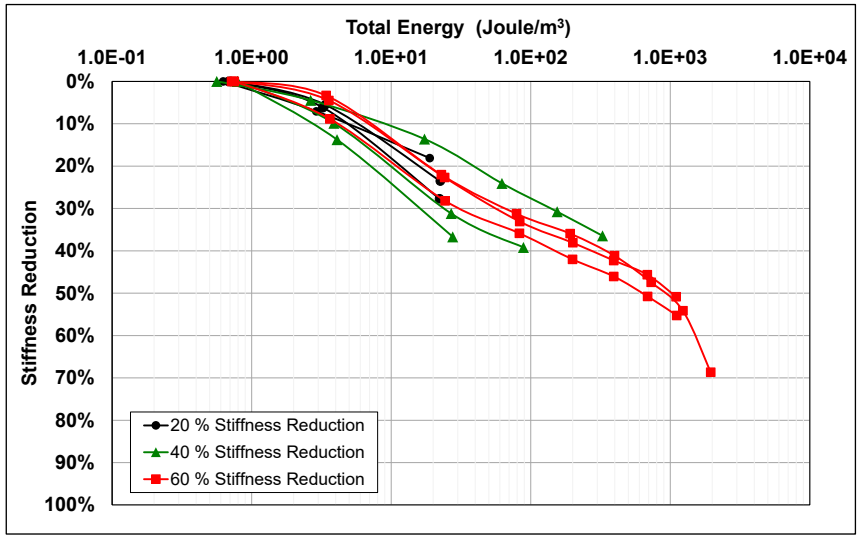

Figure A.4: 4% Cement: Retained stiffness versus energy input at 72 hours of curing.

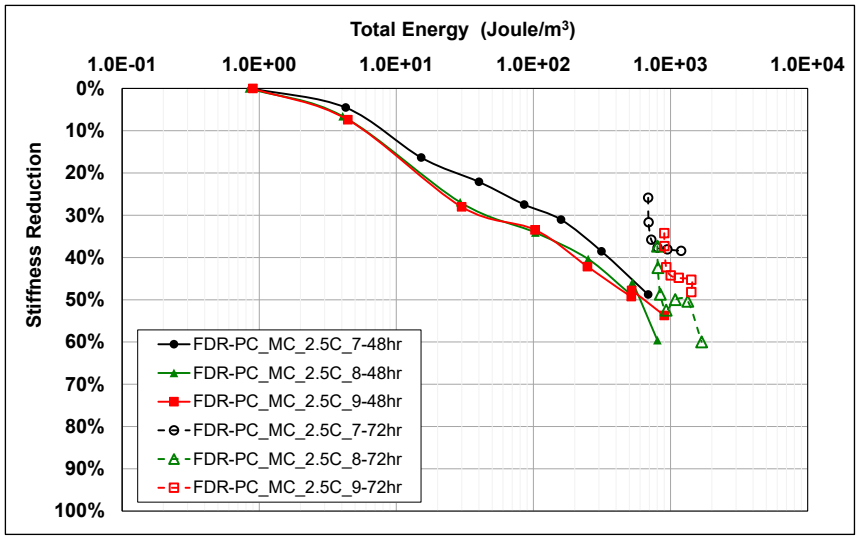

Figure A.5: 2.5% Cement: Retained stiffness versus energy input after 48 and 72 hours of curing.

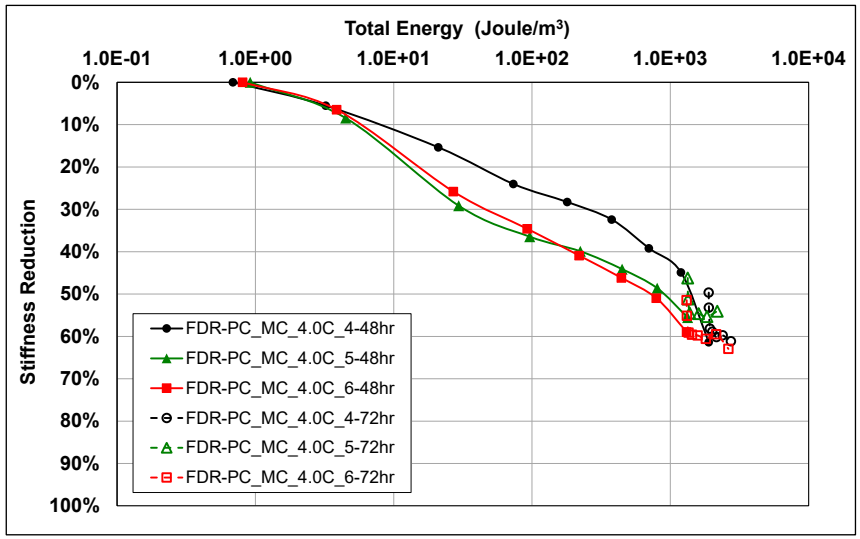

Figure A.6: 4% Cement: Retained stiffness versus energy input after 48 and 72 hours of curing.

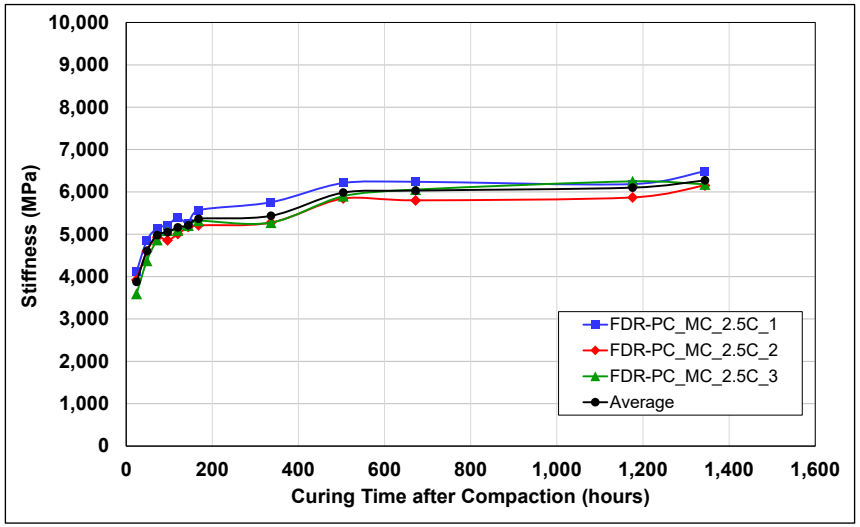

Figure A.7: 2.5% Cement: Control: Stiffness increase over time.

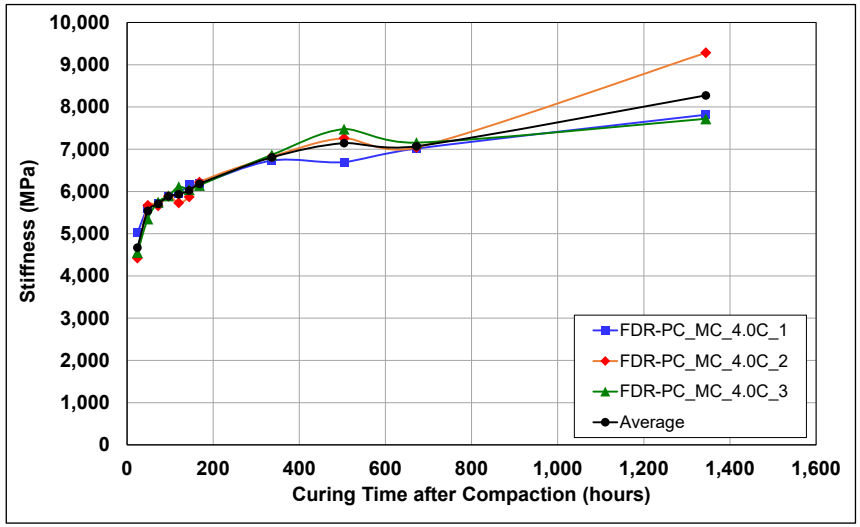

Figure A.8: 4% Cement: Control: Stiffness increase over time.

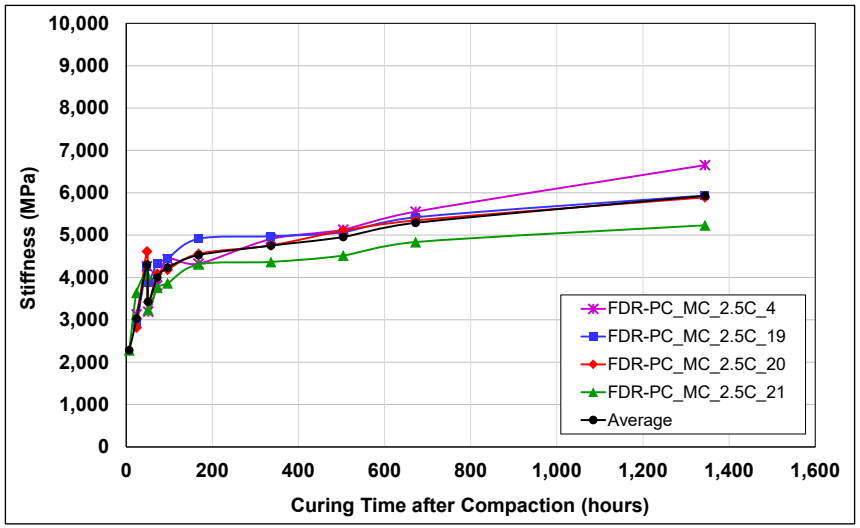

Figure A.9: 2.5% Cement: 20% reduction at 48 hours of curing.

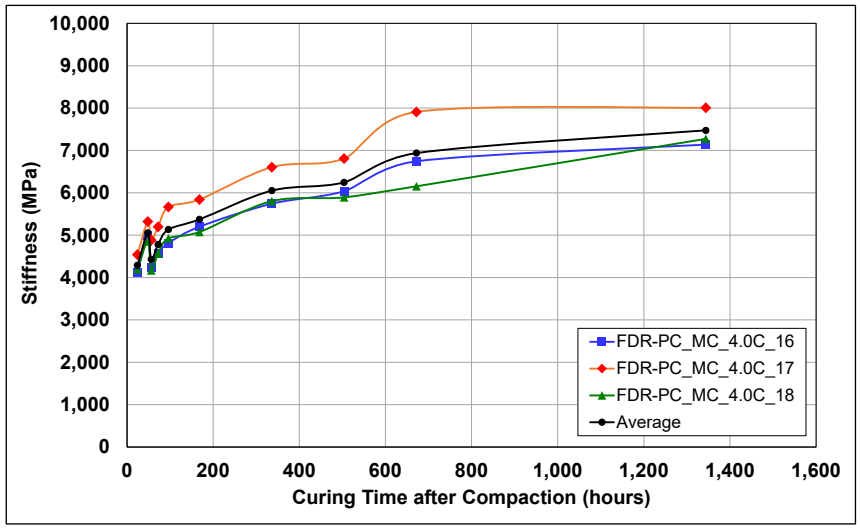

Figure A.10: 4% Cement: 20% reduction at 48 hours of curing.

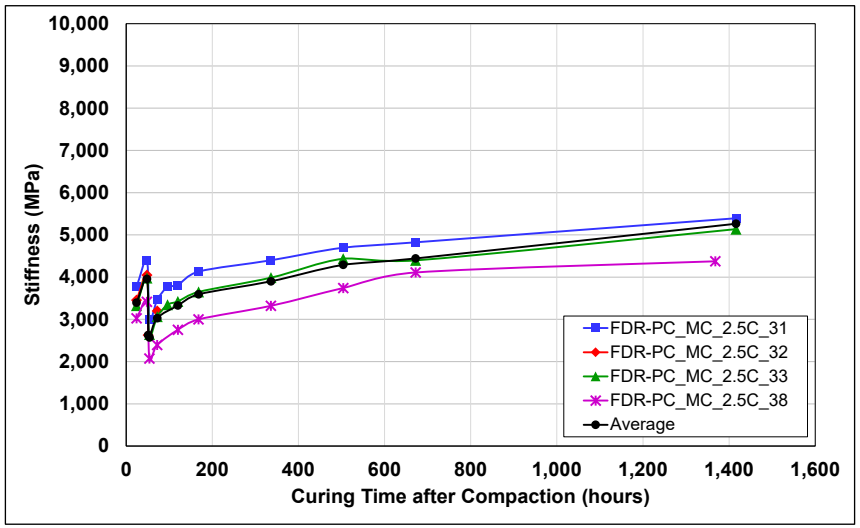

Figure A.11: 2.5% Cement: 40% reduction at 48 hours of curing.

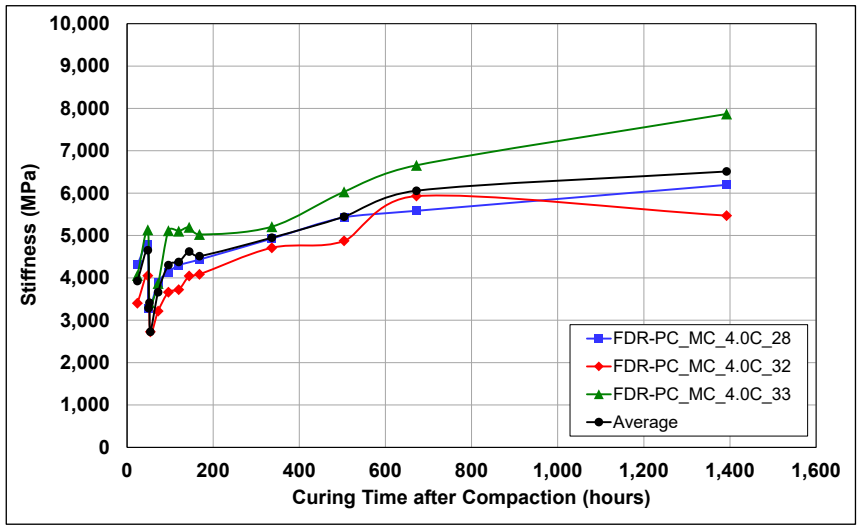

Figure A.12: 4% Cement: 40% reduction at 48 hours of curing.

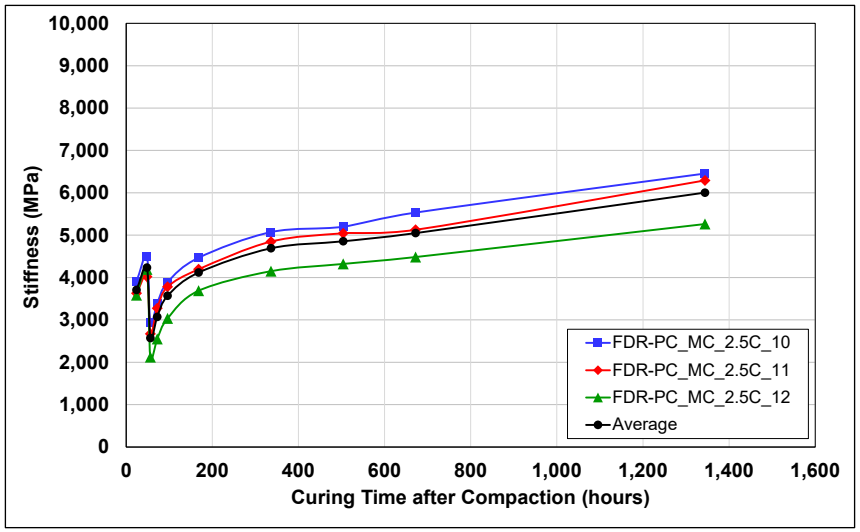

Figure A.13: 2.5% Cement: 60% reduction at 48 hours of curing.

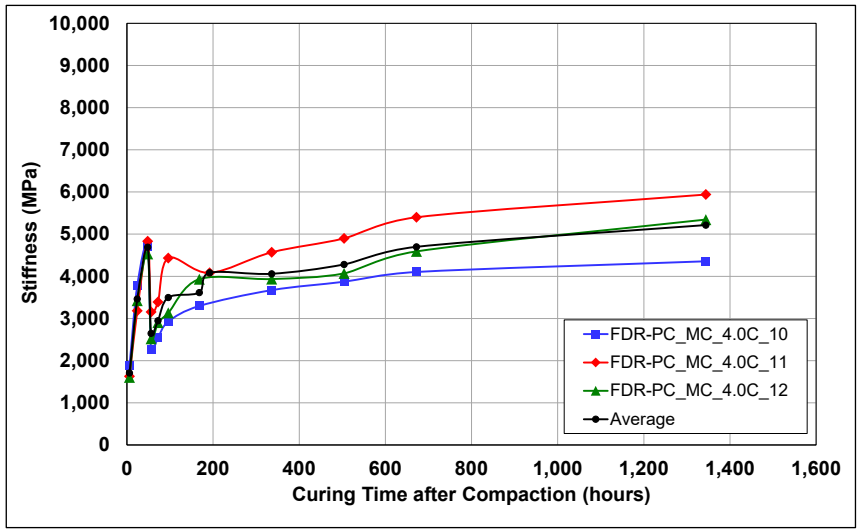

Figure A.14: 4% Cement: 60% reduction at 48 hours of curing.

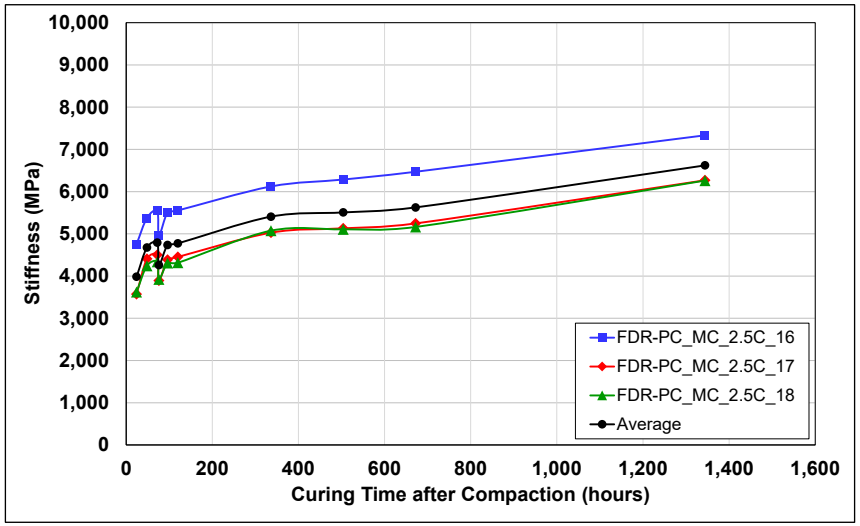

Figure A.15: 2.5% Cement: 20% reduction at 72 hours of curing.

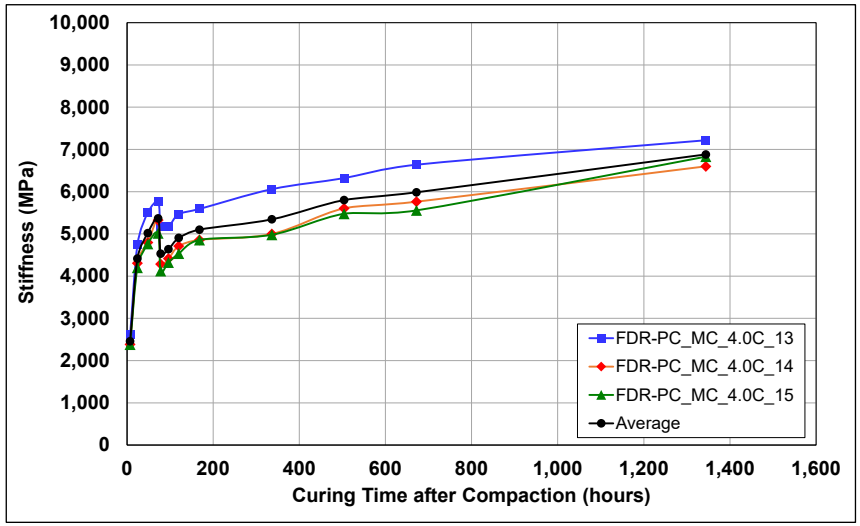

Figure A.16: 4% Cement: 20% reduction at 72 hours of curing.

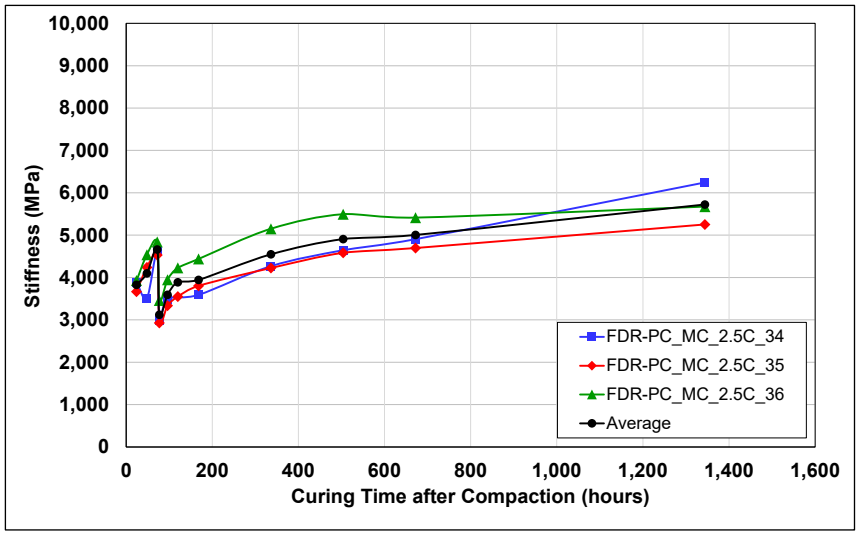

Figure A.17: 2.5% Cement: 40% reduction at 72 hours of curing.

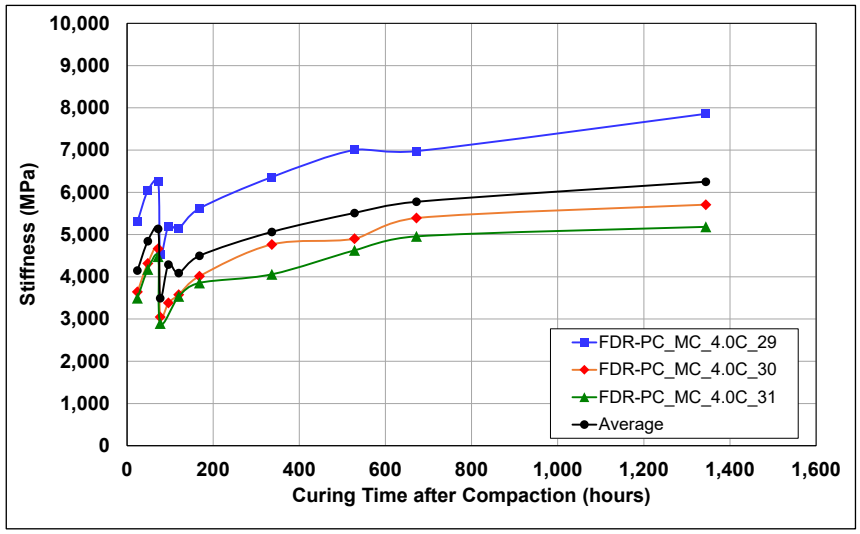

Figure A.18: 4% Cement: 40% reduction at 72 hours of curing.

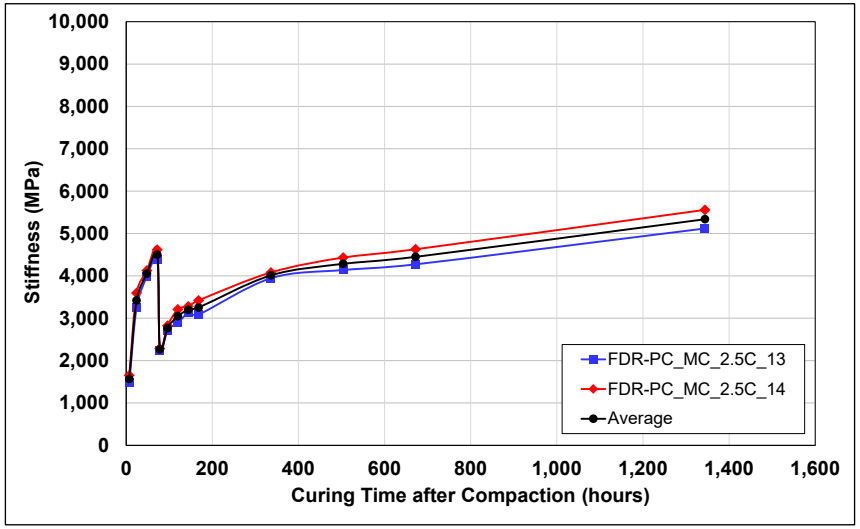

Figure A.19: 2.5% Cement: 60% reduction at 72 hours of curing.

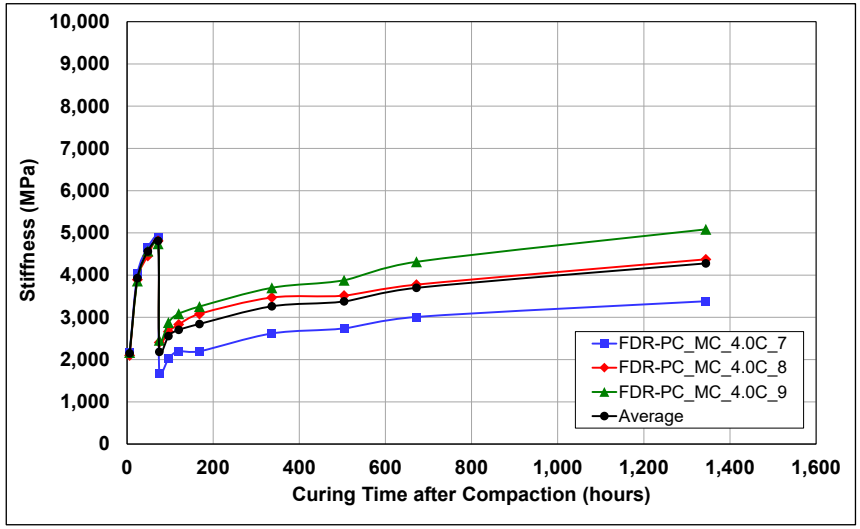

Figure A.20: 4% Cement: 60% reduction at 72 hours of curing.

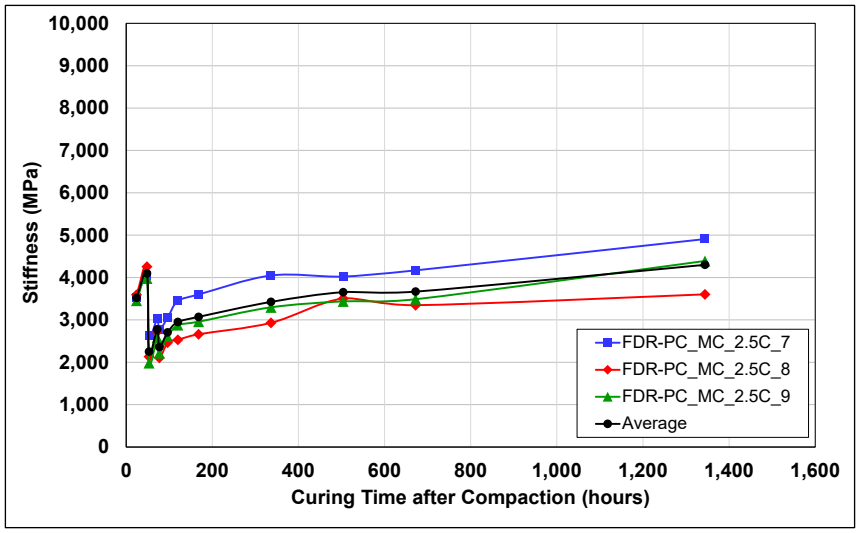

Figure A.21: 2.5% Cement: 60% reduction after 48 and 72 hours of curing.

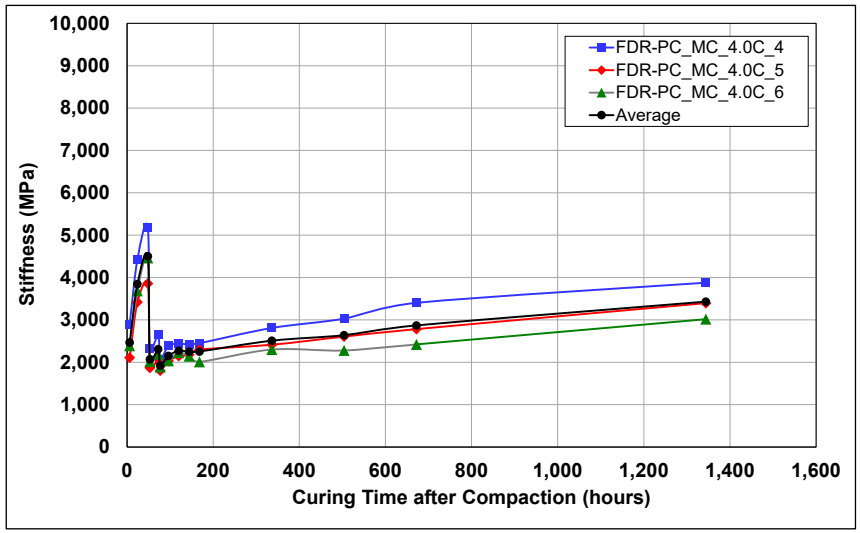

Figure A.22: 4% Cement: 60% reduction after 48 and 72 hours of curing.

APPENDIX B: MODELING AND SIMULATION RESULTS

This Appendix provides the measured and fitted results for all the laboratory-measured stiffness history with microcracking, and results from the FEM modeling to determine effective layer thickness reduction during microcracking (discussed in Section 8.3). The following results are provided:

- Stiffness history with no microcracking for the 2.5% and 4% cement-content results
- Stiffness history with one microcracking event at 48 hours curing for the 2.5% and 4% cement-content results
- Stiffness history with one microcracking event at 72 hours curing for the 2.5% and 4% cement-content results
- Stiffness history with microcracking events at 48 hours and again at 72 hours curing for the 2.5% and 4% cement-content results
- Stiffness history with three microcracking passes at 48 hours of curing for the 2.5% and 4% cement-content materials
- Stiffness history with three microcracking passes at 72 hours of curing for the 2.5% and 4% cement-content materials

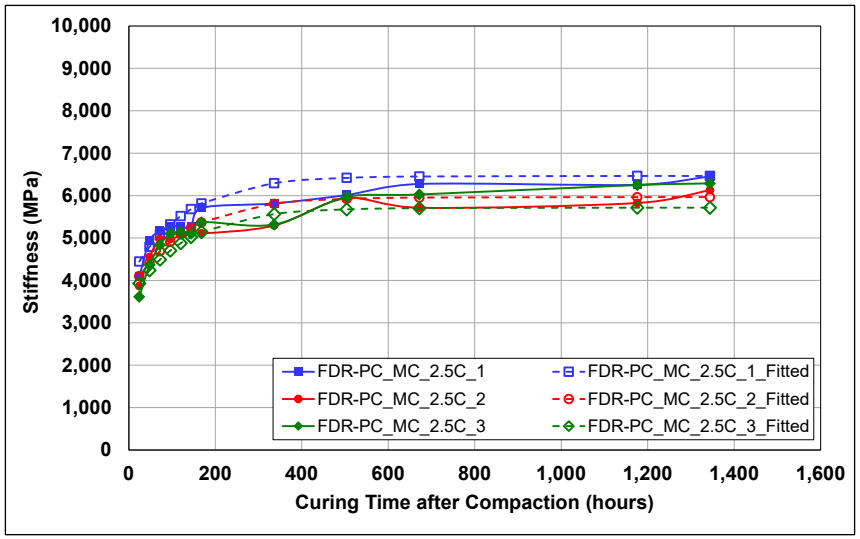

Figure B.1: 2.5% Cement with no microcracking: Comparison between fitted and measured stiffnesses.

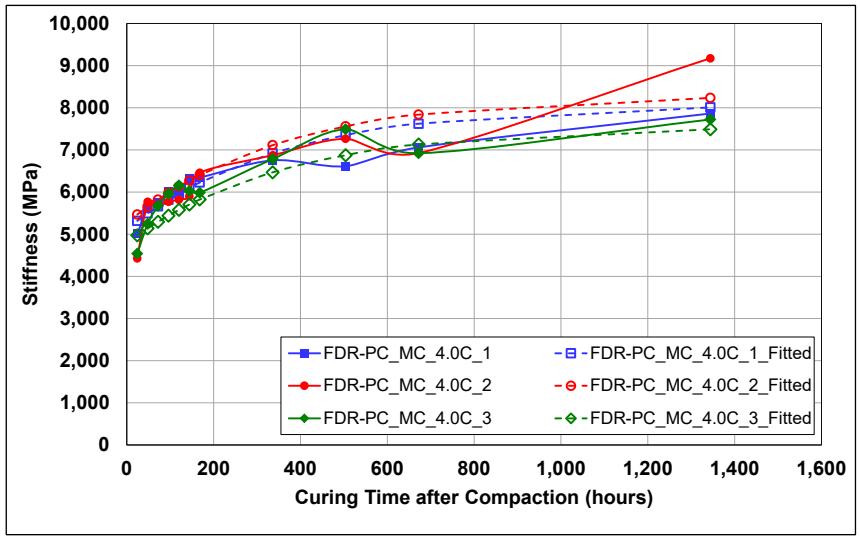

Figure B.2: 4% Cement with no microcracking: Comparison between fitted and measured stiffnesses.

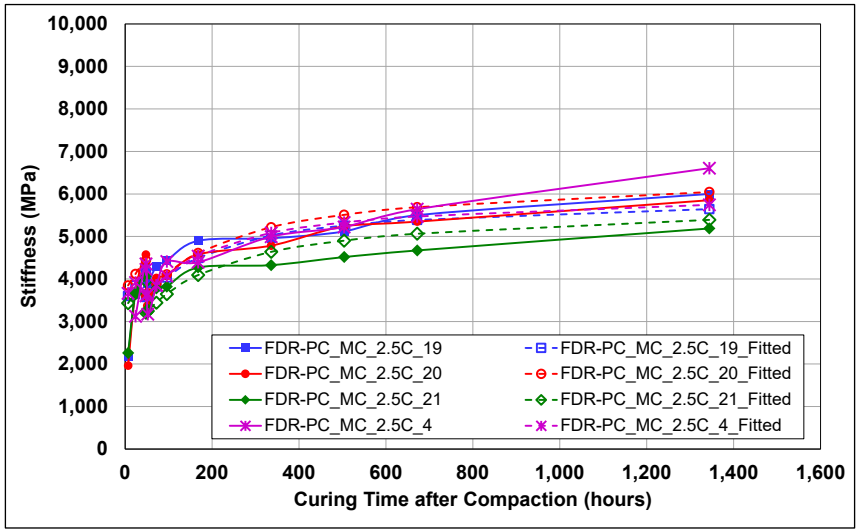

Figure B.3: 2.5% Cement with 20% stiffness reduction at 48 hours.

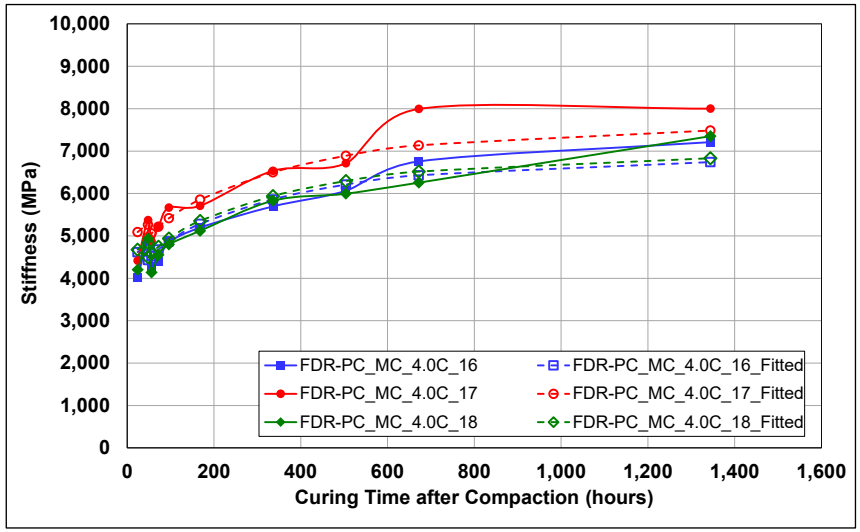

Figure B.4: 4% Cement with 20% stiffness reduction at 48 hours.

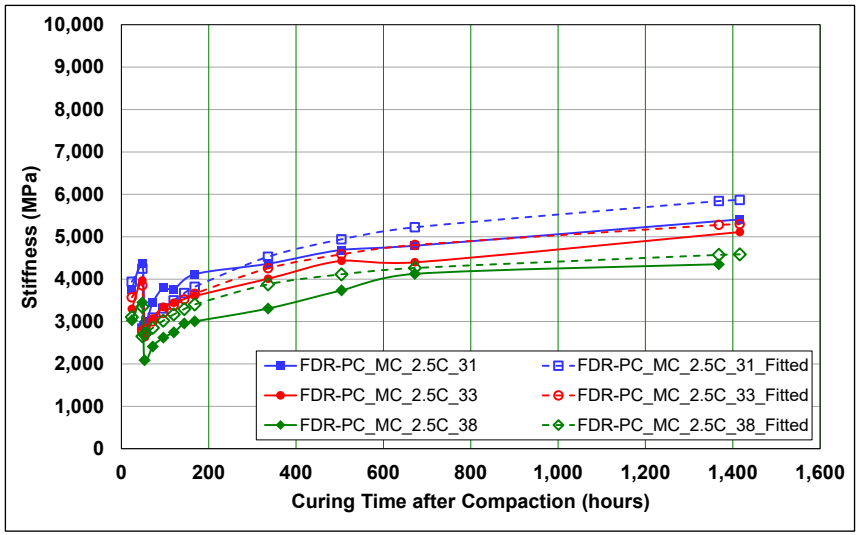

Figure B.5: 2.5% Cement with 40% stiffness reduction at 48 hours.

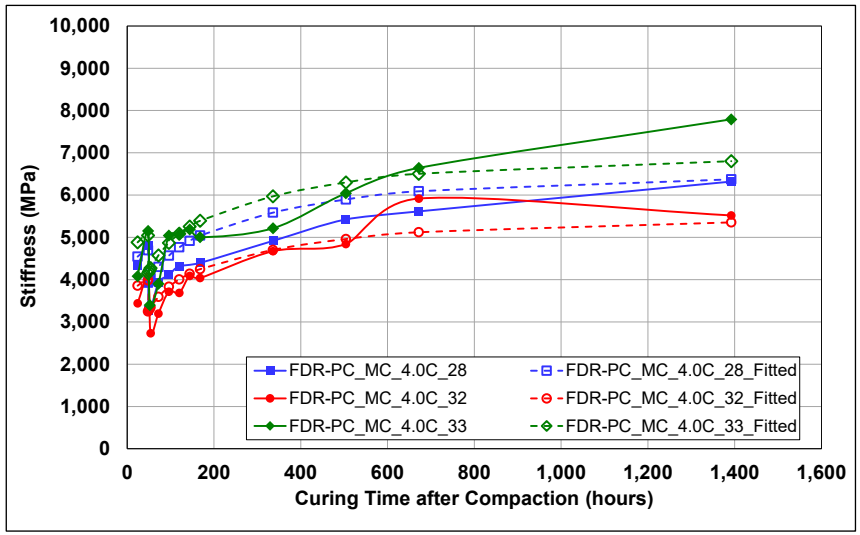

Figure B.6: 4% Cement with 40% stiffness reduction at 48 hours.

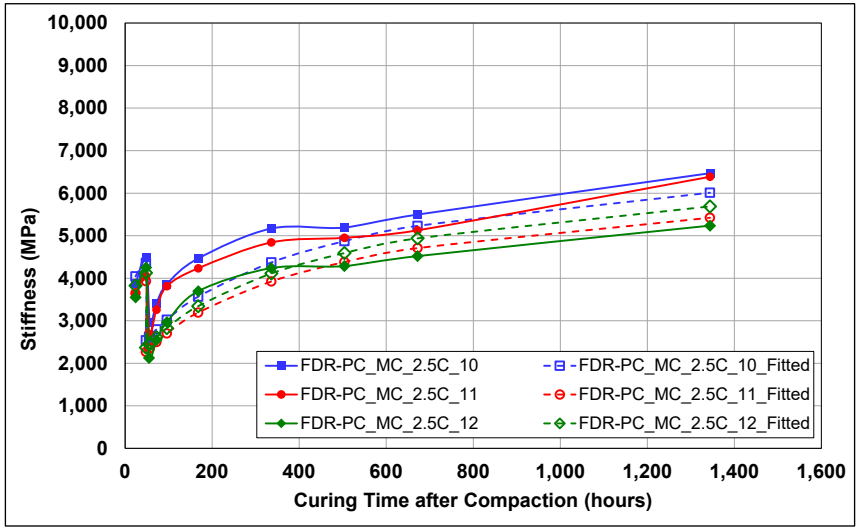

Figure B.7: 2.5% Cement with 60% stiffness reduction at 48 hours.

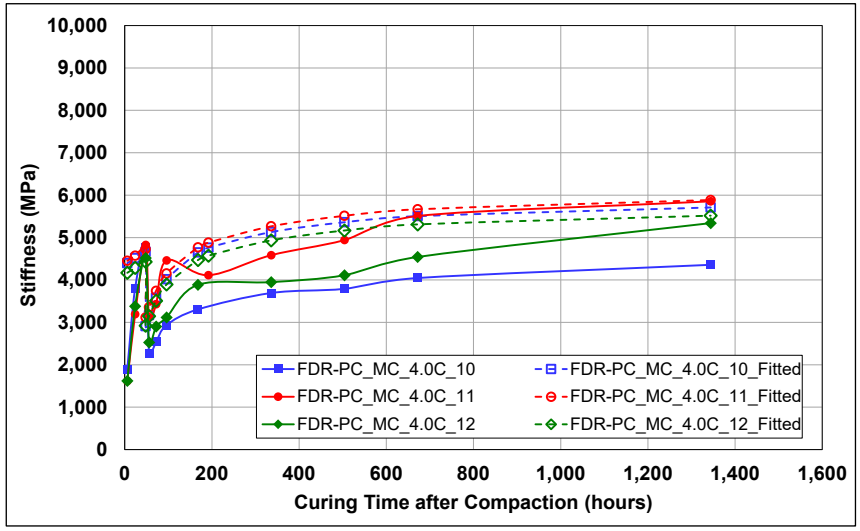

Figure B.8: 4% Cement with 60% stiffness reduction at 48 hours.

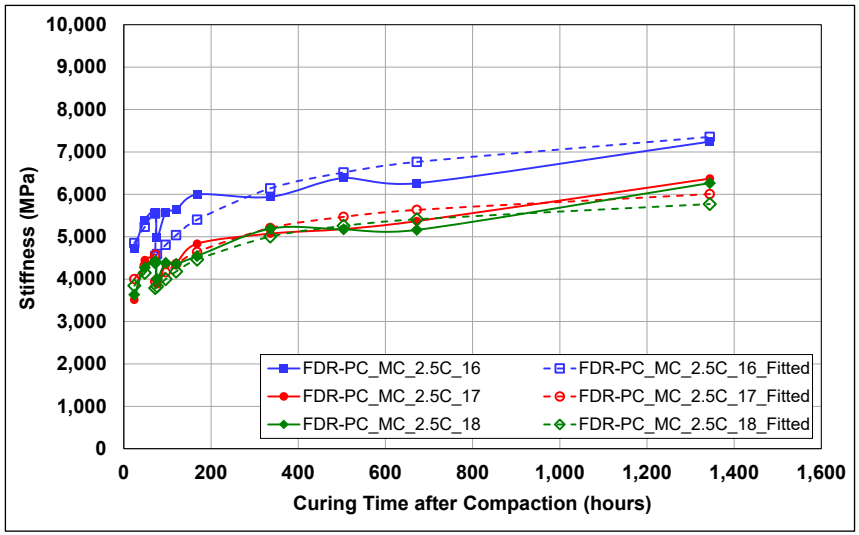

Figure B.9: 2.5% Cement with 20% stiffness reduction at 72 hours.

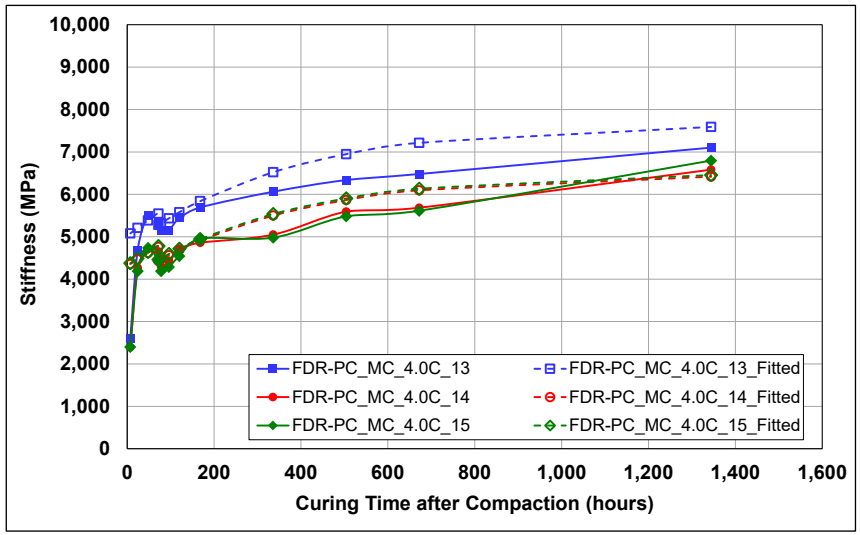

Figure B.10: 4% Cement with 20% stiffness reduction at 72 hours.

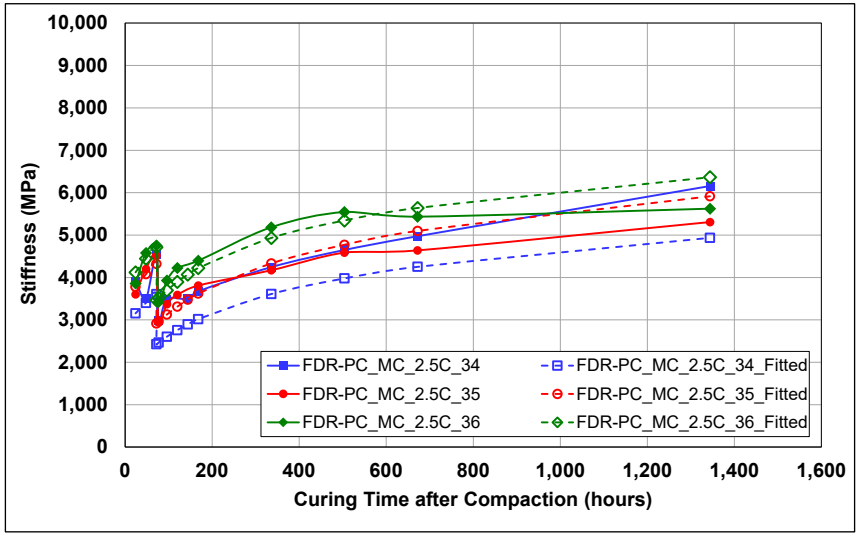

Figure B.11: 2.5% Cement with 40% stiffness reduction at 72 hours.

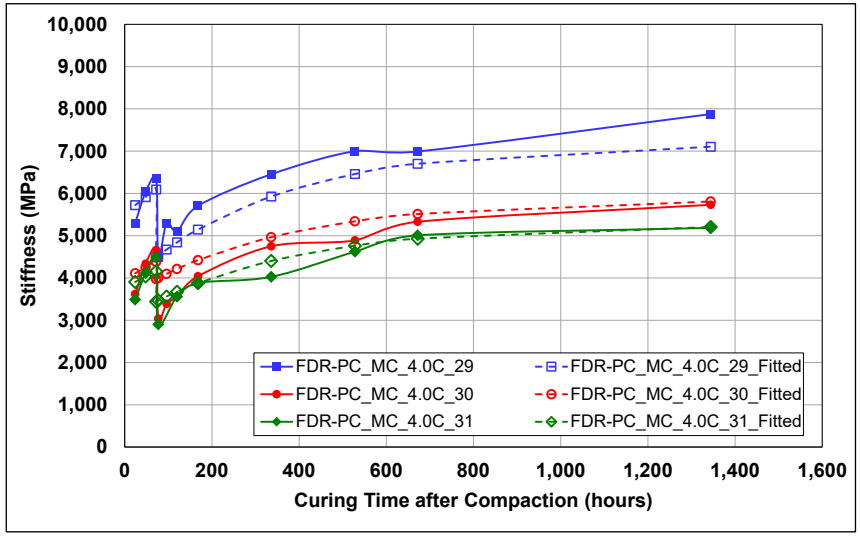

Figure B.12: 4% Cement with 40% stiffness reduction at 72 hours.

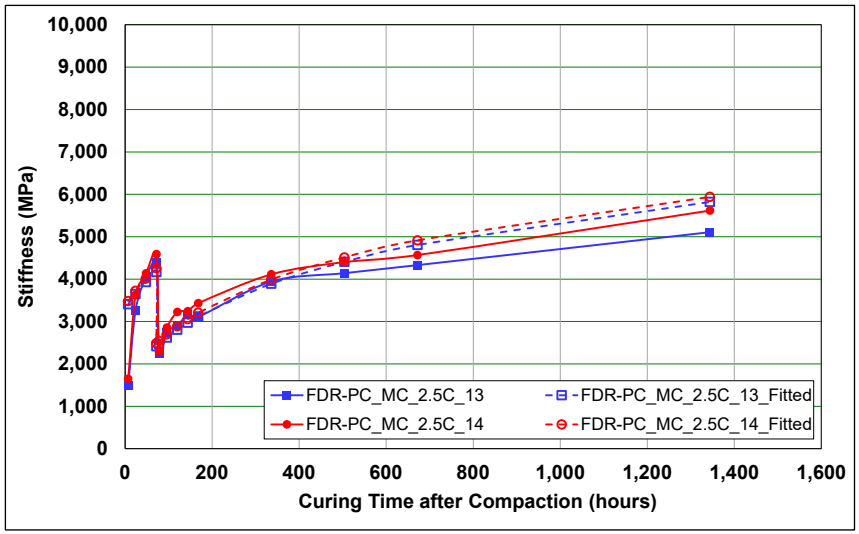

Figure B.13: 2.5% Cement with 60% stiffness reduction at 72 hours.

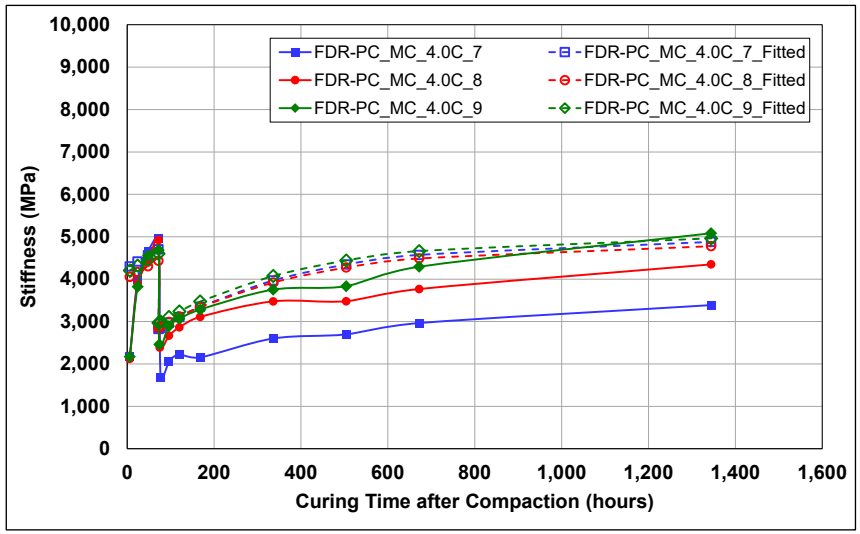

Figure B.14: 4% Cement with 60% stiffness reduction at 72 hours.

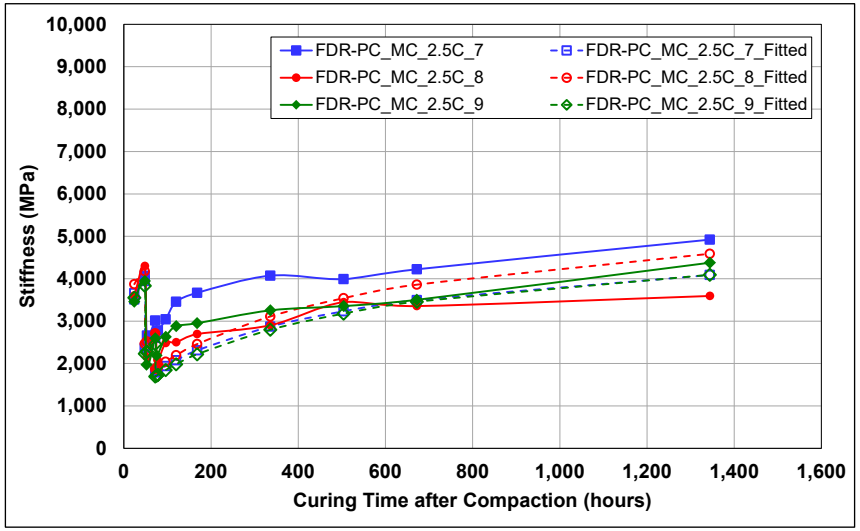

Figure B.15: 2.5% Cement with 60% stiffness reduction after 48 and 72 hours.

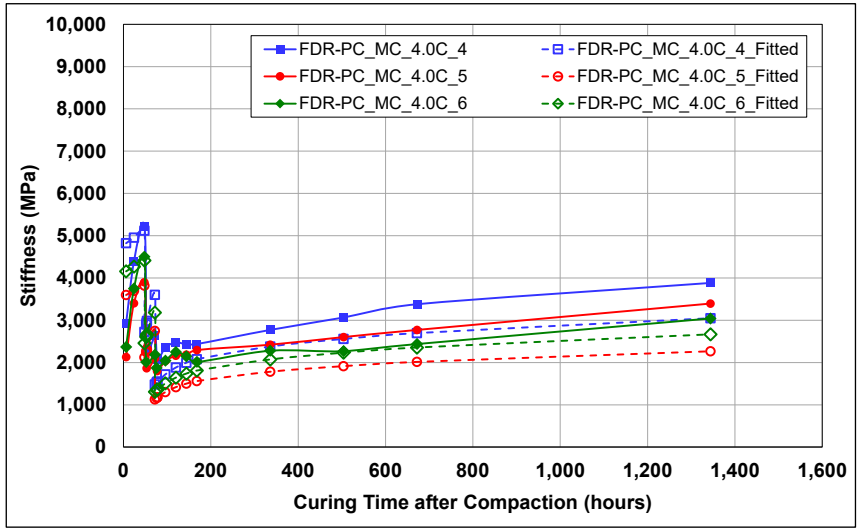

Figure B.16: 4% Cement with 60% stiffness reduction after 48 and 72 hours.

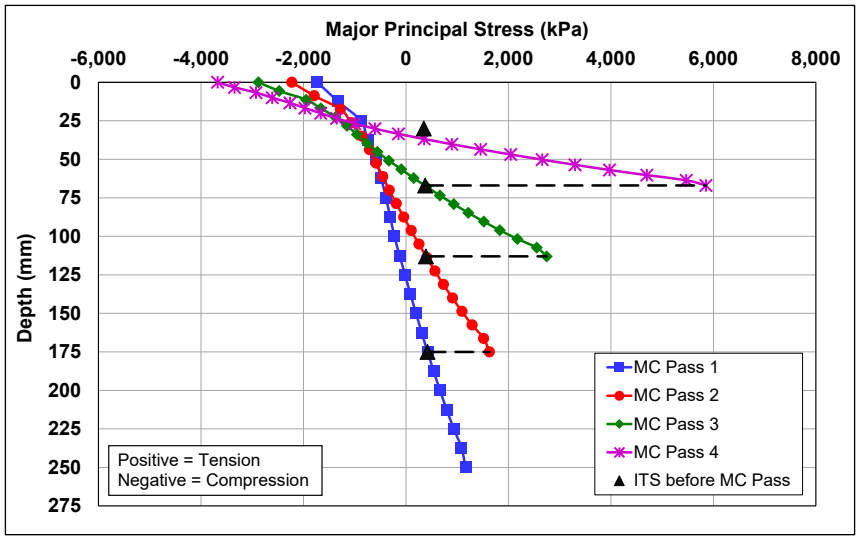

Figure B.17: 2.5% Cement with three microcracking passes at 48 hours: Effective stiffness reduction.

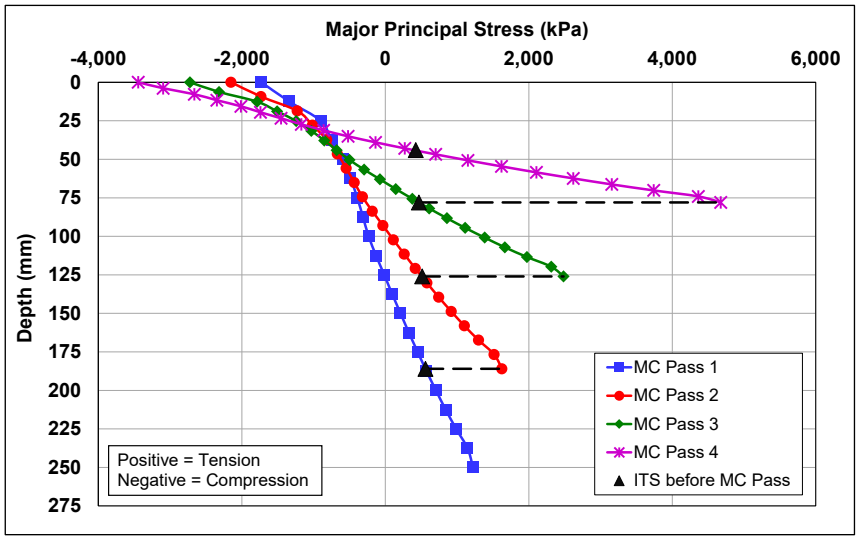

Figure B.18: 4% Cement with three microcracking passes at 48 hours: Effective stiffness reduction.

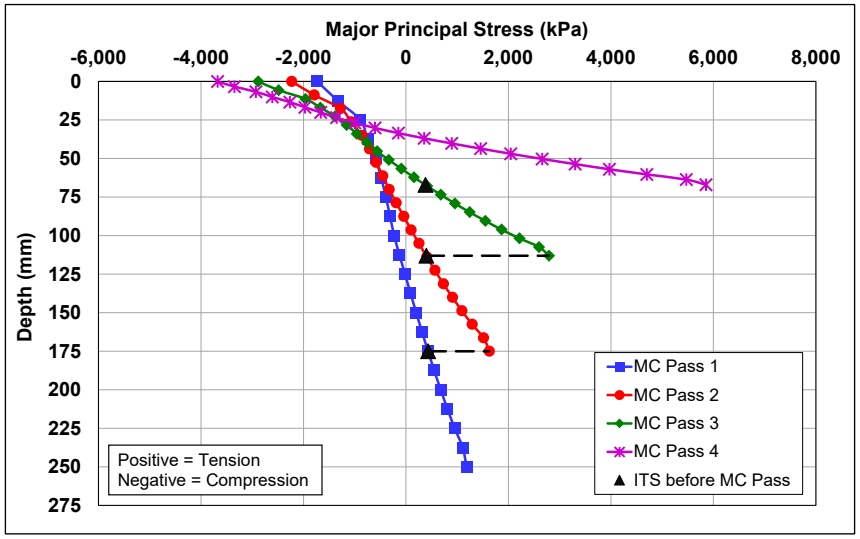

Figure B.19: 2.5% Cement with three microcracking passes at 72 hours: Effective stiffness reduction.

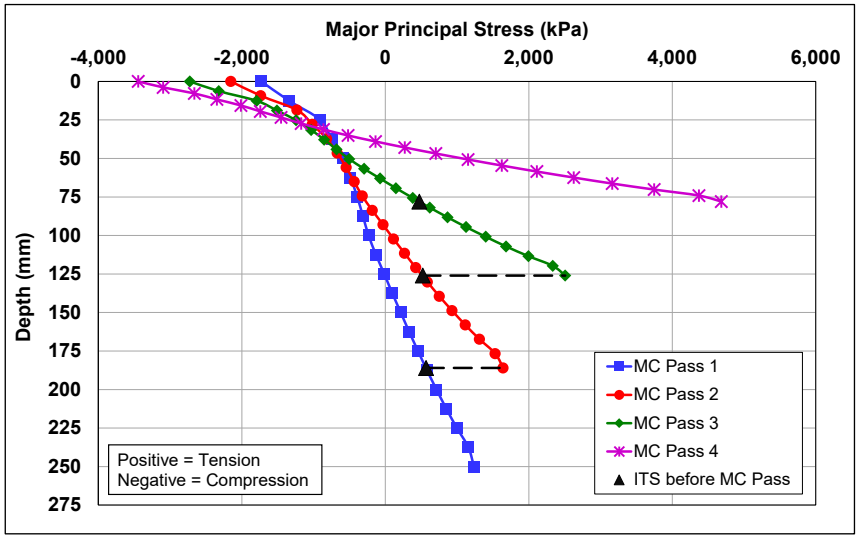

Figure B.20: 4% Cement with three microcracking passes at 72 hours: Effective stiffness reduction.